SYNTHESIS AND CHARACTERIZATION OF NOVEL MACROCYCLES BASED ON CYCLOBENZOINS

by
Maymounah Abdu M. Alrayyani

A dissertation submitted to the Department of Chemistry,
College of Natural Sciences and Mathematics
in partial fulfillment of the requirements for the degree of

DOCTOR OF PHILOSOPHY

In
CHEMISTRY

Chair of Committee: Prof. Ognjen Š. Miljanić

Committee Member: Prof. Allan J. Jacobson

Committee Member: Prof. David M. Hoffman

Committee Member: Prof. Loi H. Do

Committee Member: Prof. Yan Yao

University of Houston
May 2020

This thesis is dedicated to

My wonderful parents who have raised me to be the person I am today

My beloved husband who has been a supporter to accomplish the thesis work

My darling daughter who have made me stronger, better, and more fulfilled than I could have ever imagined

ACKNOWLEDGMENTS

This thesis is the outcome of five years of continuous and challenging work. During that time, I have been supported by many people who I am extremely grateful for them. Hence, I would like to take this opportunity to express my gratitude for all of them.

First and foremost, I would like to express my sincere thanks to my advisor **Prof. Ognjen Š. Miljanić** for his guidance, patience, helpful, suggestions, and for providing all necessary facilities which have made my research more fruitful. It has been an honor to accept me as the first graduate student from inorganic division in his group. I appreciate his willingness to offer me his time and ideas to make my PhD experience productive and stimulating. His guidance helped me in all the time of research and writing of this thesis. I am thankful to him for his outstanding scientific guidance and constructive criticism, which I have received on earlier versions of this thesis. I owe him lots of gratitude for teaching me, both consciously and unconsciously, how the good researcher and writer should be.

The studies discussed in this dissertation would not have been possible without the high-purity crystals. I have appreciated the significant collaboration, the impressive single crystal growing skills, and the inspirational discussions regarding these crystals, of the crystallographer **Dr. Xiqu Wang**. I apologize for annoying him with questions and problems regarding my single crystals. I am grateful for his patience and detailed explanations. Additionally, I am indebted to **Prof. Thomas S. Teets** and his former graduate student **Dr. Evanta Kabir** for allowing and teaching me how to use the cyclic voltammetry instrument. Their assistance and the time in which they handled all my queries are much respected. Many appreciations go to **Bunz group** in Heidelberg University at Germany for their collaboration to accomplish my first publication during the PhD journey that gives me a confidence to

pursue more. I would also like to thank my committee members: **Prof. Allan J. Jacobson**, **Prof. David M. Hoffman**, **Prof. Loi H. Do**, and **Prof. Yan Yao** for their time, insightful questions, helpful comments, and brilliant suggestions during the oral research progress examination and the PhD defense. Their questions, comments, and suggestions incented me to widen my research from various perspectives. Extended thanks go to the former and present **members in Miljanić group** for their kindness, interesting moments, motivating conversations, and endless assistance.

I am extremely grateful to my greatest family to whom I owe a great deal. Innumerable thanks go to my wonderful **parents** who have always been a constant source of prayers, support, and encouragement that sustained me thus far. I cannot forget to thank my dearest **siblings** as well for their continuous advice and guidance. I would also like to thank my beloved **husband** who has been continually supportive during the challenges and difficulties of graduate education and life. He has been patient with me when I am frustrated, and celebrate with me when even the minute things go right. Finally, I would like to express my gratitude to my darling **daughter** who donated her early childhood moments to her mom in order to finish this thesis.

Certainly, it is difficult for me to pay back what you all have provided to me, but one thing for sure, I am proud to be your student, collaborator, colleague, daughter, sister, wife, and mother; the success I have achieved is undoubtedly a glory that belongs to all of you.

Finally, I would like to acknowledge the financial support from the **Ministry of Education in Saudi Arabia** represented by **King Abdulaziz University**. This financial support fully covered both the tuitions and expenses since I arrived to the USA until I graduated, that let me focus more on achieving my goals in graduate school.

SYNTHESIS AND CHARACTERIZATION OF NOVEL MACROCYCLES BASED ON CYCLOBENZOINS

by
Maymounah Abdu M. Alrayyani

A dissertation submitted to the Department of Chemistry,
College of Natural Sciences and Mathematics
in partial fulfillment of the requirements for the degree of

DOCTOR OF PHILOSOPHY

In
CHEMISTRY

Chair of Committee: Prof. Ognjen Š. Miljanić

Committee Member: Prof. Allan J. Jacobson

Committee Member: Prof. David M. Hoffman

Committee Member: Prof. Loi H. Do

Committee Member: Prof. Yan Yao

University of Houston
May 2020

ABSTRACT

Cyclic molecules occupied a unique segment of synthetic chemistry in the last few decades. The diversity in their synthetic methodology and functionality supported their significant development to involve organic, inorganic, and supramolecular chemistry. This thesis focuses on the expansion of the research in the recently discovered class of cyclophanes, which was dubbed "cyclobenzoins".

In Chapter One, selected research literature is digested to put into perspective the challenges associated with synthetic macrocycles. Some applications of cyclophanes in molecular recognition, organic-inorganic hybrid molecules, polymer science, analytical detection, sensing, and supramolecular assembly, are also discussed. The history of benzoin condensation and the emergence of cyclobenzoin chemistry are summarized as well.

In Chapter Two, the reduction of cyclotribenzoin and the oxidation of cyclotetrabenzoin are applied to produce hexaol and octaketone macrocycles, respectively. The exceptional affinity of the crystal structures of the resultant macrocycles to host tetrahedral hydrogen-bonded water clusters or chlorinated solvent molecules within their extrinsic or intrinsic pores are discussed.

In Chapter Three, the full or partial fusion of cyclic octaketone with ortho-diamines to produce π-conjugated cyclic oligoazaacenes macrocycles is discussed. The diversity in crystal structures due to the incorporation of different motifs into the cyclic backbone is examined, as well as the optical and electronic properties of selected cyclic conjugated systems.

In Chapter Four, eight arylhydrazone arms are appended to the bridges between the phenyl rings in the octaketone scaffold. The crystal structures and crystal packing of the resulting molecules are examined and their dynamic ^{1}H NMR analyses are studied.

In summary, the chemistry of cyclobenzoins is expanded to include the host-guest chemistry, coordination polymers, and crystalline porous materials, as well as the novel optical and electronic properties resulting from the enlarged cyclic conjugated systems with azaacene subunits.

TABLE OF CONTENTS

*Note: Chapter One contains compounds labeled **1** through **112**. A separate numbering system is used for Chapters Two, Three, and Four. The compounds are numbered **1** through **29**.*

List of Charts

List of Schemes

List of Figures

List of Tables

List of Abbreviations and Acronyms

1D	one-dimistional
2D	two-dimintional
3D	three-diminsional
abs	absorption
AcOH	acetic acid
AEM	aryleneethynylene macrocycle
AIBN	azobisisobutyronitrile
ASE	aromatic stabilization energy
BET	Brunauer–Emmet–Teller
Bu	butyl
dba	dibenzylideneacetone
COP	cycloorthophenylenes
CMP	cyclometaphenylenes
CPP	cycloparaphenylenes
CV	Cyclic voltammetry
DEPT	Distortionless Enhancement by Polarization Transfer
DNT	6-dinitrotoluene
DMF	dimethyl formamide
DMSO	dimethyl sulfoxide
EM	emission
EtOH	ethanol
Et2O	diethyl ether
EX	excitation
ESI-HRMS	high resolution electrospray ionization mass spectrometry
Fc/Fc^+	ferrocene redox couple
FT-IR	Fourier-transform infrared
HOF	hydrogen-bonded organic framework

HOMO	highest occupied molecular orbital
$^{i}Pr_2O$	diisopropyl ether
ISMSC	International Symposium on Macrocyclic and Supramolecular Chemistry
IUPAC	International Union of Pure and Applied Chemistry
LUMO	lowest unoccupied molecular orbital
MeOH	methanol
MOF	metal-organic framework
MOP	metal–organic polyhedron
MWCNT	multi-walled carbon nanotubes
NHC	N-heterocyclic carbenes
NLO	non-linear optical
NMR	nuclear magnetic resonance
OFET	organic field-effect transistor
OLED	organic photovoltaic device
PA	picric acid
PAE	poly(*p*-aryleneethynylene)
PAHs	polycyclic aromatic hydrocarbons
PAV	Poly(p-arylenevinylene)
PET	polyethyleneterephthalate
PhMe	toluene
PMMA	polymethyl methacrylate
POP	porous organic polymer
PPh_3	triphenylphosphine
SAPT	Symmetry-Adapted Perturbation Theory
TBAI	tetrabutylammonium iodide
THF	tetrahydrofuran
TCNE	tetracyanoethylene
TIPS	triisopropyl silane
TsOH	p-toluenesulfonic acid

XRD	X-ray Diffraction
UH	University of Houston
UV	ultraviolet
UV/Vis	ultraviolet/visible
VOCs	volatile organic compounds

Chapter One

Cyclobenzoins: Novel Cyclophanes as Supramolecular Scaffolds

1.1 Introduction

1.1.1 Macrocycles

Macrocycles are the molecules with at least twelve atoms connected covalently in a cyclic framework.[1] This class of organic molecules has developed exponentially in the last few decades since Pedersen accidently obtained the macrocyclic polyethers which are known now as "crown ethers".[2,3] This discovery was followed by many attempts to synthesize more macrocycles. Later, Lehn and Cram developed the discipline of supramolecular chemistry by synthesize cyclic molecules with structure-specific interactions of high selectivity.[4,5] Pedersen, Lehn, and Cram were jointly awarded the Nobel Prize in Chemistry in 1987, to honor their pioneering work in developing the field of macrocycles and their applications in host-guest chemistry.[6-8] This development was followed by the syntheses of numerous macrocyclic compounds (Chart 1.1), such as torands,[9-11] calix[*n*]arenes,[12] cucurbit[*n*]urils,[13-16] pillar[*n*]arenes,[17-20] cyclodextrins,[21,22] and a variety of cyclophanes,[23-58] whose applications have been extended to cover a wide research area in organic, inorganic, and supramolecular chemistry.[59] In 2016, the Nobel Prize in Chemistry awarded to Stoddart, Sauvage, and Feringa for their research in the domain of molecular machines; the world's smallest mechanical devices which often include macrocycles in their backbones.[60-62] In this thesis, among different classes of macrocycles, novel cyclophanes and their derivatives will be highlighted.

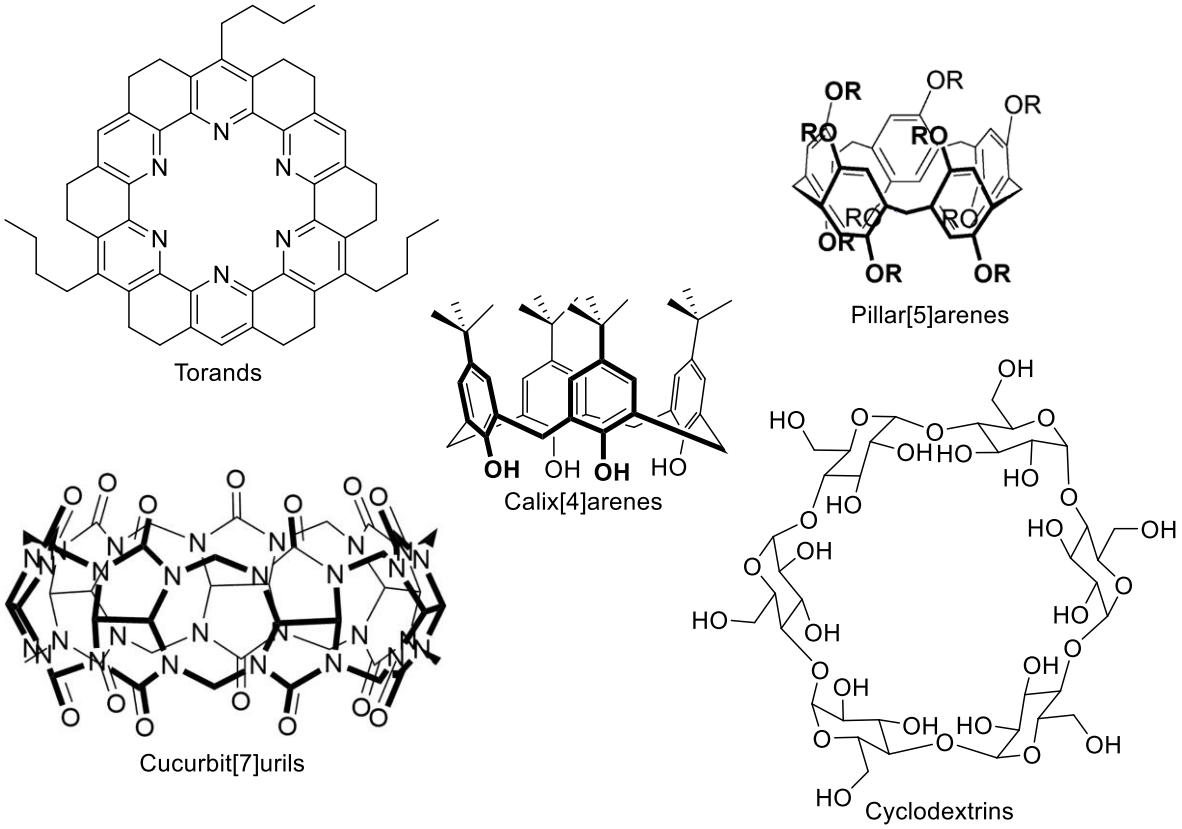

Chart 1.1 Examples of macrocyclic compounds discovered in the last few decades.

1.1.2 Syntheses of Macrocycles

Despite the syntheses of many macrocyclic compounds in last decades, the synthesis of macrocycles is still a challenge due to the presence of "ring/chain" equilibrium which leads to a relatively low yield due to the equilibrium found between the cyclic compounds and their corresponding acyclic compounds.[63,64] In order to overcome these obstacles, the essential kinetic and thermodynamic concepts behind these processes should be fully understood. On the one hand, from the kinetic point of view, using high dilution or pseudo-high dilution, which often utilizes the lessons from the solid-phase synthesis, conditions can reduce the probability of oligomerization and enhance the chance of cyclization by kinetically favoring intramolecular versus intermolecular reactions. This approach has been proven as the most efficient way to favor macrocyclization since it was discovered by Ruggli in 1912.[65] On the other hand, from the thermodynamic point of view, the given cyclic molecules can be

thermodynamically more favorable than the corresponding oligomeric ones when the stability of cyclic compound exceeds the stability of the oligomer at the equilibrium of the reversible reactions, i.e. the value of the effective molarity is high, which allows one to predict the entropic consequences of ring/chain equilibrium. This is because in the thermodynamically controlled reactions the probability of distribution at the equilibrium depends on the relative Gibbs energies of all the species involved in the reaction, which is clearly observed in shape-persistent macrocycles. In this family of macrocycles, the formation of large rings with no angle strain is thermodynamically more favorable than the formation of small rings with high angle strain.[24]

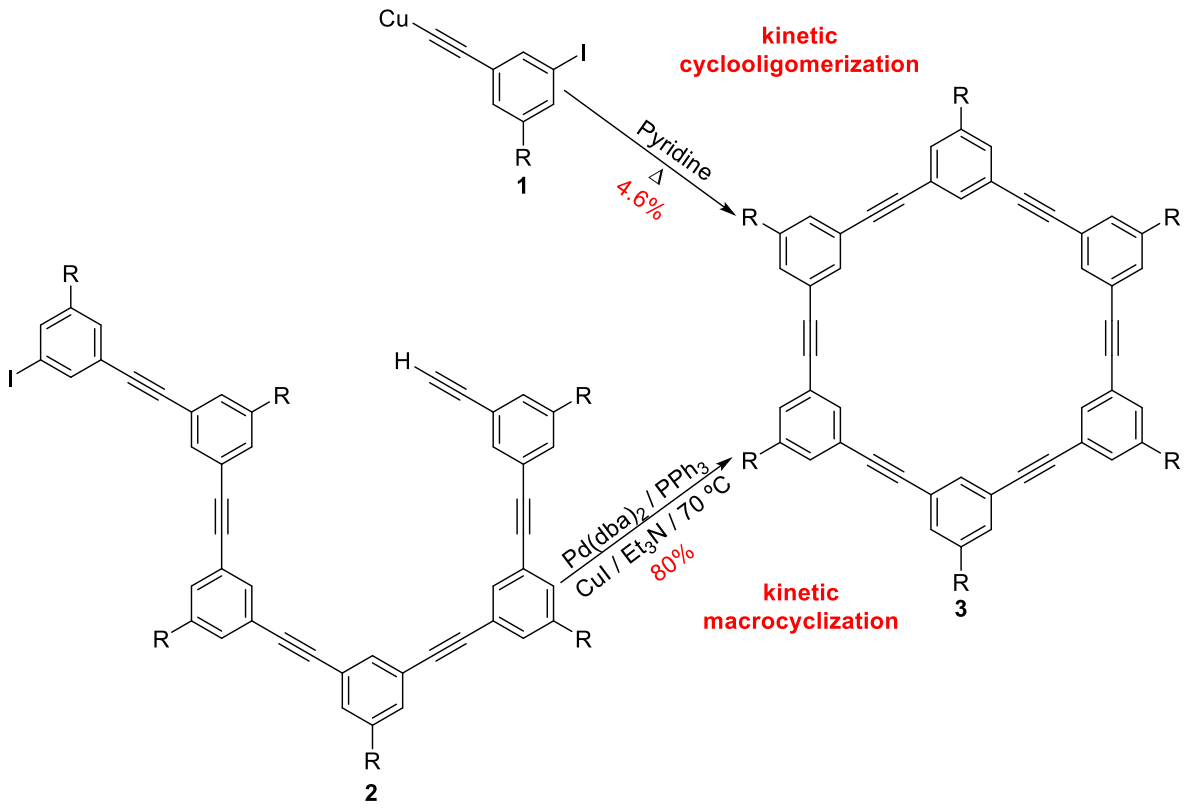

Scheme 1.1 Pathways to synthesize a hexameric phenylacetylene macrocycle.

With a vision to increase the eventual yield for a desired macrocycle molecule, the smart selection of the pathway of cyclization and the disconnection site are considered influential steps on account of their ability to induce a favorable folding of precursor in order

to help the reactive ends approach each other and then favor the macrocyclization process. For example, the yield of the final ring closure of a hexameric phenylacetylene macrocycle **3** increased from 4.6% to 80% when the reaction pathway changed from kinetic cyclooligomerization to kinetic macrocyclization (Scheme 1.1).[26] Also, different ring-disconnections were involved in [1 + 1] macrocyclization processes to prepare benzo-crown-ethers **6** of diverse sizes. The yields of the resulting benzo-crown-ethers changed dramatically—under same reaction conditions—when starting materials with different flexibilities were used (Scheme 1.2).[64]

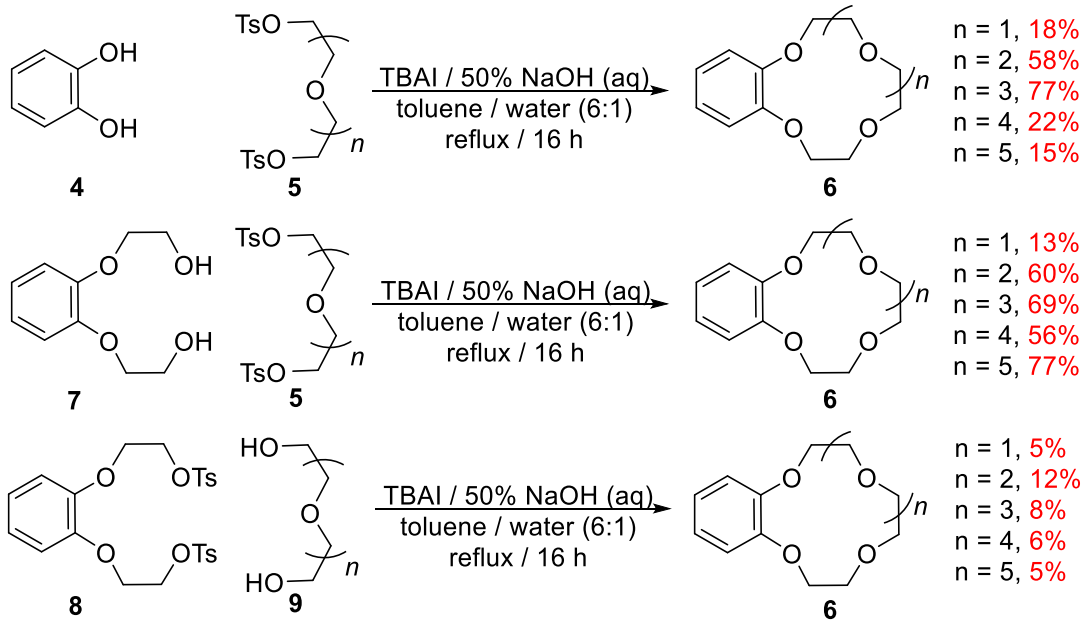

Scheme 1.2 Synthesis of benzo-crown-ethers of diverse sizes.

1.2 Cyclophanes

Cyclophanes are strained macrocycles which consist of one or more aromatic rings and saturated or non-saturated aliphatic chains that form bridges between two nonadjacent carbons in the aromatic motifs.[66] The rigidity of these macrocycles is gained from the aromatic regions while the flexibility comes from the presence of aliphatic chains. [*n*]Cyclophanes are the simplest cyclophanes and they are categorized into two main classes

(Chart 1.2A): [*n*]metacyclophane and [*n*]paracyclophane, where the prefixes *meta*- and *para*- identify the positions of the connection to the aromatic motifs while *n* represents the number of methylene groups in each aliphatic bridge of the macrocycle.[59,67] The aromatic rings which are bridged from *ortho*-positions—two adjacent carbons— do not classify as [*n*]cyclophane because, in this type of connection, the interaction between the aliphatic chains and the π-system in aromatic rings does not exist; therefore the strain is generally not observed. Moreover, as the length of the aliphatic chain in [*n*]metacyclophane or [*n*]paracyclophane increases, the ring strain decreases because the force which pulls the aromatic ring into a nonplanar shape is reduced.

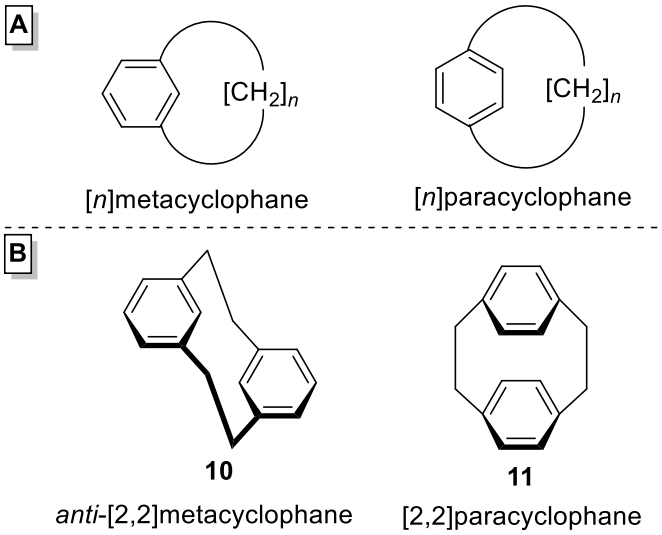

Chart 1.2 *(A)* Nomenclature of [*n*]cyclophanes and *(B)* the first discovered cyclophanes.

The research on this class of macrocycles started in 1899 when Pellegrin first synthesized *anti*-[2.2]metacyclophane (compound **10** in Chart 1.2B) through a Wurtz coupling,[68] but it did not attract the interest of many chemists until Brown and Farthing isolated [2.2]paracyclophane (compound **11** in Chart 1.2B) during the pyrolysis of *p*-xylene in 1949.[69] Two years later, [2.2]paracyclophane was synthesized using a designed strategy by Cram and Steinberg to study the electronic interactions between the "face-to-face" arranged aromatic systems.[70] Thereafter, many cyclophanes have been synthesized such as

aryleneethynylene macrocycles (AEMs),[23–27] cyclobis(paraquat-*p*-phenylene) (the so-called "blue boxes" or "ExBoxes"),[28–35] "Texas-sized" boxes,[36–38] cyanostars,[39–45] biphenarenes,[46–48] coronarenes,[49–51] and others[52–58] (Chart 1.3).

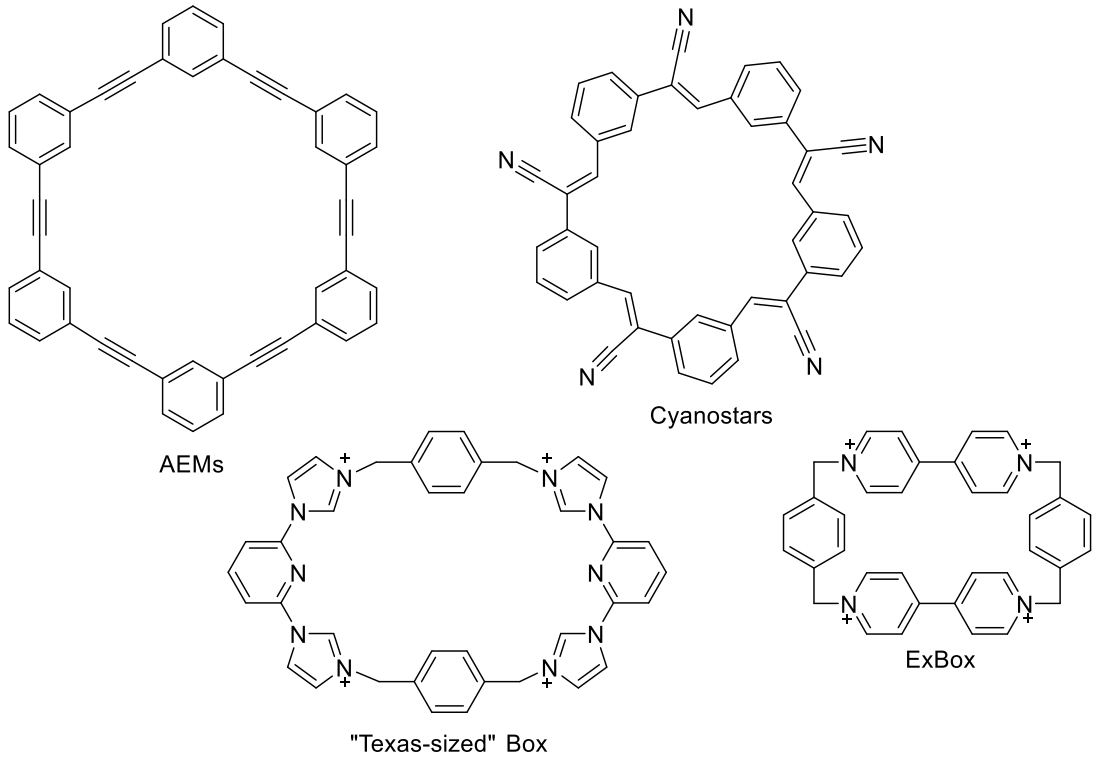

Chart 1.3 Examples of some synthesized cyclophanes.

1.2.1 General Synthetic Aspects of Cyclophanes

The synthetic methodologies for the most known cyclophanes can be classified into three main categories, according to the final synthetic event that results in the cyclophane formation (Scheme 1.3).[67] In type I strategies, a new bond is formed between the two previously unbonded atoms in order to form a bridge (type I-a) or to shrink the existing bridge (type I-b). On the one hand, type I-a reactions usually require disubstituted aromatic compounds as starting materials to perform intramolecular interaction during the cyclization step which requires high dilution conditions. On the other hand, type I-b reactions work best when the target cyclophane has two or more bridges due to the formation of a bridge-opened

reactive intermediate during the conversion process of larger cyclophane to a smaller one.[71] Despite the fact that type I strategy is considered the most popular for cyclophane synthesis, type I-a is ineffective in the synthesis of moderately strained cyclophanes and type I-b is not useful in the synthesis of highly strained cyclophanes.[72] Similar to type I-a strategy, type II strategy involves intramolecular interaction during the bond formation step, but in type II the bond connects the bridge with an aromatic ring and it is common in the synthesis of relatively unstrained cyclophanes.[73] The last strategy, type III strategy, converts a bridged pre-arene macrocycle to a cyclophane consisting of a bridged aromatic system. This reaction is mostly accompanied by a high amount of aromatic stabilization energy (ASE) due to the transformation process of pre-arene to the corresponding arene. The released energy can be utilized as a weighty counterbalance to the developing strain. In this regard, type III strategy is considered the best strategy to synthesize highly strained cyclophanes.[74]

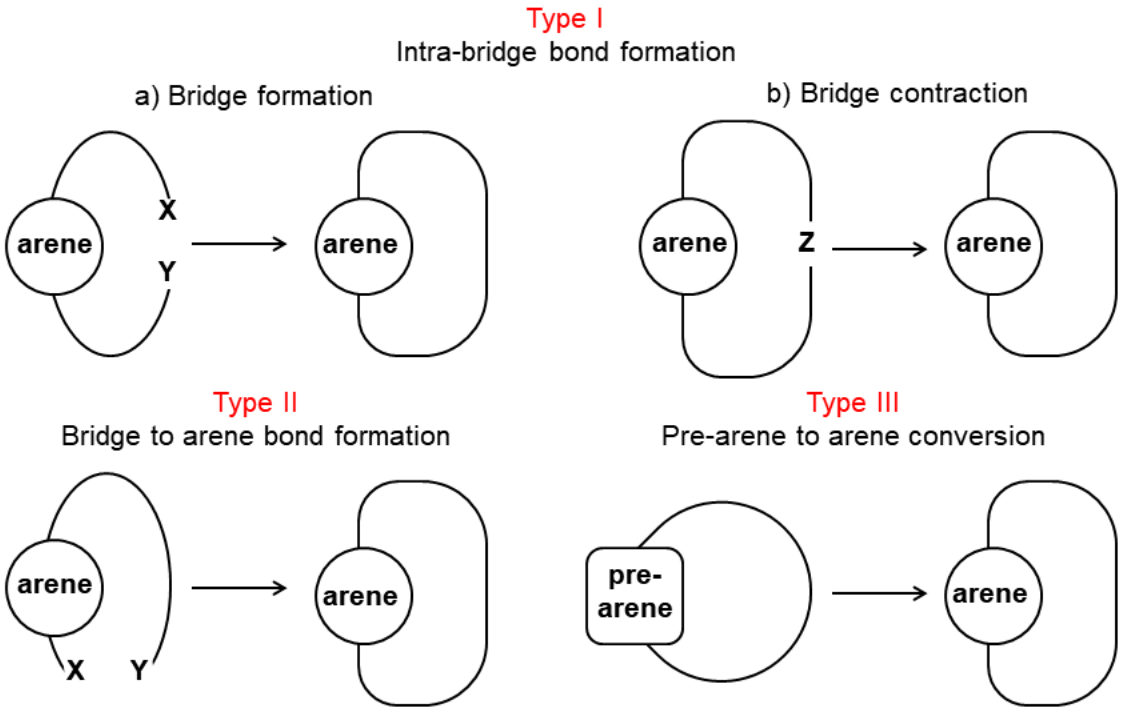

Scheme 1.3 Strategies for the synthesis of cyclophanes (adapted from ref. 67 with permission, copyright © 2015 The Royal Society of Chemistry).

1.2.2 Applications of Cyclophanes

1.2.2.1 Cyclophanes in Host-Guest Chemistry

Since the discovery of the crown ethers by Pedersen in 1976, the host-guest chemistry for the selective complexation of organic and inorganic molecules has immensely developed. Cyclophanes have been promising hosts in the field of the host-guest chemistry owing to their molecular recognition properties. These properties appear in cyclophanes due to their cyclic structure, whose backbones can be easily pre-organized to improve the affinity to accommodate different guest molecules or atoms of the suitable size and shape. In this part, some cationic, anionic, and neutral synthetic cyclophanes, which were proven as useful hosts, will be discussed in order to understand the molecular recognition capabilities of these macrocycles.

Cationic electron-poor cyclophanes usually have a high tendency to host electron-rich guest. The best example of such cyclophanes is the tetracationic cyclobis(paraquat-*p*-phenylene) molecule (**12**) which become very popular since their discovery in the Stoddart lab more than three decades ago.[28] The first synthesized tetracationic cyclobis(paraquat-*p*-phenylene) consists of two π-electron-deficient 4,4′-bipyridinium units —viologens derivatives, bridged by two *p*-xylylene linkers in a cyclic structure. The modification of parent tetracationic cyclobis(paraquat-*p*-phenylene), by adding 1,4-phenylene ring between each pair of pyridinium unit, turns it into **13** which is host capable of extracting the harmful polycyclic aromatic hydrocarbons (PAHs), ranging in size from two to seven fused aromatic rings, from both organic and aqueous media.[29] The crystal structures of the resulting complexes (Figure 1.1) exhibited that the cyclophane host crystal was colorless and it becomes colored after binding the polycyclic aromatic hydrocarbons, which is explained by the presence of charge-transfer interactions between the host and different guests.

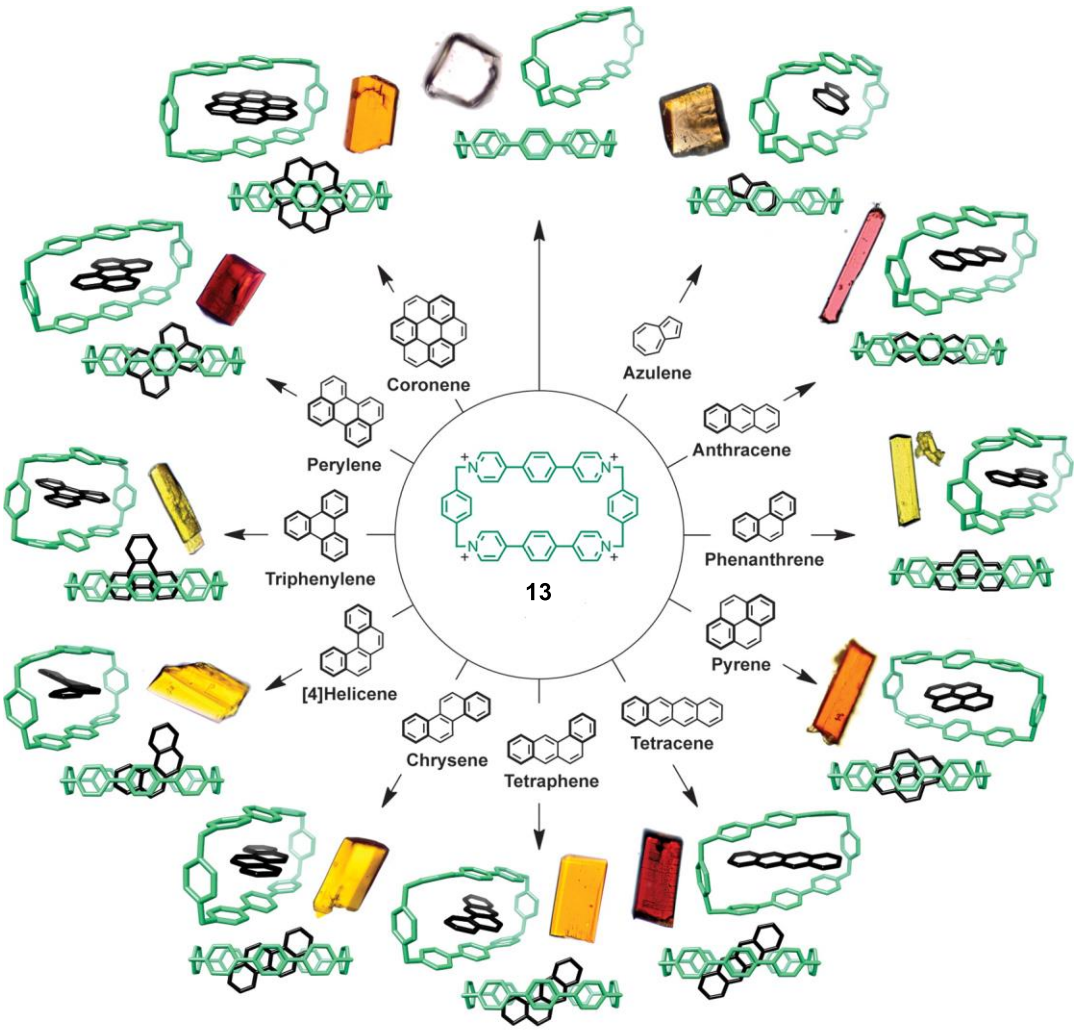

Figure 1.1 Crystal structures of polycyclic aromatic hydrocarbons-cyclophane complexes. In each case, the crystals that were used to obtain the XRD data were photographed under an optical microscope. Hydrogen atoms, counter anions, and solvent molecules have been omitted for clarity (adapted from ref. 29 with permission, copyright © 2013 American Chemical Society).

Another modification was conducted on this electron-deficient cyclobis(paraquat-*p*-phenylene) by changing the *p*-xylylene bridges to 1,2-bis(*p*-tolyl)acetylene spacers to produce a larger rigid cyclophane (compound **14** in Figure 1.2A).[75] This rigid tetracationic cyclophane can accommodate the parent cyclobis(paraquat-*p*-phenylene) through radical-pairing interactions when both are in their diradical dicationic states, forming a box-in-box complex. The strong interaction between the two cyclophanes in this complex led to the formation of a unique tetraradical tetracationic complex with a new feature. The resulting

box-in-box complex was able to host several 1,4-disubstituted benzene derivatives, as a third component, inside the cavity of the parent cyclobis(paraquat-*p*-phenylene) box (Figure 1.2B) to create hierarchical Matryoshka dolls like assemblies in solution and in the solid state which is rarely observed in the case of organic compounds.

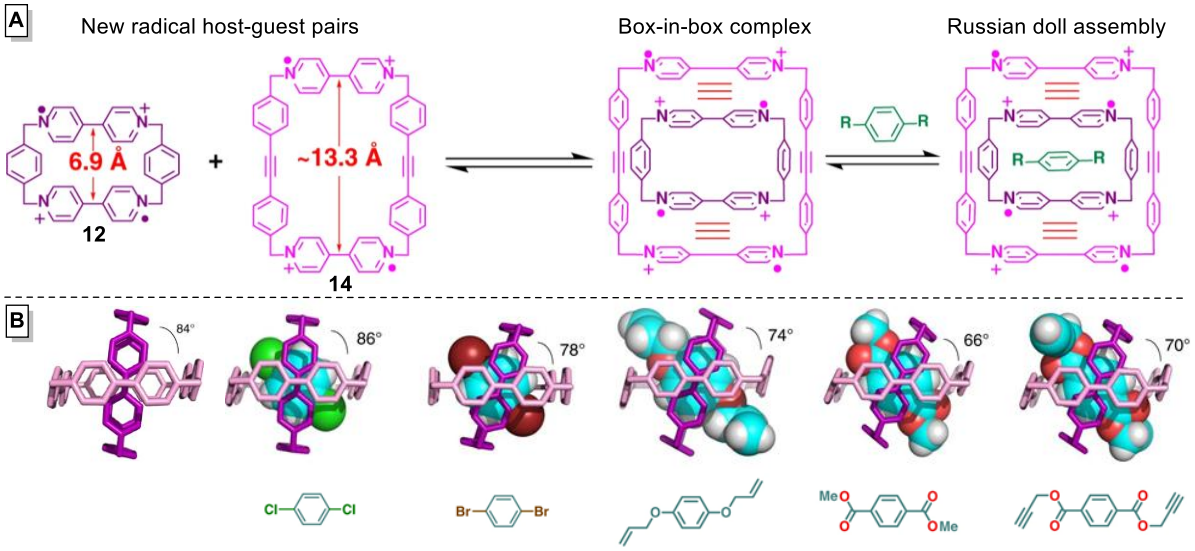

Figure 1.2 *(A)* Proposed superstructures of the tetraradical tetracationic box-in-box complex and Matryoshka dolls assembly. *(B)* The side view of the solid state superstructures of box-in-box complex and Matryoshka dolls assemblies with different guests. Hydrogen atoms have been omitted for clarity (adapted from open access ref. 75, copyright © 2018 Nature Publishing Group).

Similar to Stoddart's parent cyclobis(paraquat-*p*-phenylene), Weiss and co-workers prepared flexible positively-charged cyclophane **15** consisting of 4,4′-bipyridinium units (bis-viologens) bridged by seven carbon-long alkyl chains.[76] The ability of this electron-poor cyclophane to accommodate tetrathiafulvalene as an electron-rich guest in its well-adapted cavity was proven by X-ray crystallography (Figure 1.3). Unlike the previously mentioned electron-poor hosts which interacted with guests by charge-transfer or radical-pairing interactions, the contact between the host and guest in this complex is caused only by strong van der Waals interactions leading to a tetrathiafulvalene-viologen complex with a centroid-centroid distance of 3.82 Å.

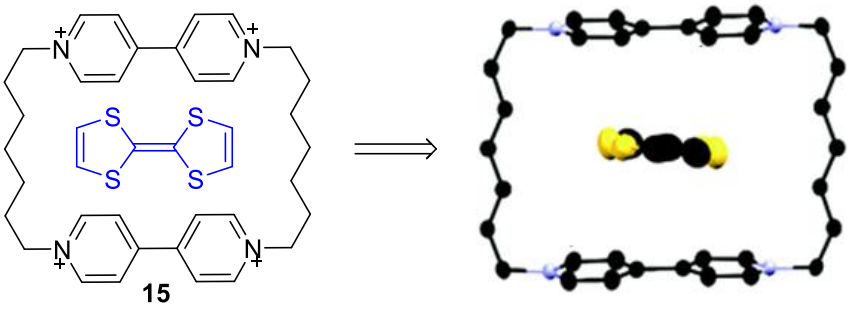

Figure 1.3 Structures of Weiss's host (black) and guest (blue) and the X-ray structure of their complex. Hydrogen atoms, counter anions, and solvent molecules have been omitted for clarity (adapted from ref. 76 with permission, copyright © 2015 The Royal Society of Chemistry).

In contrast to cationic cyclophanes, anionic electron-rich cyclophanes tend to accommodate electron-poor guests in their cavities. The most known electron-rich cyclophanes are those which have pendant carboxylate groups in their structure. The complexation of those anionic cyclophanes with the cationic molecules is mostly detected by ^{1}H-NMR spectroscopy. In 1991, Koga and co-workers designed such an anionic cyclophane **16** with eight pendant carboxylate groups which provided negatively charged environment around the cavities of the macrocycles (Chart 1.4A).[77] The ^{1}H-NMR spectroscopy indicated that the chemical shifts of the cyclophanes are changed when they form inclusion complexes selectively with positively-charged aromatic amines **17**–**22** in an alkaline aqueous medium. Inoue and co-workers also conducted NMR studies to investigate the complexation of three ammonium salts (dopamine **24**, tyramine **25**, and phenethylamine **26**) with water-soluble *para*-cyclophane **23** which has four pendant carboxylate groups distributed on the two sides of the macrocycle and go between two secondary amide groups (Chart 1.4B).[78] The NMR results confirmed that the chemical shifts of both the cyclophane host and the ammonium salt guests are shielded toward lower chemical shifts, which means the supramolecular complexes are formed with great insertion depth. The resulting host-guest complex is stabilized by an electrostatic interaction between the carboxylate anions in host molecules and ammonium

cations in guest molecules, beside the [π···π] interaction between aromatic groups. Analogous metacyclophane **27** was also prepared (Chart 1.4C); it is capable of confining the cationic histamine **28** inside its cavity based on: hydrophobic interactions, dipolar interactions, and electrostatic interactions between the carboxylate arms of the cyclophane and the alkyl ammonium arm of the histamine.[79]

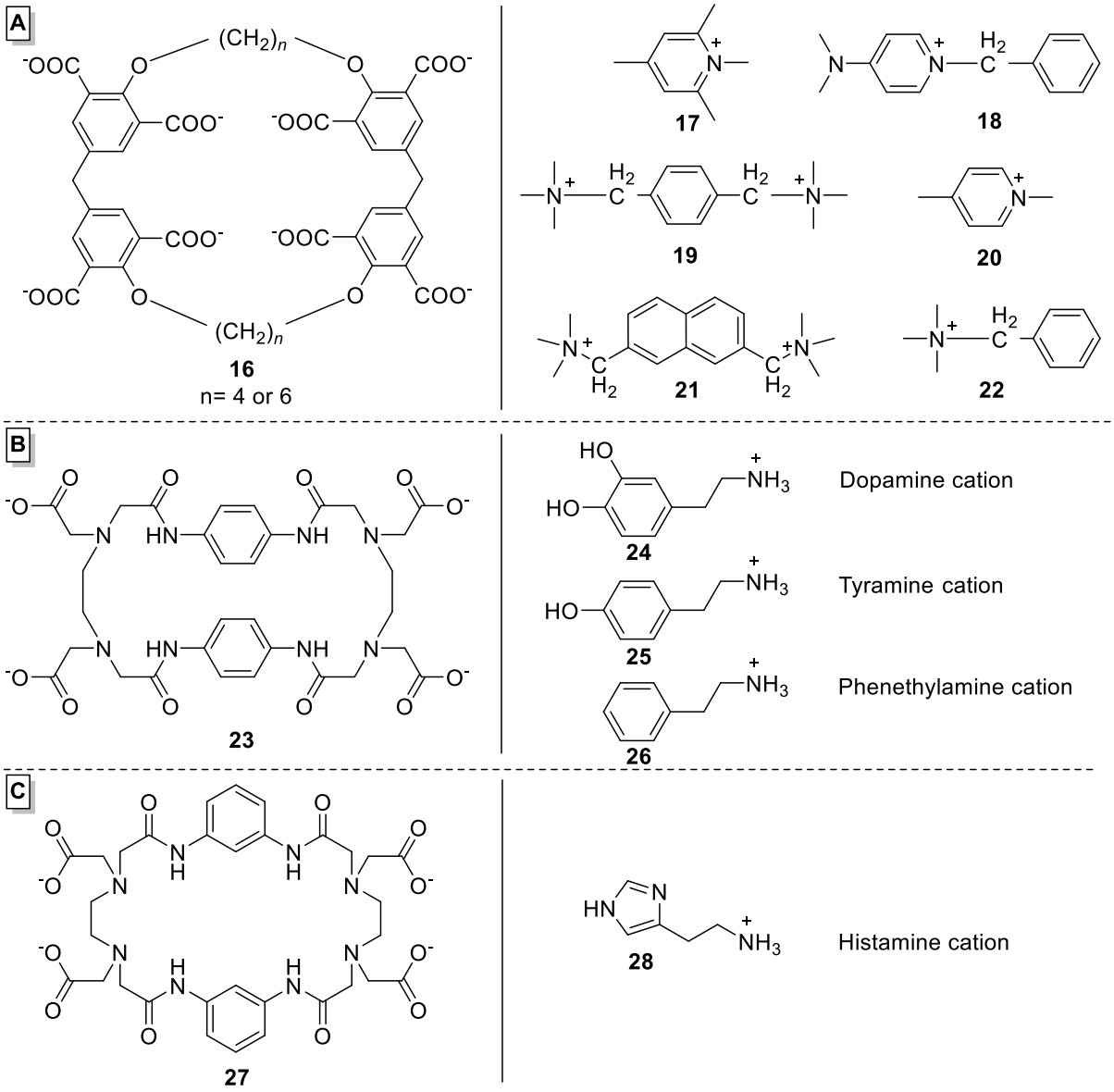

Chart 1.4 The anionic cyclophane structures (left) and their corresponding guests (right) which were designed by *(A)* Koga group; and *(B)* and *(C)* Inoue group.

The neutral synthetic cyclophanes combine the characters of both cationic and anionic cyclophanes: they can host both electron-rich and electron-poor guests in their cavities,

depending on the nature of the designed cyclophane. Shinmyozu and co-workers designed and synthesized a neutral electron-deficient cyclophane with triangular shape **29** to host a potential triangular neutral electron-rich guest through charge transfer interactions. The structure of the resulting complex was confirmed by X-ray crystallography as the first ring-in-ring complex crystallographically confirmed (Figure 1.4).[80] The host cyclophane consists of three pyromellitic diimide moieties which are π-electron acceptors, this is why it included a π-donating guest selectively in its cavity due to a charge-transfer interaction. In the inclusion complex, all benzene rings of the guest face the pyromellitic diimide moieties of host in a parallel fashion at a distance of 3.47–3.52 Å, and all the complex molecules stack regularly to form a tubular structure.

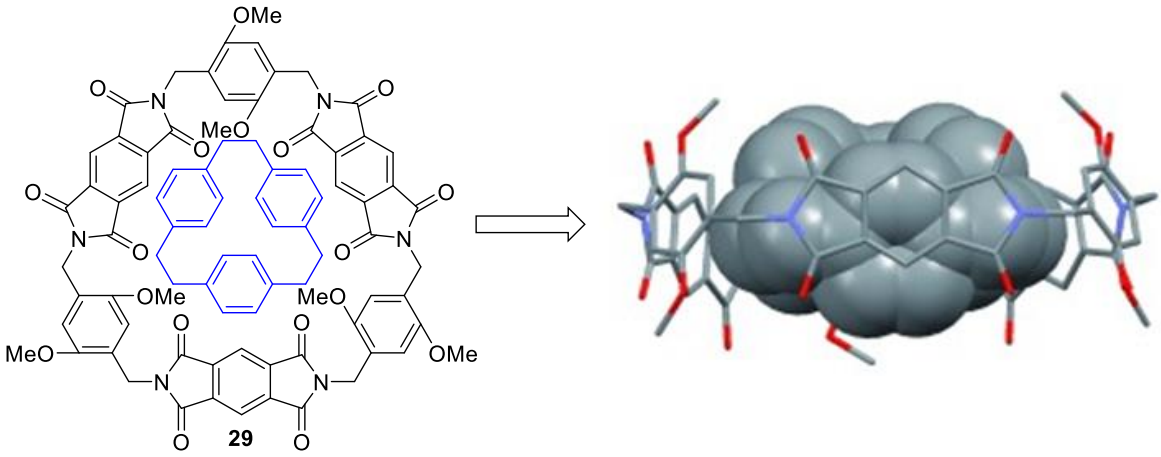

Figure 1.4 Structures of electron-deficient host (black) and electron-rich guest (blue) synthesized by the Shinmyozu group and the side view of their solid state complex at −150 °C. Hydrogen atoms have been omitted for clarity (adapted from ref. 80 with permission, copyright © 2006 John Wiley and Sons).

Similarity, Stoddart and co-workers designed triangular neutral electron-poor cyclophane **30** which consists of three naphthalenediimide units at each side of the triangle (Figure 1.5).[54] The solid state structure of this cyclophane presented supramolecular helices when linear triiodide anions were encapsulated into the electron-deficient cavity of the triangular cyclophane, with anion–π distances of about 3.8 Å. Insertion of I_3^- anions into the

cavity of the triangular cyclophane induced the [π···π] stacking of the chiral prisms to one-handed supramolecular helices, which is considered a good example of anion-induced self-assembly with potential as ion-channels.

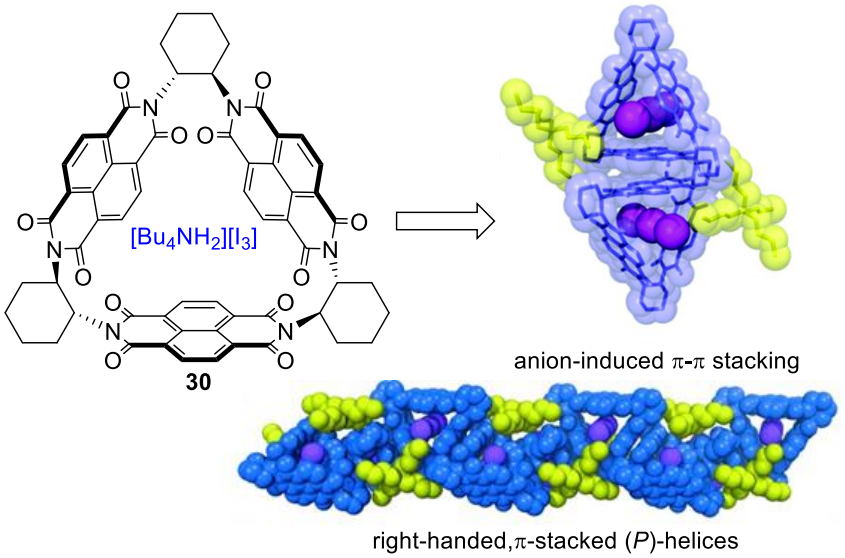

Figure 1.5 Structure of electron-deficient host **30** synthesized by the Stoddart group. Its crystal structure showed face-to-face π-stacked dimer with I_3^-, and the right-handed, π-stacked supramolecular (*P*)-helices. Macrocycle molecules are illustrated in blue, I_3^- anions in purple, and Bu_4N^+ counter ions in yellow. Hydrogen atoms have been omitted for clarity (adapted from ref. 54 with permission, copyright © 2013 John Wiley and Sons).

Cyanostar macrocycle **31**, which was designed and synthesized by Flood and co-workers, is also considered an electron-deficient cyclophane. It stacked in layers when it is engaged with bisulfate or phosphate anions.[42,43] On the one hand, the supramolecular structure of the bisulfate dimer when it is encapsulated inside the cyanostar macrocycle presented 2:2:2 stoichiometries for macrocycle : HSO_4^- : counter-cation; the bisulfate dimer was trapped within a pair of cyanostars end-capped with two tetrabutylammonium cations (Figure 1.6, right). On the other hand, the co-assembled complex of phosphate with the cyanostar macrocycle displayed a mixture of trimer 3:2:2 and tetramer 4:3:3 stoichiometry for macrocycle : $H_2PO_4^-$: counter-cation (Figure 1.6, left). The difference in the solid-state stoichiometry of the bisulfate and phosphate complexes with cyanostar macrocycle

emphasized the preference of phosphate for oligomerization over bisulfate's simpler dimerization.

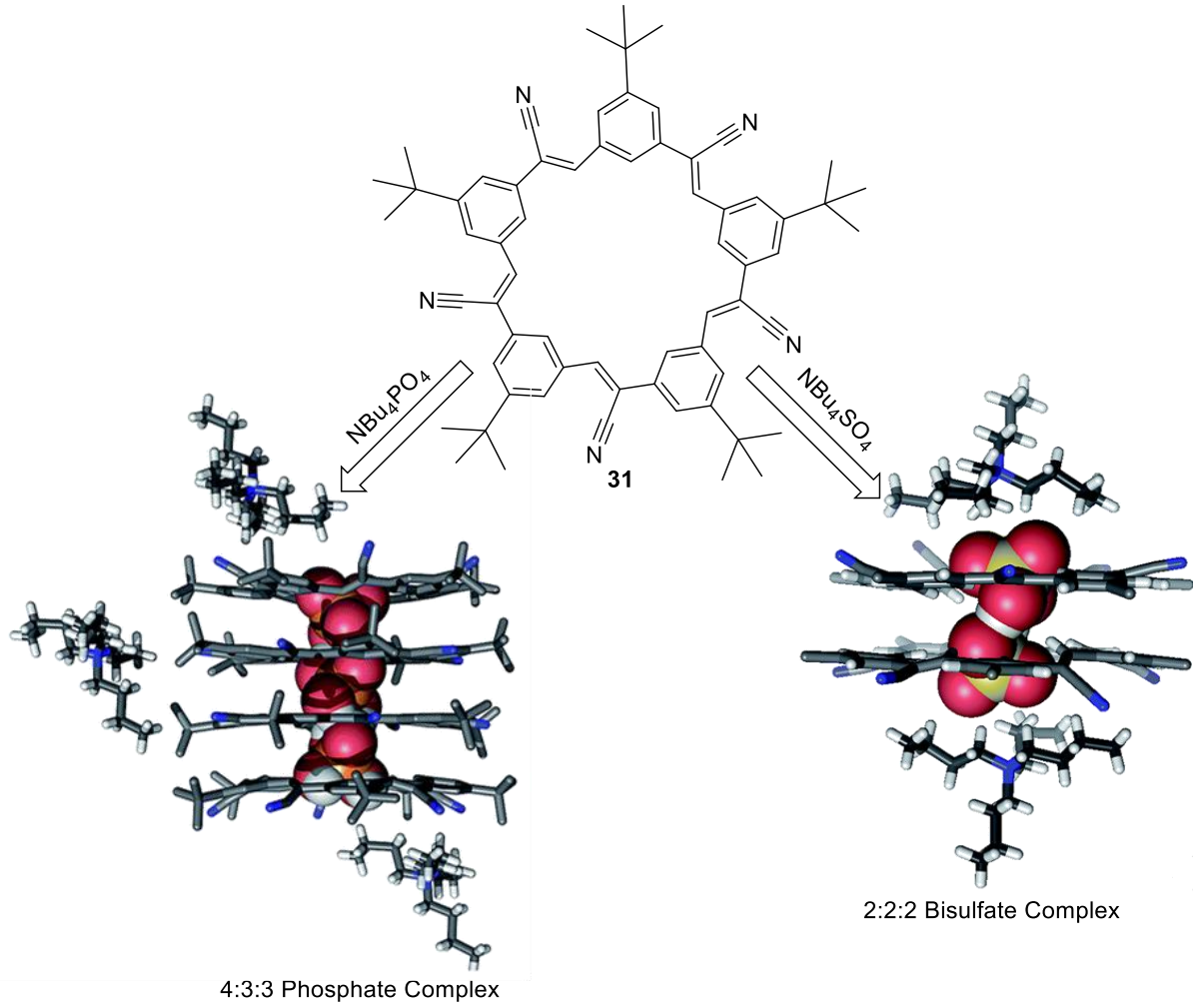

Figure 1.6 Structure of the cyanostar cyclophane before and after complexation with phosphate and bisulfate. The figures show the stack of tetrameric cyanostars with a trianionic triphosphate (left) and the stack of dimeric cyanostars with bisulfate anions (right) (adapted from ref. 42 and 43 with permission, copyright © 2016/2017 John Wiley and Sons).

Another neutral electron-deficient cyclophane was reported by Miljanić and co-workers.[27] The synthesized *m*-phenyleneethynylene macrocycle (**32**) co-crystallized with di-, tri-, tetra-, and hexafluorobenzene, with minimal structural deformations. The solid state structures of the four resulting complexes indicated the flouroarenes encapsulated into the central cavity of the host macrocycle in 1:1 ratio (Figure 1.7). It is also showed the

dimerization of two macrocycles where their large hydrophobic groups are rotated by 60° relative to one another in order to reduce the steric hindrance.

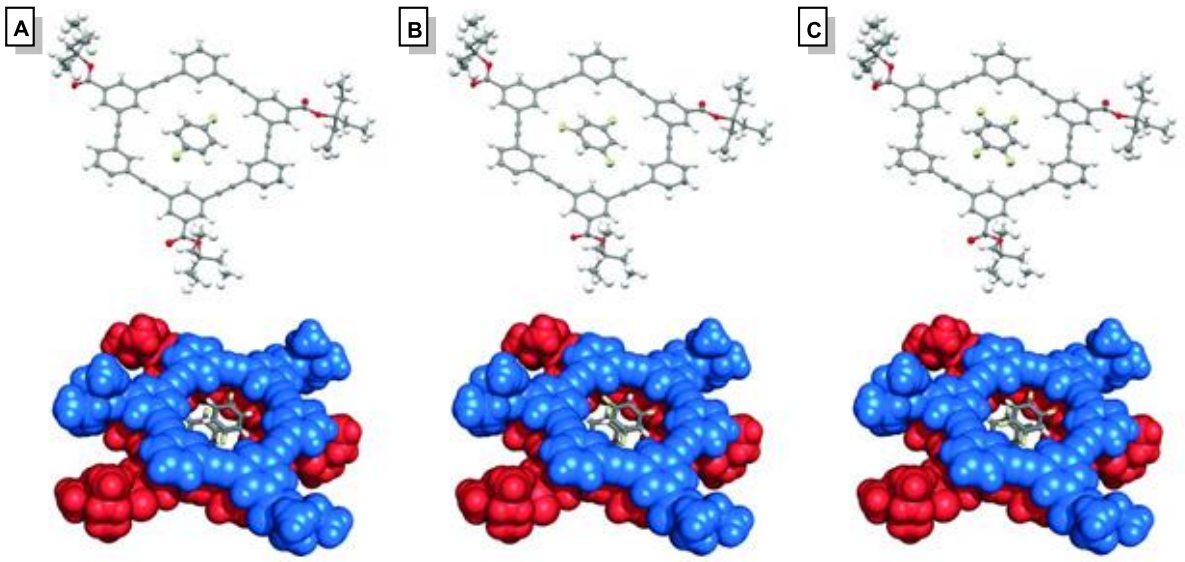

Figure 1.7 Crystal structures of *m*-phenyleneethynylene macrocycles-flouroarenes complexes (adapted from ref. 27 with permission, copyright © 2015 John Wiley and Sons).

The research in design and synthesis of neutral electron-rich cyclophanes in order to use them as hosts to accommodate electron-poor guests in their cavities has not progressed comparing with the neutral electron-poor cyclophanes. Two neutral electron-rich cyclophanes **33** and **34** were designed and synthesized by Rajakumar and Srisailas (Chart 1.5).[81] These cyclophanes possess large cavities which make their complexation with electron-poor molecules possible. The presence of the double bonds in these cyclophanes facilitates the charge-transfer interactions between the cyclophane host and the electron-poor guest. The complexation of these cyclophanes with tetracyanoethylene (TCNE) was monitored by the UV-visible spectra which showed two absorbance maxima at 416 nm and 398 nm and the calculated association constant was ranged between 59 and 62 M^{-1}.

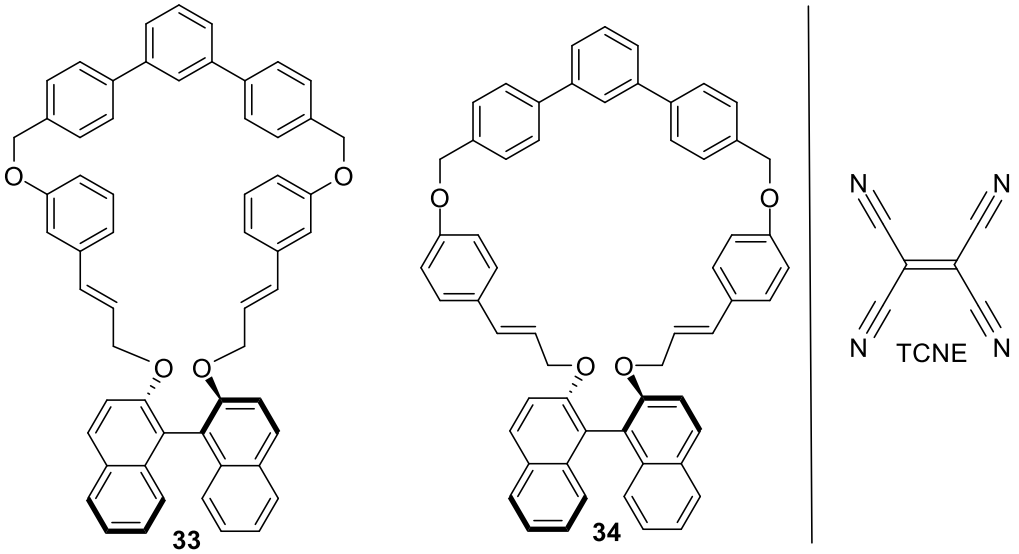

Chart 1.5 The structures of the electron-rich cyclophanes designed by Rajakumar and Srisailas (left) and the structure of the guest included in their cavities (right).

1.2.2.2 Cyclophanes in Coordination Chemistry

Cyclophanes have flexibility in designing their structures, thus they can be readily inlaid by one or more hetero atoms that can coordinate with metal ions and form mono- or poly-nuclear complexes. The complexes of cyclophanes normally follow one of these two directions: the aromatic units in cyclophanes chelate the metal through haptic covalent bonds to produce sandwich or half-sandwich compounds, or the hetero atoms in multidentate cyclophanes coordinate with metals to form coordination complexes.

Following the first direction (Chart 1.5), Cram and Wilkinson were the first to discover the reaction of [2.2]paracyclophane with hexacarbonylchromium, but their synthesis strategy led only to a mono-tricarbonylchromium complex **35a**.[82] After that Misumi and co-workers synthesized mono- and bis-tricarbonylchromium complexes of one or more layers of [2.2lparacyclophanes **36a**.[83] In the same time, Zenneck and co-workers obtained (η^{12}-[2.2]paracyclophane)chromium(0) **37** when they wanted to prepare chromium-[2.2]paracyclophane complex.[84] Then, Boekelheide and co-workers explored the π-electron

delocalized cyclophane-transition metal complexes. They inserted different transition metals: ruthenium(II), iron(I), cobalt(I), iridium (II), in the complexation process to obtain mono- and bis-(capped) R-[2.2]paracyclophane-M complexes **35b**–**e** and **36b**–**e** using different synthetic strategies.[85–87]

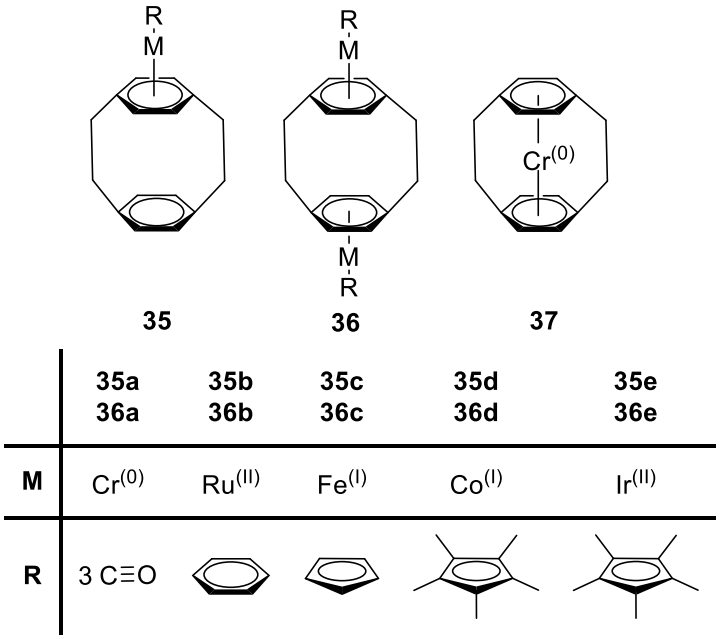

Chart 1.6 Sandwich and half-sandwich structures of [2.2]paracyclophane complexes with a variety of transition metals.

Williams and co-workers followed the second direction to fabricate two cyclophane ligands and coordinate them with transition metals. They modified the parent tetracationic cyclobis(paraquat-*p*-phenylene) (**12**) by changing one or two *p*-xylene bridges to 2,2'-bipyridine spacers to make them suitable ligands to bind a variety of transition metals.[88] These two ligands perfectly coordinated with ruthenium(II) (**38a** and **39a**), rhenium(I) **(38b** and **39b)**, silver(I) **40a**, and copper(I) **40b** which lead to a series of mono- and binuclear complexes (**Chart 1.7**).

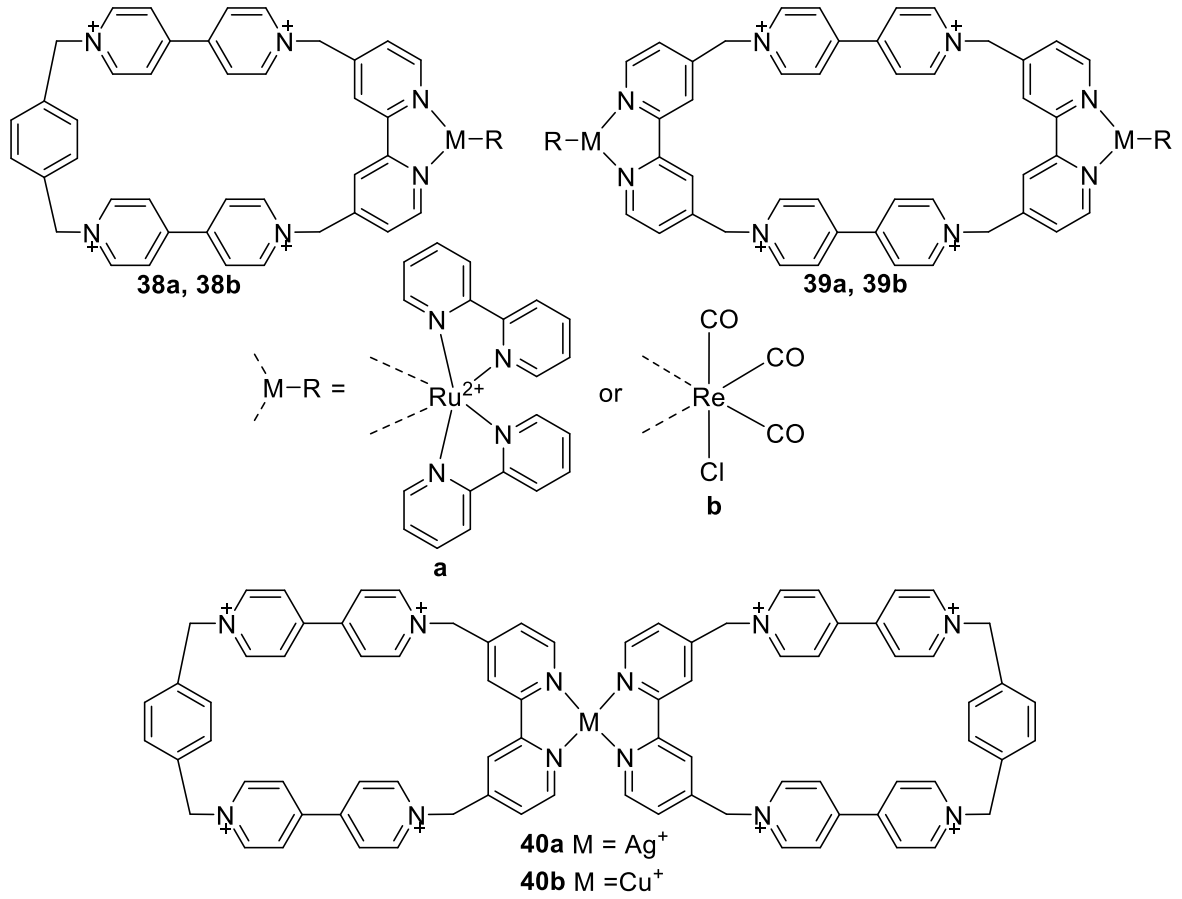

Chart 1.7 The structures of cyclophane-transition metal complexes synthesized by the Williams group.

Inoue and co-workers designed a cyclophane containing three types of donor groups: amino, amide, and pendant carboxymethyl groups, arranged in the ring system which offered many binding sites to coordinate with transition metals (Chart 1.8, top).[89,90] This multidentate cyclophane formed strong coordination bonds with zinc(II) and copper(II) ions in different ways which produced binuclear complexes **41** and **42**. The zinc(II) chelate complex **41** has an octahedral structure where each Zn atom is coordinated to two carboxylate oxygen atoms, two amine nitrogen atoms, and two amide oxygen atoms, whereas the copper(II) chelate complex **42** has a square-planar geometry with each copper atom bonded to two deprotonated amide nitrogen atoms and two amino nitrogen atoms. Another multi-dentate cyclophane ligand **43** with a large internal cavity was synthesized by Karasik and co-workers (Chart 1.8,

bottom).[91] The produced ligand is a 46-membered ring containing P, N, and O donor atoms. When this multidentate cyclophane reacted with platinum(II), palladium(II), or tungsten(0) salts, binuclear bis-P,P-chelate complexes were formed. In these complexes, the metal atoms chelate with the two phosphorous atoms, which were located in the diphosphacyclooctane moieties, and also connected with X groups (X = Cl or CO), which were directed outside of the macrocyclic cavity.

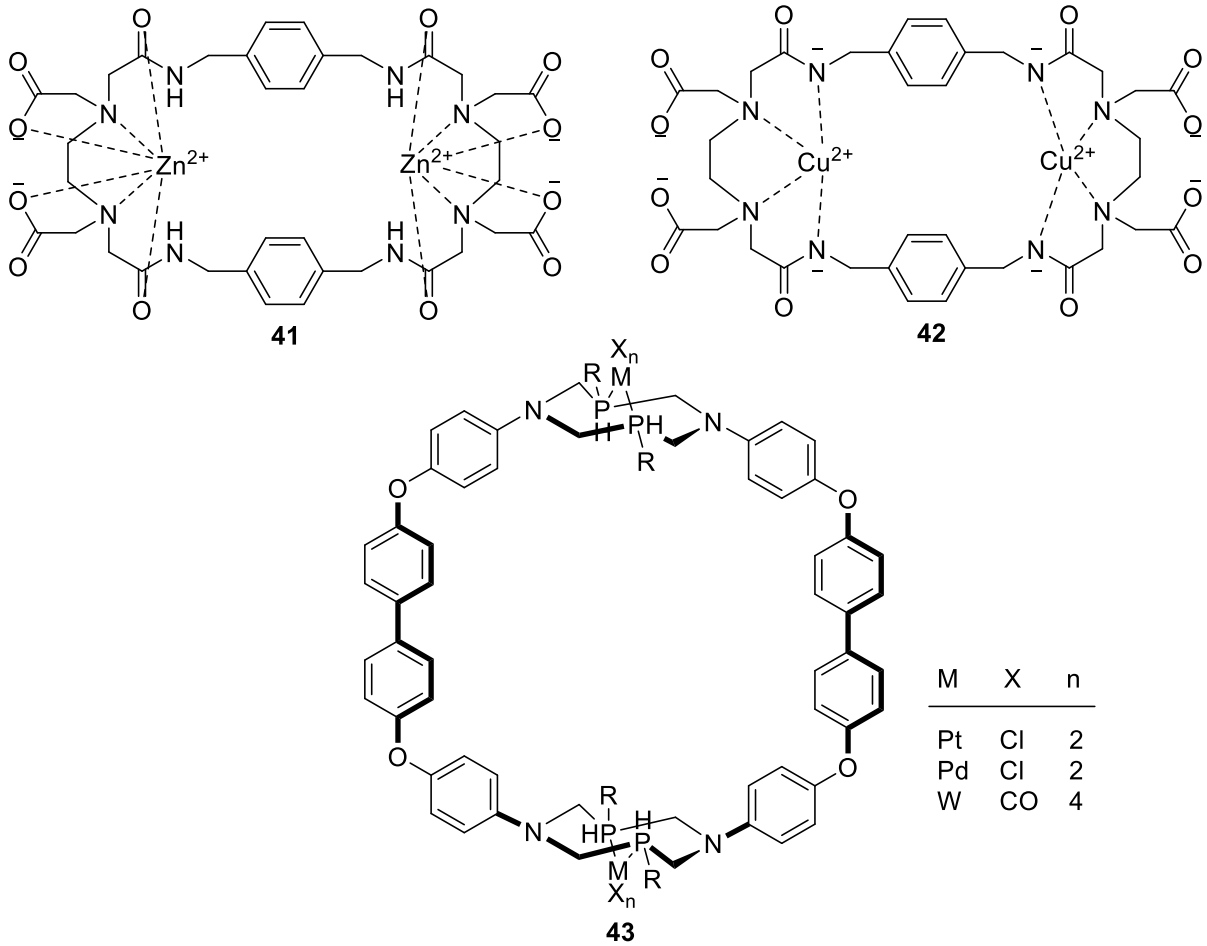

Chart 1.8 The structures of multi dentate cyclophane-transition metal complexes synthesized by the Inoue group (top) and by the Karasik group (bottom).

1.2.2.3 Cyclophanes in Polymer Science

Among the known cyclophanes, [*m*,*n*]metacyclophanes and [*m*,*n*]paracyclophanes have a special characteristics that make them versatile precursors for polymeric systems, in

that they either lose or maintain their layered structures. These two cyclophanes possess co-facial π-electron systems in their skeleton which facilitate the transannular [π···π] interaction. In this section, some of these synthesized polymers which contain [*m*,*n*]metacyclophanes or [*m*,*n*]paracyclophanes in the main chains or in the side chains as pendant groups in the polymer skeleton will be discussed, as well as the polymers that contain layers of cyclophanes and porous polymers.[92–95]

In 1966, Gorham developed a process to quantitatively cleave the bridged carbon–carbon bonds in [2.2]paracyclophane **11**, by vacuum pyrolysis to produce biradical **44**.[96] This step was followed by the reaction of the produced highly reactive biradical molecules with each other to form a linear poly(*p*-xylene) **45** films (Scheme 1.4) in quantitative yield, thus leading to use the resulting polymer for solvent-resistant coating purposes. The cyclic structure of [2.2]paracyclophane was collapsed in this reaction. The same strategy was recently applied in the derivatives of [2.2]paracyclophane which contain chemical functionalities suitable for immobilizing proteins, drugs, or anticoagulant agents, such as acetylenic [2.2]paracyclophanes, to create biologically active surfaces for diagnostics, biosensors, or biomedical device coatings.[97]

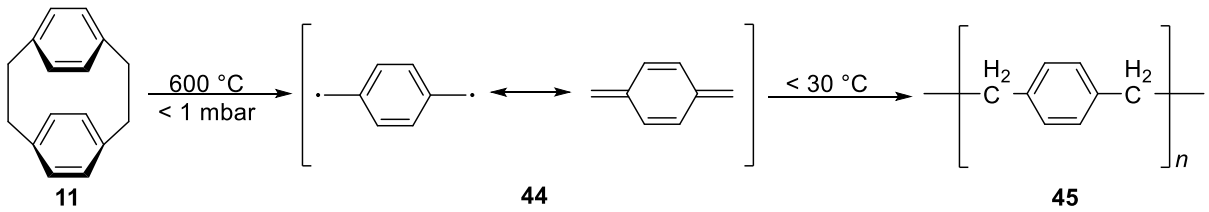

Scheme 1.4 The Gorham process for the preparation of a linear poly(*p*-xylene).

In contrast to the Gorham route in which the cyclophane monomer lost its cyclic structure during the polymerization process, it is conserved in many other methods to polymerize cyclophanes. Mizogami and Yoshimura obtained conjugated polymers, which contained cyclophane units in the main chain, by the oxidative coupling of 8,16-

dihydroxy[2.2]metacyclophane **46** (Scheme 1.5).[98] The produced polymer was composed of repeating diphenoquinone units **47**. Another study was conducted on the same cyclophane using a different strategy, where the 8,16-dihydroxy[2.2]metacyclophane **46** oxidized at first forming a dimer **48** followed by the polycondensation reaction of oxidative dimer to yield substituted poly[2.2]metacyclophane **49** (Scheme 1.5).[99]

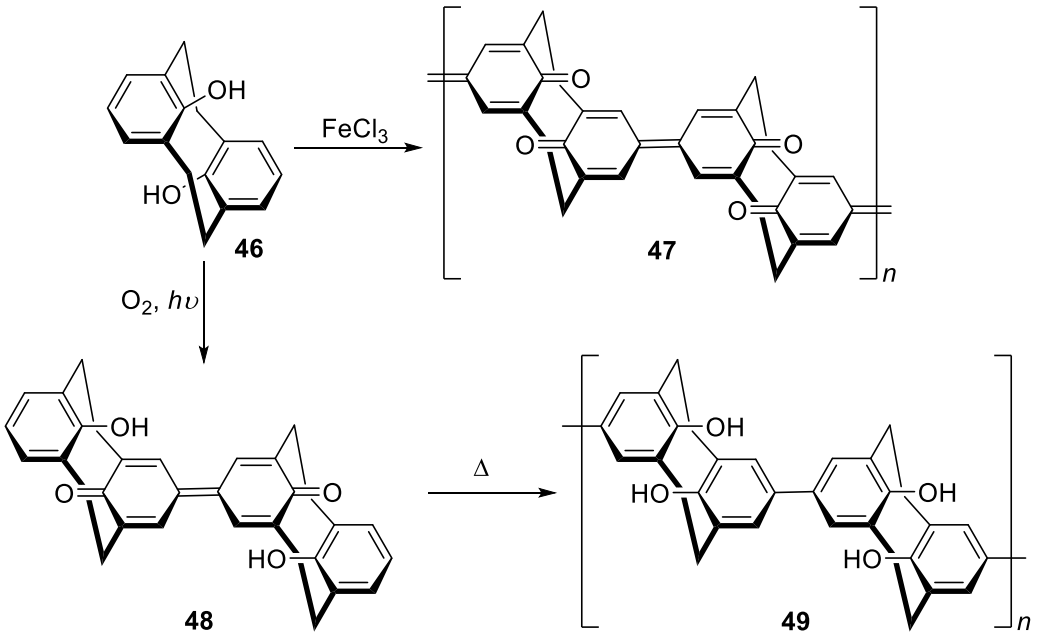

Scheme 1.5 Polymeriztion of dihydroxy[2.2]metacyclophane by oxidative coupling and polycondensation reactions.

Poly(*p*-arylene-vinylene)s (PAVs) and poly(*p*-aryleneethynylene)s (PAEs), containing a frequent [2.2]paracyclophane units in the main chain of the polymer were prepared through palladium-catalyzed cross-coupling reactions. Morisaki and Chujo applied Sonogashira–Hagihara coupling on pseudo-paradibromo[2.2]paracyclophane **50** and 2,5-didodecyloxy-1,4-diethynylbenzene **51** to synthesize poly(*p*-phenyleneethynylene) **52**, as shown in Scheme 1.6A.[100] The existence of alkyl side chains in the obtained polymer increased its solubility in common organic solvents which allowed the preparation of thin films of this polymer by casting and spin-coating from its toluene solution. The number-average molecular weight of this polymer was increased from 8000 to 14500 g mol^{-1} by treating pseudo-*p*-

diethynyl[2.2]paracyclophane **53** with 2,5-didodecyloxy-1,4-diiodobenzene **54** via Sonogashira–Hagihara coupling (Scheme 1.6A). Another π-conjugated polymer **56** containing [2.2]paracyclophane was synthesized using Mizoroki–Heck coupling of pseudo-*p*-divinyl[2.2]paracyclophane **54** with 2,5-didodecyloxy-1,4-diiodobenzene **54**, as shown in Scheme 1.6B.[101] The afforded poly(*p*-phenylenevinylene)is promising in photonic and electronic applications due to the longitudinal [π···π] interaction of the paracyclophane moiety.

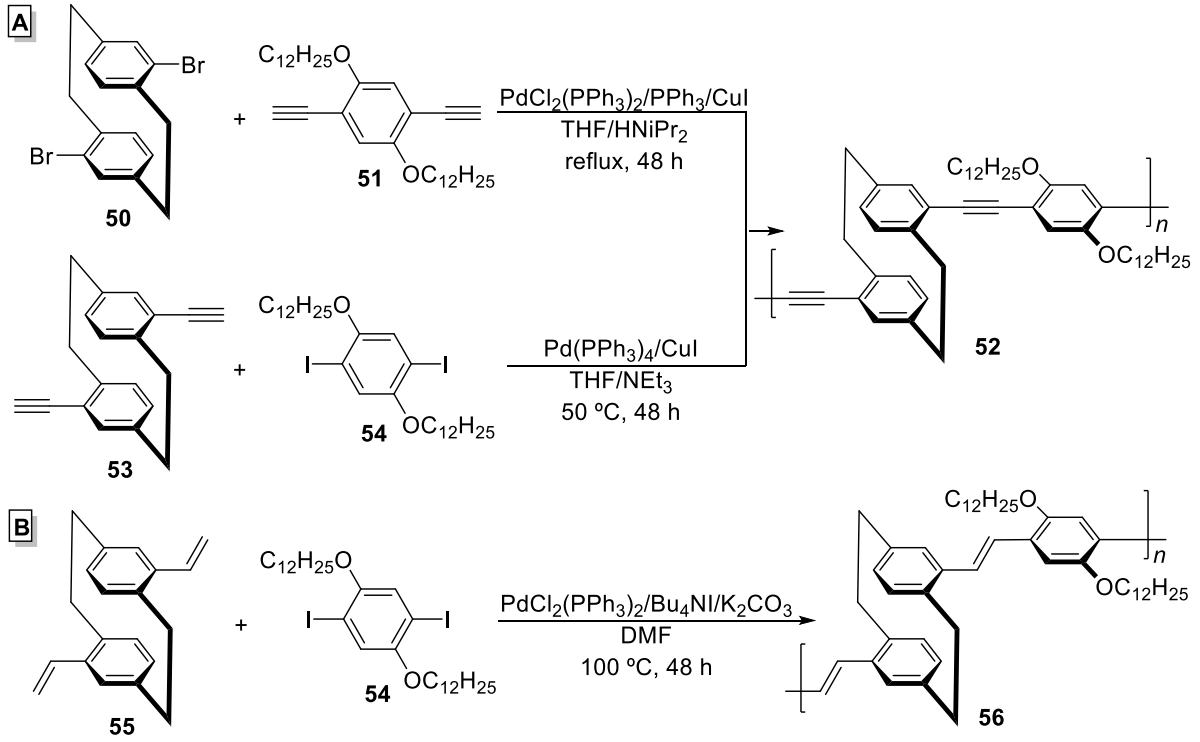

Scheme 1.6 *(A)* Synthesis of PAE-type polymer using pseudo-*p*-dibromo[2.2]paracyclophane or pseudo-*p*-diethynyl[2.2]paracyclophane. *(B)* Synthesis of a PAV-type polymer using pseudo-*p*-divinyl[2.2]paracyclophane.

The concept of π-conjugated polymers containing [2.2]paracyclophane was extended to include the multilayered conjugated polymer and the conjugated microporous polymers. The multilayered conjugated polymer, possessing [2.2]paracyclophane units in each layer which contains benzene rings aligned face-to-face, was synthesized by Jagtap and Collard (Scheme 1.7).[102] The Sonogashira–Hagihara coupling was employed on pseudo-geminal-

diethynyl[2.2]paracyclophane **57** to afford poly(aryleneethynylene) **59** conjugated polymer with the number-average molecular weight of 5000 g mol^{-1}. The anatomy of the afforded polymer consisted of the 1,4-bis(phenylethynyl)-2,5-dialkoxybenzene chromophores bridged by the pseudo-geminal disubstituted [2.2]paracyclophane units. The π-stacked fashion was seen over the entire length of the polymer and in an extended multitier arrangement which affected the optical properties of such a layered polymer.

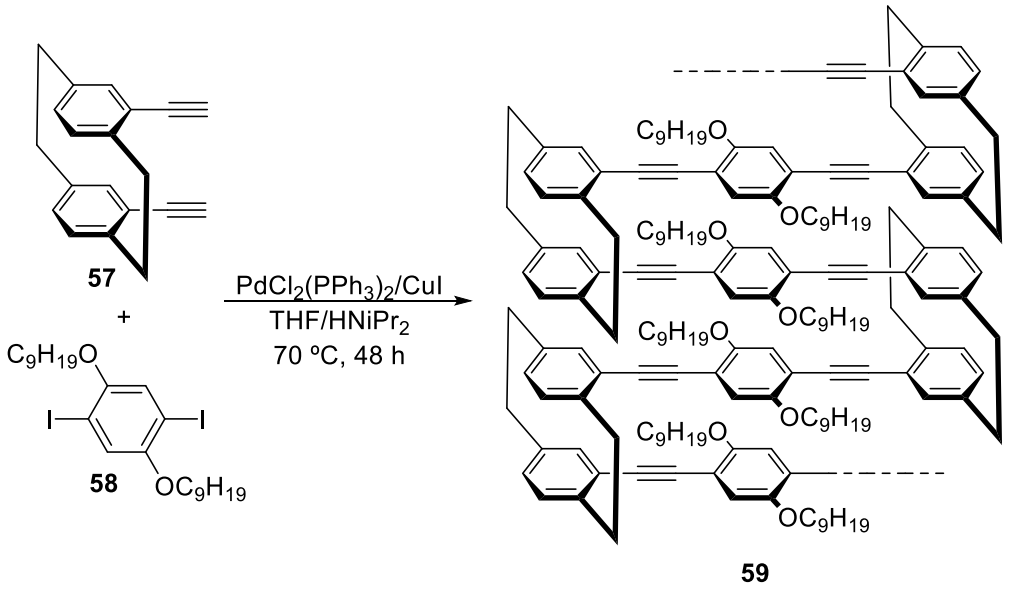

Scheme 1.7 Synthesis of a multilayered conjugated polymer possessing [2.2]paracyclophane units in each layer.

The conjugated microporous polymers **60**–**62** were synthesized by Hay, Sonogashira–Hagihara, or Yamamoto couplings of tetraethynyl[2.2]paracyclophane monomers and their derivatives (Chart 1.9).[103,104] The resulting polymers showed type I nitrogen gas adsorption profile, highlighting the existence of slit-like mesopores within the conjugated microporous polymers. The diameters of micropores were less than 2 nm. The calculated Brunauer–Emmett–Teller surface areas for the prepared polymers reached 1000 $m^{2}{\cdot}g^{-1}$, and the diameters of their particles were approximately 0.2 μm with relatively uniform morphology; as a result, they were readily dispersed in common organic solvents.

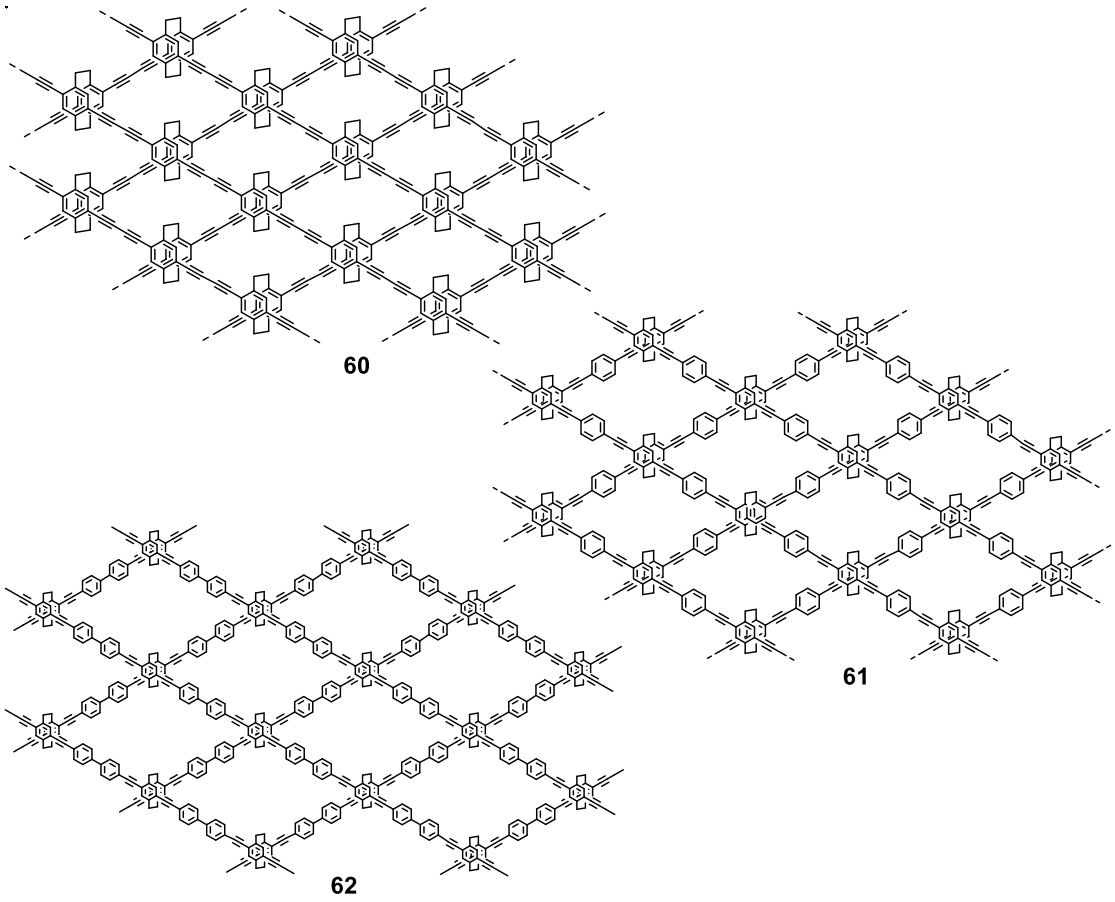

Chart 1.9 The conjugated microporous polymers synthesized through coupling reactions of tetraethynyl[2.2]paracyclophane monomers and their derivatives.

Finally, pendant [2.2]paracyclophane units were successfully appended to the side chain of polymers by Okuno and co-workers, as shown in Scheme 1.8.[105] 4-Vinyl[2.2]paracyclophane **63** was polymerized by radical, cationic, or anionic polymerization in the presence of azobisisobutyronitrile (AIBN) to obtain the target polymer **64** with the number-average molecular weight of 5400 g mol^{-1}. The distortion of a vinyl group and aromatic ring in [2.2]paracyclophane within the produced polymer reduced the conjugation compared to polystyrene. The reactivity of the produced polymer was also decreased, if compared to the reactivity of polystyrene, due to the strong electron-donating tendency of the vinyl group arising from the through-bond and through-space interaction with another aromatic ring.

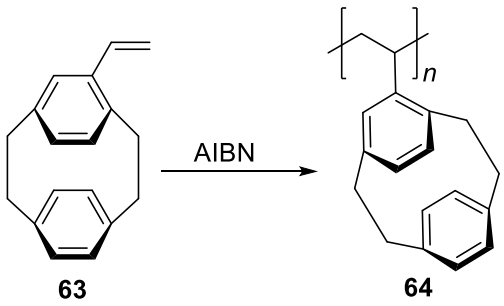

Scheme 1.8 Homopolymerization of 4-vinyl[2.2]paracyclophane.

1.2.2.4 Cyclophanes as Luminescent Materials and Sensors

Cyclophanes have a good reputation in the field of technological innovations due to the flexibility in modulating their structures to tune the desired electronic and photophysical properties. Several synthesized cyclophanes were used as sensors to detect the hazardous materials from the environment. Cyclophane **65**, in the solid phase, featured selective fluorescence recognition to detect volatile organic compounds (VOCs), particularly methanol vapors which are hazardous to the nervous system and can cause blindness and death upon prolonged exposure (Figure 1.8A).[106] Other cyclophanes **66** and **67**, which were electron-rich and highly fluorescent, could be used to detect electron-deficient nitroaromatic explosives such as picric acid (PA)[107] and 2,6-dinitrotoluene (DNT) (Figure 1.8B,C).[108]

Cyclophanes can also be used in live cell imaging as fluorescent probes for medical diagnostics and biological studies. A rigid, box-like hybrid cyclophane **68**, which was synthesized by Stoddart and co-workers, is one of the most recent synthesized cyclophanes to utilize in this field (Figure 1.9).[35] This asymmetric cyclophane is photostable in aqueous media and maintains fluorescence features when exposed to strongly acidic conditions. Also, it is bright, non-cytotoxic, and can be delivered easily into the living cells in an efficient manner. Testing this cyclophane on the lysosomes of living cells demonstrates that it allows the cells to glow brightly under irradiation with blue laser light.

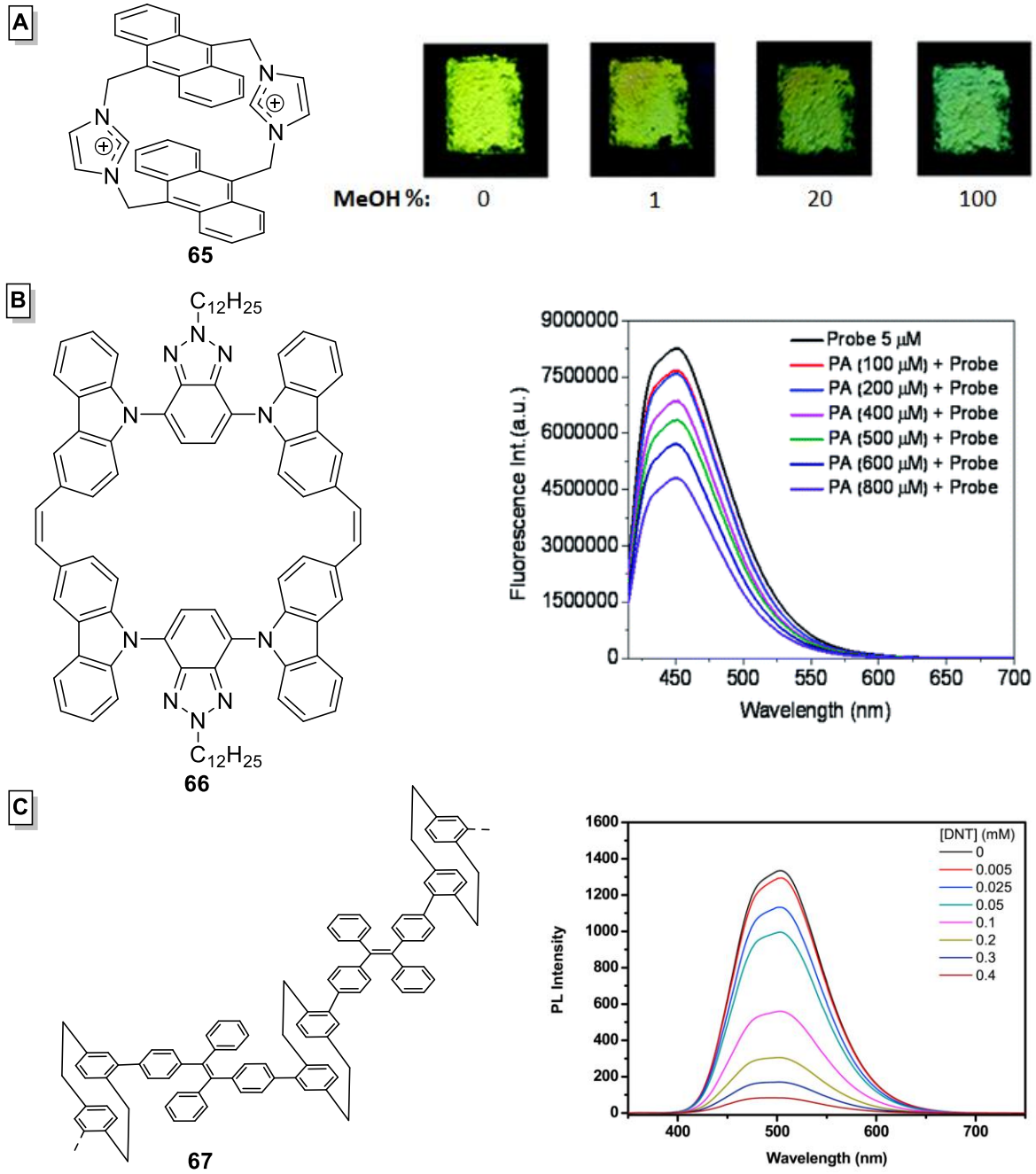

Figure 1.8 *(A)* Structure of cyclophane which detects vapor MeOH and the solid film used to show the fluorescence changes when exposed to different percentage of MeOH. *(B)* Structure of cyclophane which detects picric acid (PA) and its fluorescence emission spectra in cyclohexane at different concentration of PA (adapted from ref. 106 and 107 with permission, copyright © 2013 and 2014 The Royal Society of Chemistry, respectively). *(C)* Structure of copolymer which has cyclophane moieties and its emission spectra in a 10:90 of THF/water mixtures with addition of different amounts of 2,6-dinitrotoluene (DNT) (adapted from ref. 108 with permission, copyright © 2018 Elsevier Ltd.).

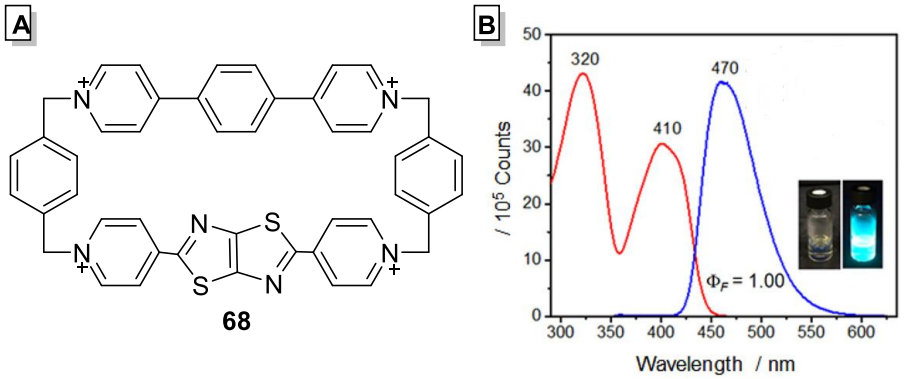

Figure 1.9 *(A)* Structure of cyclophane **68** and *(B)* its absorption (red) and emission (blue) spectra in H_2O, inset: fluorescence in H_2O under daylight and under 365 nm UV light (adapted from ref. 35 with permission, copyright © 2018 American Chemical Society).

An optically active cyclophane consisting of [2.2]paracyclophane bridged by two pyridylcyclobutyl units **69** was synthesized by MacGillivray and co-workers (Figure 1.10a).[109] The bridge-substituted [2.2]paracyclophane exhibited a strong red shift in fluorescence ($\lambda_{max(em)}$ = 414 nm) comparing to unsubstituted [2.2]paracyclophane ($\lambda_{max(em)}$ = 356 nm) as shown in Figure 1.10B. A further bathochromic shift was displayed when pyridyl moieties were functionalized by alkyl groups ($\lambda_{max(em)}$ = 493 nm) due to the polarization of the pyridinium rings. This cyclophane is a promising building block to develop the applications of optical devices.

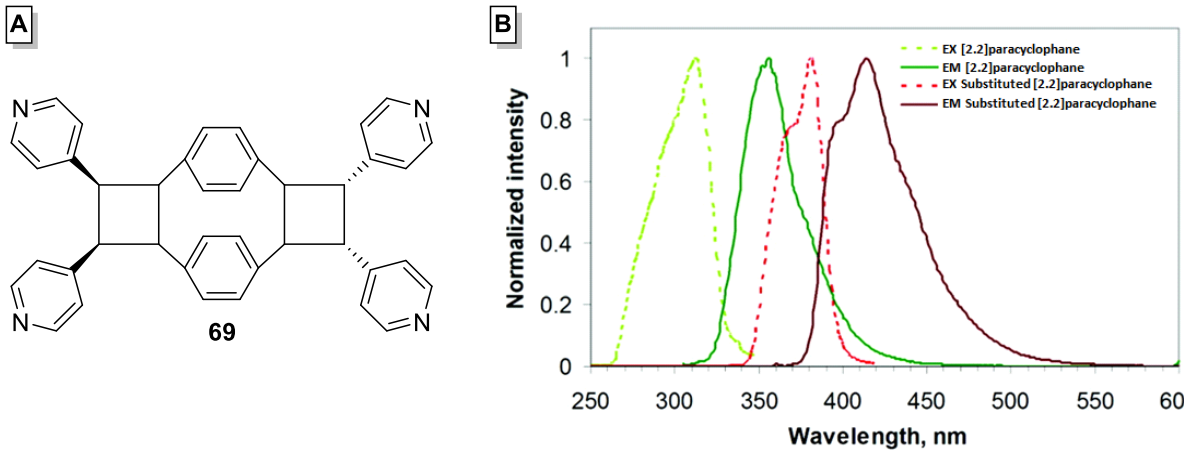

Figure 1.10 *(A)* Structure of cyclophane **69** synthesized by the MacGillivray group and *(B)* its excitation and emission spectra compared with the spectra of [2.2]paracyclophane in DMF (adapted from ref. 109 with permission, copyright © 2009 American Chemical Society).

The optically active [2.2]paracyclophane derivatives have mainly been used as chiral auxiliaries because the rotation of phenylenes is inhibited providing a conformationally stable chiral environment that makes them an ideal scaffold to synthesize circularly polarized luminescence materials. Chujo and co-workers synthesized two highly emissive enantiomers of the planar chiral [2.2]paracyclophane **70** and **71**.[110,111] These enantiomers exhibited outstanding chiroptical properties: the fluorescence quantum efficiency of 0.45 for **70** and 0.8 for 71, and the circularly polarized luminescence dissymmetry factor of 1.1×10^{-2} and 1.7×10^{-3} for Bowtie- and X-shaped optically active macrocyclic enantiomers, respectively (Chart 1.10).

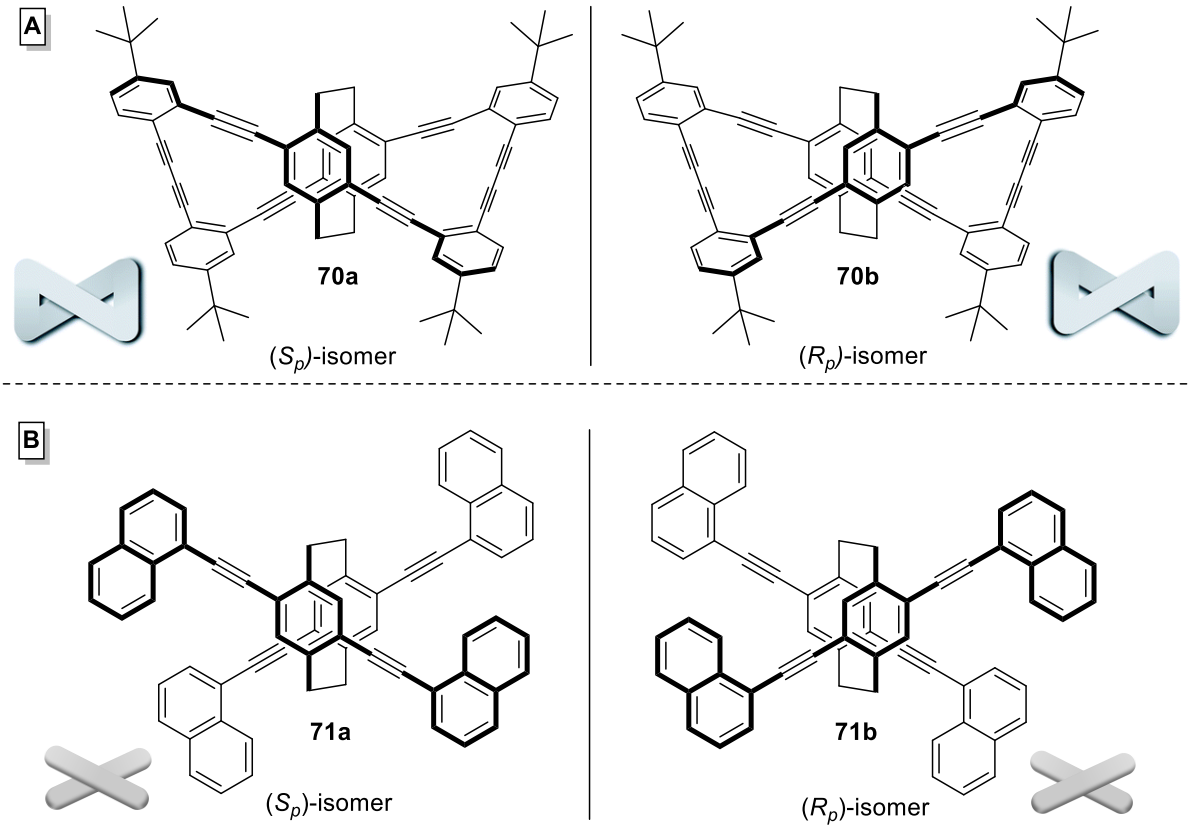

Chart 1.10 *(A)* Bowtie-shaped and *(B)* X-shaped optically active paracyclophane derivatives.

1.2.2.5 Cyclophanes as Building Blocks for Supramolecular Frameworks

Cyclophanes can be incorporated into different porous organic crystalline materials. When the framework of these materials constructed purely from organic molecules which stabilized via multiple intermolecular hydrogen-bonding interactions and other non-covalent interactions such as [π···π] stacking, it is called a hydrogen-bonded organic framework (HOF).[112] When it is composed of metal clusters 'nodes' coordinated to organic molecules 'linkers', it is called a metal-organic framework (MOF).[113]

Shimizu and co-workers constructed a large, highly symmetric cyclophane which contains bis-urea groups (compound **72** in Figure 1.11A).[114,115] The X-ray diffraction data showed that this cyclophane is assembled into columnar nanotubes held together primarily by strong hydrogen bonds leaving a sizable, robust cavity in the center. The created cavity can reversibly bind and exchange guest AcOH molecules (Figure 1.11A) and the self-assembled molecule exhibited a good thermal stability up to 180 °C with and without AcOH guest.

A series of C_3-symmetric π-conjugated planar cyclophanes **73**–**75** was built by Miyata and co-workers (Figure 1.11B), each cyclophane consisting of three 4,4′-dicarboxy-*o*-terphenyl moieties attached together by either ethynylene group(s) or phenyleneethynylene group(s) to form the cyclic structure.[116,117] The X-ray diffraction data of these cyclophanes confirmed the presence of appropriate robust hydrogen-bonded hexagonal unpenetrated networks which assembled in layers with dual or triple pores and accessible volumes up to 59%. The activated porous frameworks of the macrocycle that contains one ethynylene spacer between 4,4′-dicarboxy-*o*-terphenyl moieties presented high crystallinity, heat resistance up to 360 °C, and permanent porosity: SA_{BET} = 557 $m^2 \cdot g^{-1}$ based on CO_2 sorption at 195 K.

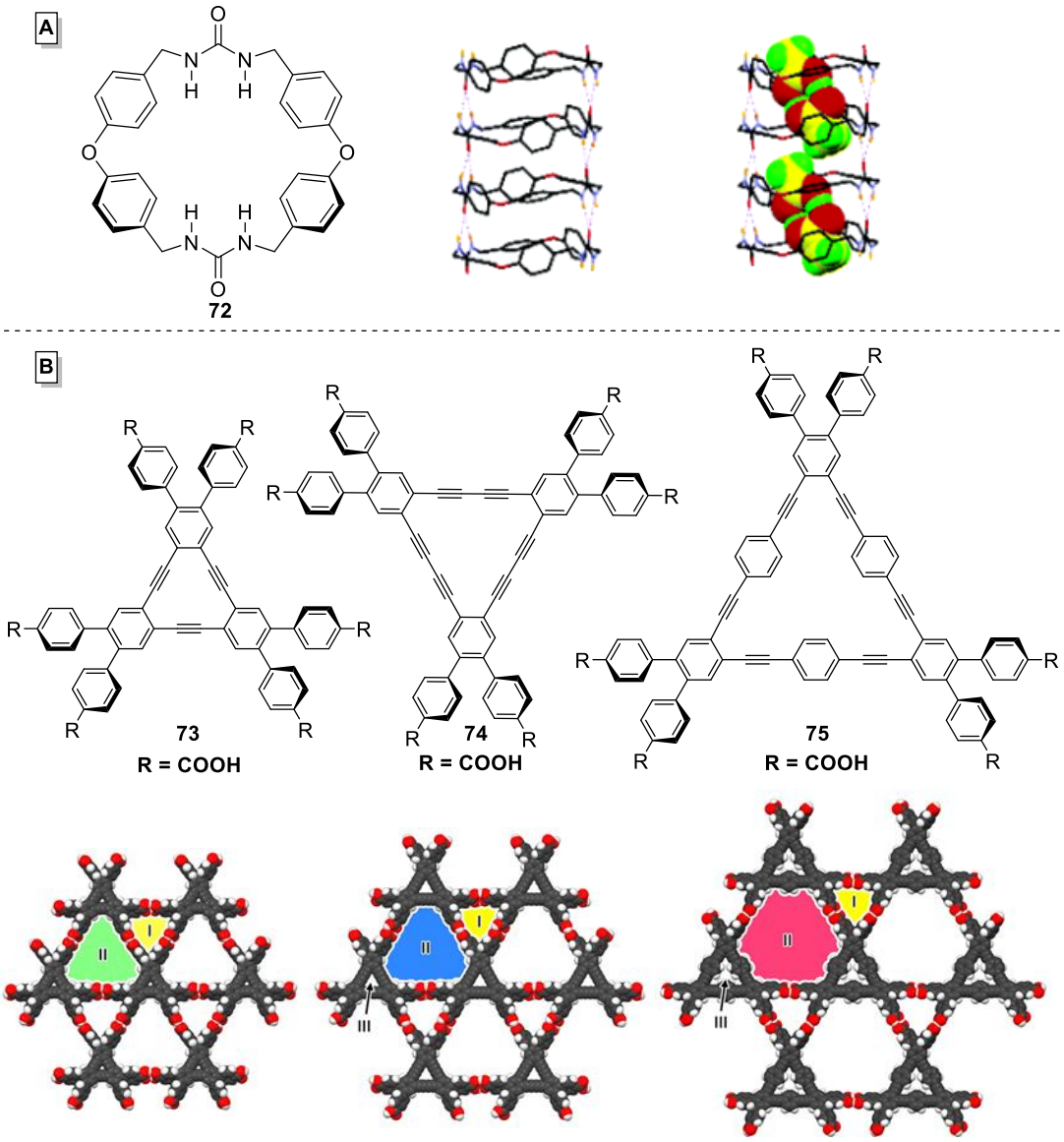

Figure 1.11 *(A)* The Shimizu's macrocycle and its columnar assembly with and without AcOH. Hydrogen atoms have been omitted for clarity (adapted from ref. 115 with permission, copyright © 2006 American Chemical Society). *(B)* Miyata's macrocycles and its X-ray packing diagrams which emphasize their porosity (adapted from ref. 116 with permission, copyright © 2016 American Chemical Society).

A shape-persistent phenyleneethynylene macrocycle **76** functionalized with three carboxylic acid groups was synthesized by Miljanić and co-workers. This macrocycle was utilized as a linker to coordinate with zinc or zirconium clusters in order to form metal–macrocycle frameworks.[118,119] The prepared macrocycle coordinated to zinc clusters contains a predesigned aperture for the 1D channels with a ~9 Å wide. In this framework, three

trinuclear zinc clusters coordinated with the carboxylic groups in the macrocycles and bridged each pair of macrocyclic molecules (Figure 1.12, left) in addition to the [π···π] stacking which was observed between the pair of macrocycles. The packing diagram of the resulting complex presented a mesoporous framework with infinite 3D channels along the crystallographic *c*-axis and a void volume of 86%. The same linker coordinated with hexanuclear clusters of zirconium forming a metal-macrocycle framework which held together through multiple weak interactions such as hydrogen bonding, [π···π] stacking, and C–H···π interactions, in addition to metal–ligand coordination (Figure 1.12, right). Utilization of the rigid macrocycle as a linker guaranteed the minimum pore size of the resultant framework forming 1D channels along the crystallographic *c*-axis. This linker was the only source of the porosity in the resultant metal-macrocycle framework.

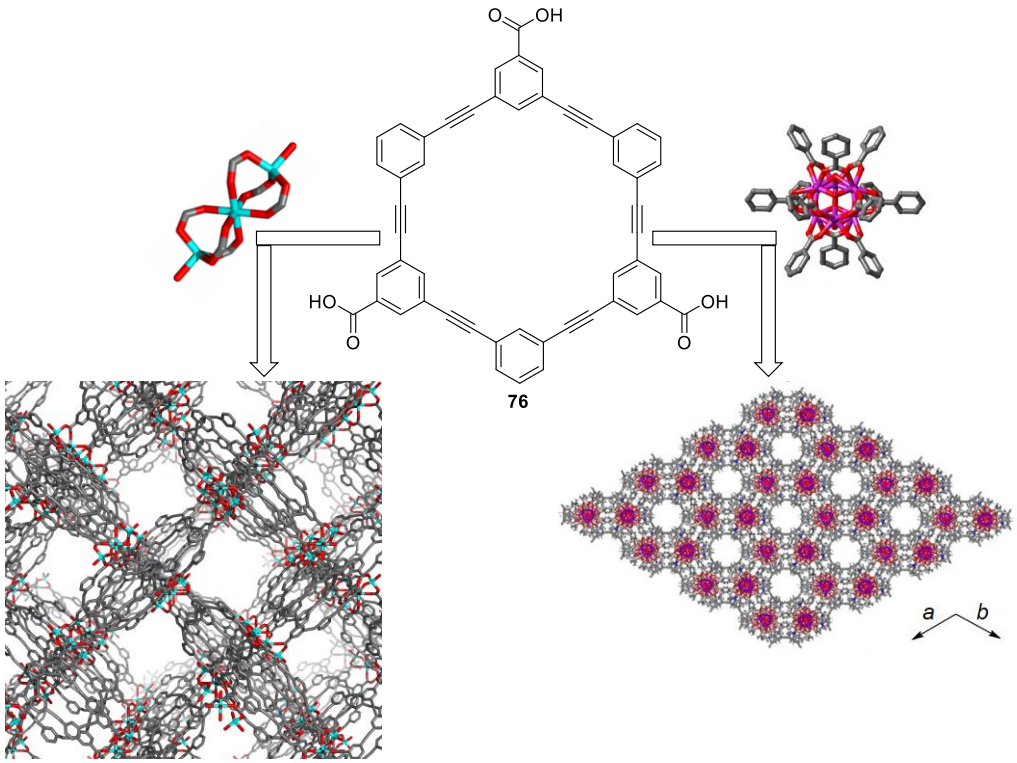

Figure 1.12 Phenyleneethynylene macrocycle **76** and its crystal packing of metal-macrocycle frameworks based on zinc cluster (left, adapted from ref. 118 with permission, copyright © 2015 The Royal Society of Chemistry) and pre-prepared zirconium cluster (right, adapted from ref. 119 with permission, copyright © 2017 John Wiley and Sons). Hydrogen atoms have been omitted for clarity. Element colors: C—gray, H—white, O—red Zn—cyan, Zr—purple.

1.3 Benzoin Condensation*

Benzoin condensation involves the formation of a carbon-carbon bond between two aldehydes, in which one aldehyde adds over the C=O bond of another, forming an anion as intermediate and ultimately an α-hydroxyketone (illustrated on the conversion of benzaldehyde **77** into parent benzoin **78**, Scheme 1.9). In fact, this addition reaction is not a condensation because no small molecule is eliminated, but the historical nomenclature persists.[120,121]

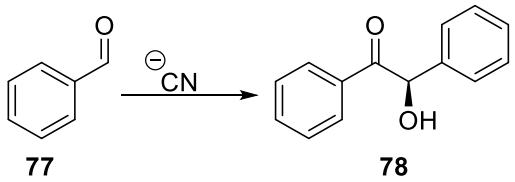

77 **78**

Scheme 1.9 Cyanide-catalyzed benzoin condensation.

The ability of nucleophiles to catalyze acylation reactions was first discovered by Wöhler and Liebig in 1832, which lead them later to discover the benzoin condensation reaction.[122,123] Shortly thereafter, Liebig's student Nikolay Zinin noticed that the coupling of two aromatic aldehyde molecules, in the presence of cyanide ion from bitter almond oil as a catalyst, produced the corresponding α-hydroxyketone which lead to the establishment of the cyanide-catalyzed version of the benzoin condensation reaction that is in most common use today.[124,125]

The mechanism of the cyanide-catalyzed benzoin condensation was established by Lapworth in 1903 and is shown in Scheme 1.10.[126] The reaction commences with the addition of cyanide to aldehyde **79** to form a tetrahedral anionic intermediate **80**. Its tautomerization results in a carbanionic nucleophile **81**; this newly created acyl anion equivalent then attacks the second molecule of **79** (which acts as the electrophile), forming the key C–C bond in **82**.

* This section of the chapter was published on ref. 120.

Another tautomerization follows, setting the stage for the expulsion of cyanide catalyst from **83** and the formation of the final benzoin product **78**.[127,128]

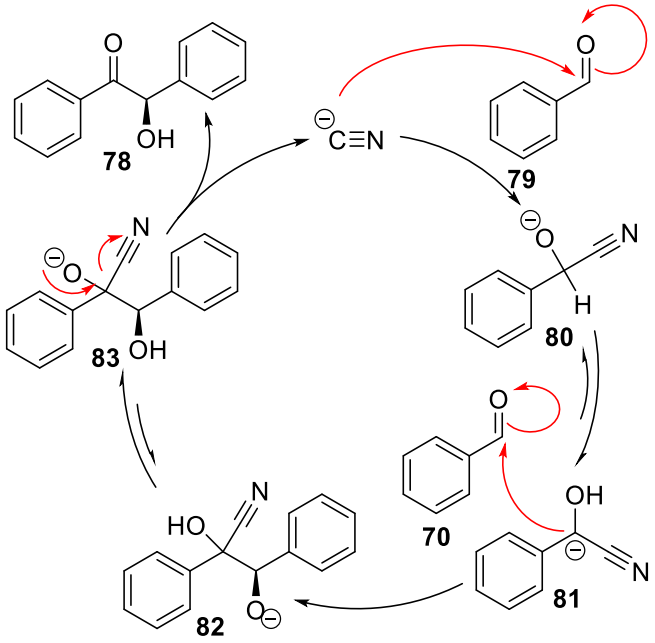

Scheme 1.10 Mechanism of cyanide-catalyzed benzoin condensation, as first proposed by Lapworth.

In cases where two different aldehyde precursors are exposed to the cyanide catalyst, the reaction typically results in a mixture of the four possible products, whose ratio is determined by their relative stabilities.[129,130] This outcome is a necessary consequence of the thermodynamic control generally observed in the benzoin condensation. In 2004, Johnson and Linghu have shown that this limitation can be circumvented by using an acyl silane as one of the coupling partners.[131] Its cyanation is followed by the [1,2]-Brook rearrangement which delivers a preferred acyl anion equivalent under the kinetic control, resulting in a single *o*-silyl protected benzoin adduct. An asymmetric version of this cross-benzoin condensation has been developed, using chiral metallophospites as catalysts.[132] Mixed aromatic benzoins can be made indirectly, by e.g. Friedel–Crafts reactions of glyoxals with aromatic hydrocarbons.[133] While benzoin condensation was initially discovered on aromatic

aldehydes, it is readily extended to their aliphatic counterparts as well; this is why sometimes it is referred as acyloin condensation.[134]

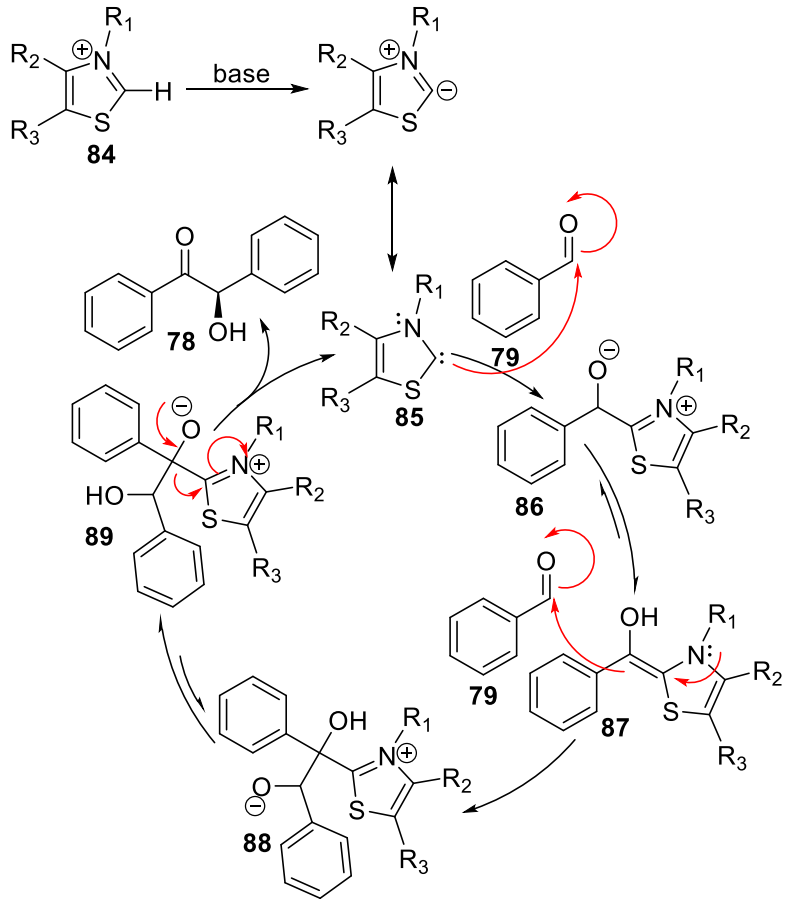

Scheme 1.11 Mechanism of carbene-catalyzed benzoin condensation, as originally proposed by Breslow.

Over a hundred years after the discovery of the cyanide-catalyzed benzoin condensation, Ugai and co-workers observed that thiazolium salts **84** (Scheme 1.11) could replace cyanide in benzoin condensation under basic conditions.[135] In 1958, Breslow suggested a mechanistic model for this reaction wherein the base deprotonates precatalyst **84** and generates carbene **85** that is the catalytically active species.[136] The initial inability to isolate the purported highly reactive carbenes made this mechanism tentative, but doubts were dispelled by the mounting evidence for carbene intermediates—including the first isolation of a free carbene by the deprotonation of a bis-adamantyl imidazolium chloride by

Arduengo and co-workers in 1991 (**90**, Chart 1.11).[137] After the isolation of this carbene, several stable *N*-heterocyclic carbenes (NHC) were discovered and used as catalysts for benzoin condensation (structures **91**–**97** in Chart 1.11).[138]

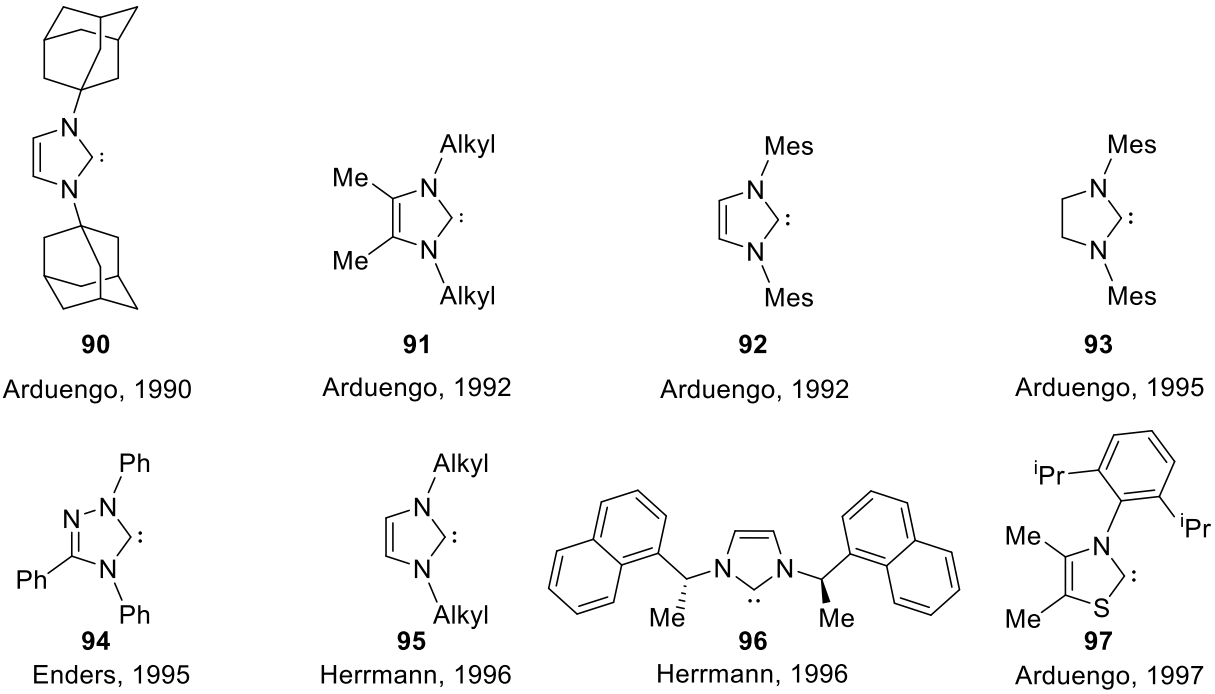

Chart 1.11 Examples of isolated stable *N*-heterocyclic carbenes.

Benzoin condensation creates a chiral center on the carbon bearing the –OH group in the new α-hydroxyketone.[134] The use of the carbene-based catalysts allowed the exploration of enantioselective variants of benzoin condensation. The first asymmetric benzoin condensation catalyzed by a chiral thiazolium salt was reported by Sheehan and Hunneman in 1966, but the enantiomeric excess (*ee*) in this reaction was just 22%.[139] Several years later, the *ee* was improved to 51% using a (*S*)-4-methyl-3-α-(1-naphthyl)ethyl-thiazolium salt **98** (Chart 1.12).[141] Several decades of investigation followed this initial report, but enantioselectivity remained modest.[140–143] Dramatic improvements came in the late 1990s with the work of Enders[144] and Leeper,[145] who discovered that triazolium-derived precatalysts **99** and **100** lead to higher enantioselectivity than their thiazolium counterparts, especially if the triazolium ring is a part of a bicyclic skeleton. With precatalyst **101**, Enders and Kallfass

subsequently improved the yields to 83% and optical purity to 90% in the case of parent benzoin.[146,147] Introduction of the pentafluorophenyl group into the structure of precatalyst **102** by Connon led to further improvement in the yield (90%) and to excellent enantioselectivity (99%).[148]

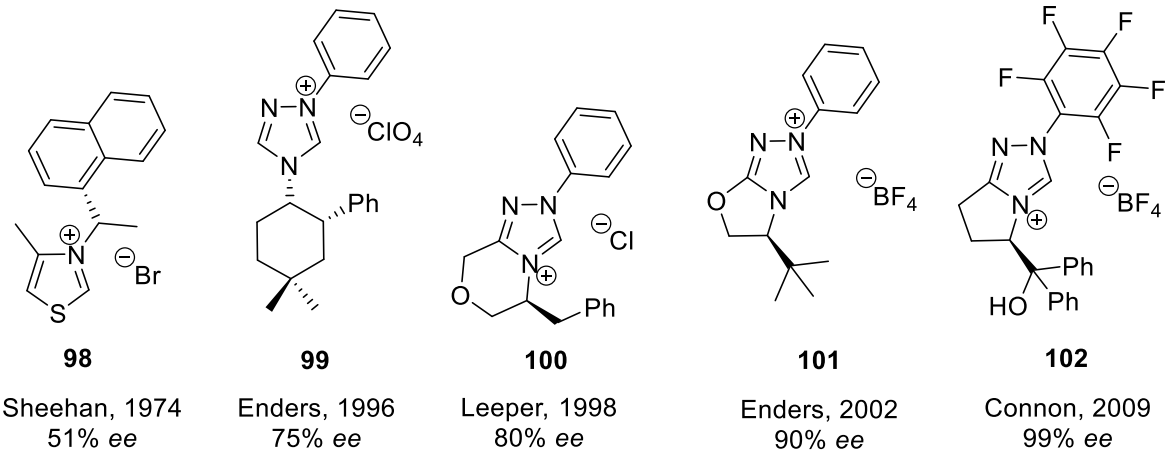

Chart 1.12 Examples of precatalysts to chiral carbene-based catalysts for asymmetric benzoin condensations.

More recently, asymmetric catalysts for benzoin condensation included desymmetrized rotaxanes substituted with a thiazolium group.[149] Observed *ee*'s were low, but this work demonstrated that a rotaxane can be used to introduce a chiral field around an otherwise achiral catalytic thread molecule. Other competent precatalysts that were recently developed included bistriazolium,[150] hydrogen bonding,[151] and spirocyclic[152] motifs, with *ee*'s ranging between 55% and 95%. An aqueous version of the NHC-catalyzed asymmetric benzoin condensation was recently reported.[153]

1.3.1 Applications of Benzoins

1.3.1.1 Benzoins in Polymer Science

Benzoins can be easily reduced into hydrobenzoins or oxidized into benzils. Benzoins, their ethers, and benzils are common photoinitiators for radical polymerizations.[154] Irradiation of benzoins with the light with wavelengths between 300 and 400 nm results in efficient α-cleavage, generating a benzoyl and benzyl alcohol radicals (Scheme 1.12).[155,156] One of the few drawbacks in using benzoin derivatives as photoinitiators is their poor absorption in the near-UV region; this feature was first addressed by Turro and co-workers by introducing methyl thioether groups to benzoin.[157] Benzoin-terminated polyurethane was used by Deka and Kakati as macrophotoinitiator in the synthesis of polyurethane–polymethyl methacrylate block copolymers.[158] Kizilcan and Akar synthesized novel oligomeric benzoin-derived photoinitiators by the reaction of the parent benzoin with depolymerization products of polyethyleneterephthalate (PET), and subsequently used it in the block copolymerization of styrene and acrylonitrile.[159] Decoration of multi-walled carbon nanotubes (MWCNT) with benzoin functional groups allowed the photoinitiation of polymer growth from the surface of the MWCNT, allowing the creation of nanotube/polystyrene hybrids.[160] Degirmenci and co-workers used propargyl ether of benzoin as a "clickable" photoinitiator that could be easily attached to azide-ornamented polymers.[161] Timpe and Rajendran studied the cationic ring-opening of epoxides using several benzoin derivatives as radical sources in polymerization process and diphenyliodonium hexafluoro-phosphate as the electron-acceptor.[162]

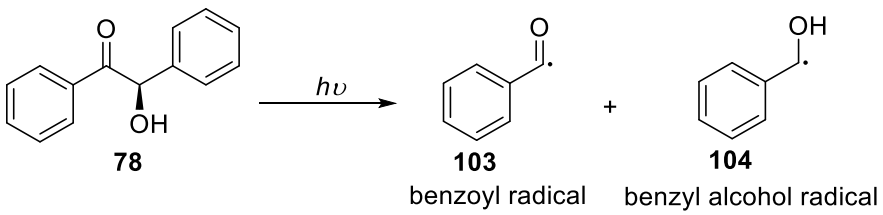

Scheme 1.12 Photolytic α-cleavage of benzoin is the basis of its use as a photoinitiator in polymerization reactions.

Attempts to incorporate benzoin motifs into polymeric structures date back to 1955, when Jones and Tinker obtained an apparent benzoin pentamer by treating terephthalaldehyde with potassium cyanide.[163] This finding contradicted a previous report by Oppenheimer in which terephthalaldehyde was shown to form only its dimer upon exposure to cyanide.[164] Kuriakose and Pillai engaged pendant benzaldehyde chains of a polymer in a cross-benzoin condensation.[165] Altomare and co-workers used free-radical copolymerization to produce optically active copolymer containing racemic α-methylolbenzoin methyl ether acrylate and (−)-menthyl acrylate monomer units.[166] Han and co-workers used rigid threefold symmetric trisaldehydes **105**–**108** (Chart 1.13) as precursors to porous organic polymers (POPs) with α-hydroxyl ketone linkages and Brunauer–Emmet–Teller (BET) surface areas as high as 726 $m^{2}{\cdot}g^{-1}$.[167]

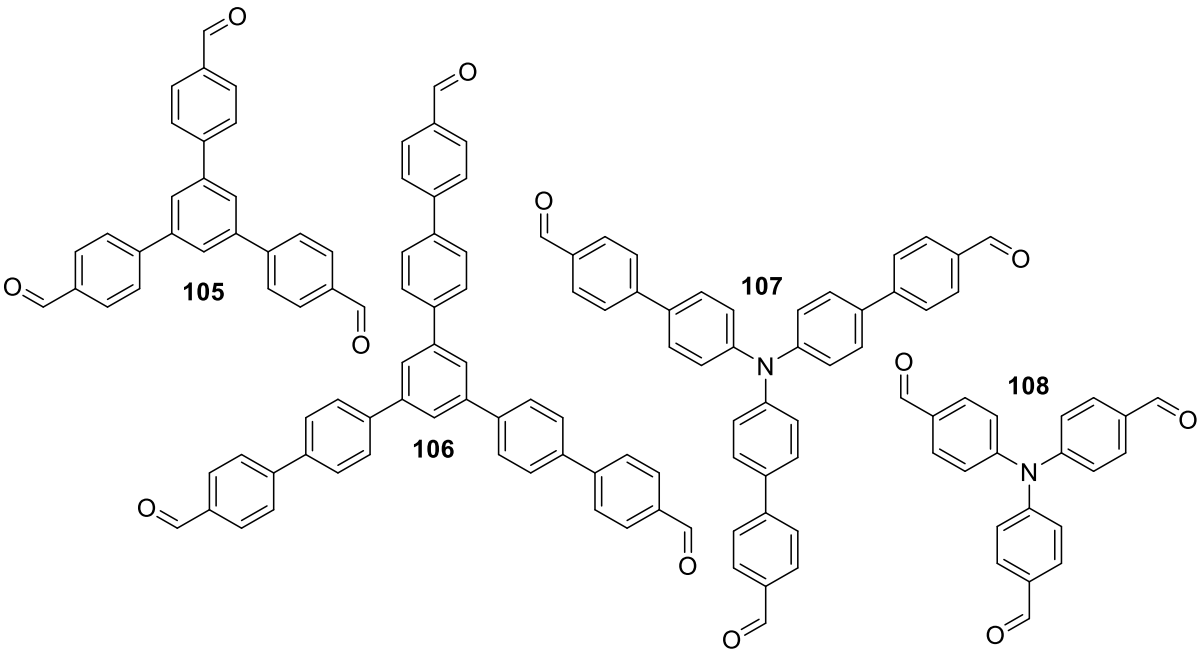

Chart 1.13 Examples of trigonally symmetric aldehydes used in the production of porous organic polymers through benzoin condensation.

1.3.1.2 Benzoins in Nanomaterials Science

Benzoin radicals can also act as reducing agents in colloidal nanomaterial synthesis. Esumi and co-workers prepared ultrafine metal particles of copper, silver, and gold from their ethanolic salt solutions by UV irradiation.[168] The photoreduction was dramatically enhanced when benzoin was added as a photoinitiator. Following the same method, silver/gold alloy particles were also obtained. Additionally, ultrathin copper nanowires with tunable diameters were grown by Yang and co-workers from the solution of oleylamine, copper chloride, and benzoin.[169] In this method, copper(II) species are first reduced to copper(I) and then to copper metal by the free radicals produced via thermal decomposition of benzoins as shown in Figure 1.13. Symmetrically ornamenting the two benzene rings in parent benzoin by electron-donating groups can promote the reducing power of benzoin radicals toward copper(II) reduction. The benzoin free radicals were also used to decrease the diameter of silver nanowires in order to improve their optoelectronic performance.[170]

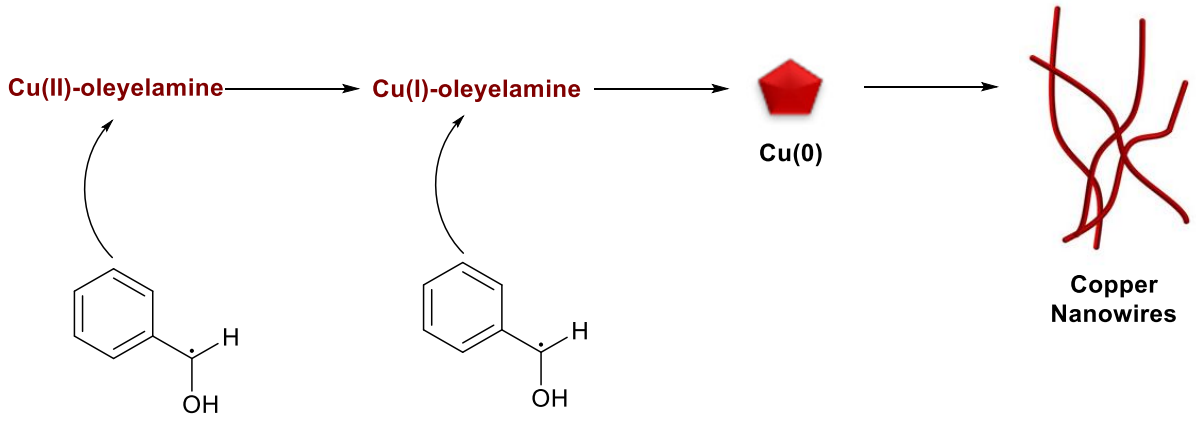

Figure 1.13 Proposed pathway of Cu-complex reduction via α-hydroxybenzyl radicals and one-dimensional copper nanowires growth (adapted from ref. 169 with permission, copyright © 2017 American Chemical Society).

1.3.1.3 Benzoins as Ligands for Transition Metals

Nitrogen condensation derivatives of benzoins have been often used as chelating ligands for metals. Vafaie and co-workers have shown that trace amounts of chromium(III) ions in water can be detected by complexing these ions with α-benzoin oxime in the presence of a non-ionic Triton X-100 surfactant,[171] building on the previous work on chromium(III) complexes of α-benzoin oxime which was reported by El-Shahat and co-workers.[172] Stamatatos and co-workers employed α-benzoin oxime and manganese (III) to construct an unusual cluster with nine metal centers (Figure 1.14, left),[173] while Joshi and Habib used the same ligand to obtain mononuclear complexes with cobalt(II), copper(II), nickel(II), and zinc(II).[174]

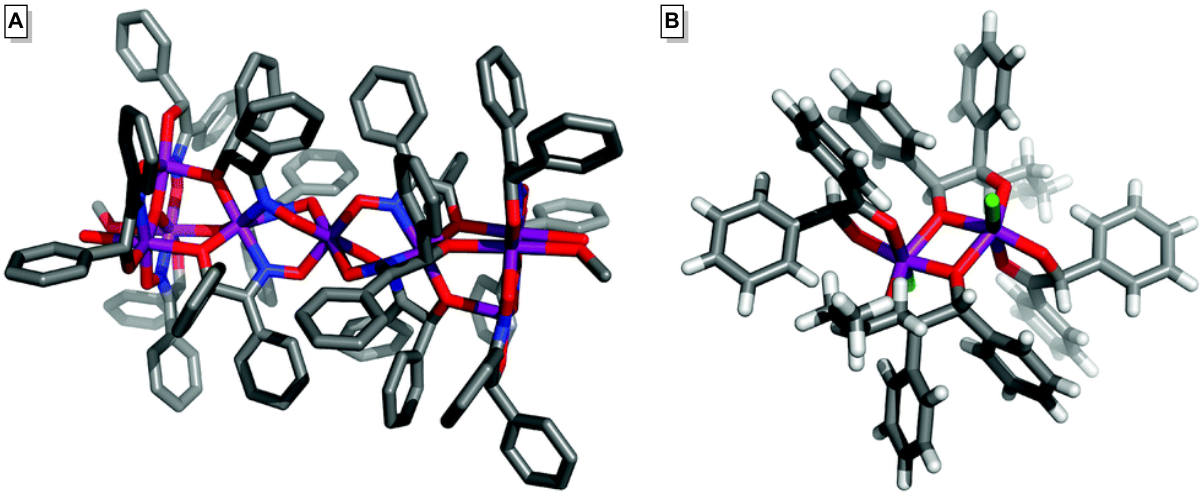

Figure 1.14 *(A)* Complexes of benzoin oxime with manganese(III) and *(B)* benzoin with titanium(IV). Element colors: C—gray, H—white, O—red, N—blue, Cl—green, metals-purple. In the structure on the left, hydrogen atoms have been omitted for clarity.

Gautam and co-workers studied complexes of benzoin's thiosemicarbazone with various copper(II) salts and found that the coordinating atoms and the coordination geometry switch as a function of a counterion.[175] Ali and co-workers synthesized cobalt(II) and nickel(II) complexes of benzoin thiosemicarbazone, and investigated their antibacterial

activities.[176] Nassef and co-workers studied homoleptic and heteroleptic complexes of benzoin thiosemicarbazone with rhodium(III), ruthenium(III), palladium(II), copper(II), and nickel(II).[177] Benzoin semicarbazone was also used as a ligand by Dahikar and Kedar to complex with some transition metals and the antimicrobial activity of the resulting complexes was studied.[178] Additionally, Aliyu and Abdullahi prepared *N,N'*-bis(benzoin)ethylenediiminato ligand to produce mononuclear complexes with manganese(II), cobalt(II), nickel(II) and copper(II) ions.[179]

Aliyu and Mohammed prepared a Schiff base from benzoin and 2-amino benzoic acid and coordinated it with iron(II) and nickel(II) salts to produce complexes with 1:1 metal-to-ligand ratio.[180] Another Schiff base, obtained by Faraj and co-workers, was derived from benzoin and glycine and complexed with a series of transition metals, yielding complexes with 1:2 metal-to-ligand ratio.[181]

Benzoins themselves are also competent ligands for catalytically active metals. Benzoin-supported titanium catalyst (Figure 1.14, right) was shown as effective in the copolymerization of norbornene and ethylene.[182] Paine and co-workers mimicked the action of non-heme enzymes in aliphatic C–C bond cleavage using complexes in which benzoins were coordinated with iron(II) and supported by a facial N3 and a tripodal N4 ligands.[183] Benzoin complex with manganese(II) was also prepared and studied by El-ajaily and Maihub.[184]

Fukuzumi and co-workers have shown that a binuclear complex of copper(II) with tridentate *N,N*-bis[2-(2-pyridyl)ethyl]-2-phenylethylamine can be quantitatively hydroxylated at the benzylic position using molecular oxygen and benzoin-derived 1,2-enediolate as the electron donor. This behavior paralleled the activity of dopamine β-hydroxylase.[185]

1.4 Cyclobenzoins[†]

Inspiring by Prof. Flood's talk from Indiana University at ISMSC (Shanghai, 2014), in which he described a very simple synthesis of the first cyanostar macrocycles, [39–45] Dr. Ji —a former graduate student in our group—decided to expand his research portfolio onto the dynamic synthesis of rigid macrocycles through (reversible) benzoin condensation. He started to test out his ideas on isophthalaldehyde (**109**, Scheme 1.13A) as the first substrate. Several weeks later, he found that a discrete oligomer had been formed in 41% yield, but only if the ratio of EtOH and H_2O solvents was adjusted so that the precipitation occurs very selectively.[186] In a couple of weeks, a crystal structure of the cyclic trimer **110** was obtained. This cyclic trimer was dubbed cyclotribenzoin to suggest its cyclic trimeric nature and its origins in the benzoin condensation.

Dr. Ji continued this project by testing terephthalaldehyde (**111**, Scheme 1.13B), whose exposure to similar benzoin condensation conditions resulted now in a cyclic tetramer **112**, which was named cyclotetrabenzoin.[187] Cyclotetrabenzoin was isolated following precipitation and recrystallization from a MeOH/DMSO mixture. While the isolated yield of 21% may appear low, it is remarkable considering how many potential isomers can be formed in the process: even just among the cyclic tetramers, there are 37 possible stereoisomers and regioisomers. Only one is isolated: this diastereomer (shown in Scheme 1.13B) is achiral on account of the presence of an S_4 rotation axis.

Benzoins have a huge volume of well-precedented chemistry, which suddenly becomes new in the context of cyclobenzoins. The hydroxyl groups can be silylated[188] or esterified;[189] both modifications remove the hydrogen bond donors, which dramatically increasing the solubility and facilitating purification.

[†] This section of the chapter was published on ref. 120.

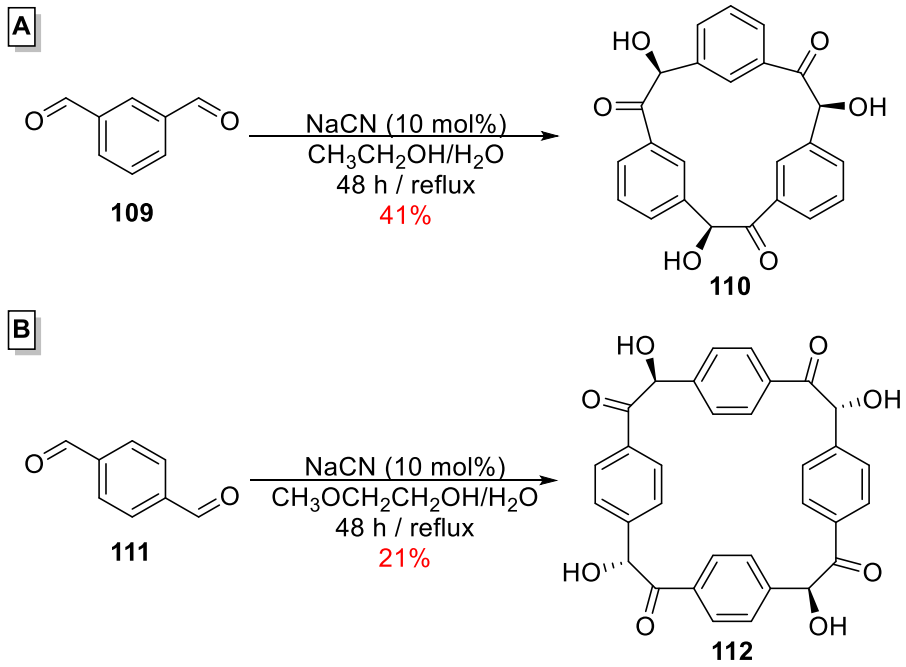

Scheme 1.13 Synthesis of *(A)* cyclotribenzoin (**110)** and *(B)* cyclotetrabenzoin **(112)**.

1.4.1 Cyclotribenzoin

The single crystal structure of cyclotribenzoin (**110**) in Figure 1.15A showed that the molecule was formed as the all-cis diastereomer, which adopted a conical shape with three benzene rings expressing a cuplike cavity. The structure is not strained, as all its carbon atoms have bonding angles within 2° of their idealized geometries. Six C–H bonds—three coming from the aromatic rings and the other three coming from the secondary carbon atoms adjacent to the hydroxyl groups—are convergently positioned pointing towards the apex of the cone. In the crystal packing of **110** (Figure 1.15B), the parallel orientation of stacked molecules to each other is clearly shown through the *a*–*b* crystallographic plane. Short [C–H···O] contacts connect each cyclotribenzoin molecule with twelve of its neighbors, with H···O distances between 2.50 and 2.60 Å. On each aromatic ring of cyclotribenzoin, the hydrogen located *ortho* to the CO group establishes a short contact with the carbonyl oxygen atom from the adjacent molecule. Likewise, the hydrogen located *meta* to the CO group

establishes short contacts with the hydroxyl oxygen atoms from neighboring molecules. This set of connections is repeated for each aromatic ring in the cyclotribenzoin molecule.

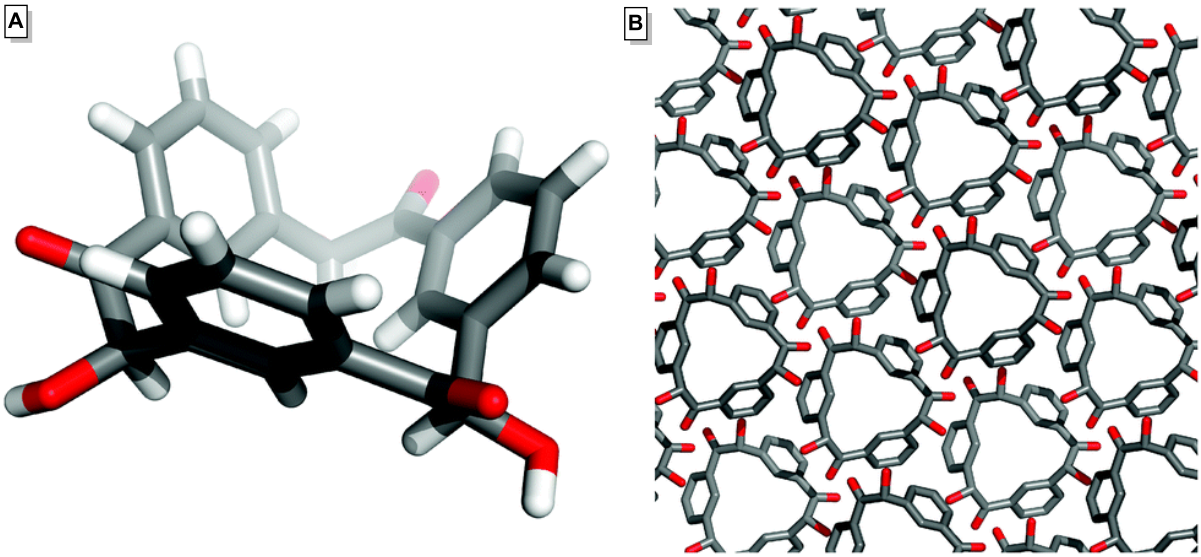

Figure 1.15 *(A)* Crystal structure and *(B)* segment of the crystal packing diagram for cyclotribenzoin (**110**). Element colors: C—gray, H—white, O—red.

1.4.2 Cyclotetrabenzoin

The crystal structure of cyclotetrabenzoin (**112**) in Figure 1.16A was obtained using synchrotron radiation. The tetrameric macrocycle is square-shaped, with a central cavity measuring 6.9 × 6.9 Å (distance between the centroids of two benzene rings located on the opposite sides). The existence of an S_4 rotation axis in the center of the cavity makes the molecule achiral although in the absence of symmetry planes. Judging by the bonding angles on all carbon atoms, **112** is not significantly strained either. The crystal packing of cyclotetrabenzoin showed that the individual macrocycles organize into 2D layers which resemble square grids (Figure 1.16B), perfectly stacked on top of one another. Molecules of cyclotetrabenzoin organize into infinite nanotubes, held in bundles through zigzagging hydrogen bonding connections (Figure 1.16C). Formed between the oxygens of the carbonyl and hydroxyl groups as acceptors and the hydrogen of the neighboring molecule's –OH group

as the donor, these hydrogen bonds repeat themselves on each of the four corners of the square-shaped macrocycle. Because of this perfect alignment, cyclotetrabenzoin is somewhat porous in the solid state, with a Langmuir surface area of 47 $m^{2} \cdot g^{-1}$.

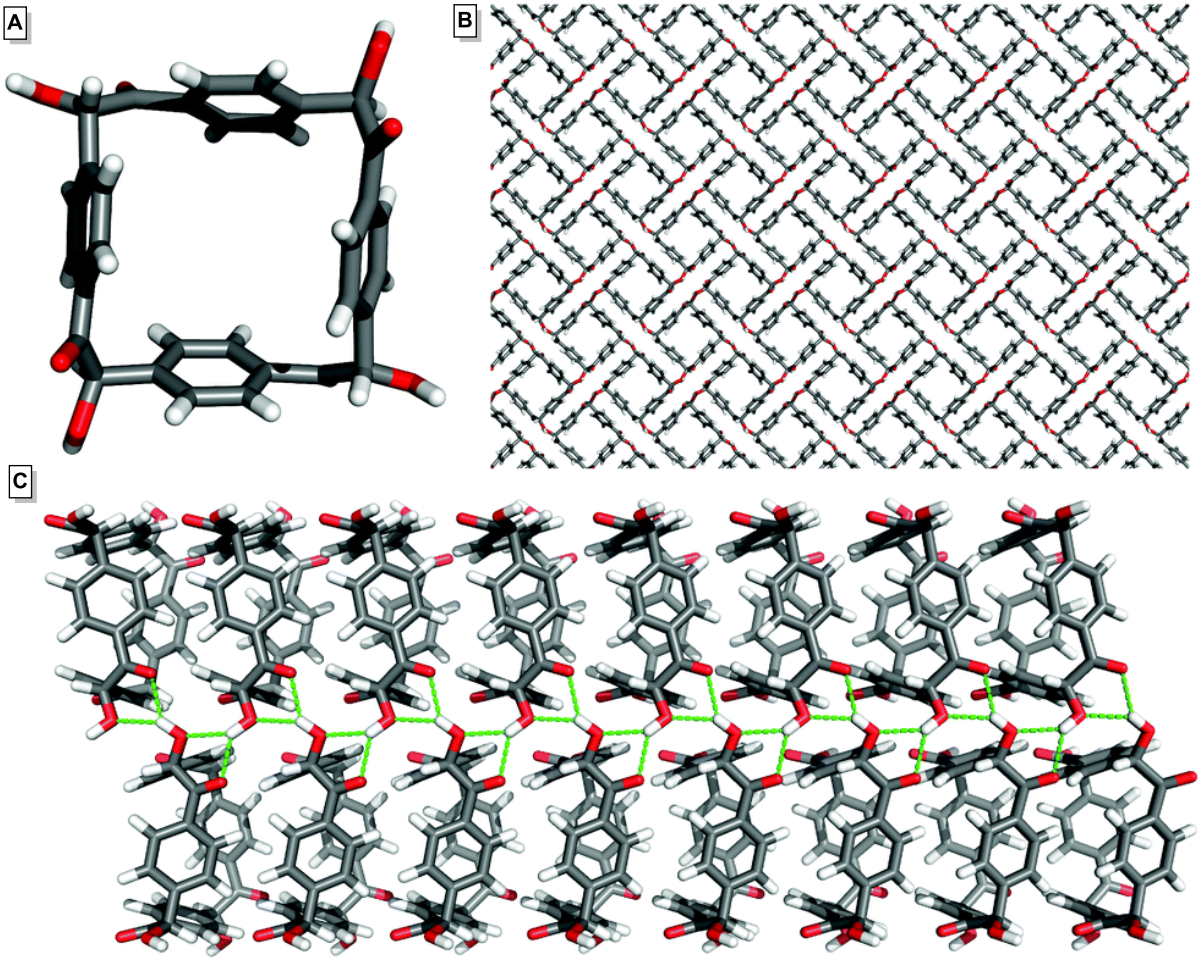

Figure 1.16 *(A)* Crystal structure and *(B)* segment of the crystal packing diagram for cyclotetrabenzoin (**112**). *(C)* Zigzagging arrays of hydrogen bonds organize molecules of cyclotetrabenzoin into perfectly aligned nanotubes (hydrogen bonds shown in green). Element colors: C—gray, H—white, O—red.

1.5 Conclusion

Chemistry of macrocycles has expanded into a broad research area that covers the fields of organic, inorganic, and supramolecular chemistry. Although the macrocyclization reaction is entropically unfavorable, many different classes of macrocyclic compounds have

been synthesized over the years. Within them, cyclophanes attracted the attention of many scientists, which is easily explained by the easy-o-functionalize the aromatic rings or the bridging chains that lead to a wide variety of cyclophanes to use in different applications including molecular recognition, organic-inorganic hybrid molecules, polymer science, analytical detection and sensing, and supramolecular assembly.

Recently, a facile one-step synthesis of novel cyclophanes, using simple building blocks, has been discovered. During the syntheses of these cyclophanes, new C–C bond has been formed through the cyanide-catalyzed benzoin condensation reaction. These cyclophanes have been dubbed "cyclobenzoins". Besides the quick assembly of the cyclobenzoins, the relatively mild conditions employed can also allow the introduction of more complex functionality into the framework, and thus provide access to a wider range of potentially useful materials, which is the aim of this thesis. Overall, the field of cyclobenzoins is still in its infancy when compared to other cyclophanes such as aryleneethynylene macrocycles and cyclobis(paraquat-*p*-phenylene), so cyclobenzoins chemistry is still under exploration in our laboratory.

Chapter Two

Reduction, Oxidation, and Oxidative Cleavage of Cyclobenzoins

2.1 Introduction

The chemical structure of a benzoin (**1**) contains both a ketone and a secondary alcohol functional group (Scheme 2.1). They provide precursors for either a reduction to a 1,2-diol—hydrobenzoin (**2**)—or oxidation to a 1,2-diketone—benzil (**3**).

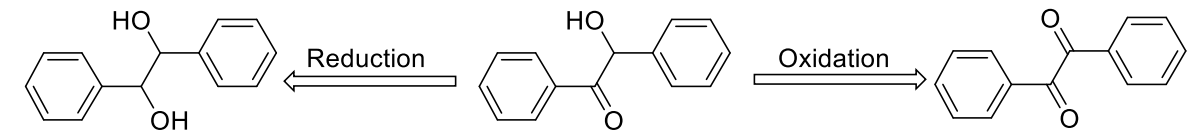

Hydrobenzoin (1,2-diol) **2** | Benzoin **1** | Benzil (1,2-diketone) **3**

Scheme 2.1 Reduction and oxidation of benzoin (**1**).

The reduction of benzoin to hydrobenzoin creates adjacent secondary alcohol groups, leading to a more polar product because alcohols are more polar than ketones.[190] But the oxidation of benzoin to benzil gives either a less polar product if the two carbonyl groups are in a *cis* configuration or a virtually non-polar product if the two carbonyl groups are in a *trans* configuration—as the dipole moments of the two opposite carbonyl groups cancel each other out in the later configuration.

2.1.1 Reduction of Benzoins

According to IUPAC, the reduction reaction in organic chemistry is defined as "the gain of hydrogen and/or loss of oxygen from an organic substrate."[190] The most common and useful reducing agents for organic compounds are complex hydrides reagents such as the

borohydrides of aluminum,[191] gallium,[192,193] beryllium,[194] lithium,[195,196] and sodium,[197,198] as well as lithium aluminum hydride[199] because they contain a metal-hydrogen bond that serves as a source of the strongly nucleophilic hydride ion. Among them, sodium borohydride seems to be of the greatest practical interest because it is inexpensive compared to its counterparts and its reactions can be carried out in water or alcohol solution at ambient conditions.[200] Additionally, sodium borohydride is more chemoselective than lithium aluminum hydride because it only reduces aldehydes and ketones to the corresponding alcohols due to the low polarity of the B–H bond.

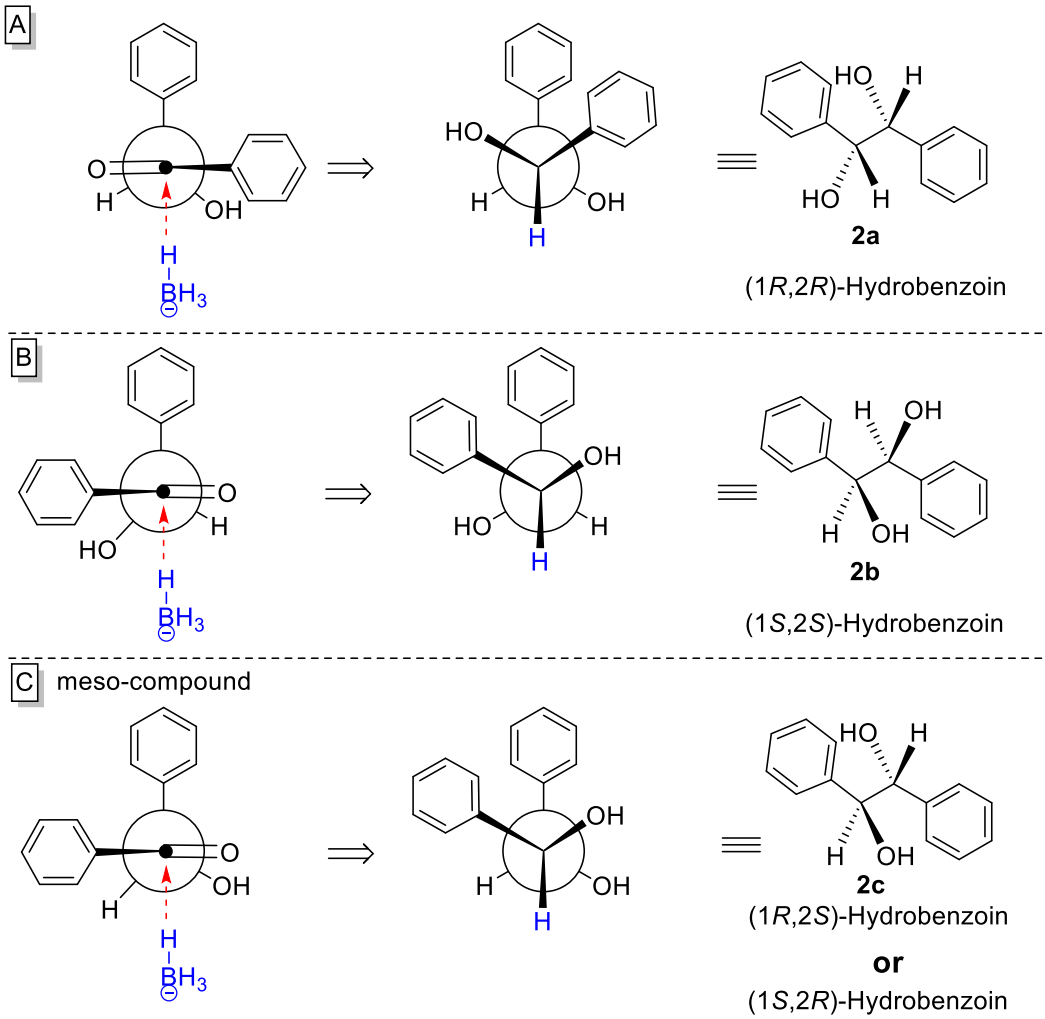

Scheme 2.2 Stereoisomeric products of hydrobenzoin **2a**–**c**.

The reduction of benzoin compounds by sodium borohydride results in three stereoisomeric hydrobenzoin products: (1*R*, 2*R*) isomer **2a**, (1*S*, 2*S*) isomer **2b**, and meso-isomer **2c**, which is not chiral although it contains two stereogenic centers since it has an internal plane of symmetry.[201,202] This is why hydrobenzoin with a total of two chiral centers cannot attain the theoretical maximum of $4 = 2^2$ stereoisomers. These three isomers are produced because the hydride ion (from sodium borohydride) can attack the carbonyl group, which has sp^2 hybridization, from different directions (Scheme 2.2). Hydrobenzoins are 1,2-diols which have been used as chiral auxiliaries and catalysts,[203] and as precursors to chiral crown ethers,[204,205] liquid crystals,[206,207] and materials with non-linear optical (NLO) properties.[208] Many efforts have been focused on the stereoselective reduction of α-hydroxyketone compounds and several useful reducing agents have been extensively examined such as $Zn(BH_4)_2$[209] and $LilnH_4$[210] which gave meso-hydrobenzoin quantitatively. This result is observed because the stereochemistry of the reduction governed by the stability of the transition state, so the benzoin is attacked from the less steric side which produces meso-hydrobenzoin.

2.1.2 Oxidation of Benzoins

In contrast with reduction reactions, IUPAC interprets the oxidation reactions in organic chemistry as "the gain of oxygen and/or loss of hydrogen from an organic substrate."[1] Based on this definition, the oxidation of α-hydroxyketone or 1,2-diol compounds leads to 1,2-diketone compounds. These compounds are distinguished by the long O=**C**–**C**=O bond which connects the adjacent carbonyl groups and measures ~1.54 Å, unlike the similar bond in buta-1,3-diene C=**C**–**C**=C, which measures 1.48 Å, or in acrolein C=**C**–**C**=O, which measures 1.45 Å.[211] This difference in bond lengths is explained by the repulsion between the partial positive charges of the carbonyl carbon atoms due to the high electronegativity of

oxygen. Benzoin (**1**) is a well-known compound belonging to α-hydroxyketone family with two phenyl groups terminated this functional unit and benzil (**3**) (1,2-diketone) is the corresponding product after the oxidation of benzoin.[122–124] Since the first observation of this reaction, numerous oxidizing agents were shown to oxidize benzoin to benzil: nitric acid,[125] chlorine,[212,213] iodine,[214] ammonium nitrate/copper(II) acetate,[215] thallium(III) nitrate,[216] iodoxybenzene,[217] oxone/alumina,[218] bismuth(III) nitrate/copper(II) acetate,[219] iron(III) nitrate,[220] *tert*-butyl hydroperoxide/titanium(IV) chloride,[221] and many others.[222–229] The first and the most common oxidizing agent that turned benzoin to benzil is nitric acid.[125] Benzils are important building blocks in synthesis of pharmaceuticals,[230–234] precursors of porphyrins,[235–237] and common photoinitiators for free radical polymerizations.[238–241]

In this chapter, the reduction of cyclotribenzoin (**4**) and the oxidation of cyclotetrabenzoin (**6**) will be discussed, and the differences between the resulting cyclic products and their acyclic analogous will be investigated.

2.2 Results and Discussion

2.2.1 Reduction of Cyclotribenzoin to Cyclotrihydrobenzoin

Using $NaBH_4$ as the reductant, cyclotribenzoin (**4**) was diastereoselectively reduced to the corresponding hexaol, which was dubbed cyclotrihydrobenzoin (**5**), in 88 % yield with all of the newly formed –OH groups *syn* to their previously existing neighbors (Scheme 2.3).[120,242] This diastereoselectivity is unusual in the absence of chelating hydride species.[209] We speculated that the diastereoselectivity of this simple reduction stemmed from the conical shape of cyclotribenzoin, which mandated the attack of the hydride reducing agent from the unencumbered lower side, pushing the newly formed –OH group upwards into the *syn* relationship with the previously existing –OH functionality (Figure 2.1).

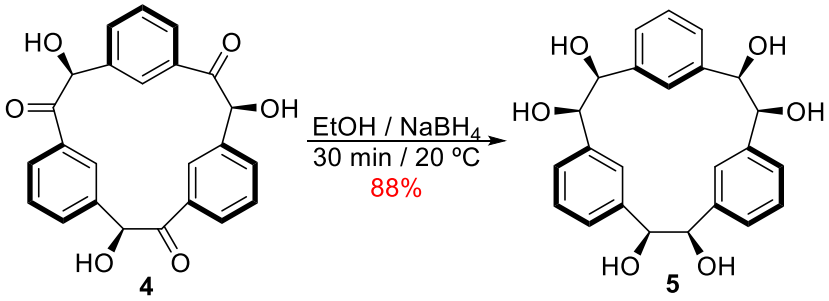

Scheme 2.3 Reduction of cyclotribenzoin **(4)** into cyclotrihydrobenzoin **(5)**.

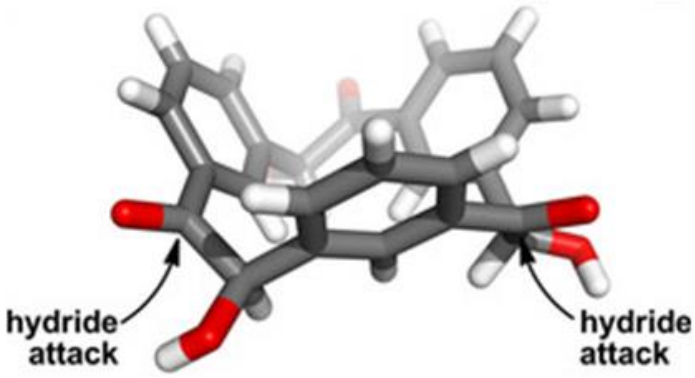

Figure 2.1 Suggested trajectory of the attack of hydride reducing agent onto cyclotribenzoin (**5**)**.** Element colors: C—gray, O—red, H—white.

2.2.2 Crystallographic Analysis of Cyclotrihydrobenzoin

Single crystals of cyclotrihydrobenzoin (**5**) suitable for X-ray diffraction analysis were obtained by vapor diffusion of either *n*-hexane or *n*-pentane into its solutions in off-the-shelf THF. The crystal structure of **5** is shown in Figure 2.2A. Cyclotrihydrobenzoin crystallized in the *C*2/*c* space group, with four molecules of **5** and twenty molecules of water per unit cell. The cone-shaped cyclotribenzoin (**4**), where all the –OH groups and all benzene rings point in the same direction, was deformed after reduction: one of the three aromatic rings in the macrocycle was flipped and its larger part points away from the rest of the molecule, while the other two aromatic rings still point in the same direction as well as all the hydroxyl groups. The adjacent –OH groups are in a gauche orientation to each other, with dihedral angles ranging from 54 to 63°. Molecules of **5** co-crystallized with water, which

presumably originated from the off-the-shelf THF that was used for crystallization of cyclotrihydrobenzoin, in a 1:3 ratio. These water molecules were extremely well-ordered within the crystal structure: atomic positions of their hydrogens could be refined directly from X-ray data (which is otherwise unusual) and elemental analysis also supported a well-defined trihydrate.

Closer inspection of the packing diagram, seen along the crystallographic *c* axis in Figure 2.2B, shows small voids where six molecules of **5** come together in a fashion reminiscent of protein subunit assembly: they orient their hydrophobic exteriors toward the outside, to enclose a highly hydrophilic interior. Within these voids, ordered pentameric water clusters are trapped.[243–245] Individual clusters are isolated in the crystal lattice, with the closest distance between two H_2O molecules in neighboring clusters being an O···O separation of 5.93 Å. In these clusters, five water molecules form a distorted tetrahedron with the central water molecule hydrogen bonded to four of its neighbors (Figure 2.2C), in the same fashion which is seen in carbon sp^3 covalent chemistry since both have four sites to form networks in a tetrahedral structure. The central water molecule acts as a hydrogen-bond donor [O−H···O distances 1.90 Å, angles 152.6°; O···O distances 2.75 Å] in the interactions with two of its water neighbors, and as a hydrogen-bond acceptor [O···H−O distances 1.76 Å, angles 166.2°; O···O distances 2.71 Å] in the other two. The [O···O] distances in this tetrahedron are comparable to the shortest observed distances in Fujita's "molecular ice" encapsulated in a self-assembled metal–organic cage (2.72 Å) and those found in the I_h-type ice (2.75 Å).[246] The [O···O···O] angles range from 97.7° to 141.8°, suggesting a "squeezed" tetrahedron relative to the I_h ice, in which the corresponding angles are 109°. In fact, the pentameric water cluster was first identified in 1964 by Walrafen, who suggested it to be one of the simplest subunits of hydrogen-bonded water networks.[247–252] In 2012, Bowman-James and coworkers isolated the Walrafen pentamer within a supramolecular host capsule.[253,254]

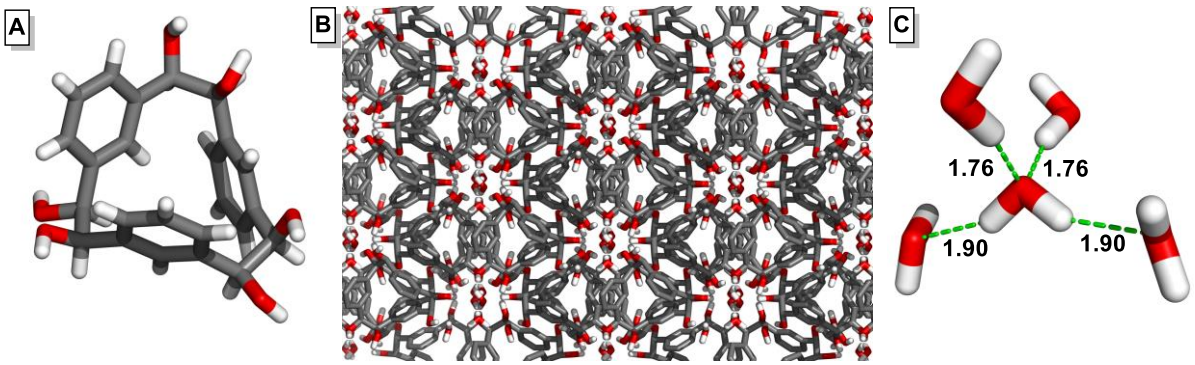

Figure 2.2 *(A)* Crystal structure of cyclotrihydrobenzoin (**5**), *(B)* packing diagram of **5** (nonpolar hydrogen atoms omitted for clarity), and *(C)* Walrafen's water pentamer cluster which are found in the voids of crystal packing of **5** (all distances are in Å). Element colors: C—gray, O—red, H—white.

Externally, the four peripheral H_2O molecules of the cluster are stabilized by hydrogen bonding and [O–H···π] interactions with the six neighboring molecules of cyclotrihydrobenzoin (**5**), color-coded in Figure 2.3A. Two symmetry-related H_2O molecules that act as hydrogen-bond donors to the central H_2O molecule also establish three additional hydrogen bonds with the –OH groups on three separate molecules of **5**. In two of these hydrogen bonds, these peripheral water molecules act as hydrogen-bond acceptors (O···H–O distances 1.82 and 1.83 Å, angles 168.0 and 163.8°; O···O distances 2.76 and 2.67 Å, respectively), and in the third one they are hydrogen-bond donors (O–H···O distances 2.03 Å, angles 142.4°; O···O distances 2.81 Å) as shown in Figure 2.3B. Moreover, each of the two symmetry-related H_2O molecules that act as hydrogen-bond acceptors from the central H_2O molecule also form a hydrogen bonds, as donors, to –OH groups in the neighboring molecules of **5** (O–H···O distances 1.91 Å, angles 170.6°). The other hydrogen atom establishes an apparent [O–H···π] contact with the benzene ring of the same molecule of **5**, characterized by an O–H···Ph centroid distance of 2.84 Å, and with the distance to the closest carbon of the ring being 2.46 Å. In addition, these peripheral H_2O molecules establish a short contact with another –OH group in a separate molecule of **5**. These contacts could be interpreted as significantly longer hydrogen bonds, wherein the H_2O molecules act as

acceptors; they are characterized by the O···H−O distances of 2.20 Å and angles of 154.7°, and O···O distances of 3.07 Å.

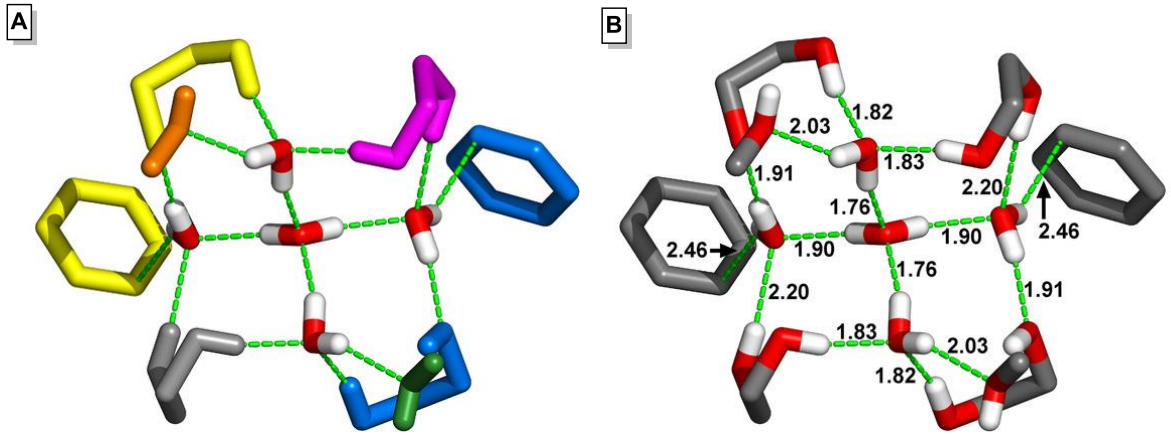

Figure 2.3 *(A)* Pentameric H_2O cluster and the fragments of six neighboring molecules of cyclotrihydrobenzoin (**5**) highlighted in different colors, and *(B)* presented with the distances (in Å) between atoms of the pentameric H_2O cluster and its neighbors of **5**. Element colors: C—gray, O—red, H—white.

2.2.3 Oxidation of Cyclotetrabenzoin to Cyclotetrabenzil

Concentrated HNO_3 was used to readily oxidize cyclotetrabenzoin into the corresponding octaketone, which we named cyclotetrabenzil (**7**), in 67% yield (Scheme 2.4). In **7**, hydrogen bond donors are no longer present, making its solubility much higher than that of cyclotetrabenzoin (**7**). The produced octaketone is soluble in several halogenated hydrocarbons, as well as in dimethyl sulfoxide.

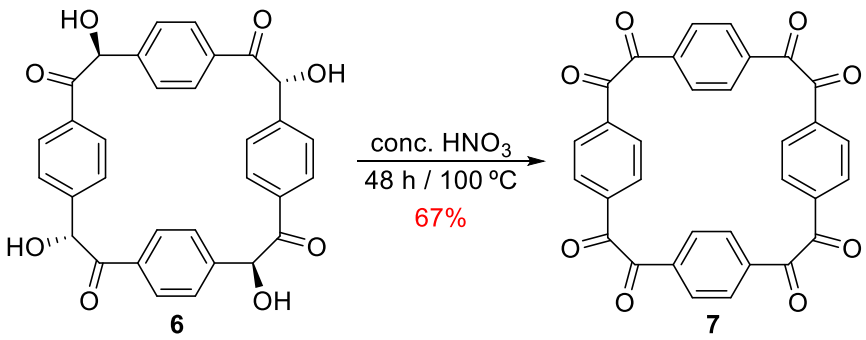

Scheme 2.4 Oxidation of cyclotetrabenzoin (**6**) into cyclotetrabenzil (**7**).

We expected the oxidation mechanism of cyclotetrabenzoin (**6**) followed the same mechanism of oxidizing its acyclic analog **1** in the presence of concentrated nitric acid (Scheme 2.5). During the oxidation, there was a release of nitrogen dioxide gas which was identified by its brown fumes. The oxidation of benzoin is completed in 1–2 hours while it took about 48 hours to finish it in cyclotetrabenzoin. This is attributed by the presence of four α-hydroxyketone units in a rigid cyclic structure.

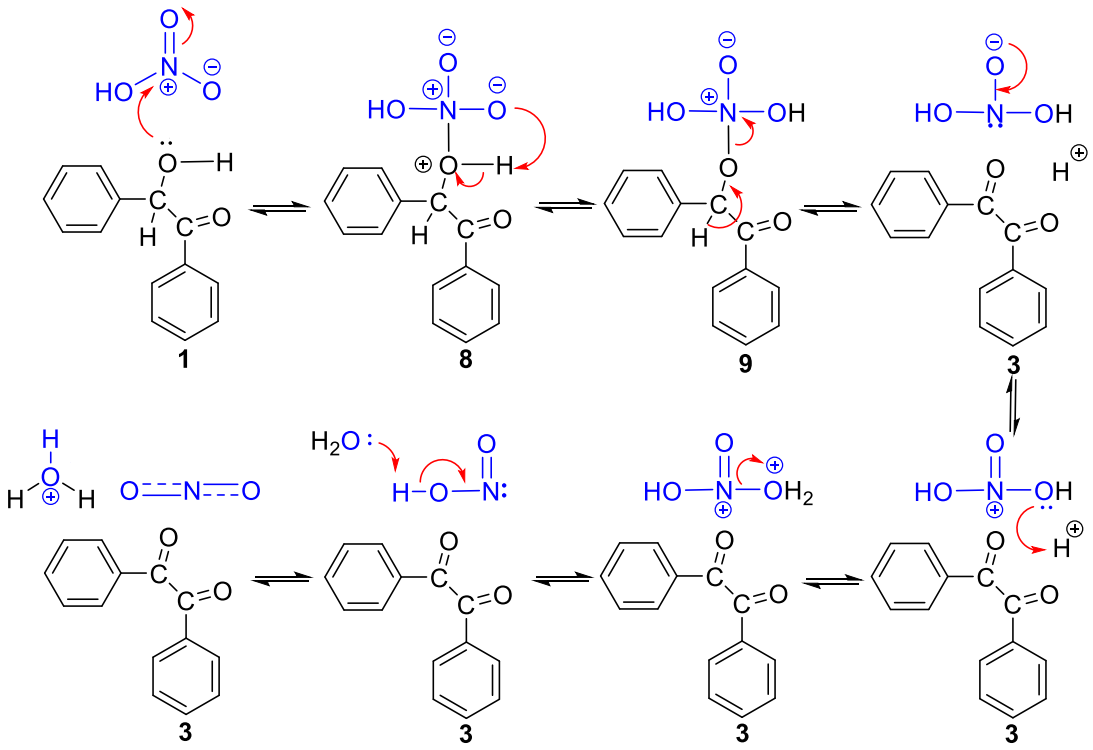

Scheme 2.5 Mechanism of the oxidation of benzoin (**1**) by concentrated nitric acid to produce benzil (**3**).

2.2.4 Crystallographic Analysis of Cyclotetrabenzil

Although the [halogen···halogen] interaction strength is considered weak,[255–262] the packing and properties of many molecular crystals are mediated by them, with [Cl···Cl] interactions being the most common. Single crystals of cyclotetrabenzil (**7**) suitable for X-ray diffraction analysis were obtained by vapor diffusion of *n*-hexane into its solutions in alkyl halide solvents: chloroform, 1,5-dichloropentane, 1,6-dichlorohexane, 1,1,2,2-

tetrachloroethane, and bromoform. Crystals of **7** which were grown from chlorinated solvents formed complexes between cyclotetrabenzil molecules and solvent molecules. The resultant complexes are stabilized by weak van der Waals forces and [Cl···Cl] interactions between solvent molecules in some cases.

2.2.4.1 Crystal Growth of Cyclotetrabenzil from Chloroform

The crystal structure of cyclotetrabenzil (**7**), which is grown from chloroform, is shown in Figure 2.4. Cyclotetrabenzil (**7**) crystallized in the $P2_1/c$ space group, with two molecules of **7** and twelve—four ordered and eight disordered—molecules of chloroform per the monoclinic unit cell. The square-shaped cyclotetrabenzoin (**6**) was deformed after oxidation: one of the four aromatic rings in the macrocycle was flipped leaving a chair-like structure shown in Figure 2.4B, and the rotation directions of the dihedral angles in the α-hydroxyketone units, which attached to the flipped benzene ring, were changed. This deformation cancelled the tilt between the aromatic rings on the opposite sides of **6** which was 40.8°, measured between the planes of each opposite aromatic rings pair: one pair of the opposite benzene rings in **7** becomes parallel and the other pair becomes antiparallel with no tilt angles. Thus delineated is a well-defined intrinsic cavity of dimensions 7.33 × 7.62 Å, measured between the centroids of the parallel and anti-parallel benzene rings, respectively, with Ph–C–C–Ph dihedral angles varying between 77.7 and 91.5° compared to 69° in **6**. Each adjacent C=O group is in a synclinal orientation to its neighbor, with O=C–C=O dihedral angles ranging from 78.8 to 96.9°, which is higher than O=C–C–OH dihedral angles of α-hydroxyketone units in **6** (13°). Each benzene ring in **7** is attached to two of carbonyl groups in *para*-positions, and these pairs are oriented in opposite directions in the case of parallel benzene rings and in same directions in the case of anti-parallel benzene rings.

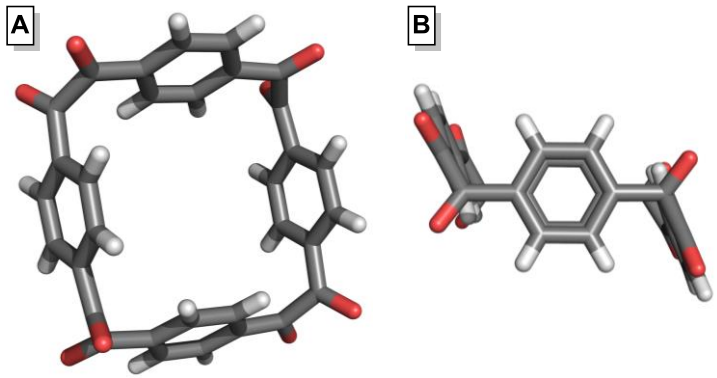

Figure 2.4 *(A)* The top-down view of the X-ray crystal structure of **7** grown from chloroform, and *(B)* the side view showing the chair-like conformation. Element colors: C—gray, O—red, H—white. All solvent molecules are omitted for clarity.

Molecules of **7** formed an inclusion complex with chloroform in a 1:3 ratio. This observation is supported by the calculated formula weight of the crystal structure (881.60 g mol^{-1}). One molecule of chloroform was included within the intrinsic pores of **7** in two orientations above and below the macrocycle, with one chlorine atom tucked in the cavity of **7** and the remaineder of the included chloroform molecule oriented away from the central cavity of the macrocycle in opposite directions (Figure 2.5A). The other two chloroform molecules were disordered within the extrinsic pores of the crystal lattice. The included chloroform molecules are aligned with the main axis of macrocycles and formed two arrays of guests within a tube of the lined up cyclotetrabenzil (**7**) molecules (Figure 2.5B). The plane of the three chlorine atoms in included chloroform formed a dihedral angle of 66.4° with the main plane of **7**. The distances between chlorine atoms tucked into the cavity and the centroids of the parallel benzene rings are 3.98 and 4.14 Å, and between them and the centroids of the anti-parallel benzene rings are 3.59 and 4.70 Å. The two chloroform molecules included into the cavity of the macrocycle form a [Cl···Cl] interaction with a distance of 3.47 Å, measured between the chlorine atoms directed toward the cavity; the [C−Cl···Cl] and [Cl···Cl−C] angles are 171.2°. This [Cl···Cl] distance is comparable to the calculated equilibrium distance in literature for chloroform dimer (3.43 Å), which has similar

dipole moment orientation, when [C−Cl···Cl] and [Cl···Cl−C] angles are 180° and the dipole moment between the two molecules is 1.28 Debye.[263]

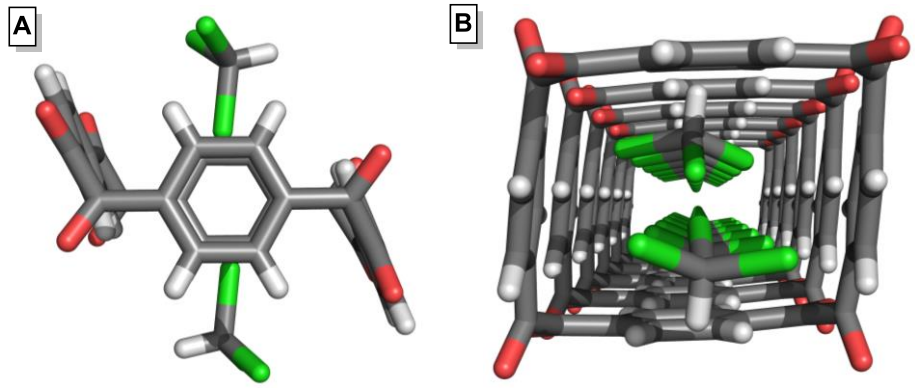

Figure 2.5 *(A)* The complex of cyclotetrabenzil with chloroform **7**·$CHCl_3$ and *(B)* the orientation of chloroform molecules with respect to cyclotetrabenzil (**7**) tubes. Element colors: C—gray, O—red, H—white, Cl—green.

Interestingly, neither electrostatic interactions nor isotropic van der Waals forces were detected between the host macrocycles and the chloroform guest, but common cyclotetrabenzil molecules were found connected with the host-guest complex by short contacts in the 2.40–3.16 Å range. The binding patterns of **7**·$CHCl_3$ indicated the cyclotetrabenzil-chloroform complex is uniquely stabilized by its short contacts with neighboring molecules, as well as the [Cl···Cl] interaction.

The supramolecular network derived from the packing of **7**·$CHCl_3$ is shown along the crystallographic *a* axis in Figure 2.6. The molecules of **7** similarly stack in a parallel orientation and each molecule establishes short contacts with neighboring molecules, whether they are macrocycle or chloroform molecules. Specifically, three hydrogen atoms from each anti-parallel benzene ring at **7** establish three short [C–H···O] contacts (H···O distances between 2.48 and 2.70 Å) with carbonyl oxygens from three neighboring molecules. The parallel benzene rings did not establish any short contacts with the neighboring molecules. Additionally, one carbonyl oxygen from each corner of **7** establishes a short [C=O···H]

contact (O···H distances between 2.40 and 2.48 Å) with one of the chloroform molecules included into the central cavities of neighboring macrocycles. Another carbonyl oxygen from the opposite corner of **7** establishes a short [C=O···H] contact (O···H distance 2.32 Å) with two of the disordered chloroform molecules which are located in the extrinsic cavities of the crystal lattice. This binding pattern is repeating itself in three dimensions, forming symmetrical multi-layers of the **7**·$CHCl_3$ complex.

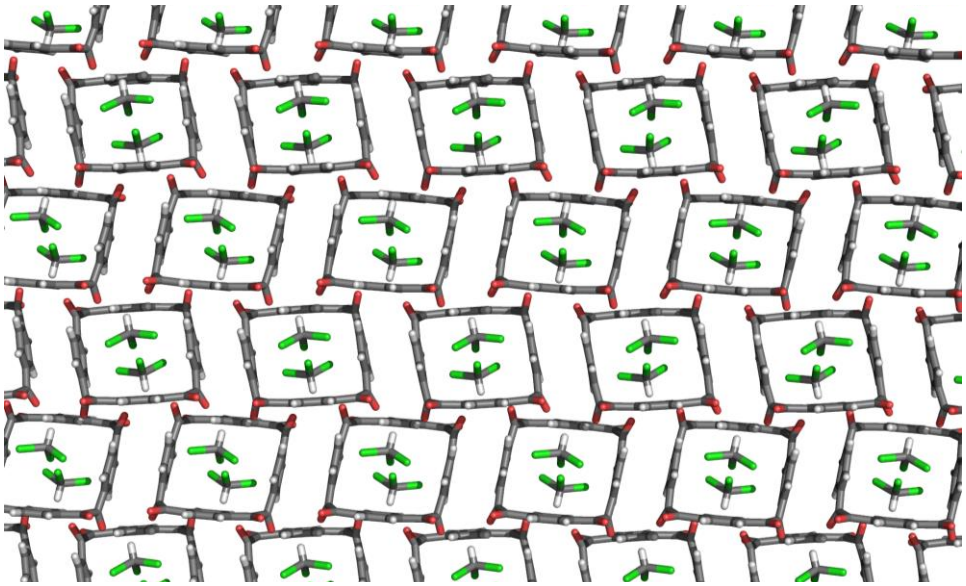

Figure 2.6 Segment of the crystal packing diagram of **7**·$CHCl_3$, shown along the crystallographic *a* axis. Element colors: C—gray, O—red, H—white, Cl—green. Disordered solvent molecules are omitted for clarity.

2.2.4.2 Crystal Growth of Cyclotetrabenzil from 1,5-Dichloropentane

The crystal structure of cyclotetrabenzil (**7**)**,** which is grown from 1,5-dichloropentane, is shown in Figure 2.7. Cyclotetrabenzil (**7**) crystallized in the *C*2/*c* space group, with four molecules of **7** and four molecules of 1,5-dichloropentane per monoclinic unit cell.

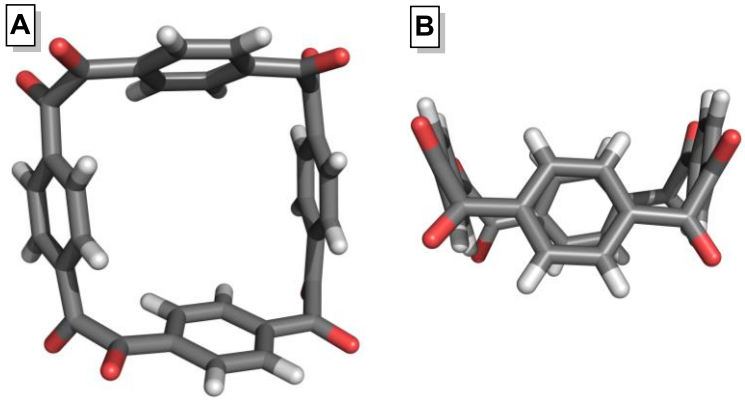

Figure 2.7 *(A)* The top-down view of the X-ray crystal structure of **7** grown from 1,5-dichloropentane, and *(B)* the side view showing the boat-like conformation. Element colors: C—gray, O—red, H—white. All solvent molecules are omitted for clarity.

The crystal structure of **7** grown from 1,5-dichloropentane is slightly changed compared with the crystal structure of cyclotetrabenzoin (**6**): the central cavity is expanded and its dimensions are now 7.22 × 7.39 Å, measured between the centroids of each opposite pair of benzene rings, revealing a boat-like crystal structure (Figure 2.7B). The tilt angle between a pair of the opposite benzene rings of **7** decreased to 23.0° while the other pair did not change, compared to 40.8° in cyclotetrabenzoin (**6**), measured between the planes of each two opposite benzene rings. The Ph–C–C–Ph dihedral angles ranged between 77.8 and 89.3° compared to 69° in **6**, which means the cyclotetrabenzil structure is unsymmetrically twisted. The O=C–C=O dihedral angles ranging from 81.3 to 92.4° in the adjacent C=O groups, which are arranged in a synclinal directions to each other. These angles are higher than the O=C–C–OH dihedral angles of α-hydroxyketone units in **6** (13°). Each two carbonyl groups attached to *para*-positions of the same benzene ring in **7** are pointed in the same directions.

Cyclotetrabenzil (**7**) complexed with 1,5-dichloropentane molecules in a 1:1 ratio. Molecules of 1,5-dichloropentane are seen in two orientations aligned with the main axis of macrocycles, and their chlorine atoms are tucked into the cavities of two neighboring cyclotetrabenzil molecules, forming a sandwich-like structure (Figure 2.8A). The distances

between chlorine atoms tucked into the cavity and the centroids of the benzene rings of the macrocycle ranged from 3.79 to 4.46 Å. The complexation pattern of **7**·$C_5H_{10}Cl_2$ repeated itself producing a continuous chain of 1,5-dichloropentane molecules surrounded by successive macrocycles, seen along the crystallographic *a* axis in Figure 2.8B. The chlorine atoms in 1,5-dichloropentane chain are separated by a distance of 3.77 Å with no apparent [Cl···Cl] interaction. This distance was measured between the chlorine atoms when [C–Cl···Cl] and [Cl···Cl–C] angles were 151.5 and 154.0°. It is noted that the [Cl···Cl] distance measured in complex **7**·$C_5H_{10}Cl_2$ is longer than the corresponding distance observed in complex **7**·$CHCl_3$.

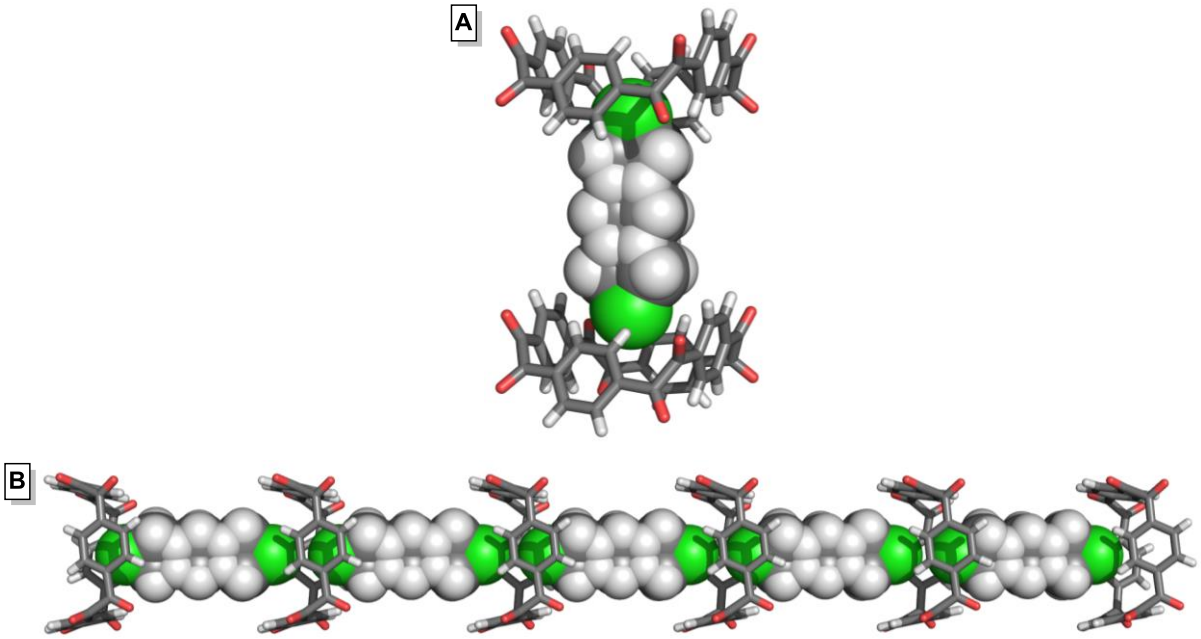

Figure 2.8 *(A)* Sandwich-like complex of **7**·$C_5H_{10}Cl_2$, and *(B)* continuous chain of 1,5-dichloropentane molecules included into consecutive cyclotetrabenzil (**7**), shown along the crystallographic *a* axis. Element colors: C—gray, O—red, H—white, Cl—green.

Same as in **7**·$CHCl_3$ complex, the electrostatic interactions and the isotropic van der Waals forces were not observed between the host macrocycles and the 1,5-dichloropentane guest molecules, but common cyclotetrabenzil molecules were found connected with the host-guest complex by short contacts in the range of 2.48–3.19 Å. This means the binding

pattern of **7**·$C_5H_{10}Cl_2$ is stabilized by the common short contacts established between the complex and the neighboring molecules.

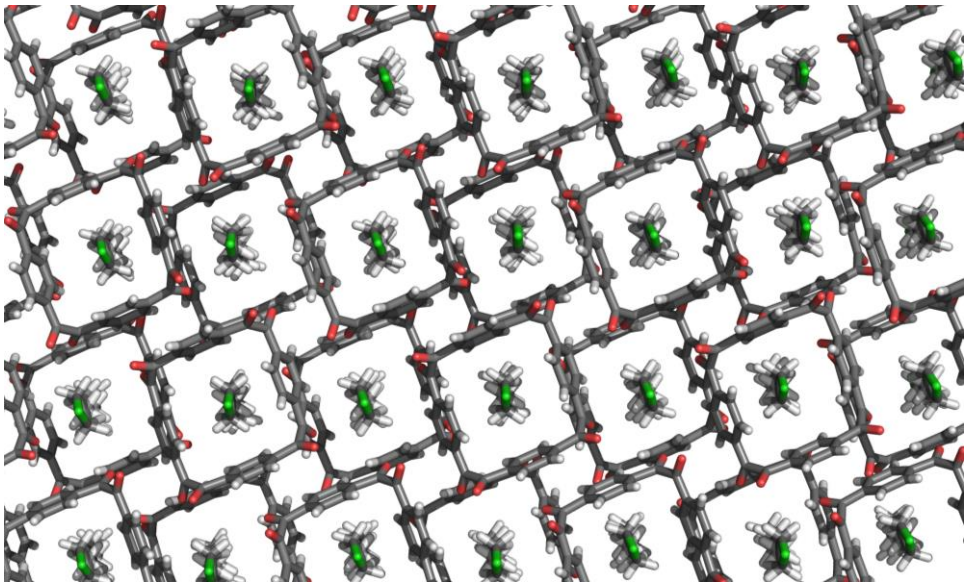

Figure 2.9 Segment of the crystal packing diagram of **7**·$C_5H_{10}Cl_2$, shown along the crystallographic *b* axis. Element colors: C—gray, O—red, H—white, Cl—green.

The crystal packing for **7**·$C_5H_{10}Cl_2$ is shown in Figure 2.9, viewed along the crystallographic *b* axis. Cyclotetrabenzil (**7**) similarly stacks in a parallel orientation and each molecule establishes a variety of short contacts with eight macrocycles and four 1,5-dichloropentane molecules. Specifically, two hydrogen atoms from each benzene rings in an opposite pair at **7** establish short [C–H···O] contacts (H···O distances are 2.60 and 2.68 Å) with two carbonyl oxygen atoms from two different neighboring molecules. Similarly, one hydrogen atom from each benzene rings in the other opposite pair at **7** establishes a short [C–H···O] contact (H···O distances are 2.53 Å) with one carbonyl oxygen from a neighboring molecule. Additionally, several short [C=O···H] contacts, with O···H distances ranging from 2.48 to 2.71 Å, were seen between the oxygen atoms in the carbonyl groups of **7** and the hydrogen atoms from the neighboring 1,5-dichloropentane molecules or neighboring macrocycles. This binding pattern is repeating itself in three dimensions forming symmetrical multi-layers of **7**·$C_5H_{10}Cl_2$ complex.

2.2.4.3 Crystal Growth of Cyclotetrabenzil from 1,6-Dichlorohexane

The single crystal of cyclotetrabenzil (**7**) grown from 1,6-dichlorohexane showed a preliminary crystal structure and packing diagram analogous to those found for the single crystal grown from 1,5-dichloropentane (Figure 2.10). There are slight differences noticed in measurements summarized in Table 2.1. The poor solubility of cyclotetrabenzil in 1,6-dichlorohexane led to the growth of very small crystals, which showed the molecules' connectivity but it could not be refined.

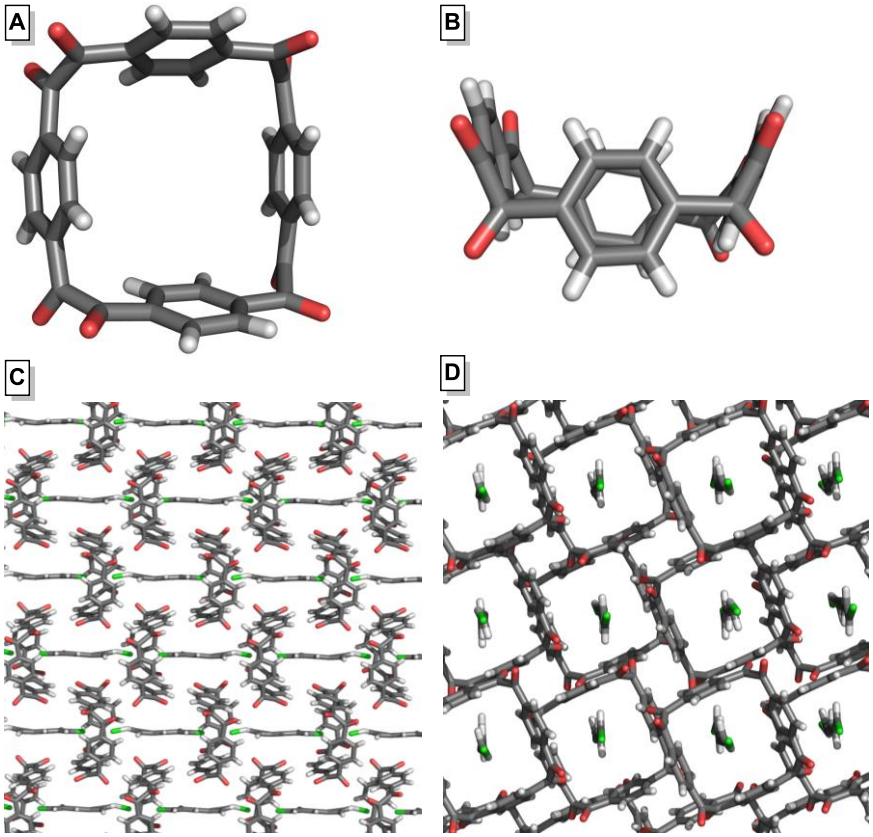

Figure 2.10 *(A)* The top-down view of the X-ray crystal structure of **7** grown from 1,6-dichlorohexane, *(B)* the side view showing the boat-like conformation, *(C)* segment of the crystal packing diagram of **7**·$C_6H_{12}Cl_2$ shown along the crystallographic *a* axis, and *(D)* same as *(C)* but shown along the crystallographic *b* axis. Element colors: C—gray, O—red, H—white, Cl—green. All solvent molecules are omitted in *(A)* and *(B)* for clarity.

Table 2.1 The differences in the measured distances and angles between **7**·$C_5H_{10}Cl_2$ and **7**·$C_6H_{12}Cl_2$ complexes.

	8b	**8c**
The distances between the centroids of each opposite pairs of benzene rings in cyclotetrabenzil, Å	7.22 7.39	7.31 7.39
The tilt angles between the planes of each opposite pairs of benzene rings in cyclotetrabenzil, º	23.0 40.8	18.9 33.7
The Ph–C–C–Ph dihedral angles, º	77.8–89.3	86.2–89.5
The O=C–C=O dihedral angles, º	81.3–92.4	87.9–94.6
The distances between chlorine atoms tucked into the cavity and the centroids of the benzene rings of the macrocycle, Å	3.79–4.46	3.72–4.34
The distances between the chlorine atoms from neighboring solvent molecules, Å	3.77	3.07

2.2.4.4 Crystal Growth of Cyclotetrabenzil from 1,1,2,2-Tetrachloroethane

The crystal structure of cyclotetrabenzil (**7**), which is grown from 1,1,2,2-tetrachloroethane, is shown in Figure 2.11. Cyclotetrabenzil (**7**) crystallizes in the $P\bar{1}$ space group, with two molecules of **7** and four molecules of 1,1,2,2-tetrachloroethane per the triclinic unit cell. The crystal structure of **7** shows a chair-like structure (Figure 2.11B) similar to the structure of cyclotetrabenzil grown from chloroform, but the single crystal of **7** grown from 1,1,2,2-tetrachloroethane is twinned in two different orientations with different dimensions of the same structure. In this molecule, one opposite pair of benzene rings is parallel and the other opposite pair of benzene rings is anti-parallel; all four benzene rings enclose a clear intramolecular cavity of dimensions 7.37 × 7.53 Å or 7.28 × 7.45 Å measured from the centroids of the parallel and anti-parallel benzene rings, respectively, with Ph–C–C–

Ph dihedral angles ranging from 73.0 to 89.9°. The neighboring C=O groups at each 1,2-diketone unit are synclinal with O=C–C=O dihedral angles varying between 73.8 and 92.7°.

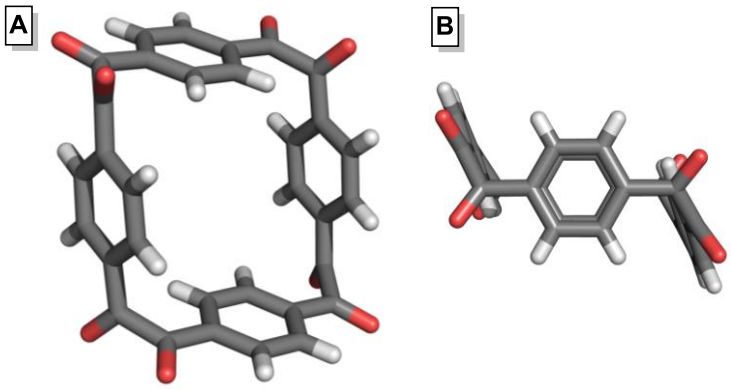

Figure 2.11 *(A)* The top-down view of the X-ray crystal structure of **7** grown from 1,1,2,2-tetrachloroethane, and *(B)* the side view showing the chair-like conformation. Element colors: C—gray, O—red, H—white. All solvent molecules are omitted for clarity.

Molecules of cyclotetrabenzil (**7**) formed an inclusion complex with 1,1,2,2-tetrachloroethane in a 1:2 ratio; one of 1,1,2,2-tetrachloroethane molecules is ordered and the other one is disordered and both are oriented to face the central cavity in **7**. Here, the measurements will be focused on the ordered molecule and ignore the disordered ones. The ordered 1,1,2,2-tetrachloroethane molecules are in a gauche conformation, with [H–C–C–H] dihedral angle of –63.7º, and distributed between the macrocycle molecules. One chlorine atom, from each two molecules aligned up and down with the main axis of macrocycles, is tucked into the central cavity of **7** in two orientations, leaving the rest of the molecule directed away from the central cavity of the macrocycle (Figure 2.12A). A tube of lined up cyclotetrabenzil molecules is seen along the crystallographic *b* axis. In this tube, the 1,1,2,2-tetrachloroethane molecules seemingly locate between the corners of cyclotetrabenzil molecules although they are oriented toward the central cavity of the **7** (Figure 2.12B,C). This was seen because cyclotetrabenzil molecules are inclined out of the main plane of the crystal lattice.

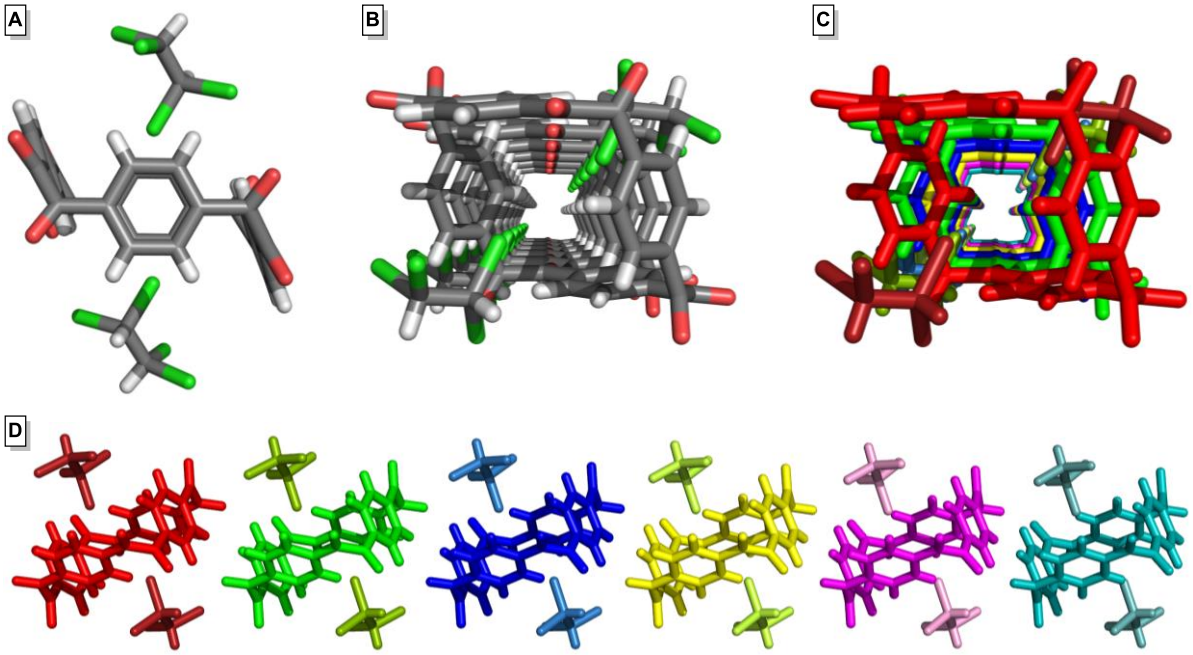

Figure 2.12 *(A)* The complexation of cyclotetrabenzil (**7**) with two molecules of 1,1,2,2-tetrachloroethane, *(B)* the positions of 1,1,2,2-tetrachloroethane molecules relative to cyclotetrabenzil tubes viewed along the crystallographic *b* axis, *(C)* same as *(B)* but highlighted in different colors, and *(D)* the **7**·$C_2H_2Cl_4$ complex viewing along the reciprocal cell axis a^*. Element colors: C—gray, O—red, H—white, Cl—green.

The distances between chlorine atoms tucked into the cavity and the centroids of the parallel benzene rings are 4.40 and 4.46 Å, and between them and the centroids of the anti-parallel benzene rings are 3.78 and 5.12 Å. The distance between the chlorine atoms directed toward the cavity is 5.05 Å, which means there is no interaction between these chlorine atoms. Same as in cyclotetrabenzil crystal grown from chloroform, no direct interaction was seen between the host macrocycles and 1,1,2,2-tetrachloroethane guest molecules except the common short contacts which were found connected the host-guest complex with neighboring molecules and they helped in stabilization the complex.

The extended structure of **7**·$C_2H_2Cl_4$ viewed along the crystallographic *b* axis is shown in Figure 2.13. Cyclotetrabenzil (**7**) molecules stack in a herringbone pattern with 1,1,2,2-tetrachloroethane molecules trapped between the voids of crystal lattice. Each cyclotetrabenzil molecule establish a collection of short contacts with ten macrocycles and

four 1,1,2,2-tetrachloroethane molecules of its neighbors: short [C–H···O] contacts, with H···O distances ranging between 2.45 and 2.71 Å, and short [C=O···C] contacts, with O···C distances ranging between 3.04 and 3.40 Å, as well as some short contacts established between the macrocycle and 1,1,2,2-tetrachloroethane. Specifically, one hydrogen atom from the anti-parallel benzene rings at one of the twins cyclotetrabenzil molecules establishes short contacts with carbonyl oxygen from neighboring molecule, and the anti-parallel benzene rings at the other twins cyclotetrabenzil molecules establishes [π···π] interaction with the anti-parallel benzene rings in neighboring molecules (centroid-centroid distance is 3.79 Å). Contrasting to cyclotetrabenzil crystal grown from chloroform, all the hydrogen atoms in parallel benzene rings from both twinned molecules of **7** establish short contacts with carbonyl oxygen atoms from neighboring molecules. An endless three dimensional network is formed due to the repeat of this contact pattern on each cyclotetrabenzil molecule.

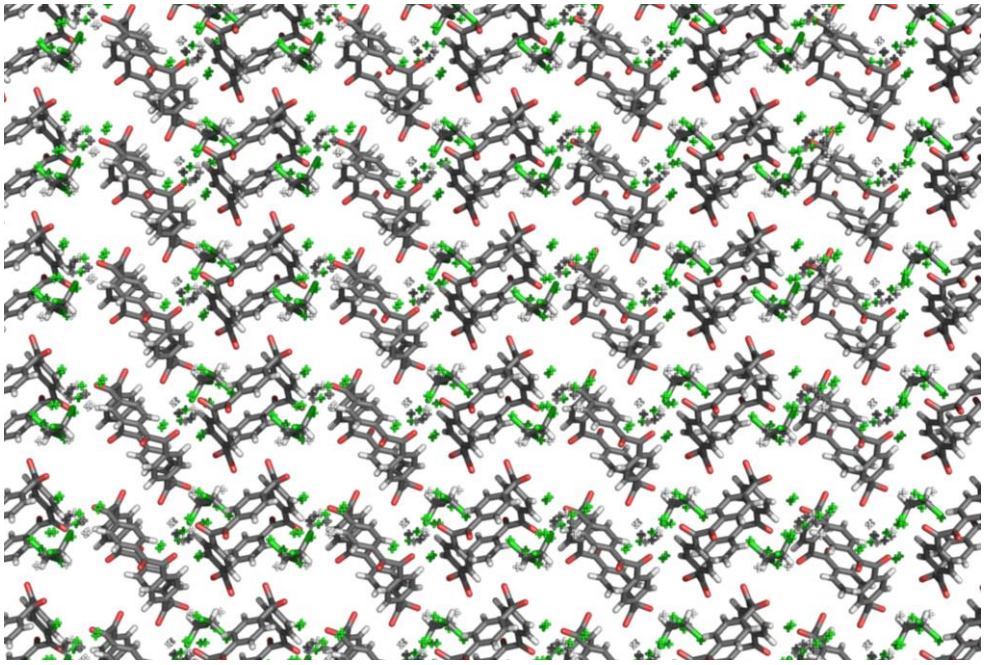

Figure 2.13 Segment of the crystal packing diagram of **7**·$C_2H_2Cl_4$, shown along the crystallographic *b* axis. Element colors: C—gray, O—red, H—white, Cl—green.

2.2.4.5 Crystal Growth of Cyclotetrabenzil from Bromoform

The crystal structure of cyclotetrabenzil grown from bromoform is shown in Figure 2.14. Cyclotetrabenzil (**7**) crystallizes in the $P2_1/n$ space group, with only two molecules of **7** per the monoclinic unit cell. Similar to the crystal structure of cyclotetrabenzil grown from chloroform, the macrocycle was deformed to make a chair-like structure as shown in Figure 2.14B. In this structure, one opposite pair of benzene rings is parallel and the other opposite pair is anti-parallel with no tilt angles between the rings on the opposite sides of the macrocycle. Thus, they define a clear intramolecular cavity of dimensions 7.63 × 7.42 Å measured between the centroids of the parallel and anti-parallel benzene rings, respectively, with Ph–C–C–Ph dihedral angles varying between 80.2 and 88.9°. The 1,2-diketone units in this crystal structure have O=C–C=O dihedral angles ranging from 82.1 to 88.3° and the neighboring C=O groups are in a synclinal stereochemical arrangement.

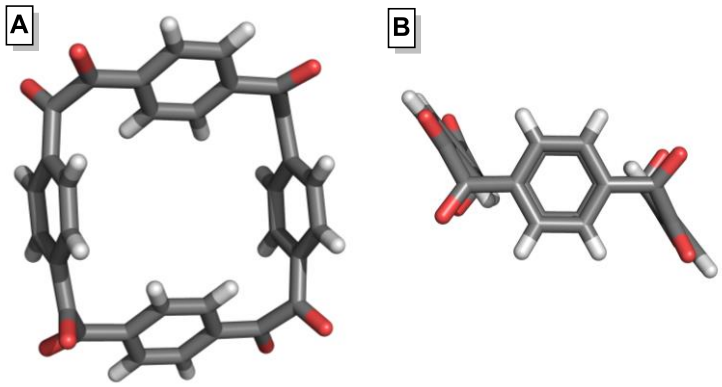

Figure 2.14 *(A)* The top-down view of the X-ray crystal structure of **7** grown from bromoform, and *(B)* the side view showing the chair-like conformation. Element colors: C—gray, O—red, H—white.

The crystal packing diagram of cyclotetrabenzil (**7**), grown from bromoform, viewed along the crystallographic *c* axis in Figure 2.15. Cyclotetrabenzil closely stack in a herringbone pattern with no voids between the molecules. Each cyclotetrabenzil (**7**) molecule establishes an assortment of short contacts with fourteen neighboring molecules: short [C–

H···O] contacts (H···O distances range between 2.34 and 2.69 Å) with ten of its neighboring molecules and short [C=O···C] contacts (O···C distance is 3.20 Å) with four of its neighboring molecules. Specifically, one hydrogen atom from the anti-parallel benzene rings at **7** establishes short contacts with carbonyl oxygen from neighboring molecule, and the carbon attached to this hydrogen establishes short contact with the same carbonyl oxygen. Unlike the crystal structure of cyclotetrabenzil grown from chloroform, where the hydrogen atoms of parallel benzene rings did not establish any short contacts with the neighboring molecules, here each hydrogen atom in parallel benzene rings establishes short contact with carbonyl oxygens from four neighboring molecules. These contacts are reproduced on each cyclotetrabenzil molecule, forming an infinite network. In contrast to the crystal structure of cyclotetrabenzil grown from chloroform, there is no evidence for the presence of the bromoform molecules neither in the intrinsic nor in the extrinsic pores in this crystal lattice.

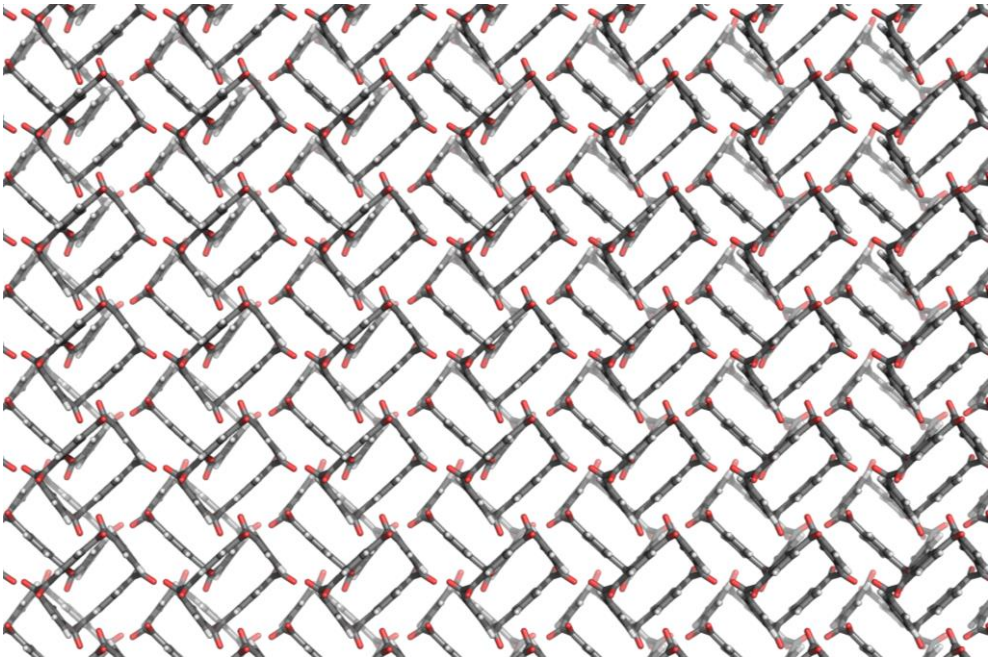

Figure 2.15 Segment of the crystal packing diagram of cyclotetrabenzil (**7**) grown from bromoform and shown along the crystallographic *c* axis. Element colors: C—gray, O—red, H—white.

From all crystal structures of cyclotetrabenzil (**7**) obtained from different alkyl halide solvents, it is noted that cyclotetrabenzil (**7**) has a high affinity to solvate with chlorinated alkanes but not with brominated ones. This feature was demonstrated by the high exchange-repulsion energy between [Br···Br] in the modeled bromoform dimer (2.19 kcal mol^{-1}), compared to 1.25 kcal mol^{-1} between [Cl···Cl] in chloroform dimer, which destabilize the dimer and almost compensates for the stabilizing dispersion energy of −2.60 kcal mol^{-1} as shown in Table 2.2.[263,264] Although the difference between the exchange-repulsion energy of bromoform dimer and chloroform dimer is minimal (0.94 kcal mol^{-1}), sometimes minor differences can make a significant change such as the barrier to rotation in ethane which needs only 2.90 kcal mol^{-1} to turn the molecule from the least stable conformer (eclipsed) to the most stable one (staggered).[265–267]

Table 2.2 Calculated interaction energy (MP2) and SAPT decomposition of the $(CHCl_3)_2$ and $(CHBr_3)_2$ dimers. All energy values are given in (kcal mol^{-1}). The equilibrium [Cl···Cl] and [Br···Br] distances, and dipole moment of each isolated monomer are also indicated.

	r (Å)	μ (d)	E_{el}	E_{ex}	E_{ind}	E_{disp}	$E_{int,SAPT}$	$E_{int,MP2}$
$(CHCl_3)_2$	3.43	1.28	–0.03	1.25	–0.21	–1.61	–0.59	–0.55
$(CHBr_3)_2$	3.53	1.05	–0.08	2.19	–0.50	–2.60	–0.99	–0.95

From the structural point of view, this difference in solvation between cyclotetrabenzil (**7**) and alkyl chloride solvents can be explained by 'bumps fit into hollows' and 'nature abhors a vacuum' principles. Since close packing is very important to build organic crystals, the solvate forms to decrease the voids between molecules, thus leading to more efficient packing.[268,269] In the crystal packing of **7** grown from bromoform, the

macrocycle molecules arranged themselves tightly in order to prevent the presence of any void, therefore no space was left to accommodate bromoform molecules (Figure 2.16B).

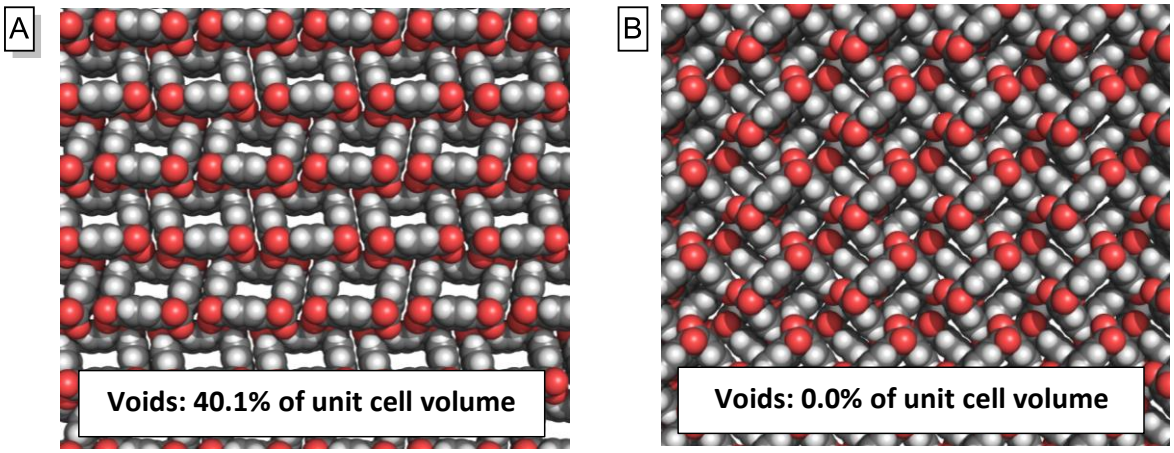

Figure 2.16 Comparison between the crystal packing of cyclotetrabenzil (**7**) grown from *(A)* chloroform and *(B)* bromoform. Element colors: C—gray, O—red, H—white. All solvent molecules are omitted for clarity. The % of voids are measured by Mercury 4.3.1 software.

Moreover, the host cavity of cyclotetrabenzil (**7**) could be too small to encapsulate halide ions which have van der Waals radii larger than that of chlorine; van der Waals radii of chlorine and bromine atoms are 1.80 and 1.95 Å, respectively.[270,271] In this case, the host cavity of **7** could lose its electrostatic binding affinity due to the introduction of brominated solvents which have bromine atoms larger than the capacity of the cavity (Figure 2.17). These phenomena are qualitatively similar to the binding interactions which were seen during the filling of the cavity of protein folding by mutants.[272,273] The introduction of bulky mutants within the core of the protein causes strain which is observed through the distortion of bond angles and the formation of unfavorable van der Waals contacts.

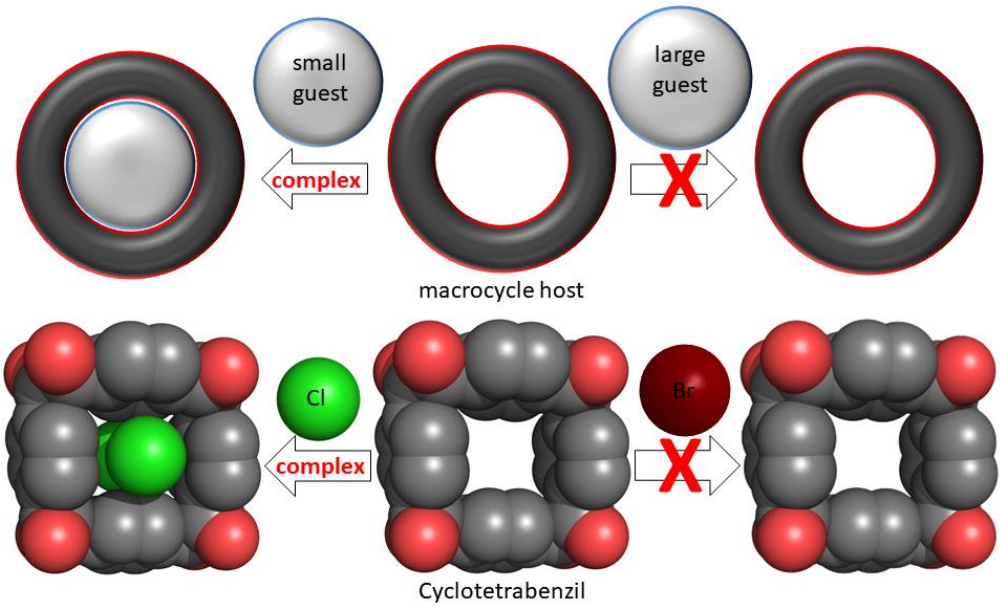

Figure 2.17 The capability of cyclotetrabenzil (**7**) to host chlorinated alkanes but not brominated ones.

In collaboration with Dr. Wu group, the explanation of the solvation behavior of cyclotetrabenzil (**7**) with chloroform and bromoform was theoretically attempted. The electrostatic potential (ESP) plot of cyclotetrabenzil (**7**) shows that the inner region of the macrocycle is electropositive (blue region in Figure 2.18), so solvent molecules may complex to the macrocycle through electrostatic interactions.

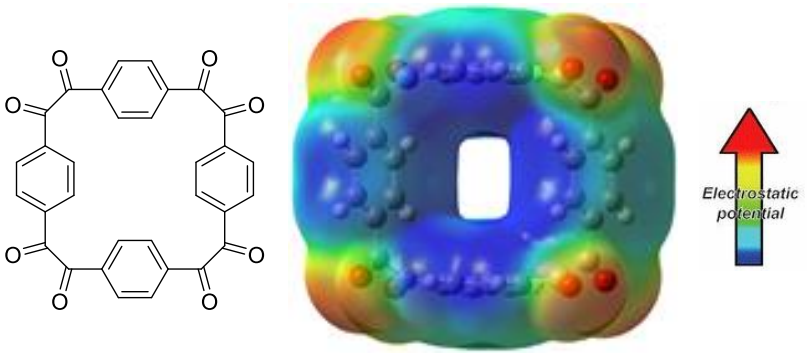

Figure 2.18 Electrostatic potential plot of the cyclotetrabenzil (**7**) computed at isovalue = 0.0004.

The optimized structures of cyclotetrabenzil (**7**) before and after complexation with chloroform and bromoform showed that the calculated complexation to bromoform

significantly distorted the macrocycle structure (Figure 2.19). This may prevent the dimerization of bromoform within the cavity of **7**.

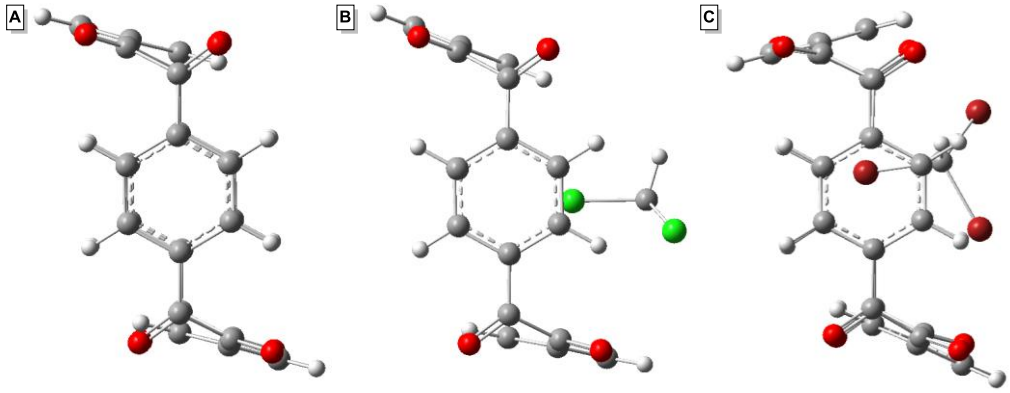

Figure 2.19 *(A)* The optimized structures of cyclotetrabenzil (**7**) before complexation, *(B)* after complexation with chloroform, and *(C)* after complexation with bromoform, performed at the B3LYP-D3/6-31+G(d) level of theory.

The interaction energies between optimized cyclotetrabenzil (**7**), when it was complexed with one and two molecules of chloroform or bromoform, were calculated. The interaction energy of complexing one molecule of bromoform with **7** (–50.44 kcal mol^{-1}) was significantly higher than that when one chloroform molecule complexing with **7** (–10.66 kcal mol^{-1}). Dimerization of the guest molecule slightly increases the energy of **7**·$CHCl_3$ complex (–11.05 kcal mol^{-1}) and dramatically decreases the energy of **7**·$CHBr_3$ complex (–36.54 kcal mol^{-1}), thus illustrating that the complexation of **7** with one bromoform molecule weakens the interaction with the second bromoform molecule. Unfortunately, the calculated interaction energies did not explain why cyclotetrabenzil (**7**) prefers to solvate with chlorinated solvents but not bromoform because the interaction energy between optimized cyclotetrabenzil (**7**) with two molecules of bromoform is still higher than the interaction energy of it with two molecules of chloroform.

All of the previous proposed reasons did not explain exactly why cyclotetrabenzil crystals tend to solvate with chlorinated solvents but not bromoform. Changing the crystal

growth methodology probably produces crystals have a potential to solvate with bromoform or with other brominated solvents.

2.2.5 Oxidative Cleavage of Cyclotribenzoin and Cyclotetrabenzoin

Two novel oligomers: 3,3'-dibenzoic acid (**10**) and 4,4'-dibenzoic acid (**11**), were obtained from the oxidative cleavage of cyclotribenzoin (**4**) and cyclotetrabenzoin (**6**), respectively, using concentrated nitric acid (Scheme 2.6).

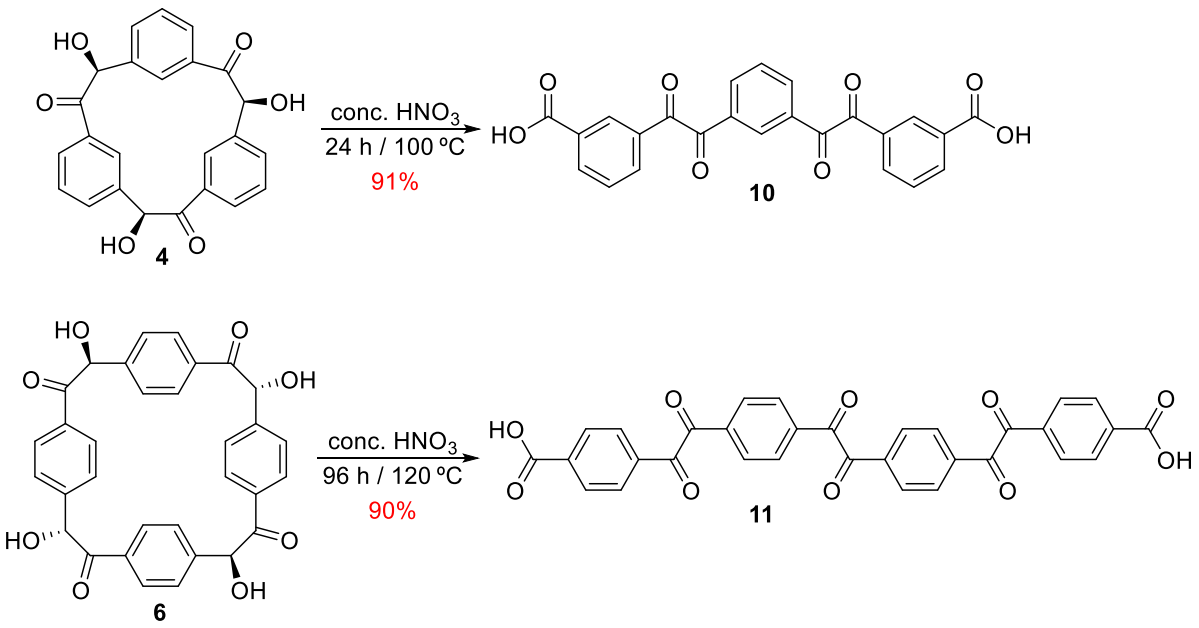

Scheme 2.6 The oxidative cleavage of cyclotribenzoin (**4**) (top) and cyclotetrabenzoin (**6**) (bottom).

The exact oxidation conditions of **6** were applied on cyclotribenzoin **4** in order to get cyclotribenzil, but the result was unexpected: cyclotribenzoin (**4**) was oxidatively cleaved to give 3,3'-dibenzoic acid (**10**) in 91% yield after one day. Oligomeric 4,4'-dibenzoic acid (**11**) was first seen as a by-product during the oxidation process of cyclotetrabenzoin (**6**), but then it was isolated as a pure compound in a 90% yield by increasing the time, the temperature, and the number of equivalents of nitric acid.

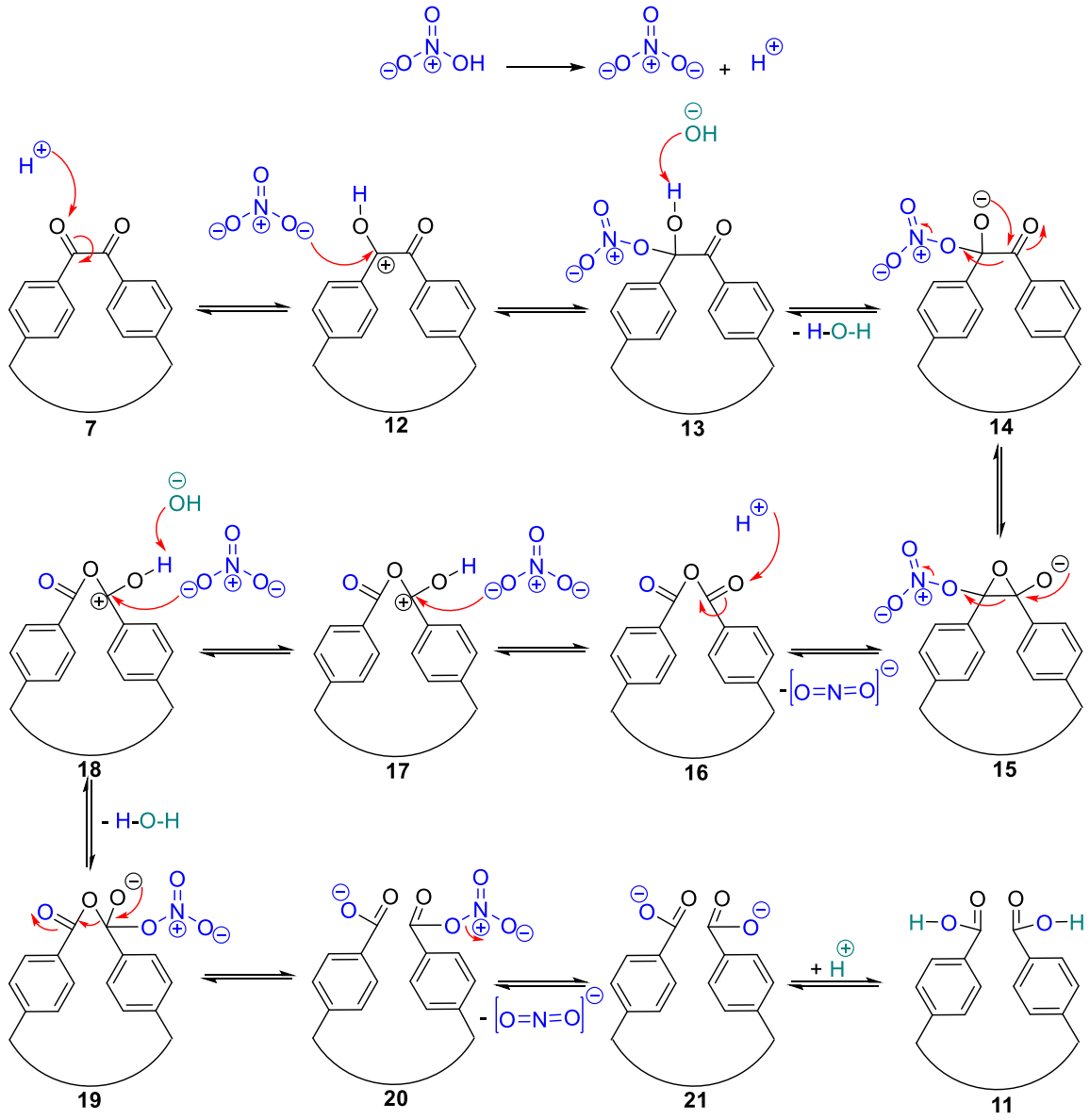

Scheme 2.7 Proposed mechanism for the oxidative cleavage of 1,2-diketones units in cyclic octaketone (**7**) to dicarboxylic acids (**11**).

When cyclotribenzoin (**4**) and cyclotetrabenzoin (**6**) were oxidized under vigorous conditions, the initial cyclic products underwent carbon–carbon oxidative bond cleavage [O=**C–C**=O] in one of the 1,2-diketone units, producing dibenzoic acid compounds **10** and **11**. The oxidation of **4** could not cleanly produce the corresponding hexaketone; instead, a significant amount of ring-opened product **10** was observed, whereas octaketone which produced from the oxidation of **6** was isolable as illustrated in the previous section, and its

ring-opened analog **11** was observed as a by-product during the oxidation under harsh conditions. This is a proof for that the carbon–carbon oxidative bond cleavage occurred after the oxidation of α-hydroxyketone units to 1,2-diketone units following the suggested mechanism shown in Scheme 2.7. The oxidation of **4** *in situ*, immediately followed imine condensation with 1,2-phenylenediamines, produces isolable trisquinoxaline compounds which have very twisted structures.[274]

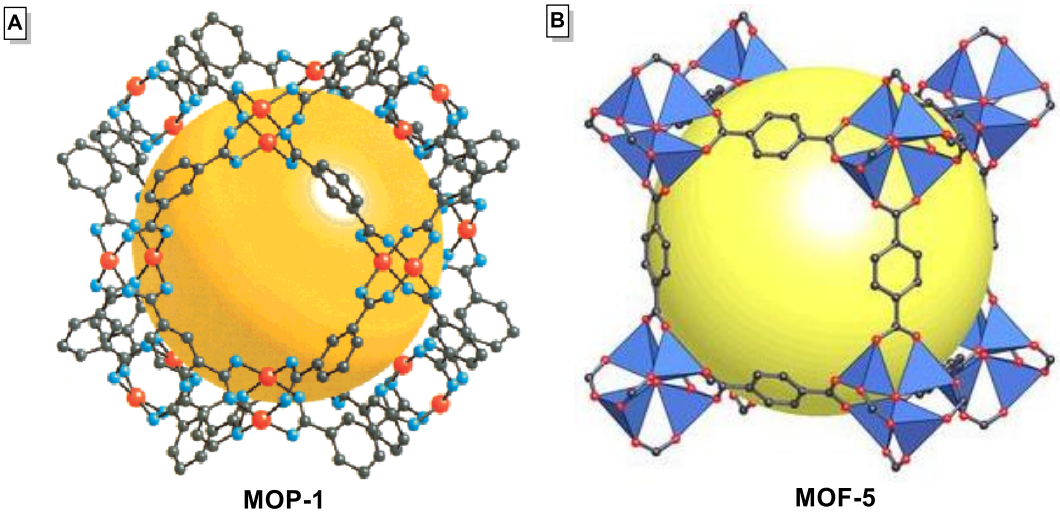

Figure 2.20 *(A)* Structure of MOP-1 (adapted from ref. 275 with permission, copyright © 2001 American Chemical Society) and *(B)* Structure of MOF-5 (adapted from ref. 276 with permission, copyright © 1999 Nature Publishing Group) synthesized by Yaghi and co-workers.

As new dicarboxylic acid compounds were produced, utilizing them as linkers to synthesize metal-organic frameworks (MOFs) was an experiment worth trying. Compounds 3,3'-dibenzoic acid (**10**) and 4,4'-dibenzoic acid (**11**) were solvothermally treated with transition metal salts. The results were disappointing: the single crystal X-ray diffraction analysis for the obtained crystals exhibited that the mixture of **10** and hydrated $Cu(NO_3)_2$ in DMF at 100 ºC produced porous metal−organic polyhedron MOP-1 (Figure 2.20A) and the product of the reaction of **11** with hydrated $Zn(NO_3)_2$ in DMF at 100 ºC was metal-organic frameworks MOF-5 (Figure 2.20B).[275,276] This means that both dicarboxylic acid compounds

underwent further oxidative cleavages of C–C bonds at all 1,2-diketone units at high temperatures, producing the corresponding monomers (isophthalic acid and terephthalic acid) which then reacted with metal salts and produced MOP-1 and MOF-5.

2.3 Conclusions and Outlook

In conclusion, we have shown that the reduction of cyclotribenzoin and the oxidation of cyclotetrabenzoin can be achieved by using sodium borohydride as the reducing agent and nitric acid as the oxidizing agent. The resulting cyclotrihydrobenzoin and cyclotetrabenzil were fully characterized by ^{1}H NMR, ^{13}C NMR, mass spectroscopy, infrared spectroscopy, elemental analysis, and X-ray crystallography. On one hand, the crystallographic analysis of cyclotrihydrobenzoin showed that the individual molecules oriented their –OH groups convergently in order to create extrinsic hydrophilic voids to accommodate tetrahedral hydrogen-bonded water clusters. On the other hand, the crystal structures of cyclotetrabenzil in different alkyl halide solvents revealed the ability of such macrocycles to solvate with chlorinated solvents but not with bromoform. The future work will be oriented at exploring the possibility to oxidize cyclotribenzoin and reduce cyclotetrabenzoin in order to produce analogously intrinsic or extrinsic functional pores and study their potential to stabilize other species. Additionally, the capability to use synthesized cyclotrihydrobenzoin and cyclotetrabenzil as scaffolds for further reactions, such as the reaction between cyclotrihydrobenzoin with diboronic acid and aldol condensation between cyclotetrabenzil with dibenzyl ketone, will be attempted.

Under harsh oxidation conditions, cyclotribenzoin and cyclotetrabenzoin were oxiditively cleaved and two dibenzoic acid molecules were obtained. The poor solubility of these compounds precluded further studies of their reactivity.

2.4 Experimental Section

2.4.1 General Materials and Physical Methods

Materials. All reactions were performed in a fume hood in oven-dried glassware. All starting materials and solvents, which were used for syntheses or crystal growth, were obtained from the commercial sources and used without further purification. Cyclotribenzoin **5** and cyclotetrabenzoin **7** were synthesized according to the procedures reported in literature.[187,188]

Physical Methods. All NMR spectra were recorded on a JEOL ECA-500 and ECA-600 spectrometers, with working frequencies for ^{1}H nuclei of 500 and 600 MHz, and for ^{13}C nuclei of 125 and 150 MHz, respectively. ^{1}H and ^{13}C NMR chemical shifts (δ) were reported in parts per million (ppm) units relative to the residual signals of deuterated solvent (^{1}H: DMSO-d_6, 2.50 ppm; ^{13}C: DMSO-d_6, 39.5 ppm). All NMR spectra were recorded at ambient temperature. The multiplicities of ^{1}H NMR signals were described as follows: s = singlet, d = doublet, t = triplet, q = quartet, m = multiplet, dd = doublet of doublet. The ^{13}C NMR signal structure was analyzed by DEPT (Distortionless Enhancement by Polarization Transfer), which is a tool used to assign ^{13}C NMR peaks, and described as follows: (+) = primary or tertiary C atom "positive signal", (−) = secondary C atom "negative signal", and (Cq) = quaternary C atom "no signal". Melting points were measured in a Barnstead International 1101D MeL-Temp capillary MP apparatus equipped with a Fluke 51-2 Thermometer, and are uncorrected. Mass spectra were recorded using electrospray ionization high resolution mass spectrometry (ESI-HRMS) and were collected at University of Texas at Austin by Dr. Ian M Riddington and his assistants. Infrared spectra (IR) were recorded on a Nicolet iS10 FT-IR spectrometer equipped with a Thermo Scientific iTR for multi-purpose ATR sampling and reported in wavenumbers (cm^{-1}) as solid phase measurement. Elemental analyses were conducted by Intertek USA Inc. Single crystal XRD measurement was performed by Dr.

Wiqu Wang (UH) using a Bruker DUO platform diffractometer equipped with a 4K CCD APEX II detector and an Incoatec 30 Watt Cu microsource with compact multilayer optics.

2.4.2 Syntheses and Characterization of Compounds 5, 7, 10, and 11

2.4.2.1 Synthesis and Characterization of Cyclotrihydrobenzoin (5)

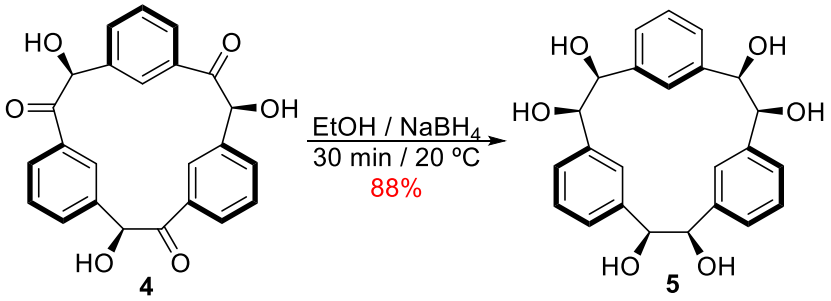

Cyclotribenzoin (**4**, 2.5 mmol, 1.01 g) was suspended in EtOH (25 mL) in a 100-mL round-bottomed flask equipped with a stirring bar. While the suspension was stirring, sodium borohydride (10.0 mmol, 378.3 mg, 4.00 equiv.) was carefully added to the mixture in small portions over the course of 5 min. The suspension was stirred for 30 min, and then placed in an ice bath. Then, deionized water (25 mL) and 6M HCl (3 mL) were added, while the temperature was kept under 5 ºC. Another portion of deionized water (25 mL) was added after a while, and the mixture was left to stir overnight at ambient temperature. The resulting white product was collected by suction filtration and rinsed with water (50 mL) and ether (50 mL), to afford a white product of cyclotrihydrobenzoin (**5**). Yield: 899 mg, 2.2 mmol, 88%, m.p. > 260 °C for the dehydrated material, but the loss of crystallization H_2O is apparent in the 120–130 °C range. ^{1}H NMR (DMSO-d_6, 500 MHz): δ = 7.00–7.09 (m, 9H), 6.14 (s, 3H), 5.01 (s, 6H), 4.62 (s, 6H) ppm. ^{13}C NMR (DMSO-d_6, 125 MHz): δ = 140.50 (Cq), 126.72 (+), 126.55 (+), 125.98 (+), 76.98 (+) ppm. IR (neat): $\tilde{\nu}$ = 3322, 2860, 1396, 1281, 1211, 1162, 1107, 1065, 1050, 1032, 919, 901, 781, 737, 699, 665, 604, 532 cm^{-1}. ESI-HRMS: *m/z* [M+Na]$^{+}$: Calcd for [$C_{24}H_{24}O_6$·Na]$^{+}$: 431.43; Found 431.15, with correct isotope distribution.

Elemental analysis Calcd (%) for $C_{24}H_{24}O_6$: C 62.33, H 6.54, O 31.13, N 0.00; Found: C 62.34, H 6.48, O 31.18, N < 0.05.

2.4.2.2 Synthesis and Characterization of Cyclotetrabenzil (7)

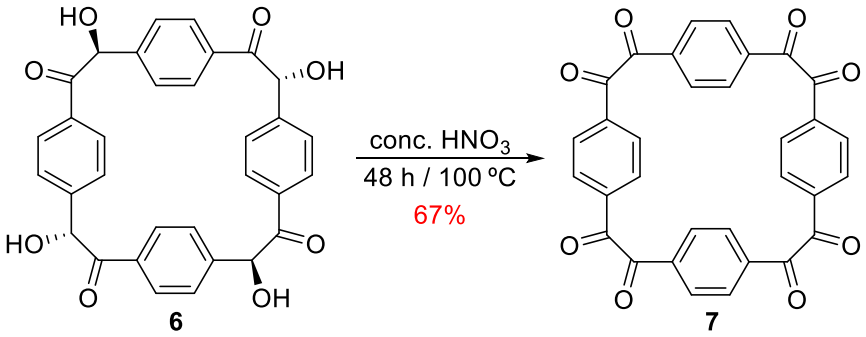

Cyclotetrabenzoin (**6**, 10.0 mmol, 5.37 g) and concentrated nitric acid (200 mL) were added to a 500-mL round-bottomed flask equipped with a stirring bar. The mixture was heated at 100 °C and the brown fumes of NO_2 started evolving after 1 h. After 48 h, when the evolution of NO_2 seized, the mixture was cooled to room temperature and carefully quenched the excess nitric acid with deionized water (200 mL), filtered by suction, and washed with deionized water (100 ml), EtOH (100 mL), and Et_2O (100 mL), respectively. The resulting crude solid was purified by Soxhlet extraction using dichloromethane (500 mL). The extract was evaporated using rotary evaporator to afford a pure yellow solid of cyclotetrabenzil (**7**). Yield: 3.51 g, 6.65 mmol 67%. m.p. > 350 °C (decomposition). ^{1}H NMR (DMSO-d_6, 500 MHz): δ = 7.86 (s, 16H) ppm. ^{13}C NMR (DMSO-d_6, 125 MHz): δ = 195.04 (Cq), 136.34 (Cq), 130.97 (+), 130.2 (+) ppm. IR (neat): $\tilde{\nu}$ = 1692, 1678, 1497, 1404, 1273, 1204, 1182, 896, 737, 691, 672, 646, 626 cm^{-1}. ESI-HRMS: *m/z* [M+Cl]$^-$: Calcd for [$C_{32}H_{16}O_8$·Cl]$^-$: 563.92; Found 563.05, with correct isotope distribution. Elemental analysis Calcd (%) for $C_{32}H_{16}O_8$: C 72.73, H 3.05; Found: C 71.26, H 3.02.

2.4.2.3 Synthesis and Characterization of Oligomeric 3,3'-Dibenzoic Acid (10)

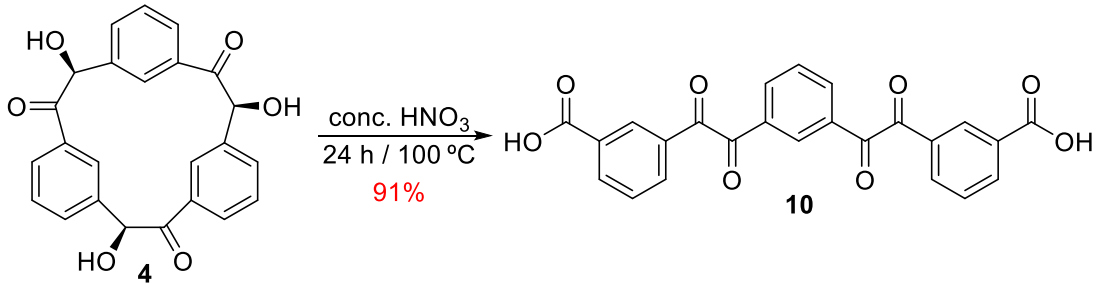

Cyclotribenzoin (**4**, 3.8 mmol, 1.51 g) and concentrated nitric acid (75 mL) were added to a 250-mL round-bottomed flask equipped with a stirring bar. The mixture was heated at 100 °C. After 24 h, the mixture was cooled to room temperature and carefully quenched with deionized water (75 mL). The resulting solid was collected by suction filtration and rinsed with water (75 ml), EtOH (75 mL), and Et_2O (75 mL), respectively, to afford a yellow 3,3'-dibenzoic acid product (**10**). Yield: 1.47 g, 3.41 mmol, 91%, m.p. ~ 310 °C. ^{1}H NMR (DMSO-d_6, 600 MHz): δ = 8.52 (s, 1H), 8.43 (s, 2H), 8.34 (d, J=7.6 Hz, 2H), 8.27 (d, J=7.6 Hz, 2H), 8.20 (d, J=7.6 Hz, 2H), 7.83 (t, J=7.6 Hz, 1H), 7.73 (t, J=7.6 Hz, 2H) ppm. ^{13}C NMR (DMSO-d_6, 150 MHz): δ = 192.48 (Cq), 192.39 (Cq), 166.73 (Cq), 136.68 (+), 136.13 (+), 134.59 (+), 133.34 (Cq), 132.99 (Cq), 132.21 (Cq), 131.46 (+), 131.04 (+), 130.99 (+), 130.44 (+) ppm. IR (neat): $\tilde{\nu}$ = 3073, 2562, 1665, 1602, 1418, 1312, 1181, 1165, 1108, 969, 935, 734, 718, 686, 668, 661, 649, 554 cm^{-1}. ESI-HRMS: *m/z* $[M+Na]^+$: Calcd for $[C_{24}H_{14}O_8 \cdot Na]^+$: 453.35; Found 453.06, with correct isotope distribution. Elemental analysis Calcd (%) for $C_{24}H_{14}O_8$: C 66.98, H 3.28, O 29.74; Found: C 65.83, H 2.90, O 28.22.

2.4.2.4 Synthesis and Characterization of Oligomeric 4,4'-Dibenzoic Acid (11)

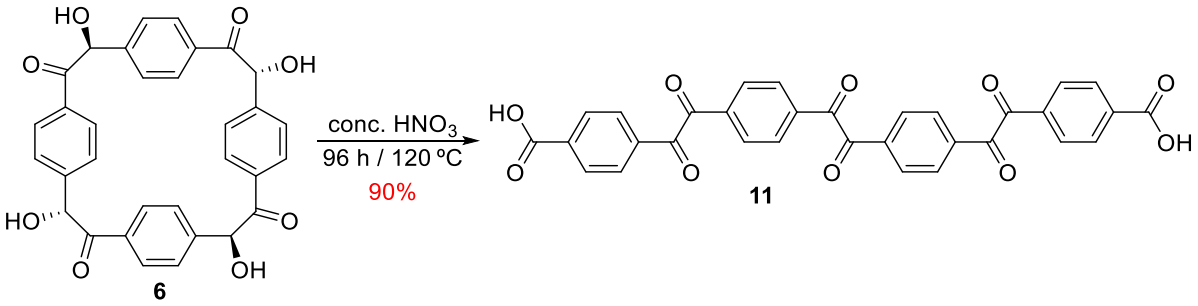

Cyclotetrabenzoin (**6**, 2.5 mmol, 1.34 g) and concentrated nitric acid (100 mL) were added to a 250-mL round-bottomed flask equipped with a stirring bar. The mixture was heated at 120 °C. After 96 h, the mixture was cooled to room temperature and carefully quenched with deionized water (100 mL). The resulting solid was collected by suction filtration and rinsed with water (100 ml), EtOH (100 mL), and Et_2O (100 mL), respectively, to afford a yellow 4,4'-dibenzoic acid product (**11**). Yield: 1.27 g, 2.25 mmol, 90%, m.p. ~ 416 °C. ^{1}H NMR (DMSO-d_6, 600 MHz): δ = 8.17 (d, J=8.9 Hz, 4H), 8.14 (d, J=8.2 Hz, 4H), 8.10 (d, J=8.2 Hz, 4H), 8.06 (d, J=8.9 Hz, 4H) ppm. ^{13}C NMR was not measured for this compound because it is slightly soluble in DMSO-d_6 and completely insoluble in the other common deuterated solvents. IR (neat): $\tilde{\nu}$ = 3058, 1664, 1405, 1296, 1201, 886, 864, 848, 831, 811, 795, 778, 723, 690, 533, 524 cm^{-1}. ESI-HRMS: *m/z* [M-H]$^-$: Calcd for [$C_{32}H_{18}O_{10}$·H]$^-$: 561.49; Found 561.08, with correct isotope distribution. Elemental analysis Calcd (%) for $C_{32}H_{18}O_{10}$: C 68.33, H 3.23, O 28.44; Found: C 66.11, H 3.48, O 29.72.

2.4.3 X-ray Crystallographic Analyses of Compounds 5, 7, and 11

2.4.3.1 Crystal Growth and Crystal Data of Cyclotrihydrobenzoin (5)

Single crystals of cyclotrihydrobenzoin (**5**) suitable for X-ray diffraction analyses were obtained by dissolving crude **5** (15 mg) in off-the-shelf THF (3 mL). The product

solution was heated and filtered using PTFE syringe filters (0.22 μm, 30 mm). The resulting filtrate (0.15 mL) was added to a 0.75 mL round-bottomed culture tube, and this tube was placed inside a 2 dram scintillation vial containing either *n*-hexane or *n*-pentane (1 mL) as the diffusing solvent. The vial was tightly closed and kept at ambient conditions without external disturbances. After five days, colorless needle-like crystals were obtained by vapor diffusion technique. Slow evaporation crystallization strategy also produced single crystals suitable for X-ray diffraction analysis during two weeks when the crude cyclotrihydrobenzoin (5 mg) was dissolved in isopropanol (1 mL) and the solution added to capped NMR tube equipped with a needle to facilitate the evaporation process.

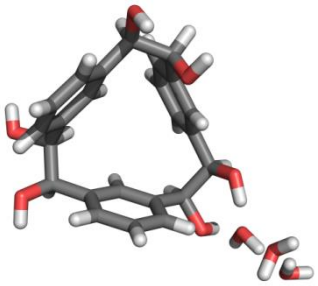

Table 2.3 Crystallographic Data and Structure Refinement of **5**·3H_2O.

Empirical formula	$C_{48}H_{58}O_{17}$	
Formula weight	906.94	
Temperature	123(2) K	
Wavelength	CuKα (λ = 1.54178 Å)	
Crystal system	Monoclinic	
Space group	*C*2/*c*	
Unit cell dimensions	a = 29.7217(3) Å	α = 90°
	b = 9.6922(10) Å	β = 132.61°
	c = 20.5407(4) Å	γ = 90°
Volume	4354.88(11) $Å^3$	
Z	4	
Density (calculated)	1.383 Mg/m^3	

Table 2.3 Continued

Absorption coefficient	0.875 mm^{-1}
$F(000)$	1928
Crystal size	0.15 × 0.06 × 0.01 mm^3
2θ range for data collection	4.042 to 66.678°.
Index ranges	$-35 \leq h \leq 34$, $-11 \leq k \leq 11$, $-24 \leq l \leq 23$
Reflections collected	19409
Independent reflections	3827 [$R_{(int)} = 0.0271$]
Completeness to $2\theta = 66.678°$	99.1 %
Absorption correction	Empirical
Refinement method	Full-matrix least-squares on F^2
Data / restraints / parameters	3827 / 0 / 321
Goodness-of-fit on F^2	1.048
Final R indices [$I>2\sigma(I)$]	$R_1 = 0.0410$, w$R_2 = 0.1124$
R indices (all data)	$R_1 = 0.0447$, w$R_2 = 0.1158$
Largest diff. peak and hole	0.46 and –0.26 e $Å^{-3}$

2.4.3.2 Crystal Growth and Crystal Data of Cyclotetrabenzil (7)

Single crystals of cyclotetrabenzil (**7**) suitable for X-ray diffraction analyses were obtained by dissolving crude **7** (20 mg) in alkyl halide solvents (3 mL): chloroform, 1,5-dichloropentane, 1,6-dichlorohexane, 1,1,2,2-tetrachloroethane, or bromoform. The product solution was heated and filtered using PTFE syringe filters (0.22 μm, 30 mm). The resulting filtrate (0.15 mL) was added to a 0.75 mL round-bottomed culture tube, and this tube was placed inside a 2 dram scintillation vial containing *n*-hexane (1 mL) as the diffusing solvent. The vial was tightly closed and kept at ambient conditions without external disturbances. After seven days, yellow crystals were obtained by vapor diffusion technique.

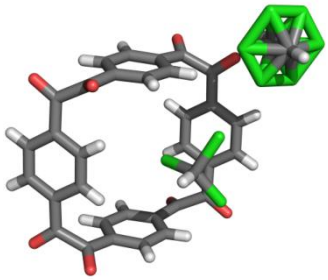

Table 2.4 Crystallographic Data and Structure Refinement of **7**·$CHCl_3$.

Empirical formula	$C_{35}H_{19}Cl_9O_8$	
Formula weight	881.60	
Temperature	123(2) K	
Wavelength	CuKα (λ = 1.54178 Å)	
Crystal system	Monoclinic	
Space group	$P2_1/c$	
Unit cell dimensions	a = 11.2293(3) Å	α = 90°
	b = 10.9699(3) Å	β = 101.158(2)°
	c = 15.0913(4) Å	γ = 90°
Volume	1823.87(9) $Å^3$	
Z	2	
Density (calculated)	1.605 Mg/m^3	
Absorption coefficient	6.685 mm^{-1}	
F(000)	887	
Crystal size	0.20 × 0.12 × 0.10 mm^3	
2θ range for data collection	5.017 to 66.598°	
Index ranges	$-10 \le h \le 12$, $-12 \le k \le 13$, $-17 \le l \le 17$	
Reflections collected	12954	
Independent reflections	3129 [$R_{(int)}$ = 0.0253]	
Completeness to 2θ = 66.598°	97.4 %	
Absorption correction	Empirical	
Refinement method	Full-matrix least-squares on F^2	
Volume	4354.88(11) $Å^3$	
Z	4	
Data / restraints / parameters	3129 / 6 / 254	

Table 2.4 Continued

Goodness-of-fit on F^2	0.995
Final R indices [$I>2\sigma(I)$]	R_1 = 0.0746, wR_2 = 0.2228
R indices (all data)	R_1 = 0.0801, wR_2 = 0.2312
Largest diff. peak and hole	1.21 and –0.62 e Å^{-3}

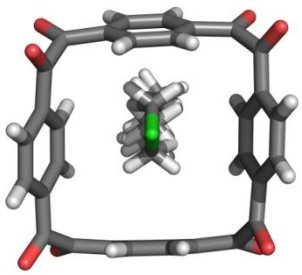

Table 2.5 Crystallographic Data and Structure Refinement of **7**·$C_5H_{10}Cl_2$.

Empirical formula	$C_{37}H_{26}Cl_2O_8$	
Formula weight	669.48	
Temperature	123(2) K	
Wavelength	CuKα (λ = 1.54178 Å)	
Crystal system	Monoclinic	
Space group	*C*2/c	
Unit cell dimensions	a = 17.4031(5) Å	α = 90°
	b = 11.8413(3) Å	β = 95.452(10)°
	c = 15.3028(4) Å	γ = 90°
Volume	3139.26(15) Å^3	
Z	4	
Density (calculated)	1.417 Mg/m^3	
Absorption coefficient	2.326 mm^{-1}	
F(000)	1384	
Crystal size	0.11 × 0.06 × 0.05 mm^3	
Theta range for data collection	4.523 to 67.959°	
Index ranges	$-20 \le h \le 19$, $-13 \le k \le 14$, $-18 \le l \le 18$	
Reflections collected	22422	
Independent reflections	2845 [$R_{(int)}$ = 0.0354]	

Table 2.5 Continued

Completeness to theta = 67.959°	99.2 %
Absorption correction	Empirical
Refinement method	Full-matrix least-squares on F^2
Data / restraints / parameters	2845 / 0 / 236
Goodness-of-fit on F^2	1.035
Final R indices [$I>2\sigma(I)$]	R_1 = 0.0471, wR_2 = 0.1243
R indices (all data)	R_1 = 0.0623, wR_2 = 0.1403
Largest diff. peak and hole	0.43 and –0.60 e Å^{-3}

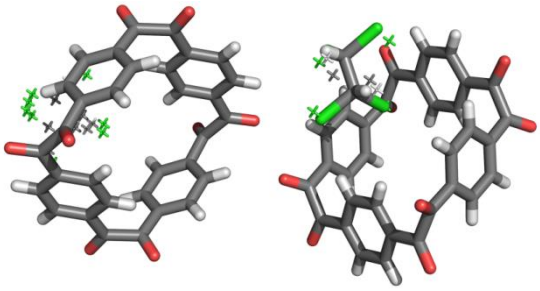

Table 2.6 Crystallographic Data and Structure Refinement of **7**·$C_2H_2Cl_4$.

Empirical formula	$C_{36}H_{20}Cl_8O_8$	
Formula weight	864.12	
Temperature	123(2) K	
Wavelength	CuKα (λ = 1.54178 Å)	
Crystal system	Triclinic	
Space group	$P\bar{1}$	
Unit cell dimensions	a = 9.9531(4) Å	α = 86.664(10)°
	b = 10.4448(3) Å	β = 88.983(10)°
	c = 19.1859(5) Å	γ = 65.459(10)°
Volume	1811.23(10) Å^3	
Z	2	
Density (calculated)	1.584 Mg/m^3	
Absorption coefficient	6.140 mm^{-1}	
F(000)	872	
Crystal size	0.36 × 0.28 × 0.16 mm^3	

Table 2.6 Continued

Theta range for data collection	4.614 to 133.166°
Index ranges	$-14 \leq h \leq 14$, $-14 \leq k \leq 14$, $-20 \leq l \leq 19$
Reflections collected	37776
Independent reflections	6224 [$R_{(int)} = 0.0607$]
Completeness to theta = 66.583°	97.3 %
Absorption correction	Empirical
Refinement method	Full-matrix least-squares on F^2
Data / restraints / parameters	6224 / 812 / 579
Goodness-of-fit on F^2	1.060
Final R indices [$I>2\sigma(I)$]	$R_1 = 0.0643$, w$R_2 = 0.1696$
R indices (all data)	$R_1 = 0.0656$, w$R_2 = 0.1704$
Largest diff. peak and hole	0.85 and –0.38 e Å^{-3}

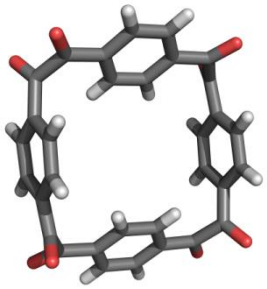

Table 2.7 Crystallographic Data and Structure Refinement of **7** grown from Bromoform.

Empirical formula	$C_{32}H_{16}O_8$	
Formula weight	528.45	
Temperature	123(2) K	
Wavelength	CuKα (λ = 1.54178 Å)	
Crystal system	Monoclinic	
Space group	$P2_1/n$	
Unit cell dimensions	a = 11.3502(3) Å	α = 90°
	b = 9.1551(3) Å	β = 112.962(1)°
	c = 12.6550(4) Å	γ = 90°
Volume	1210.81(5) Å^3	
Z	2	

Table 2.7 Continued

Density (calculated)	1.449 Mg/m^3
Absorption coefficient	0.879 mm^{-1}
$F(000)$	544
Crystal size	0.08 × 0.05 × 0.01 mm^3
2θ range for data collection	4.446 to 66.563°
Index ranges	$-13 \leq h \leq 13, -10 \leq k \leq 10, -15 \leq l \leq 15$
Reflections collected	8922
Independent reflections	2129 [$R_{(int)} = 0.0253$]
Completeness to $2\theta = 66.563°$	99.5 %
Absorption correction	Empirical
Refinement method	Full-matrix least-squares on F^2
Data / restraints / parameters	2129 / 0 / 181
Goodness-of-fit on F^2	1.032
Final R indices [$I>2\sigma(I)$]	$R_1 = 0.0357$, w$R_2 = 0.0964$
R indices (all data)	$R_1 = 0.0395$, w$R_2 = 0.1008$
Largest diff. peak and hole	0.21 and –0.16 e $Å^{-3}$

2.4.3.3 Crystal Growth of Oligomeric 4,4'-Dibenzoic Acid (11)

Single crystals of oligomeric 4,4'-dibenzoic acid (**11**) were obtained by dissolving crude **11** (20 mg) in pyrrolidine (2 mL). The product solution was heated and filtered using PTFE syringe filters (0.22 μm, 30 mm). The resulting filtrate (0.2 mL) was added to a 0.75 mL round-bottomed culture tube, and this tube was placed inside a 2 dram scintillation vial containing either Et_2O or $^{i}Pr_2O$ (1 mL) as the diffusing solvent. The vial was tightly closed and kept at ambient conditions without external disturbances. On the third day, colorless hair-like aggregated crystals were obtained by vapor diffusion technique. Unfortunately, the resultant crystals are unsuitable for X-ray diffraction analyses because they are too small. Since many tiny crystals are seen in the vials, we concluded that under the mentioned crystal growth conditions the crystal nucleation rate was faster than the crystal growth rate.

Chapter Three

Synthesis and Characterization of π-Conjugated Cyclic Oligoazaacenes Based on Cyclotetrabenzil

3.1 Introduction

3.1.1 Fully π-Conjugated Linear Acenes

The IUPAC definition of "acenes" is the following: polycyclic aromatic hydrocarbons consisting of fused benzene rings in a rectilinear arrangement (Chart 3.1).[190]

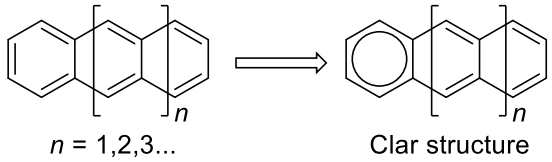

Chart 3.1 Oligoacenes general formula and the corresponding Clar structure.

The smallest acenes, anthracene (n = 1), is easily isolated from petroleum resources, and readily obtained on large scale.[277] Tetracene, which is also called naphthacene (n = 2), was first synthesized in 1985 by Onan and co-workers,[278] and the discovery of pentacene (n = 3) dates back 90 years when Clar and John first reported its synthesis and properties.[279] Since then, a number of reports have been published on their (and their derivatives') use as semiconductors in organic field-effect transistors (OFETs), organic light-emitting diodes (OLEDs), and organic photovoltaic devices, owing to their high charge-carrier mobility.[280–287] By increasing the number of benzene rings in oligoacenes, whose topology includes only one Clar aromatic sextet spread over the entire molecule, the HOMO–LUMO gap is decreased and the chemical reactivity is increased.[288] Synthesis of oligoacenes with $n > 3$ is a challenge since they are insoluble in common organic solvents and extremely sensitive towards oxidation by O_2 and dimerize under formal [4+4] cycloadditions, leading to butterfly

dimers. The synthesis of hexacene (n = 4) was independently reported by Clar and Marschalk in 1939;[289,290] after that, subsequent research was reported in an attempt to synthesize heptacene (n = 5),[291–294] but its existence remained dubious until it was isolated in 2006 by Neckers and co-workers and fully characterized in 2017 by Bettinger and co-workers.[295,296] Functionalization of oligoacenes (where n = 3, 4, or 5) with bis(triisopropylsilylethynyl) (TIPS) group overcomes the solubility and stability obstacles and the azacenes become soluble in common organic solvents and stable under ambient conditions.[297,298] Octacene (n = 6) and nonacene (n = 7) were synthesized by Bettinger and co-workers before heptacene was fully characterized,[299] and their synthesis disproved Clar's assertion that it is impossible to synthesize acenes with $n > 5$.[300] Decacene (n = 8) was generated for the first time in 2017 by Peña and co-workers and oligoacenes up to undecacene (n = 9) were synthesized in 2018 by Echavarren and co-workers.[301,302] Dodecacene (n = 10), the longest acene obtained so far, was recently generated on Au(111) surface by Moresco and co-workers.[303]

The considerable interest in oligoacenes was extended to include the nitrogen-containing heteroacenes which show potential as electron-transport materials.[304–306] Bunz and co-workers pioneered the chemistry of azaacenes:[307,308] heterocyclic analogs of acenes which offer many new lessons in electron mobility and fundamental studies of (anti)aromaticity.[309] Linear azaacenes with their electron-accepting properties are attractive materials in the field of organic electronics.[310–314] Additionally, the electronic properties of TIPS-pentacene were enhanced where two or four carbon atoms were substituted by nitrogen atoms.[315] Electronegative substitution also affected the electronic properties of azaacenes: a significant bathochromic shift in the optical transitions was seen when compared with their non-halogenated azaacenes.[316,317]

3.1.2 Fully π-Conjugated Cyclic Arylenes

Fully unsaturated macrocycles are considered to be models for infinitely conjugated π systems with well-defined shapes and noncollapsible backbones which make them exhibit unique optical and electronic behaviors.[318] The sub-units of these unsaturated macrocycles are arylenes which are produced by the removal of two hydrogen atoms from the benzene rings of an aromatic compound.[319] These fully π-conjugated cyclic arylenes are useful building blocks for building columnar 1D nanotubes, 2D porous surface networks, and 3D inclusion complexes by self-assembly. Annulenes were the first fully π-conjugated cyclic arylenes studied in the early 1960s,[24,320,321] and then the study expanded to include the π-conjugated macrocycles which were composed of arylene or heteroarylene moieties in their backbones over the last three decades.[322–330] Cyclic oligophenylenes are a notable subclass of fully π-conjugated cyclic arylenes, in which benzene rings cyclized via *ortho*-([*n*]COPs),[331–334] *meta*-([*n*]CMPs),[335–338] or *para*-([*n*]CPPs) positions, with [*n*] denoting the number of phenyl rings in the macrocycle (Chart 3.2A).[339–346] Cyclic oligophenylenes containing two or three mixed linkages are also synthesized and mostly the ring strains were released in such macrocycles, especially in *ortho*/*para* connection fashion, because the central cavity lost its circular shape and adapted triangular or square conformation (Chart 3.2B).[347–350] These macrocycles are characterized by their thermal, light, and air stability, aromaticity, [π···π] interactions, optoelectronic properties, and molecular recognition, therefore they have attracted the attention of many chemists to conduct more research in this field. The insertion of heteroarylenes moieties within the interior, such as cyclothiophenes and cyclopyrroles, or exterior, such as quinoxaline-based oligophenylene macrocycles, areas of the cyclic oligophenylenes backbone can strongly affect the shape of the macrocycles, the [π···π] stacking properties, the HOMO–LUMO energy levels, and the intermolecular interactions (Chart 3.2C).[351–360] Trisquinoxalines macrocycles were isolated by Bunz group by adding the

requisite 1,2-phenylenediamines *in situ* to the oxidation of cyclotribenzoin **5**.[90] The resultant macrocycles were good emitters for organic light-emitting diodes (OLED) devices.

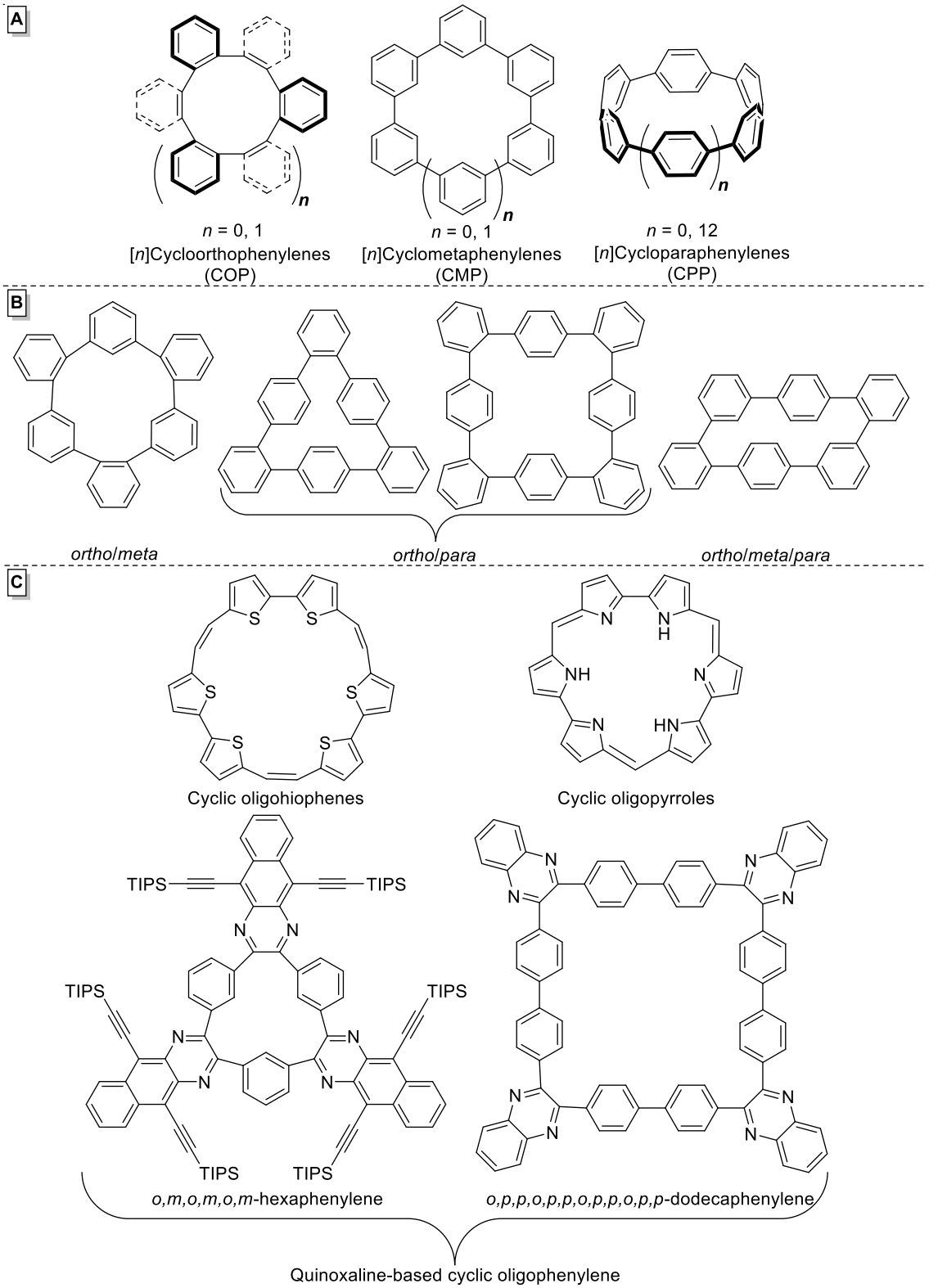

Chart 3.2 *(A)* Different cyclization positions, *(B)* mixed linkages, and *(C)* heteroarylenes moieties inserted into cyclic oligophenylenes.

Syntheses of most previously mentioned fully π-conjugated cyclic arylenes are a significant challenge: cyclic oligophenylenes are generally synthesized by transition metal-mediated cross-coupling reactions or aryl halides homo-coupling reactions, and both mostly produce cyclic products with analogous macrocycles and open-chain oligomers. Additionally, the couplings have to overcome a large steric strain in the final cyclization steps which impedes high yields and thus hinders large-scale applications. Therefore, the cyclization has to be improved or carried out at the very beginning of the synthesis to avoid loss of complex building blocks and allow the introduction of further functionalities.[361,362]

Synthesis of cyclotetrabenzil (**7**), which is described in details at Chapter One, opened up a very productive collaboration between our group and the team of Prof. Uwe Bunz at the Ruprechts-Karls-Universität in Heidelberg (Germany). As most azaacenes are synthesized through a convenient condensation of 1,2-diketones with 1,2-phenylenediamines, cyclotetrabenzil (**7**) presented itself as an interesting precursor that could orient four azaacenes around the central macrocyclic core. Structural, optical, and electronic properties of the resulting cyclic oligoazaacenes were investigated.[120,363] The results are expected to combine the electronic properties of both linear azaacenes and cyclic π-conjugated arylenes.

3.2 Results and Discussion

3.2.1 Syntheses of π-Conjugated Cyclic Oligoazaacenes

Two macrocycles **23a**–**b** were prepared in good yields by condensation of **7** with four equivalents of chiral diamines **22a**–**b** which indicated the possibility of inserting saturated functionalities into the cyclic backbone (Scheme 3.1).

A series of fully π-conjugated oligoazaacenes macrocycles was synthesized using acid-mediated imine condensation reaction between 1,2-phenylenediamine derivatives **24a**–**n**

and the octaketone **8**, in EtOH or $CHCl_3$, producing the corresponding tetraquinoxaline macrocycles **25a**–**n** in yields ranging from 34% to 85% (Scheme 3.1). The resulting products are soluble in chlorinated solvents such as dichloromethane, $CHCl_3$, and 1,2-dichloroethane, and introducing [tris(isopropyl)silyl]ethynyl substituents improved the solubility of the resulting compounds in most organic solvents. In these reactions the cyclization takes place in the first step before derivatization which enhanced the final yields and prevented the collapse of the cyclic structure when further functionalities were introduced within the macrocycle backbone.[360] The central cavities of these dodecaphenylene macrocycles consist of an all-carbon macrocycle in which adjacent benzenoid rings connect in *para*- and *ortho*-positions, alternately.

Interestingly, when the relative amount of the parent 1,2-phenylenediamine **24a** in the coupling was decreased to 3 equivalents, bisquinoxaline macrocycle **26a** could be isolated, in which the two quinoxaline condensations occurred on the opposite corners of the cyclic octaketone. The bisquinoxalines macrocycles were also seen when 4 equivalents of heteroaromatic diamines **24i**, **24j**, and **24n** were used as precursors in condensation reaction. These macrocycles, which were functionalized on only two opposite corners, offered the possibility for the synthesis of mixed condensation products such as **25ac**, **25ad**, and **25nl** (Scheme 3.2), which were formed in good yields. The stepwise nature of the condensation allows incorporation of different azaacene fragments into the same molecule, opening up the space for the modulation of optoelectronic properties.

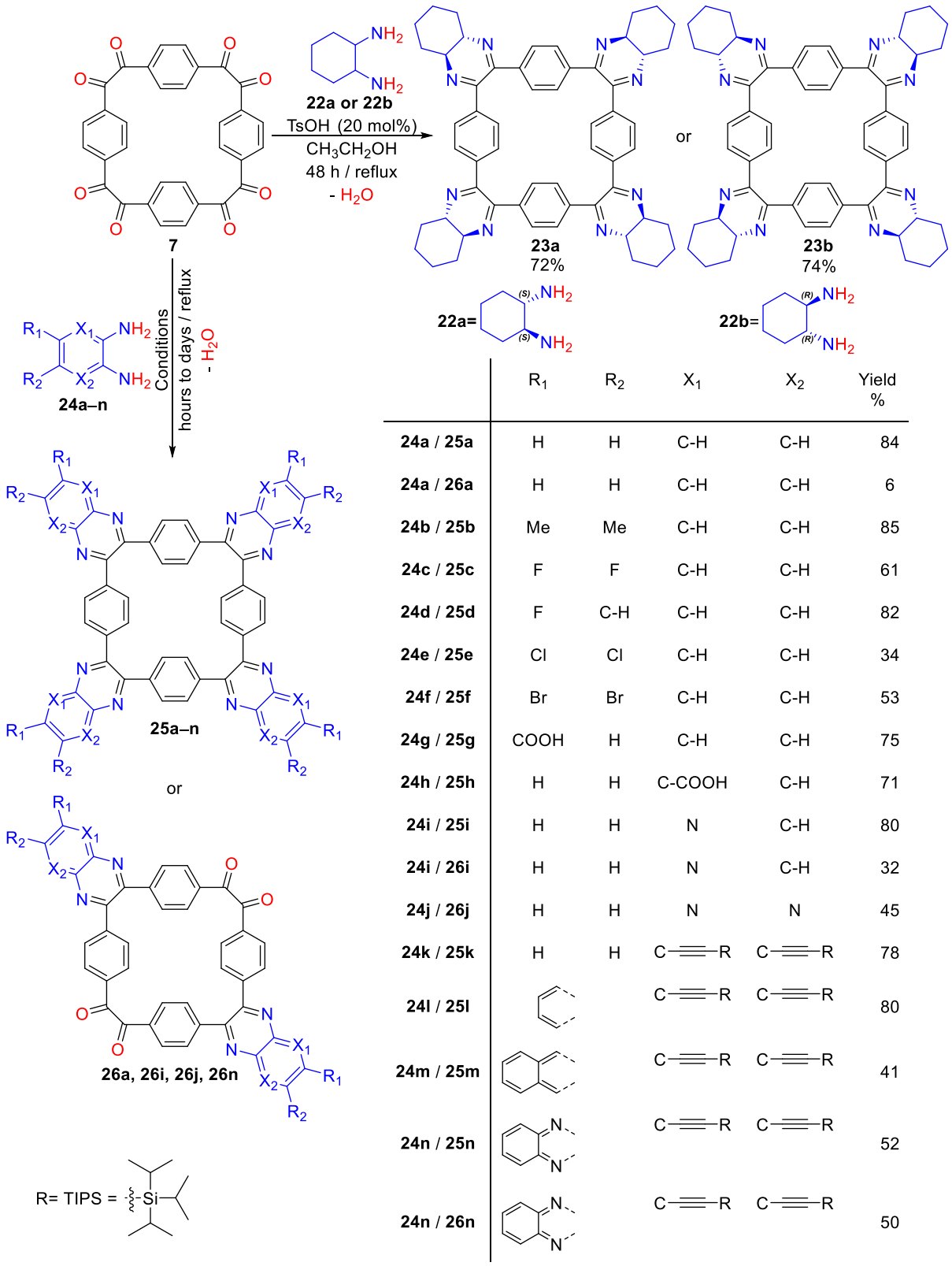

	R_1	R_2	X_1	X_2	Yield %
24a / 25a	H	H	C-H	C-H	84
24a / 26a	H	H	C-H	C-H	6
24b / 25b	Me	Me	C-H	C-H	85
24c / 25c	F	F	C-H	C-H	61
24d / 25d	F	C-H	C-H	C-H	82
24e / 25e	Cl	Cl	C-H	C-H	34
24f / 25f	Br	Br	C-H	C-H	53
24g / 25g	COOH	H	C-H	C-H	75
24h / 25h	H	H	C-COOH	C-H	71
24i / 25i	H	H	N	C-H	80
24i / 26i	H	H	N	C-H	32
24j / 26j	H	H	N	N	45
24k / 25k	H	H	C≡R	C≡R	78
24l / 25l			C≡R	C≡R	80
24m / 25m			C≡R	C≡R	41
24n / 25n			C≡R	C≡R	52
24n / 26n			C≡R	C≡R	50

Scheme 3.1 Imine condensation of cyclotetrabenzil (**7**) with chiral diamines **22a**–**b** and 1,2-phenylene diamines **24a**–**n**. The condensation of **7** with **22a**–**b** and **24a**–**j** was done in TsOH/EtOH system, the condensation of **7** with **24k**–**m** was done in AcOH/$CHCl_3$ system, and the condensation of **7** with **24n** was done in PhMe/EtOH system.

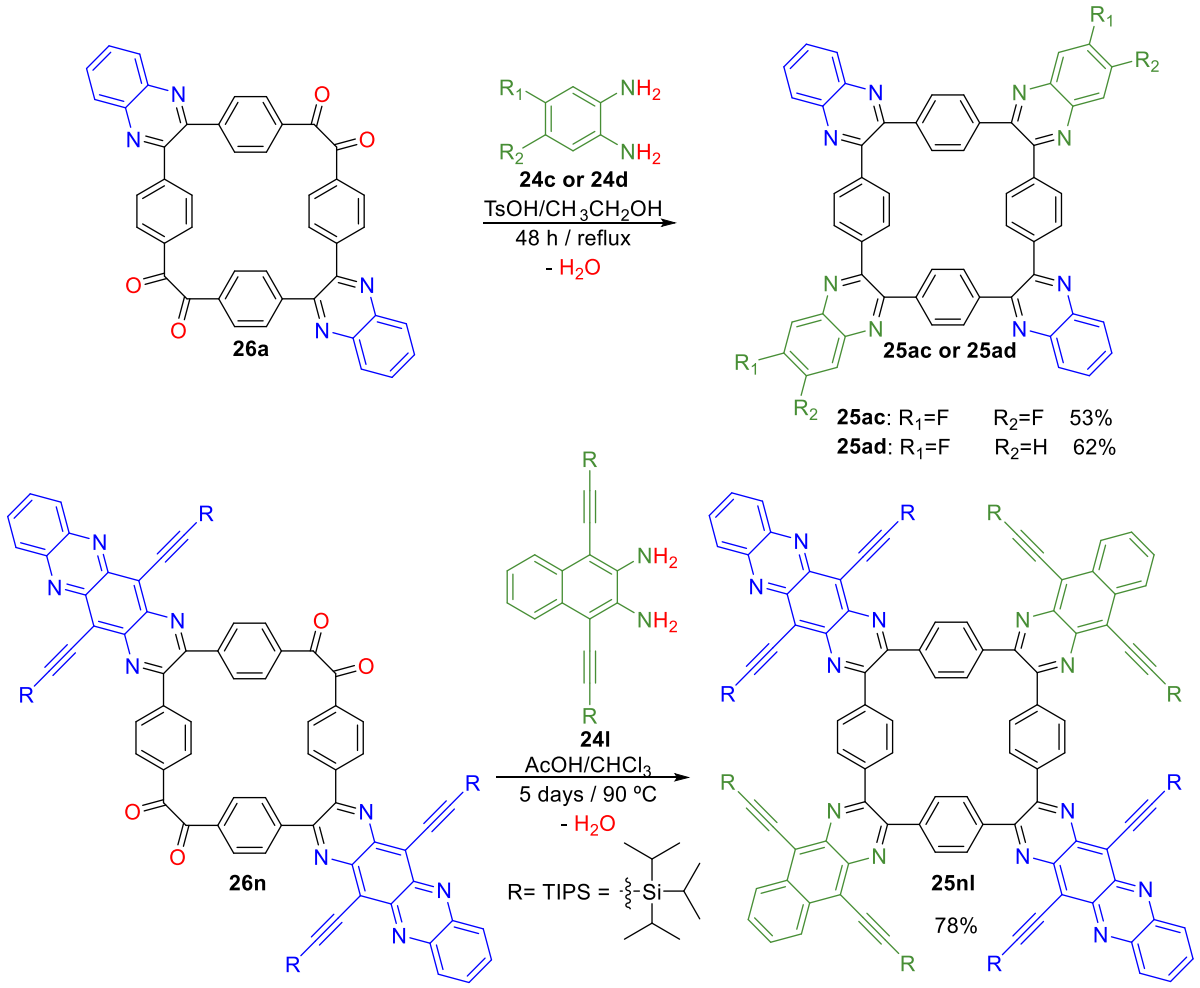

Scheme 3.2 Stepwise condensation leads to the incorporation of mixed azaacenes moieties into the same molecule.

Many attempts were performed to imitate Suzuki's approach to produce fully π-conjugated oligoazaacenes macrocycles for functionalized *N*-hetero [8]circulenes—macrocyclic compounds containing a central polygon which is completely surrounded and fused by benzenoids—[364] but the ring closing cyclodehydrogenation was unsuccessful by the well-established and specialized methods.[350] Additionally, compounds **25g** and **25h** were synthesized to use them as tetratopic linkers in metal organic frameworks, but all experiments done for this purpose failed.

3.2.2 Syntheses of π-Conjugated Acyclic Oligoazaacenes

To elucidate the effect of cyclization on the physical properties of linear azaacenes, acyclic model compounds **27k**–**n** were prepared through imine condensation of benzil (**3**) with the 1,2-phenylenediamines **24k**–**n** (Scheme 3.3). The yields of produced acyclic azaacenes **27k**–**n** ranged between 69–91%.

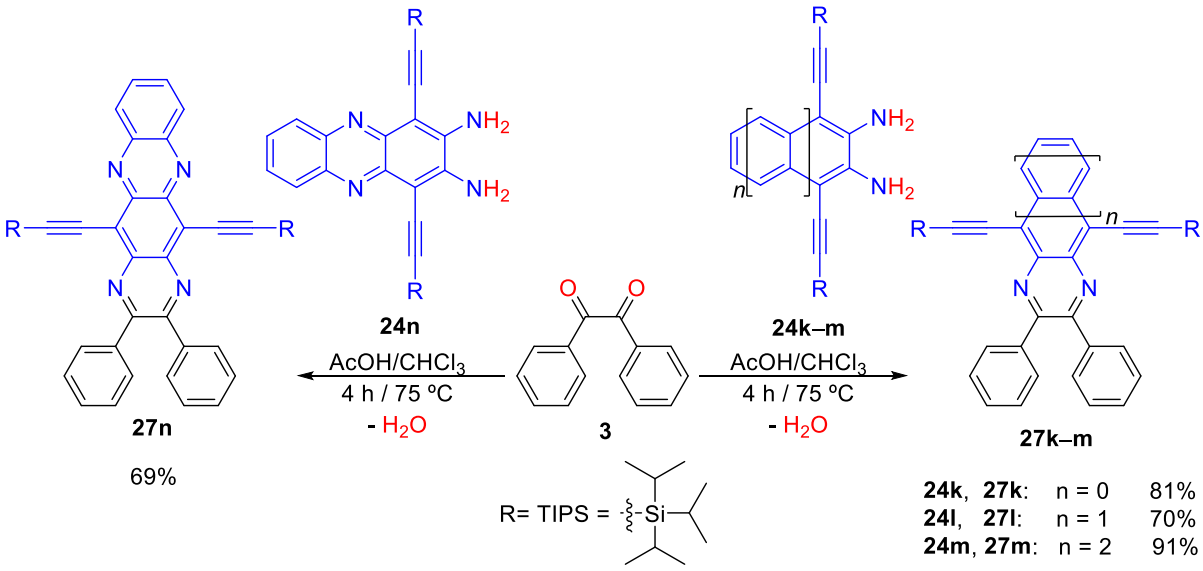

Scheme 3.3 Imine condensation of benzil **(3)** with 1,2-phenylene diamines **24k**–**n**.

3.2.3 General Crystal Structures of Selected π-Conjugated Cyclic Oligoazaacenes

Diffraction-quality single crystals of most prepared cyclic oligoazaacenes were grown by slow vapor diffusion, and the analyses of their diffraction patterns confirm the cyclic structures and illustrate the solid-state conformations. The progressing of crystal structure from **7** to **26** and finally to **25** increases the number of rigidifying fusions of quinoxaline rings around the central cavity, which results in first elongating for **26**, and later twisting of the macrocycles into the saddle-shaped structures of **25** (Figure 3.1).

When two quinoxaline rings are fused on the opposite sides of the central cavity of macrocycle, the originally square-shaped cyclotetrabenzil (**7**) is dramatically deformed into a rhombus shape with an approximate distance along the long diagonal of 10.58 Å, connecting the centroids of the fused bonds between the central macrocycle and quinoxaline nucleus, and 7.73 Å an approximate distance along the short diagonal between the centroids of the two C–C bonds between the adjacent carbonyl groups.

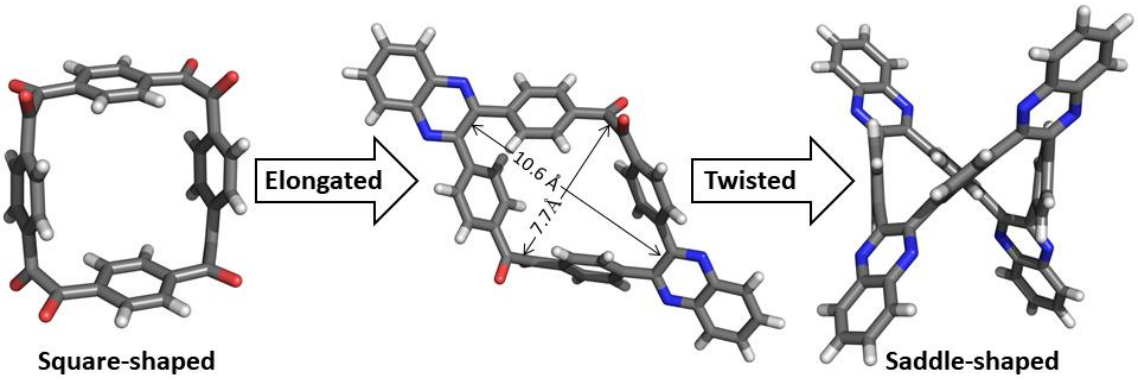

Figure 3.1 The progressive deformation of the cyclotetrabenzil structure when it is subject to condensation conditions. Element colors: C—gray, O—red, N—blue, H—white.

Deformation is further evidenced by the increased torsion angles between the adjacent C=O groups, which vary between 102.3 and 105.9º in compound **26a**. In the extended structure, notable short contacts are found between the C–H bonds on benzene rings of the central macrocycle and carbonyl oxygens (range from 2.41 to 2.66 Å) and nitrogens on the quinoxaline nuclei of the neighboring molecules (2.66 Å). By increasing the fused quinoxaline rings around the central cavity to four (compound **25a**), the core macrocycle twisted further, forming a saddle-shaped conformation. The core macrocycle is contracted relative to **26a**, measuring about 7.29 × 7.72 Å (distances between the centroids of the macrocycle-quinoxaline fused bonds on the opposite sides of the macrocycle). During the growth of single crystals for both **25a** and **26a**, two inter-grown molecules are made in a symmetrical fashion forming "twinned crystals". In compound **25a**, the distances between the

two opposite quinoxaline moieties in one molecule are 8.53 and 9.10 Å with tilt angles of 67.3 and 78.2º, and 8.51 and 9.13 Å with tilt angles of 65.5 and 72.6º in its twin (measured between the centroids and planes of pyrazine rings). Looking at the inclination of the phenyl rings of the core macrocycle in compound **25a** with respect to the quinoxaline moieties, one can see that the inclination angles range between 27.9 and 61.0º in one molecule and between 33.8 and 61.4º in its twin (measured between the planes of pyrazine rings and their phenyl ring neighbors in the core macrocycle). The packing structure of compound **25a** is very complex and it displayed voids that occupied 9.4% of unit cell volume. This packing structure revealed pseudo-cage formed by the arrangement of six molecules of **25a** in a star-shaped structure which indicated that **25a** could be used to intercalate small molecules within its crystal lattice (Figure 3.2).

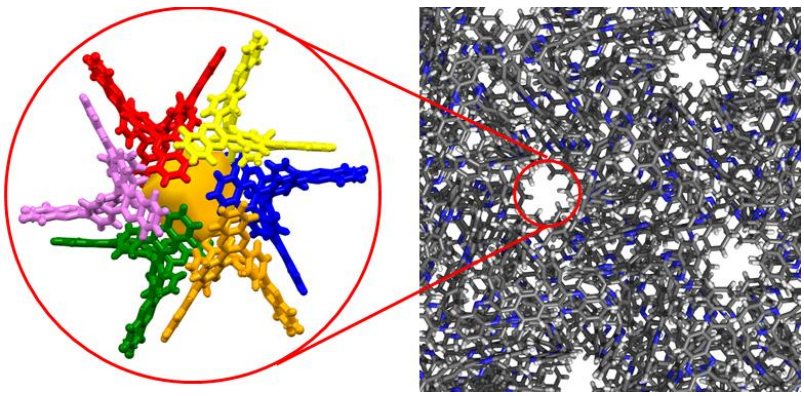

Figure 3.2 The crystal packing of compound **25a** and the pseudo-cage formed within its crystal lattice.

Replacing the four quinoxaline moieties by four 6,7-dimethylquinoxaline moieties in compound **25b** did not affect the saddle-shaped solid-state conformation of the macrocyclic structure but influenced the distances between the centroids of pyrazine rings in each two opposite quinoxaline moieties and the tilt angles between their planes which become 10.93 Å and 70.8º, respectively (Figure 3.3). Notably, the distances between each opposite pair of quinoxaline moieties and the tilt angles between them are identical which indicates that the

fusion of 6,7-dimethyl quinoxaline leads to a more symmetrical structure than with the unsubstituted quinoxaline. The symmetry was further observed in the inclination angles between the phenyl rings of the core macrocycle and 6,7-dimethylquinoxaline moieties where same inclinations are seen between all quinoxaline moieties with their phenyl ring neighbors in the core macrocycles (16.2 and 59.6º; measured between the planes of pyrazine rings and their phenyl ring neighbors in the core macrocycle). The crystal packing diagram of compound **25b** is shown in Figure 3.3C, viewed along the crystallographic *c* axis. Molecules of compound **25b** tightly stack in a parallel orientation with no voids showed between molecules through two packing factors: the [π···π] interaction between all aromatic moieties at each molecule with their neighboring molecule (centroid-centroid distance is 4.94 Å) and a variety of short contacts which range between 2.38 and 3.27 Å, connecting the phenyl rings in core macrocycle and the terminal aryl rings in quinoxaline moieties with their neighboring molecules.

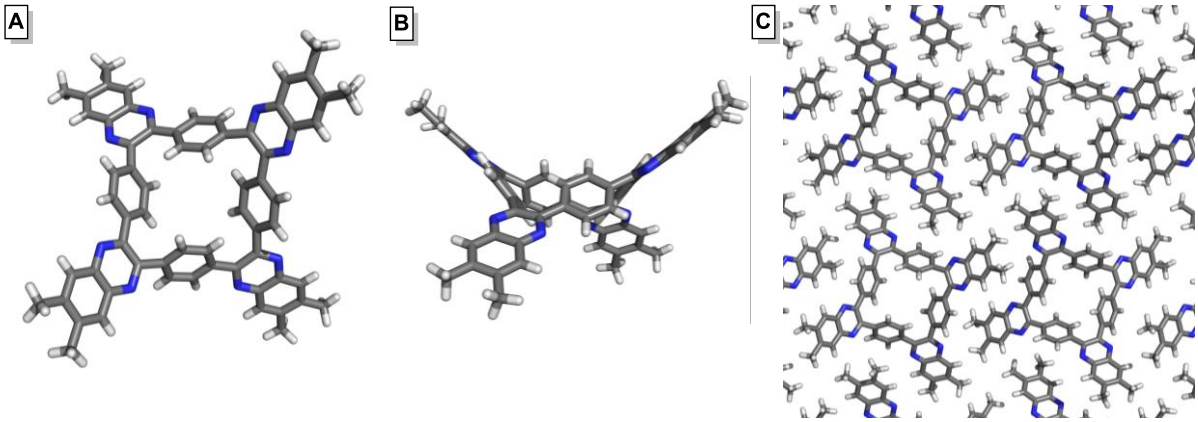

Figure 3.3 Crystal structure of compound **25b** *(A)* top view, *(B)* side views, and *(C)* segment of its crystal packing diagram viewed along the crystallographic *c* axis. Element colors: C—gray, N—blue, H—white.

Quinoxaline moieties were substituted by fluoroquinoxaline where one or two fluorine atoms occupied all the four corners of the macrocycle (compounds **25c** and **25d**) or just two opposite corners (compounds **25ac** and **25ad**). Inserting fluorine atoms in the

macrocycle maintained the saddle-shaped solid-state conformation of the macrocyclic structure but altered its symmetry. Compound **25c**, where 6,7-difluoroquinoxaline moieties fuse to the core macrocycle from the all four corners, is the most symmetrical compound within this fluorinated family, with equal distances between each two opposite quinoxaline moieties (10.18 Å) and equal tilt angles (79.0º) measured between the centroids and planes of each opposite pyrazine rings (Figure 3.4A). The measured inclination angles between the phenyl rings of the core macrocycle and 6,7-difluoroquinoxaline moieties range from 14.8 to 58.4º, measured between the planes of pyrazine rings and their phenyl rings neighbors in the core macrocycle. The less symmetrical structure was seen in compound **25ac** when 6,7-difluoroquinoxaline moieties fused to macrocycle **26a**. The distances between the centroids and planes of each opposite pyrazine rings from two opposite quinoxaline moieties is 10.20 Å and between the two opposite 6,7-difluoroquinoxaline moieties is 10.03 Å; the tilt angles between the planes of quinoxaline or 6,7-difluoroquinoxaline moieties are 80.4 and 81.6º (Figure 3.4B). The inclination angles between the quinoxaline or 6,7-difluoroquinoxaline moieties and the neighboring phenyl rings in the core macrocycle varied from 17.8 to 59.1º. When 6-fluoroquinoxaline moieties fused to the core macrocycle from the all four corners in compound **25d**, fluorine atoms were disordered over two possible sites (positions 6 and 7 in each quinoxaline moiety) with 34% and 66% fractional occupancies (Figure 3.4C). The distances between each two opposite 6-fluoroquinoxaline moieties in compound **25d** are 9.59 and 9.72 Å, and the tilt angles are 87.8 to 88.7º (measured between the centroids and planes of each opposite pyrazine rings). The inclination angle between 6-fluoroquinoxaline moieties and the nearest phenyl rings in the core macrocycle range from 21.9 to 59.1º. In the last compound of this fluorinated family, 6-fluoroquinoxaline moieties fused to two vacant opposite 1,2-diketone units in compound **26a** to produce compound **25ad**. Twinned crystals were formed during the single crystal growth of compound **25ad** and the fluorine atoms were

disordered over several possible sites with fractional residences, but the total occupancy was still two fluorine atoms per macrocycle (Figure 3.4D). The distances between each two opposite 6-fluoroquinoxaline moieties in twin crystals of compound **25ad** vary from 8.52 to 9.19 Å, and the tilt angles range from 65.2 to 75.7º (measured between the centroids and planes of each opposite pyrazine rings). The inclination angle between 6-fluoroquinoxaline moieties in their phenyl rings neighbors in the core macrocycle range from 25.7 to 62.5º.

The extended crystal structures, seen along the crystallographic *a* axis in Figure 3.4A and 3.5B, for compounds **25c** and **25ac** appeared seemingly similar. Both contains small voids between the packed molecules that occupy 21.1% in **25c** and 22.4% in **25ac** of the unit cell volume, which could highlight the porosity of these structures. Attempts to perform N_2 adsorption/desorption (77 K) measurements for these two crystals failed due to the collapse of crystal structure during the removal of the solvent. The molecules of these two compounds are held together within the crystal lattice through [$\pi\cdots\pi$] interaction between the aromatic moieties at each molecule with their neighboring molecule (centroid-centroid distances range from 3.84 and 3.90 Å in **25c** and from 4.74 and 4.83 Å in **25ac**), and an assortment of short contacts ranging between 2.40 and 3.04 Å in **25c** and between 2.34 and 3.02 in **25ac**, connecting the phenyl rings in the core macrocycle and quinoxaline moieties with their neighboring molecules. The crystal packing diagram of compounds **25d** (seen along the crystallographic *b* axis in Figure 3.4C) displayed voids that occupied 15.7% of unit cell volume. The molecules of **25d** stacked together by [$\pi\cdots\pi$] interaction between the aromatic moieties at each molecule with their neighboring molecule (centroid-centroid distances ranging from 3.61 and 4.94 Å) and short contacts ranging between 2.18 and 3.42 Å. Finally, the packing diagram of the twin crystals of **25ad** (seen along the crystallographic *c* axis in Figure 3.4D) is very complicated and it showed the same packing pattern as in the packing diagram of compound **25a** (Figure 3.4). Small voids, which occupied 8.6% of unit cell

volume, were displayed and revealed pseudo-cage formed by the arrangement of six molecules of **25ad** in a star-shaped structure which indicated that **25ad** could also be used to host small molecules within its crystal lattice.

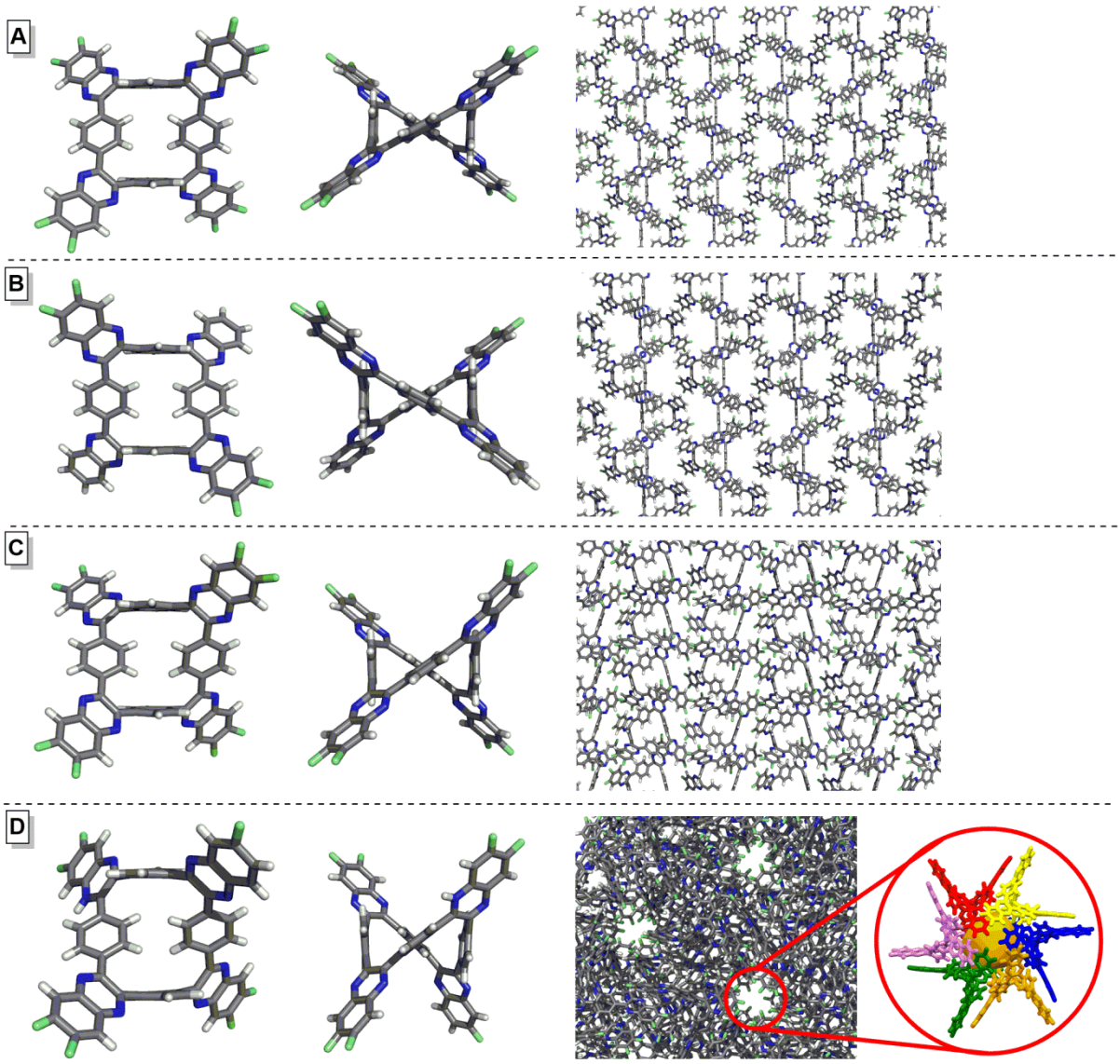

Figure 3.4 Top and side views of crystal structures of compounds *(A)* **25c**, *(B)* **25ac**, *(C)* **25d**, and *(D)* **25ad**, and segment of their crystal packing diagrams viewed along the crystallographic (*a* and *b*) *a* axis, *(C) b* axis, and *(D) c* axis. Element colors: C—gray, N—blue, H—white, F—lime.

In X-ray measurements of compound **25e**, where the core macrocycle fused with four 6,7-dichloroquinoxaline moieties, the structure could be solved but refined poorly. These preliminary measurements indicated a saddle-shaped structure which was observed in all

previously discussed four-fold macrocycles (Figure 3.5). In this macrocycle, the distances between the opposite pairs of 6,7-dichloroquinoxaline moieties are 9.49 and 9.63 Å and the tilt angles are 80.9 to 87.7º, measured between the centroids and planes of each opposite pyrazine rings. The inclination angles between the phenyl rings of the core macrocycle and 6,7-dichloroquinoxaline moieties range from 21.2 to 76.7º, measured between the planes of pyrazine rings and their phenyl rings neighbors in the core macrocycle. The extended structure of **25e**, seen along the crystallographic *b* axis in Figure 3.5C, displayed the tight packing of molecules with no voids between them. This packing occurred by the presence of [π···π] interaction between the pyrazine moieties with the neighboring molecules and assortment of short contacts in the range between 2.66 and 3.41 Å.

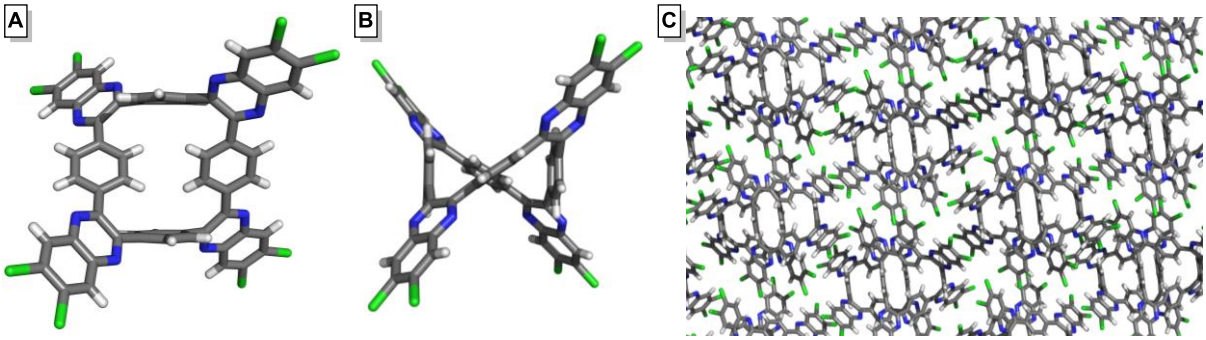

Figure 3.5 Crystal structure of compound **25e** *(A)* top view, *(B)* side view, and *(C)* segment of its crystal packing diagram viewed along the crystallographic *b* axis. Element colors: C—gray, N—blue, H—white, Cl—green.

3.2.4 Inclusion Complexes of Selected π-Conjugated Cyclic Oligoazaacenes

The skeleton of innumerable macrocycles can be modified by inserting new functional groups, which bring about additional chemical or physical features in comparison to the parent compounds.[365] Functionalization the prepared cyclic oligoazaacenes by increasing the number of aza-groups in the structure was applied, which allowed the macrocycles to host small aromatic rings within their crystal lattice. Compounds **25i** and **26j**

were made by fusing 1,4,5-triazanaphthalene or 1,4,5,8-tetraazanaphthalene moieties in the four or two opposite corners of the core macrocycle instead of quinoxaline moieties.

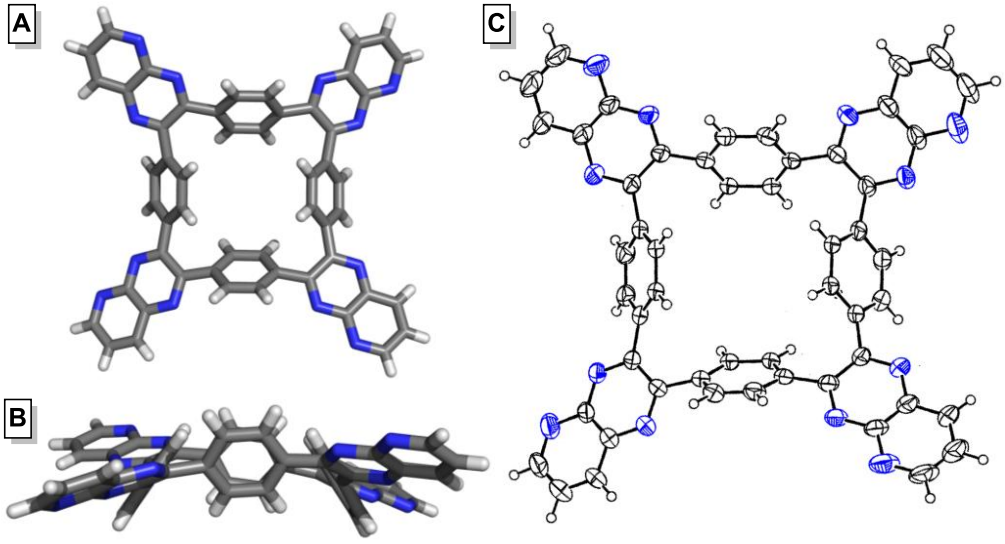

Figure 3.6 *(A)* Top-down view and *(B)* side view of the X-ray crystal structure of compound **25i**. *(C)* Thermal ellipsoid plot of **25i** shown at the 50% probability level. Element colors: C—gray, N—blue, H—white. All solvent molecules are omitted for clarity.

The conformation of compound **25i** (Figure 3.6) was proven by single crystal X-ray diffraction analysis. Adding one aza-group at each quinoxaline moiety in the four corners of the macrocycles did not affect the solid-state conformation of the original macrocycle as much as the previously mentioned substituents did. The macrocycle **25i** maintained the square-shaped structure of the parent macrocycle **7** with slight changes in the distances and tilt angles between opposite pairs of phenyl rings in the core macrocycle: they were 7.31×7.62 Å with no tilt angles and become 7.12×7.12 Å with 67.2º tilt angles. The distances and tilt angles between each two opposite 1,4,5-triazanaphthalene moieties are identical: 11.70 Å and 42.6º, respectively, measured between the centroids and planes of each opposite pyrazine rings. The identical distances and tilt angles refer to the presence of high symmetry in **25i**. This symmetry was further proved by measuring the inclination angles between the phenyl rings of the core macrocycle and 1,4,5-triazanaphthalene moieties. Same inclinations

of 38.6 and 48.8º were seen between the planes of pyrazine rings in all quinoxaline moieties and the planes of their phenyl rings neighbors in the core macrocycle.

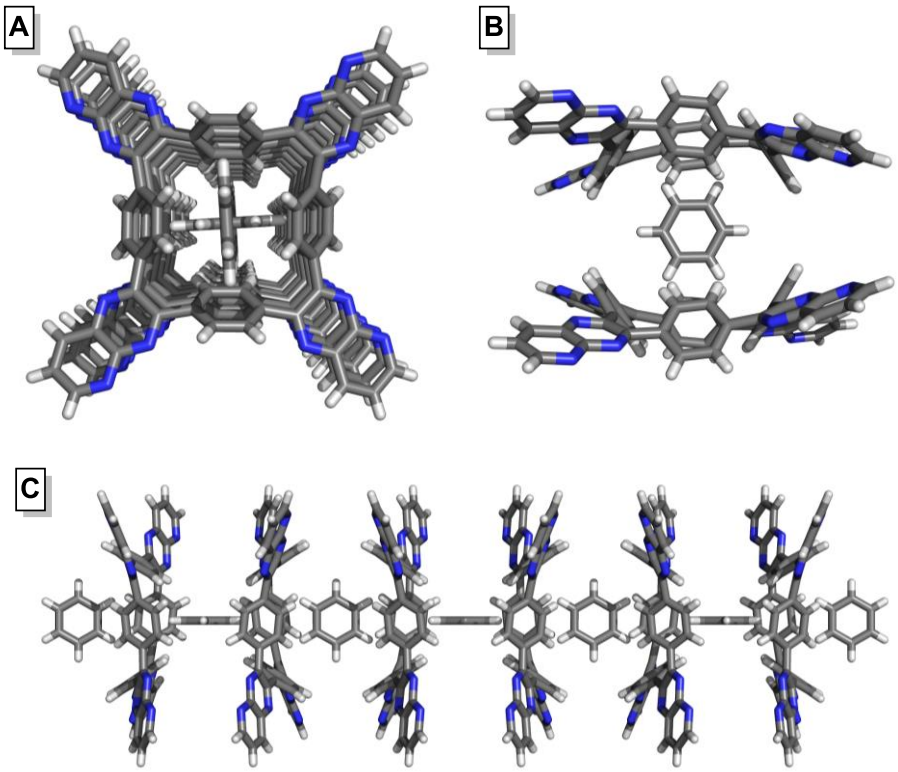

Figure 3.7 *(A)* Benzene rings included into the intrinsic cavities of **25i** in two orientations, *(B)* sandwich-like complex of compound **25i**, and *(C)* alternative co-sequence of benzene rings (guests) and macrocycle molecules (hosts), viewed along crystallographic *b* axis. Element colors: C—gray, N—blue, H—white.

Compound **25i** formed an inclusion complex with benzene in a 1:2 ratio. One of these benzene molecules was included within the intrinsic pores of compound **25i** in two orientations aligned with the main axis of the macrocycle (Figure 3.7A). The other benzene molecule is disordered within the extrinsic pores of the crystal lattice in two overlapping orientations. The included benzene molecules are lined up with the main axis of the macrocycles, with two opposite edges tucked into the cavities of two neighboring molecules of **25i**, forming a sandwich-like complex (Figure 3.7B). This complexation pattern repeated itself within the crystal lattice, producing an infinite alternating sequence of benzene rings and macrocycle molecules, seen along the crystallographic *b* axis in Figure 3.7C. The

distance between the centroids of the benzene rings above and below the macrocycle average plane is 7.92 Å and their planes are perpendicularly intersected. These planes almost are perpendicularly intersected also with the macrocycle plane that is dividing the phenyl rings in the core macrocycle (87.2 and 89.9°). The distances between the centroid of benzene ring tucked into the cavity and the centroids of the phenyl rings in the core macrocycle range from 5.08 to 5.58 Å. The binding patterns of compound **25i** indicated that the resultant inclusion complex is stabilized by four short [C–H···C] contacts measuring 2.82 Å, established between the tucked edges of benzene rings with two opposite phenyl rings in the nearest host macrocycle.

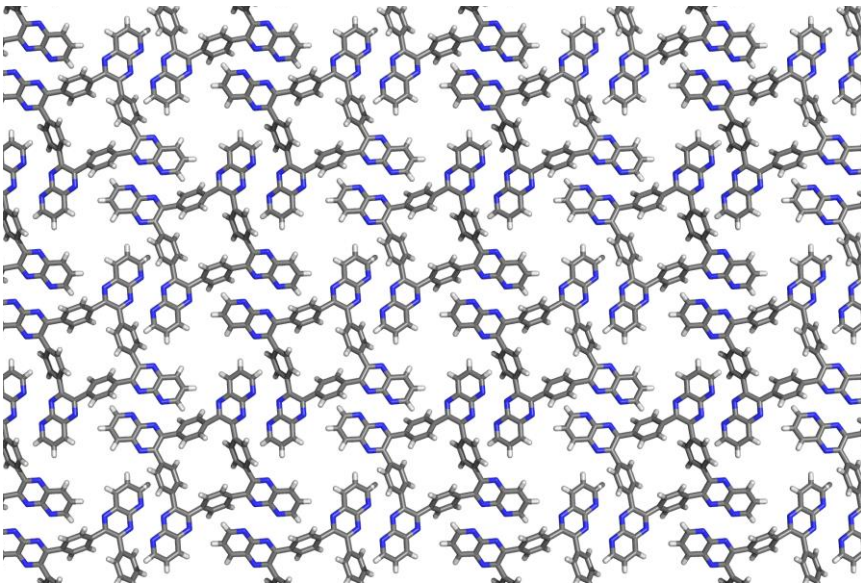

Figure 3.8 Segment of the crystal packing diagram of compound **25i**, shown along the crystallographic *c* axis. Element colors: C—gray, N—blue, H—white. All solvent molecules are omitted for clarity.

The crystal packing diagram of compound **25i** is shown in Figure 3.8 viewed along the crystallographic *c* axis. Molecules of compound **25i** tightly stack in a parallel orientation through short [C–H···N] contacts measuring 2.68 Å, established between the hydrogen atoms located in the *meta*-positions of pyridine rings and the nitrogen atoms in pyrazine rings which are on the opposite side of pyridine nitrogens. Two more short contacts measuring 3.34 and

3.39 Å were established between one of the shared carbons between pyrazine and pyridine rings which were located in the *ortho*-position for pyridine and two adjacent carbons of disordered benzene rings.

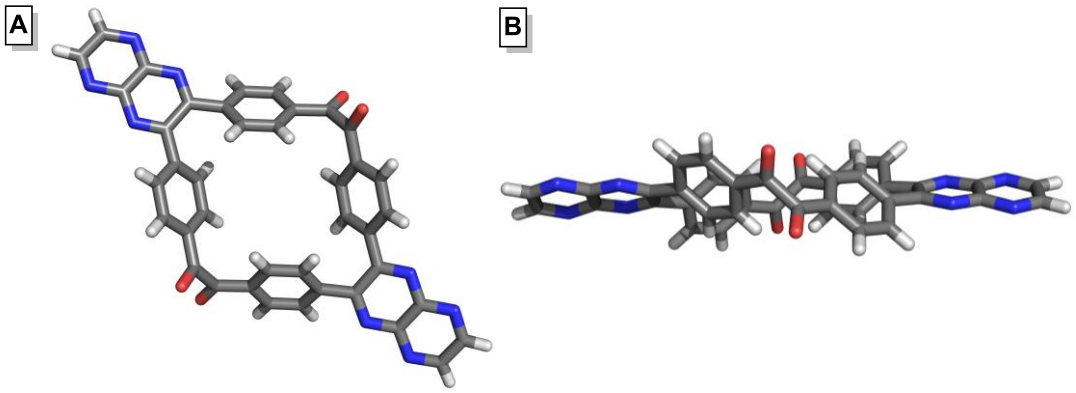

Figure 3.9 (A) Top-down view, and (B) side view of the X-ray crystal structure of compound **26j**. Element colors: C—gray, O—red, N—blue, H—white. All solvent molecules are omitted for clarity.

X-ray diffraction analysis of compound **26j**, which is produced by the fusion of 1,4,5,8-tetraazanaphthalene moieties with two opposite corners of **7**, showed that the crystal structure of compound **26j** is very similar to compound **26a**. In compound **26j**, the square-shaped central cavity of cyclotetrabenzil (**7**) elongated to adapt a rhombus shape with a long diagonal of 10.22 Å connecting the centroids of the fused bonds between the central macrocycle and tetraazanaphthalene nucleus, and a 8.45 Å short diagonal between the centroids of the two C–C bonds between the adjacent carbonyl groups (Figure 3.9). This deformation of the central cavity was clearly observable, although the torsion angles (79.3º) between the adjacent C=O groups mostly did not change. The planes of each opposite pair of phenyl rings in the core macrocycle form an acute angle (75.4 and 76.1º) in two opposite directions with centroid-centroid distances of 7.40 and 7.42 Å. The distance between the centroids of pyrazine rings in tetraazanaphthalene moieties and the tilt angle between their planes are 12.50 Å and 35.1º, respectively. The phenyl rings in the core macrocycle are

inclined, and the angles between the tetraazanaphthalene planes and the phenyl rings planes are almost similar (38.5 and 39.6º) for both phenyl rings attached to the same tetraazanaphthalene moiety in the both fusion corners of macrocycle.

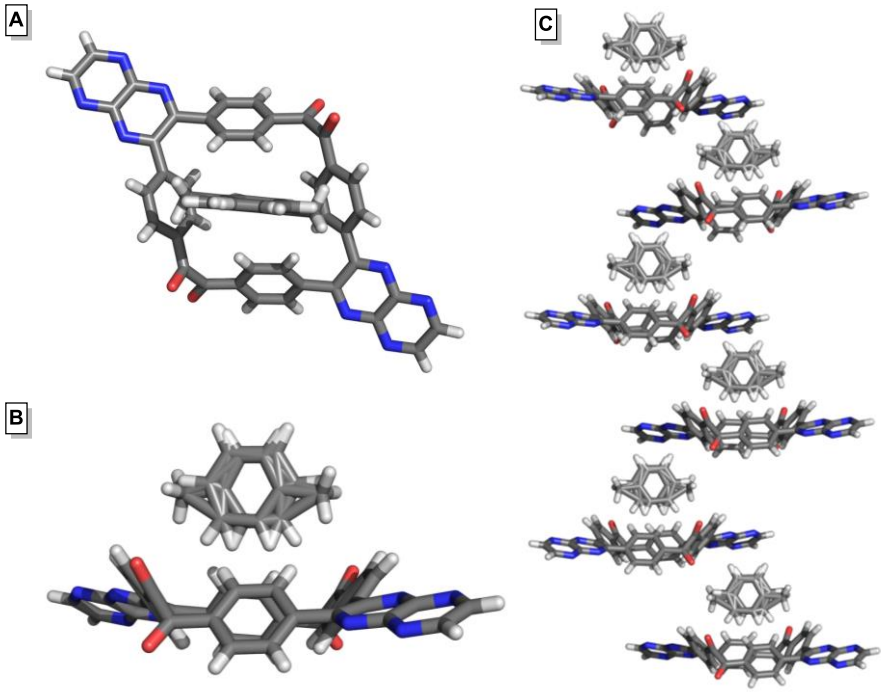

Figure 3.10 Disordered PhMe molecule included into the cavity of **26j** in two orientations *(A)* top-down view, *(B)* side view, and *(C)* alternative zig-zag co-sequence of PhMe guests and host macrocycle molecules of **26j**, viewed along crystallographic *c* axis. Element colors: C—gray, O—red, N—blue, H—white.

Compound **26j** formed an inclusion complex with PhMe in a 1:1 ratio. The included PhMe molecules are located on the same level with the macrocycle **26j** in two overlapped orientations. One edge from the included PhMe is tucked into the cavities of **26j** from the side that has 7.40 Å distance between the centroids of the opposite phenyl rings as seen in Figure 3.10A,B. This complexation pattern repeated itself within the crystal lattice generating an infinite zig-zag alternative sequence of PhMe guests and macrocycle hosts, seen along the crystallographic *c* axis in Figure 3.10C. The plane of PhMe molecule and the plane of core macrocycle are almost perpendicularly intersected with an inclined angle of 84.6º. The distances between the centroids of PhMe guest and the phenyl rings in the host macrocycle

range from 5.14 to 5.64 Å. The binding patterns of the resultant inclusion complex of compound **26j** indicated that there are two short [C–H···N] and [C–H···O] contacts measuring 2.64 and 2.65 Å, respectively, established between two of the hydrogen atoms of the methyl group in PhMe guests with two neighboring macrocycles.

The extended structure of compound **26j** is shown in Figure 3.11, viewed along the crystallographic *a* axis. A variety of short contacts were found to stabilize this extended structure: short [C–H···N] contacts of 2.54 Å, short [C=O···N] contacts of 2.97 Å, short [C=O···C] contacts range from 2.93 to 3.18 Å, short [C–H···O] contacts of 2.45 and 2.61 Å, short [C–H···C] contacts of 2.79 and 2.83 Å, and finally short [C···C–H] contacts of 3.39 Å. The other stabilization factor is face-to-face [π···π] stacking with distance of 4.13 Å between the centroids of the phenyl rings in the host macrocycle and the terminal pyrazine rings in the neighboring molecules.

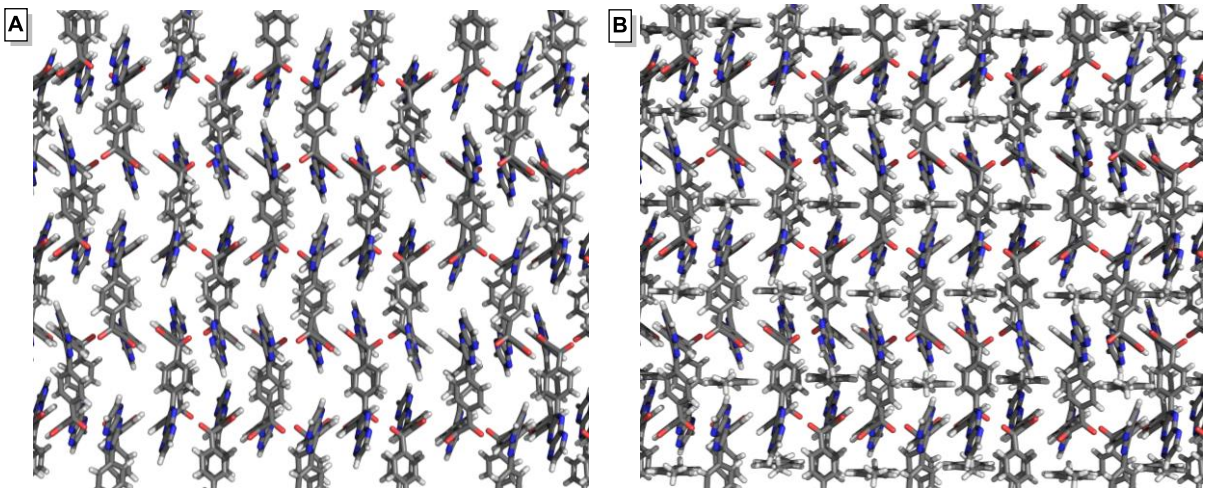

Figure 3.11 Segment of the crystal packing diagram of compound **26j** *(A)* without guest molecules and *(B)* with guest molecules, shown along the crystallographic *a* axis. Element colors: C—gray, O—red, N—blue, H—white.

3.2.5 Crystal Structure of Cyclic Oligoazaacene 26i and Its Coordination Polymer

The fusion of 1,4,5-triazanaphthalene moieties with only two opposite corners of the parent cyclotetrabenzil (**7**) produced compound **26i** which is very similar to compound **26a**.

This compound is expected to have two pyridine rings terminating the two opposite quinoxaline sides instead of the two benzene rings in compound **26a**. The changes make the structure confusing since the nitrogen atoms in terminal pyridine rings could be oriented in the same direction (*cis*) or oriented in opposing direction (*trans*) as shown in Figure 3.12A.

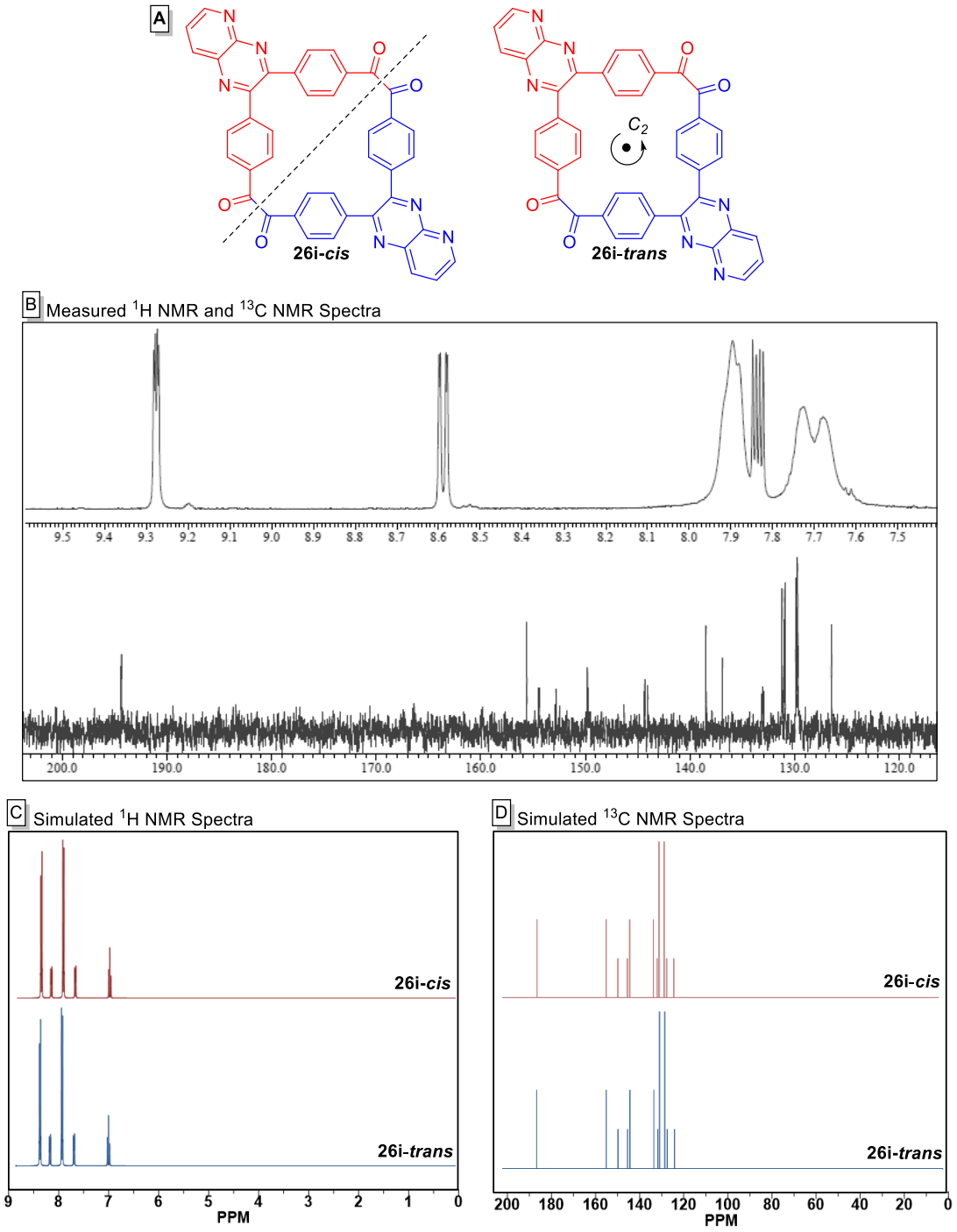

Figure 3.12 *(A)* The *cis* and *trans* expected isomers for compound **26i** highlighting their symmetry operations, *(B)* the measured ^{1}H NMR and ^{13}C NMR spectra, and *(C)* and *(D)* simulated ^{1}H NMR and ^{13}C NMR spectra.

The physical characterization techniques such as mass spectrometry, FT-IR spectroscopy, elemental analysis, ^{1}H NMR, and ^{13}C NMR spectroscopy cannot differentiate between the two expected constitutional isomers and the results of these analyses were unsatisfactory. Both isomers have the same molecular weight, functional groups, and element ratio which make the characterization of resultant compound **26i** by mass spectrometry, FT-IR spectroscopy, or elemental analysis is ambiguous. The measured and simulated ^{1}H NMR and ^{13}C NMR spectra, which created by ChemDraw Professional software, for both isomers are mostly the same (Figure 3.12B–D) since the *cis*-isomer has a symmetry plane dividing the molecule into two symmetrical parts, and the *trans*-isomer has a two-fold rotation axis perpendicular to the plane of the molecule, which also dividing the molecule into two symmetrical parts.

Applying single-crystal X-ray diffraction analysis on compound **26i** could be a good choice to identify the right structure. Confirming the expectations, structure of compound **26i** is very similar to the structure of compound **26a** where the central cavity is elongated, forming a rhombus shape with a long diagonal of 10.67 Å connecting the centroids of the fused bonds between the central macrocycle and triazanaphthalene nucleus, and 7.54 Å short diagonal between the centroids of the two C–C bonds between the adjacent carbonyl groups (Figure 3.13). The elongation of the central cavity was obviously noticeable through the identical torsion angles (101.1º) between the adjacent C=O groups. The tilt angles between the planes of each opposite pair of phenyl rings in the core macrocycle are 57.4 and 70.2º, with centroid-centroid distances of 7.59 and 7.20 Å. The phenyl rings in the core macrocycle are inclined, and the angles between the triazanaphthalene planes and the neighboring phenyl rings planes range from 46.2 to 51.1º.

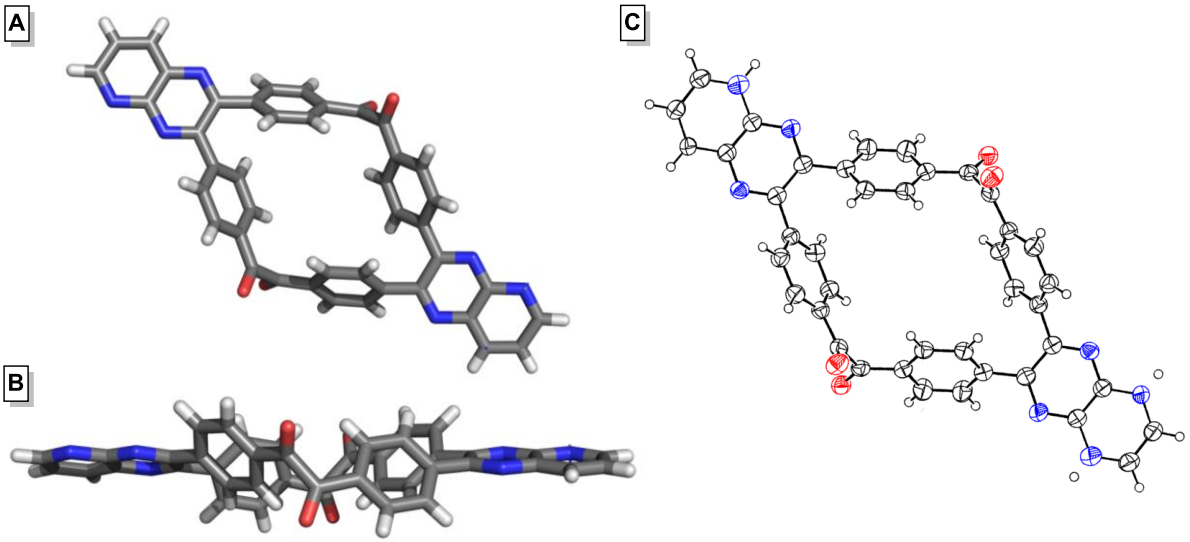

Figure 3.13 *(A)* Top-down view, and *(B)* side view of the X-ray crystal structure of compound **26i**. *(C)* Thermal ellipsoid plot of **26i** shown at the 50% probability level. Element colors: C—gray, O—red, N—blue, H—white. All solvent molecules are omitted for clarity.

The packing diagram of compound **26i** is shown in Figure 3.14 viewed along the reciprocal a^* cell axis. The extended structure is stabilized by two types of short contacts: short [C=O···C] contacts which range from 3.01 to 3.22 Å and short [C–H···O] contacts of 2.56 and 2.68 Å.

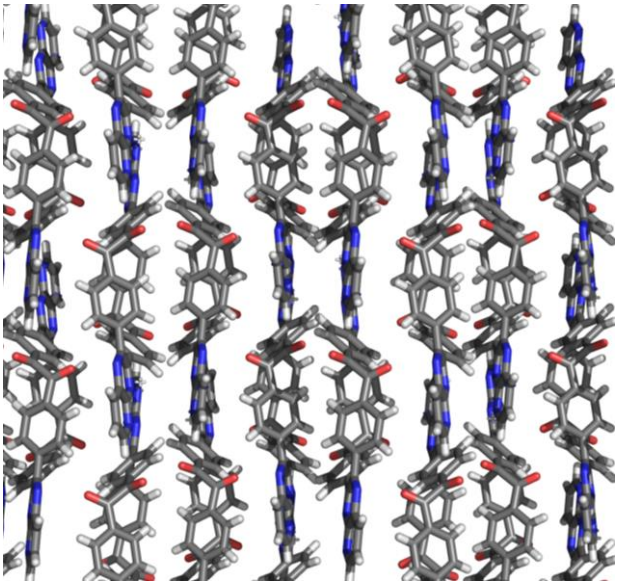

Figure 3.14 Segment of the crystal packing diagram of compound **26i**, shown along the reciprocal *a** cell axis. C—gray, O—red, N—blue, H—white. All solvent molecules are omitted for clarity.

Unfortunately, the results of the single crystal X-ray analysis were disappointing; the minimal difference between the electron density of carbon and nitrogen atoms makes the assignment of these atoms very confusing, thus not allowing us to clarify which regioisomer was formed.

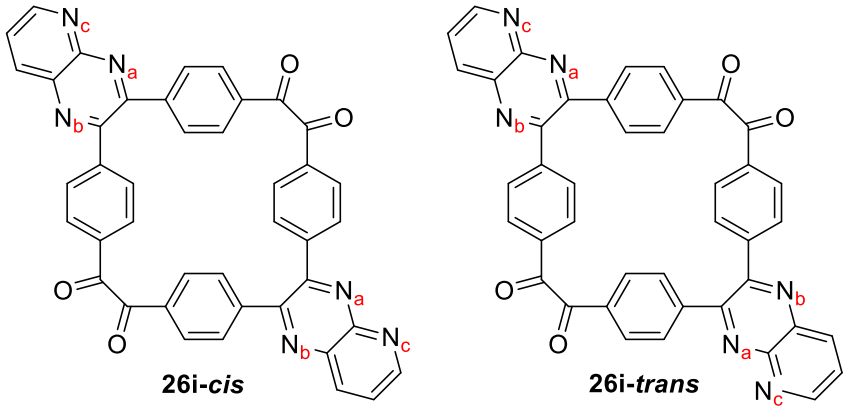

Chart 3.3 The possible sites in compound **26i** to coordinate with transition metals.

After the failure of all the performed physical analyses to identify the identity of compound **26i**, the experiments turned into studying the chemical properties for this compound that may direct the project in another way in order to elucidate the correct structure. Two opposite sides in compound **26i** fused with triazanaphthalene moieties which have been studied as potential transition metals chelators to copper;[366–375] this type of fusion makes compound **26i** an excellent candidate ligand to coordinate with different transition metals. Since the structure of **26i** has six accessible sites to coordinate with metals and there are two likely structures (Chart 3.3), it has a possibility to act as a bidentate ligand from both symmetrical sides in macrocycle through N_a, N_b, or N_c, or act as a tetradentate ligand through N_a–N_c or N_b–N_c, at each isomer, so several possible complexes can be produced. The pK_a values of the conjugated acids of the ligands can possibly be used to predict relative coordination abilities of the N-containing ligands. The pK_a of protonated quinoxaline is 0.56 which makes it a weaker base than 1,4,5-triazanaphthalene whose pK_a (in the protonated

state) is 1.20. These pK_a values indicated that protonation of 1,4,5-triazanaphthalene occurs at N_c.[376,377] Therefore, N_c will be the best site to coordinate with transition metals which reduced the total of expected complexes to two possibilities.

In this experiment, the slow diffusion of methanolic solution of copper salts into a $CHCl_3$ solution of compound **26i** in 1:1 adduct using liquid-liquid diffusion technique were applied. The copper salts used in this experiment were $Cu(NO_3)_2 \cdot 2.5H_2O$, $Cu(ClO_4)_2 \cdot 6H_2O$, $Cu(CO_2CH_3)_2 \cdot H_2O$, $CuCl_2 \cdot 2H_2O$, and CuCl, but only $CuCl_2 \cdot 2H_2O$ afforded single crystals with **26i** after a pair of days. The resulting bright blue crystals were analyzed by single crystal X-ray diffraction and the resulting structure is shown in Figure 3.15.

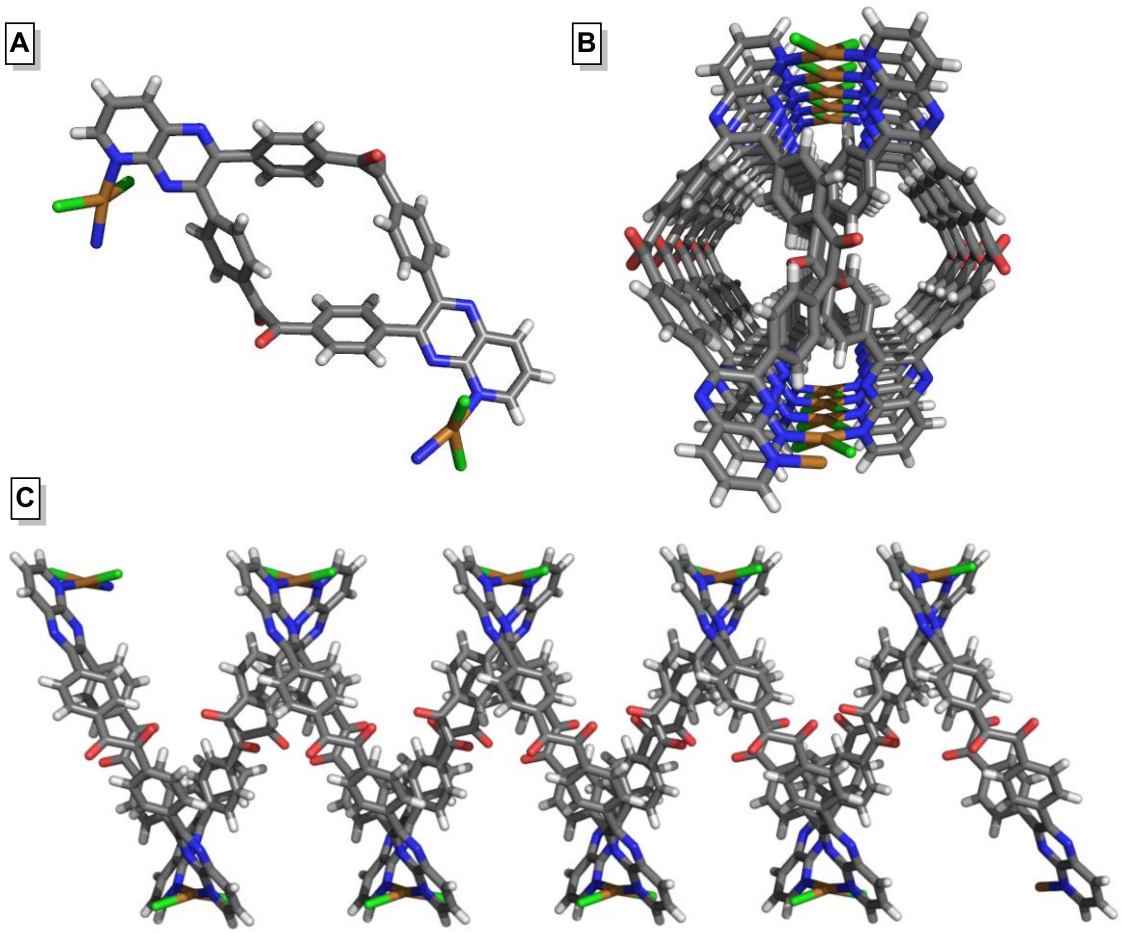

Figure 3.15 *(A)* The interaction between nitrogen atoms of the terminal pyridine rings in compound **26i** with $CuCl_2 \cdot 2H_2O$. *(B)* and *(C)* a single infinite, one-dimensional, and twin-tubular strand of alternating $CuCl_2$ and macrocycle showing from different orientations.

The crystallographic results relieved all the doubts about the correct structure. It proved that the nitrogen atoms of the terminal pyridine rings in compound **26i** are oriented in the same direction forming the *cis*-isomer. The results also confirmed the prediction of the most probable site in triazanaphthalene moieties to coordinate with metal. Every Cu(II) ion in this structure coordinates simultaneously to N-sites in two terminal pyridine rings from two cyclic ligands forming an infinite one-dimensional twin-tubular helices which were seen as basic skeletal structures. Each turn of the helical structure consists of two $CuCl_2$ units and two macrocyclic units that make a single strand of alternating $CuCl_2$ and macrocycle. The Cu(II) ion is four-coordinated with a geometry index (τ) of 0.21, measured by Okuniewski method, where τ is the number ranging from 0 to 1 that indicates the geometry of the coordination center (for four coordinated compounds: τ_4 = 1.0 for perfect tetrahedral geometry and 0.0 for perfect square planar geometry).[378] Consequently, the local geometry approximates to be almost square planar with two chlorine atoms and two nitrogen atoms from two cyclic ligands: the average bond length of Cu–Cl and Cu–N bonds are 2.24 and 2.02 Å, while the basal angles of Cl– Cu–Cl and N– Cu–N are 154.9 and 168.7º, and the average angle of Cl–Cu–N is 91.2º.

The rhombus-shaped central cavity of the macrocycle is slightly elongated and twisted after the coordination with Cu(II) ion: the long and short diagonals became 10.74 and 7.41 Å, respectively, and the torsion angles between the adjacent C=O groups became 108.4 and 118.5º. The centroid-centroid distances between the opposing pairs of phenyl rings in the core macrocycle are 7.45 and 7.47 Å, with tilt angles between their planes of 64.4 and 62.3º. The distance between the centroids of pyrazine rings in triazanaphthalene moieties and the tilt angle between their planes are 12.99 Å and 37.3º, respectively. The inclined angles between the triazanaphthalene planes and the neighboring phenyl rings planes in the core macrocycle range from 39.4 to 47.1º. The large distance between the Cu(II) ions in this structure

precludes any direct interaction between them: 17 Å between two Cu(II) ions coordinate to the same macrocycle and 10.9 Å between two Cu(II) ions starting each turn of the helical strand.

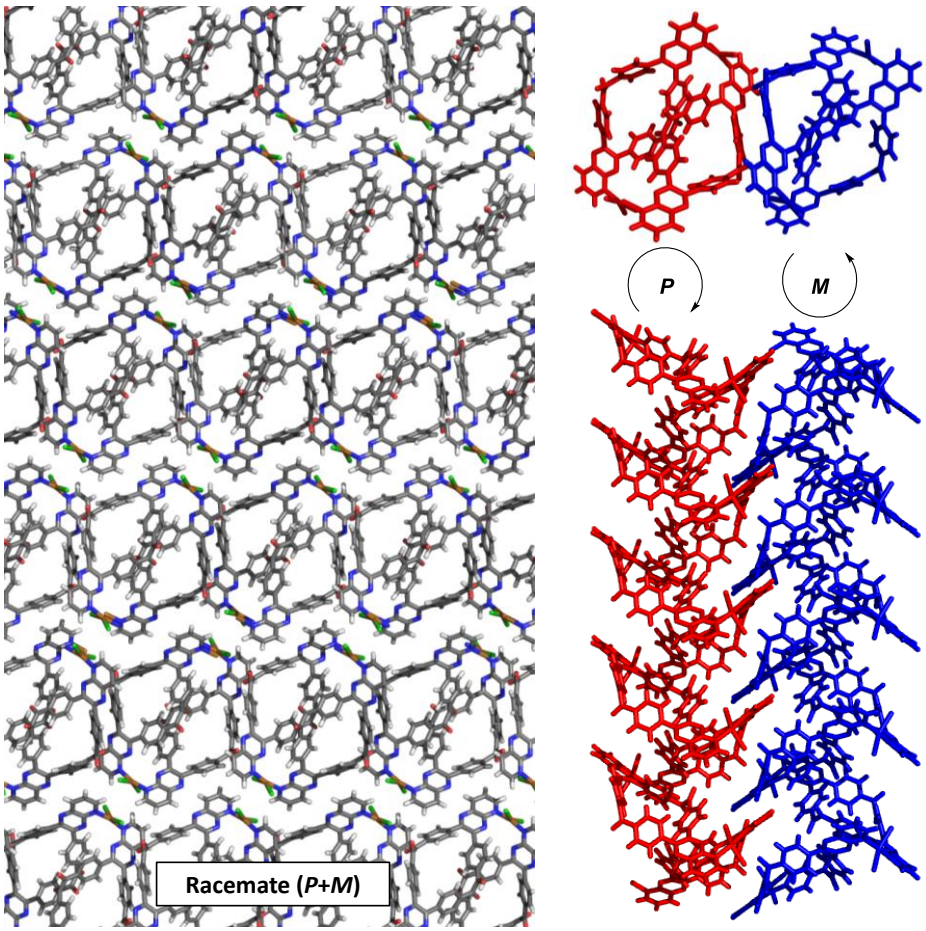

Figure 3.16 Crystal packing on the crystallographic *b* axis for **26i** showing the alternating right-handed (*P*)/left-handed (*M*) fashion and forming a racemate in the solid state.

The twin-tubular helices were found to be packed on the *b*-axis in an alternating right-handed (*P*)/lefthanded (*M*) fashion forming a racemic mixture in the solid state (Figure 3.16). This packing style generates a 3D network with spaces in the cavities accessible to small solvent molecules. The crystal lattice of the alternating helices stabilized with different short contacts: short [C=O···C] contacts range from 3.01 to 3.22 Å, short [C–H···Cl] contacts of 2.65 Å, short [C–H···C] contacts of 2.79 to 2.88 Å, and finally short [C=O···C] contacts with an average of 3.17 Å.

Table 3.1 Optical and electrochemical properties of selected oligoazaacenes molecules.

Compd.	$\lambda_{max,\,abs.}$ [nm]	λ_{onset} [nm]	$\lambda_{max,\,em.}$ [nm]	ε [L(mol*cm)$^{-1}$]	$E_{(0/-)}$ [V] [a]	HOMO [eV] [b]	LUMO [eV] [c]	gap [eV] [d]	Φ [e]
7	269	294	369	24000	–1.40	–7.62	–3.40	4.22	0.03
23a	303	356	426	8600	–2.06	–6.22	–2.74	3.48	0.02
23b	302	355	427	14000	–2.09	–6.20	–2.71	3.49	0.02
25a	368	394	406	36000	–2.13	–5.82	–2.67	3.15	0.06
26a	343	380	408	19000	–1.69	–6.37	–3.11	3.26	0.06
25b	377	399	408	46000	–1.67	–6.24	–3.13	3.11	0.06
25c	370	395	409	36000	–1.62	–6.32	–3.18	3.14	0.03
25d	372	396	409	40000	–1.97	–5.96	–2.83	3.13	0.03
25k	378	415	422	197000	–1.50	–6.29	–3.30	2.99	0.03
25l	497	512	508	146000	–1.63	–5.59	–3.17	2.42	0.14
25m	597	612	604	125000	–1.50	–5.28	–3.30	1.98	0.17
25n	595	616	607	74000	–1.09	–5.72	–3.71	2.01	0.09
26n	598	617	609	298000	–1.63	–5.18	–3.17	2.01	0.38
25nl	595	616	608	117000	–0.98	–5.83	–3.82	2.01	0.16
27k	369	405	427	43000	–1.85	–6.01	–2.95	3.06	0.02
27l	485	501	497	50000	–1.56	–5.71	–3.24	2.47	0.41
27m	582	598	590	46000	–1.40	–5.47	–3.40	2.07	0.46
27n	586	606	599	66000	–1.03	–5.82	–3.77	2.05	0.45

UV/Vis measurements for **7**, **23a**–**b**, **25a**–**d**, and **26a** were performed in CH_2Cl_2; **25k**–**n**, **26n**, **25nl**, and **27k**–**n** in *n*-hexane. [*a*] First reduction potentials measured by cyclic voltammetry (CV) in CH_2Cl_2 or THF with Bu_4NPF_6 as the electrolyte against Fc/Fc^+ as an internal standard (−4.80 eV) at 200 mV s^{-1}. [*b*] E_{HOMO}=$E_{LUMO\,CV}$−$E_{gap\,UV}$. [*c*] Calculated from CV measurements ($E_{LUMO\,CV}$=−4.80 eV–$E_{(0/-)}$). [*d*] Calculated from λ_{onset} in CH_2Cl_2 for **7**, **23a**–**b**, **25a**–**d**, and **26a** and in *n*-hexane for **25k**–**n**, **26n**, **25nl**, and **27k**–**n**. [*e*] Quantum yields as solutions in CH_2Cl_2 or *n*-hexane from average values of three independent measurements.

3.2.6 Physical Properties of Selected Cyclic Oligoazaacenes

To evaluate the suitability of synthesized macrocycles for applications in organic electronics—such as photovoltaics and light-emitting diodes—the optical and electrochemical properties of some prepared oligoazaacene macrocycles were analyzed by UV/Vis absorption and fluorescence spectroscopy, and cyclic voltammetry, and were found to be dominated by the linear azaacene fragments. From the UV/Vis (λ_{onset}) and cyclic voltammetry ($E_{(0/-)}$) measurements, the ionization potentials, HOMO/LUMO energy levels and optical band gaps were estimated; the results are summarized in Table 3.1.

3.2.6.1 Optical Properties of Selected Prepared Oligoazaacenes

Cyclotetrabenzil (**7**) has a relatively featureless UV/Vis absorption spectrum, with absorption not extending beyond 300 nm. Compounds **23a** and **23b**, macrocycles fused to saturated fragments, have one broad peak at around 300 nm, while bisquinoxalines macrocycle **26a** has two main absorption bands at 343 and 290 nm coming from n–π* and π–π* transitions. Tetraquinoxaline macrocycles **25a**–**d** have two main features in their absorption spectra: λ_{max} 368 nm (**25a**), 377 nm (**25b**), 370 nm (**25c**), and 372 nm (**25d**) and another band centered around 281 nm. Spectra of **25a**, **25c**, and **25d** are largely superimposable, suggesting a relatively minimal effect of substitution. The attachment of methyl or TIPS groups onto compound **25a** led to a noticeable redshift of the UV-vis spectra from 368 nm (**25a**) to 377 nm (**25d**) and 378 nm (**25k**), as a consequence of decreasing the polarity of macrocycles. A significant redshift in the UV/Vis spectra is also observed by increasing the size of the TIPS-azaacene appendix from diazanaphthalene (**25k**) to diazaanthracene (**25l**) and to di- and tetraazatetracenes (**25m**, **25n**, and **25nl**). The related tetraquinoxalines derivatives **25m** and **25n** show similar absorption around 597–595 nm

while the shape of the spectra differs. The tetraazatetracene compound **25n** exhibits a broad absorption between 400–510 nm. Compared to their noncyclic relatives **27k**–**n**, the cyclic compounds **25k**–**n** show red shifts of 9 nm for **25k**/**27k** and **25n**/**27n**, 12 nm for **25l**/**27l**, and 15 nm for **25m**/**27m**. This trend in bathochromic shifts is seen due to the increase of the polyconjugated structures which lower the band gaps between the HOMO and LUMO energy levels in cyclic oligoazaacenes. Regardless of their cyclic/acyclic nature, all absorption profiles of the differently substituted acenes are quite similar. Thus a large influence of the fourfold cyclisation on the optical properties in solution is not observed with the expectation of the bathochromic shift and peak intensities.

The octaketone **7** has a significantly more structured emission with a maximum at 369 nm. Compounds **23a**–**b** have superimposable spectra with a single emission peak at ~426 nm, and compounds **25a**–**d** and **26a** have also essentially superimposable spectra with a single emission peak at ~408 nm. All the compounds **8**, **23a**–**b**, **25a**–**d**, **26a** have low fluorescence quantum yields of under 6%. The attachment of TIPS motifs on compound **25a** led to a noticeable redshift of the emission spectra from 406 nm for **25a** to 422 nm for **25k** (TIPS-diazanaphthalene motifs). This shift is gradually increased with the increasing size of the acene appendix: 508 nm for **25l** (TIPS-diazaanthracene motifs) and 604–609 nm for **25m**–**n**, **26n**, and **25nl** (TIPS-diazatetracene or TIPS-tetraazatetracene motifs). In comparison with their noncyclic relatives **27l**–**n**, the cyclic compounds **25l**–**n** show bathochromic shifts of 11 nm for **25l**/**27l**, 14 nm for **25m**/**27m**, and 8 nm for **25n**/**27n**.

To examine the influence of different size of TIPS-azaacenes motifs within the macrocycles, the quantum yields (Φ) of the TIPS-azaacene derivatives **25k**–**n**, **26n**, **25nl**, and **27k**–**n** in *n*-hexane were compared. The acyclic compounds **27l**–**n** have quantum yields Φ from 41% (**27l**), 46% (**27m**), and 45% (**27n**) in *n*-hexane. The Φ for the corresponding four-fold cyclic oligoazaacenes compounds **25l**–**n**, **26n**, and **25nl** decrease to 14%, 17%, 38%, and

9% in *n*-hexane. The space-filling phenyl groups of **27l**–**n** could prevent aggregation of the acenes in solution due to them being twisted out of the molecular plane, thus inhibiting the quenching of the fluorescence.

Compounds **25l**–**n** and **25nl** were spin-coated as thin-films and as thin-film composites with polymethyl methacrylate (PMMA) as a host material on glass substrate, to inhibit the aggregation of the emitters. However quantum yields are not greatly influenced, as they were determined to be 19% (**25l**), 10% (**25m**), 12% (**25n**), and 13% (**25nl**) in thin-films and 10% (**25l**), 12% (**25m**), 12% (**25n**), and 7% (**25nl**) in thin-film composites.

The effect of the integration of azaacene subunits on the optical properties of macrocycles is clearly shown in Figure 3.17. The colors of the compounds **25k**–**l**, **25n**, **27k**–**l** and **27n** under daylight and illumination at 365 nm are different. The color of the substances in solution is determined by the acene fragment: **25k** and **27k** are colorless (TIPS-diazanaphthalene motifs), **25l** and **27l** are deep yellow (TIPS-diazaanthracene motifs), and **25n** and **27n** are deep red (TIPS-tetraazatetraacene motifs). The three cyclic compounds show the azaacene-typical fluorescence.

Figure 3.17 Photographs of **25k**–**l**, **25n**, **27k**–**l** and **27n** under UV light with illumination at 365 nm (left) in *n*-hexane and in daylight (right).

3.2.6.2 Electronic Properties of Selected Prepared Oligoazaacenes

To approximate the ionization potentials and electron affinities, we performed cyclic voltammetry (CV) measurements. All studied compounds display one pseudo reversible reduction peak $E_{(0/-)}$ and no oxidation peak. The first reduction potentials for the cyclic oligoazaacenes ranged from −2.13 V to −0.98 V, and for the acyclic relatives range from −1.03 V to −1.85 V.

From the CV and UV/Vis spectra, the HOMO/LUMO energy levels and optical bandgaps were estimated. The bandgap for parent macrocycle **7** is 4.22 eV, and for its derivatives with saturated motifs **23a**–**b** or with quinoxaline motifs **25a**–**d**, and **26a** range from 3.11 eV to 3.49 eV. For the cyclic TIPS-azaacene compounds **25k**–**m** the gap decreases by enlarging the azaacene subunit: it shifted from 2.99 eV for **25k**, to 2.42 eV for **25l** and finally to 1.98 eV for **25m**. The gaps of the acyclic TIPS-azaacene compounds **27k**–**m** are subtly increased compared with the cyclic analogous: 3.06 eV for **27k**, to 2.47 eV for **27l** and finally to 2.07 eV for **27m**.

3.3 Conclusions and Outlook

In conclusion, a new and highly modular synthetic strategy to access a class of conjugated functionalized cyclic oligoazaacenes molecules was developed by doing the yield-limiting cyclization step at the beginning of the synthesis. Through various unsaturated, halogenated, and TIPS-ethynylated *ortho*-diamines, the effect of incorporating different motifs into the cyclic backbone structure were examined. Stabilizing and solubilizing side groups turn the produced compounds into easy-to-handle macrocycles. Constructing structures from cyclic octaketone building block with multiple 1,2-phenylenediamines gives rise to novel optical and electronic properties resulting from the enlarged cyclic conjugated

systems with azaacene subunits. The optical and electronic properties are primarily determined by the linear azaacene subunit; however, a small bathochromic shift compared to the linear counterparts is observed. The fusion of cyclic octaketone with nitrogen-rich 1,2-phenylenediamines produced large macrocycles with molecular recognition and complexation properties.

In the future, the unique physical properties of cyclic oligoazaacenes molecules will be investigated. The increased absorptivity by the cyclization combined with a high solubility could be applied in many areas of organic electronics such as for organic photovoltaics (OPV). Furthermore, mixed macrocycles with donor and acceptor units at opposing sides could prove to be exciting candidates for novel donor/acceptor systems. Also, the fusion of octaketone with 1,2-phenylenediamine derivatives of highly electron-withdrawing or electron-donating ability could make them a candidate host to accommodate small molecules with electron-rich or electron-poor characters. Finally, the coordination of the two-fold or four-fold macrocycles with abundant nitrogen atoms or carboxylic acid groups to different transition metals could lead to the formation of two- or three-dimensional hybrid porous membranes or frameworks.

3.4 Experimental Section

3.4.1 General Materials and Physical Methods

Materials. All reactions were performed in a fume hood in oven-dried glassware. All starting materials and solvents, which were used for syntheses or crystal growth, were obtained from the commercial sources and used without further purification. Cyclotetrabenzil (**7**) was synthesized according to the procedures described in Chapter Two.

Physical Methods. All NMR spectra were recorded on a JEOL ECA-500 spectrometer, with working frequencies for ^{1}H nuclei of 500, for ^{13}C nuclei of 125, and for ^{19}F nuclei of 470 MHz. ^{1}H, ^{13}C , and ^{19}F NMR chemical shifts (δ) were reported in parts per million (ppm) units relative to the residual signals of deuterated solvent (^{1}H: DMSO-d_6 = 2.50 ppm; $CDCl_3$ = 7.24 ppm; THF-d_8 = 3.58 and 1.73 ppm; ^{13}C: DMSO-d_6 = 39.50 ppm; $CDCl_3$ = 77.23 ppm; THF-d_8 = 67.57 and 25.37 ppm). All NMR spectra were recorded at ambient temperature. The multiplicities of ^{1}H NMR signals were described as follows: s = singlet, d = doublet, t = triplet, q = quartet, m = multiplet, dd = doublet of doublet). The ^{13}C NMR signal structure was analyzed by DEPT (Distortionless Enhancement by Polarization Transfer), which is a tool used to assign ^{13}C NMR peaks, and described as follows: (+) = primary or tertiary C atom "positive signal", (−) = secondary C atom "negative signal", and (Cq) = quaternary C atom "no signal". Melting points were measured in a Barnstead International 1101D MeL-Temp capillary MP apparatus equipped with Fluke 51-2 Thermometer, and are uncorrected. Mass spectra were recorded using electrospray ionization high resolution mass spectrometry (ESI-HRMS) and were collected at University of Texas at Austin by Dr. Ian M Riddington and his assistants. Infrared spectra (IR) were recorded on a Nicolet iS10 FT-IR spectrometer equipped with a Thermo Scientific iTR for multi-purpose ATR sampling and reported in wavenumbers (cm^{-1}) as a solid phase measurement. Elemental analyses were conducted by Intertek USA Inc. UV-Vis absorption spectra were recorded in dichloromethane in 1 cm quartz cuvettes using PerkinElmer LAMBDA 25 UV-Vis spectrophotometer. Excitation spectra were recorded in dichloromethane in 1 cm quartz cuvettes using PerkinElmer LS 55 spectrofluorometer. Quantum yields (Φ) were obtained by the absolute method using an Ulbricht sphere.[379] Given Φ for solutions in dichloromethane are average values of three independent measurements for solutions. Cyclic voltammetry (CV) experiments were performed with a CH Instruments 602E potentiostat using a three-

electrode system in a nitrogen-filled glove-box. A 3 mm diameter glassy-carbon, Pt wire, and silver wire were used as working electrode, auxiliary or counter electrode, and pseudoreference electrode, respectively. Measurements were carried out in dichloromethane with 0.1 M NBu_4PF_6 as a supporting electrolyte. Ferrocene was used as an internal standard, and potentials were referenced to the ferrocene/ferrocenium redox system and internal standard (−4.8 eV). To determine the first reduction potentials ($E_{(0/-)}$) and the first oxidation potential of ferrocene, the half-wave potentials were used. Single crystal XRD measurements were performed by Dr. Xiqu Wang (UH) using a Bruker DUO platform diffractometer, unless otherwise specified, equipped with a 4K CCD APEX II detector and an Incoatec 30 Watt Cu microsource with compact multilayer optics.

3.4.2 Syntheses and Characterization of Cyclic Oligoazaacenes

3.4.2.1 Synthesis and Characterization of Compound 23a

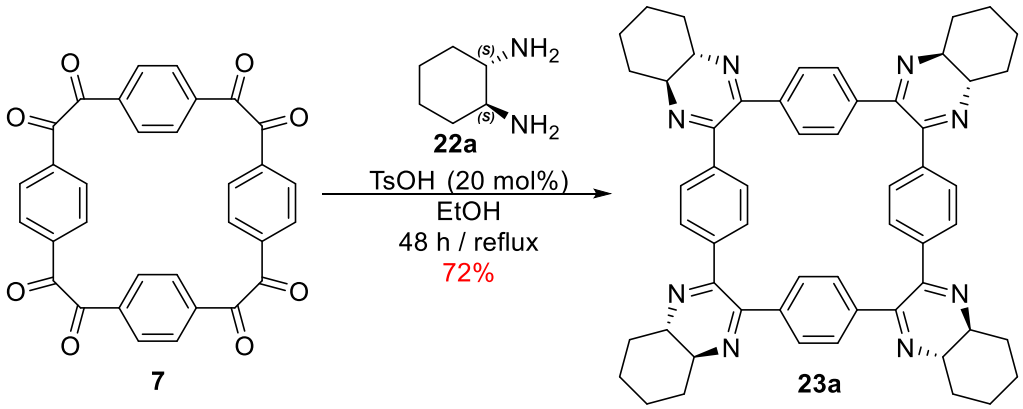

A solution of **7** (0.05 g, 0.10 mmol), (1*S*,2*S*)-(+)-1,2-diaminocyclohexane **22a** (0.05 g, 0.40 mmol, 4.00 equiv.), and *p*-toluenesulfonic acid (3.8 mg, 0.02 mmol, 0.20 equiv.) in EtOH (4 mL) was prepared in a 10-mL round-bottomed flask fitted with a Dean-Stark condenser. The solution was heated to reflux for 48 h, then cooled to room temperature, filtered, and washed with EtOH (10 mL) and then Et_2O (10 mL). After filtration, the product

was dissolved in $CHCl_3$ and the solution passed through a 2 cm thick Celite pad on a glass-fritted Büchner funnel and a clear solution was seen. The solvent was evaporated from the clear solution using rotary evaporator to afford a pure solid of compound **23a** (yield: 61 mg, 0.072 mmol, 72%, m.p. > 300 ºC, with decomposition). ^{1}H NMR (500 MHz, $CDCl_3$) δ 7.23 (s, 16H), 2.83 (m, 8H), 2.49 (m, 8H), 1.90 (m, 8H), 1.62 (m, 8H), 1.42 (m, 8H) ppm. ^{13}C NMR (125 MHz, $CDCl_3$) δ 157.34 (Cq), 137.85 (Cq), 128.63 (–), 59.24 (–), 33.53 (+), 25.49 (+) ppm. IR (neat): $\tilde{\nu}$ = 2924, 2856, 1534, 1448, 1287, 1258, 1231, 1065, 979, 842, 571, 549 cm^{-1}. ESI-HRMS: *m/z* $[M+H]^+$: Calcd for $[C_{56}H_{56}N_8 \cdot H]^+$: 840.46; Found 841.47, with correct isotope distribution. Elemental analysis Calcd (%) for $C_{56}H_{56}N_8$: C 79.97, H 6.71, N 13.32; Found: C 78.67, H 6.53, N 13.06.

3.4.2.2 Synthesis and Characterization of Compound 23b

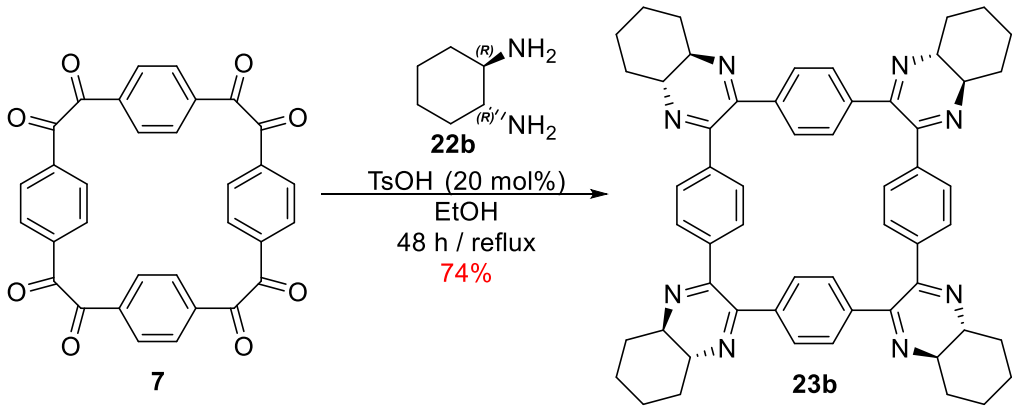

A solution of **7** (0.05 g, 0.10 mmol), (1*R*,2*R*)-(–)-1,2-diaminocyclohexane **22b** (0.05 g, 0.40 mmol, 4.00 equiv.), and *p*-toluenesulfonic acid (3.8 mg, 0.02 mmol, 0.20 equiv.) in EtOH (4 mL) was prepared in a 10-mL round-bottomed flask fitted with a Dean-Stark condenser. The solution was heated to reflux for 48 h, then cooled to room temperature, filtered, and washed with EtOH (10 mL) and then Et_2O (10 mL). After filtration, the product was dissolved in $CHCl_3$ and the solution passed through a 2 cm thick Celite pad on a glass-

fritted Büchner funnel and a clear solution was seen. The solvent was evaporated from the clear solution using rotary evaporator to afford a pure solid of compound **23b** (yield: 62 mg, 0.074 mmol, 74%, m.p. > 300 ºC, with decomposition). ^{1}H NMR (500 MHz, $CDCl_3$) δ 7.23 (s, 16H), 2.83 (m, 8H), 2.49 (m, 8H), 1.90 (m, 8H), 1.62 (m, 8H), 1.42 (m, 8H) ppm. ^{13}C NMR (125 MHz, $CDCl_3$) δ 157.34 (Cq), 137.81 (Cq), 128.63 (–), 59.24 (–), 33.53 (+), 25.49 (+) ppm. IR (neat): $\tilde{\nu}$ = 2925, 2856, 1534, 1449, 1288, 1258, 1231, 1066, 979, 842, 571, 549 cm^{-1}. ESI-HRMS: *m/z* $[M+Na]^+$: Calcd for $[C_{56}H_{56}N_8 \cdot Na]^+$: 840.46; Found 863.45, with correct isotope distribution. Elemental analysis Calcd (%) for $C_{56}H_{56}N_8$: C 79.97, H 6.71, N 13.32; Found: C 77.98, H 6.39, N 12.90.

3.4.2.3 Synthesis and Characterization of Compound 25a

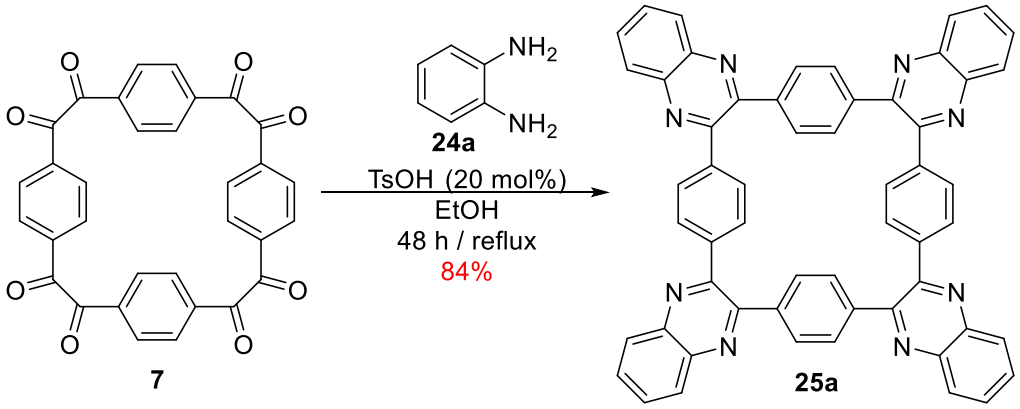

A solution of **7** (0.53 g, 1.00 mmol), *o*-phenylenediamine **24a** (0.43 g, 4.00 mmol, 4.00 equiv.), and *p*-toluenesulfonic acid (38.0 mg, 0.20 mmol, 0.20 equiv.) in EtOH (40 mL) was prepared in a 100-mL round-bottomed flask fitted with a Dean-Stark condenser. The solution was heated to reflux for 48 h, then cooled to room temperature, filtered, and washed with EtOH (30 mL) and then Et_2O (30 mL). After filtration, the product was dissolved in $CHCl_3$ and the solution passed through a 5 cm thick Celite pad on a glass-fritted Büchner funnel and a clear solution was seen. The solvent was evaporated from the clear solution

using rotary evaporator to afford a pure solid of compound **25a** (yield: 686 mg, 0.84 mmol, 84%, m.p. > 450 ºC, with decomposition). ^{1}H NMR (500 MHz, $CDCl_3$) δ 8.18 (dd, J=6.3 Hz, 8H), 7.79 (dd, J=6.3 Hz, 8H), 7.57 (s, 16H) ppm. ^{13}C NMR (125 MHz, $CDCl_3$) δ 152.24 (Cq), 141.43 (Cq), 139.17 (Cq), 130.54 (+), 130.20 (+), 129.36 (+) ppm. IR (neat): $\tilde{\nu}$ = 1337, 1220, 1124, 1064, 1017, 976, 845, 757, 637, 625, 610, 561, 541 cm^{-1}. ESI-HRMS: *m/z* $[M+H]^+$: Calcd for $[C_{56}H_{32}N_8 \cdot H]^+$: 816.27; Found 817.28, with correct isotope distribution.

3.4.2.4 Synthesis and Characterization of Compound 26a

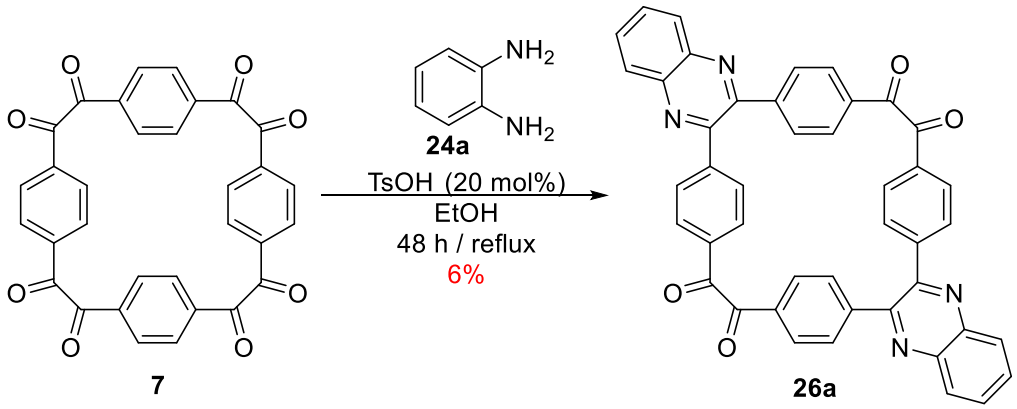

A solution of **7** (0.11 g, 0.20 mmol), *o*-phenylenediamine **24a** (0.06 g, 0.60 mmol, 3.00 equiv.), and *p*-toluenesulfonic acid (7.6 mg, 0.04 mmol, 0.20 equiv.) in EtOH (8 mL) was prepared in a 25-mL round-bottomed flask fitted with a Dean-Stark condenser. The solution was heated to reflux for 48 h, then cooled to room temperature, filtered, and washed with EtOH (10 mL) and then Et_2O (10 mL); the resulting product is mixture of **25a** and **26a** as shown in Figure 3.18. After filtration, the product was dissolved in boiling $CHCl_3$ (10 mL) and then filtered to afford a pure solid of compound **26a** (yield: 38 mg, 0.06 mmol, 6%, m.p. > 450 ºC, with decomposition). ^{1}H NMR (500 MHz, DMSO-d_6) δ 8.23 (dd, J=7.0 Hz, 4H), 7.96 (dd, J=6.0 Hz, 4H), 7.84−7.82 (d, J=7.5 Hz, 8H), 7.69−7.68 (d, J=7.0 Hz, 8H) ppm. ^{13}C NMR (125 MHz, DMSO-d_6) δ 195.52 (Cq), 152.21 (Cq), 145.43 (Cq), 141.19 (Cq), 132.09

(Cq), 131.95 (+), 131.74 (+) 129.80 (+), 129.60 (+) ppm. IR (neat): $\tilde{\nu}$ = 1664, 1601, 1556, 1507, 1477, 1406, 1342, 1318, 1290, 1215, 1175, 1124, 1053, 978, 832, 766, 720, 711, 686, 596, 541, 505 cm^{-1}. ESI-HRMS: *m/z* $[M+H]^+$: Calcd for $[C_{44}H_{24}O_4N_4 \cdot H]^+$: 672.18; Found 673.19, with correct isotope distribution. Elemental analysis Calcd (%) for $C_{44}H_{24}O_4N_4$: C 78.56, H 3.60, N 8.33; Found: C 76.07, H 3.50, N 7.79.

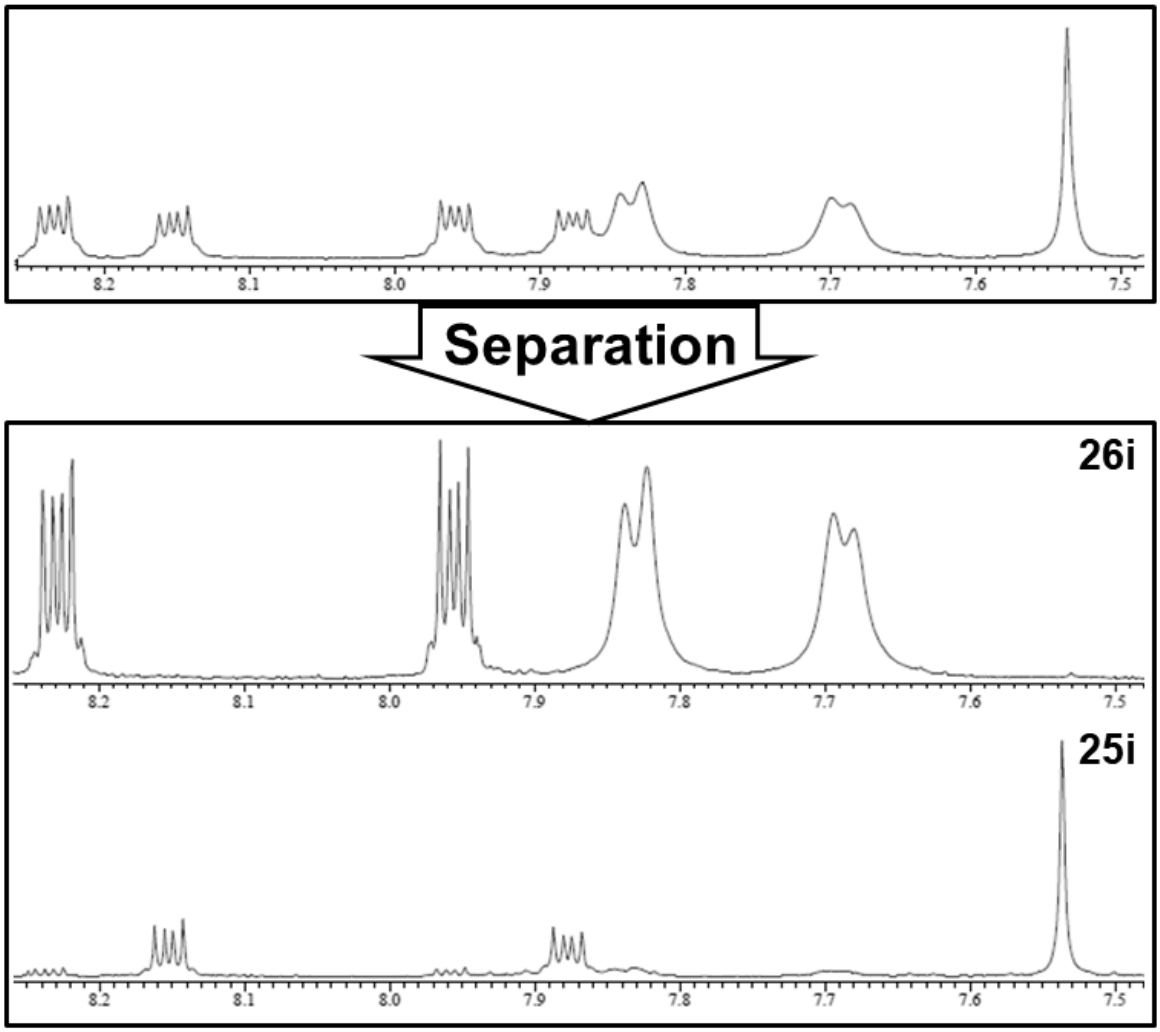

Figure 3.18 ^{1}H NMR spectra of the reaction of cyclotetrabenzil (**7**) with three equivalents of *o*-phenylenediamine before and after separation.

3.4.2.5 Synthesis and Characterization of Compound 25b

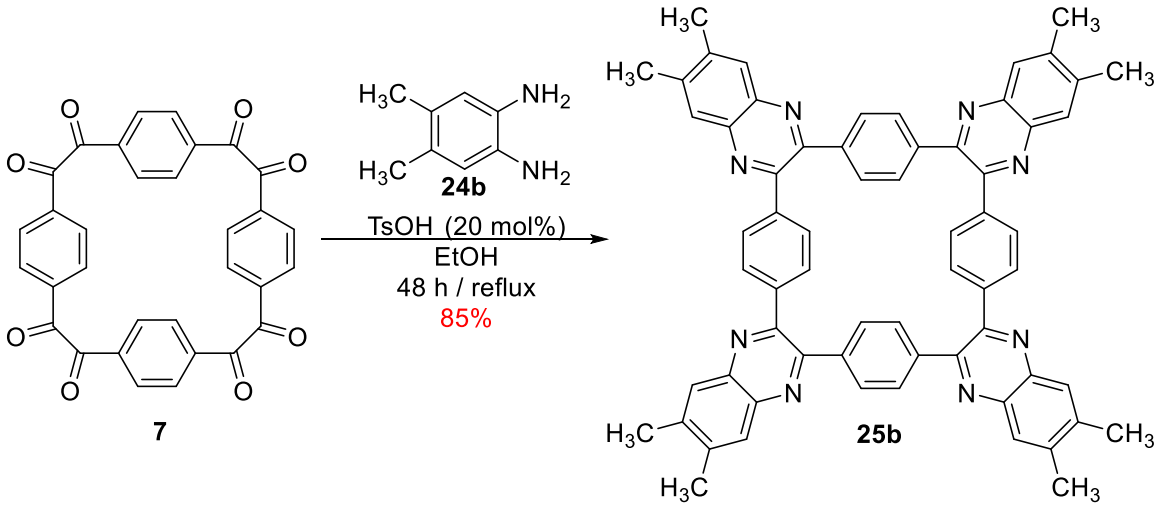

A solution of **7** (0.53 g, 1.00 mmol), 4,5-dimethyl-1,2-phenylenediamine **24b** (0.54 g, 4.00 mmol, 4.00 equiv.), and *p*-toluenesulfonic acid (38.0 mg, 0.20 mmol, 0.20 equiv.) in EtOH (40 mL) was prepared in a 100-mL round-bottomed flask fitted with a Dean-Stark condenser. The solution was heated to reflux for 48 h, then cooled to room temperature, filtered, and washed with EtOH (30 mL) and then Et_2O (30 mL). After filtration, the product was dissolved in $CHCl_3$ and the solution passed through a 5 cm thick Celite pad on a glass-fritted Büchner funnel and a clear solution was seen. The solvent was evaporated from the clear solution using rotary evaporator to afford a pure solid of compound **25b** (yield: 789 mg, 0.85 mmol, 85%, m.p. > 450 ºC, with decomposition). ^{1}H NMR (500 MHz, $CDCl_3$) δ 7.90 (s, 8H), 7.51 (s, 16H), 2.51 (s, 24H) ppm. ^{13}C NMR (125 MHz, $CDCl_3$) δ 151.42 (Cq), 141.09 (Cq), 140.41 (Cq), 139.21 (Cq), 130.09 (+), 128.32 (+), 20.60 (+) ppm. IR (neat): $\tilde{\nu}$ = 2970, 1682, 1606, 1475, 1339, 1263, 1208, 1058, 1016, 1005, 968, 863, 607, 564 cm^{-1}. ESI-HRMS: *m/z* $[M+H]^+$: Calcd for $[C_{64}H_{48}N_8 \cdot H]^+$: 928.40; Found 929.41, with correct isotope distribution. Elemental analysis Calcd (%) for $C_{64}H_{48}N_8$: C 82.73, H 5.21, N 12.06; Found: C 80.25, H 4.95, N 11.21.

3.4.2.6 Synthesis and Characterization of Compound 25c

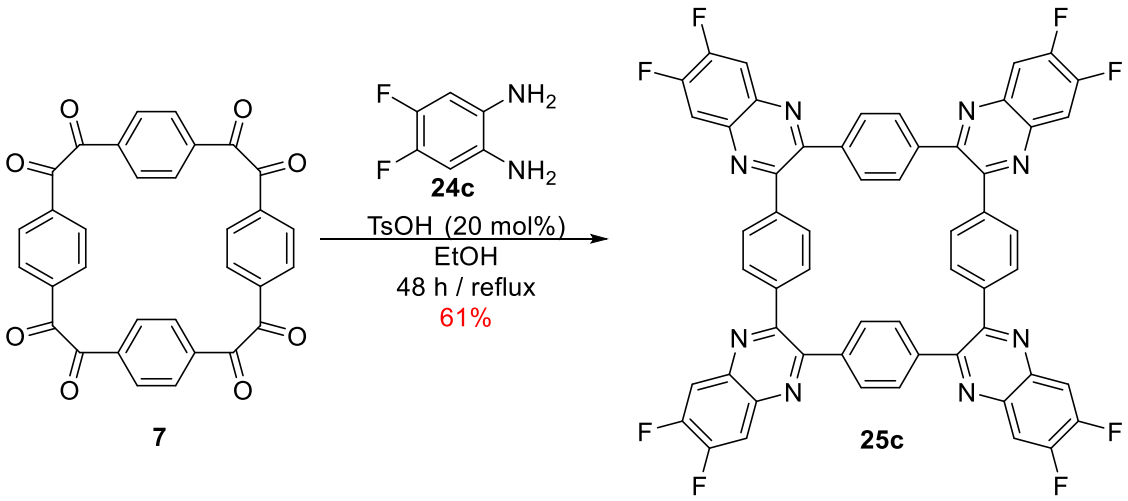

A solution of **7** (0.53 g, 1.00 mmol), 4,5-difluoro-1,2-phenylenediamine **24c** (0.58 g, 4.00 mmol, 4.00 equiv.), and *p*-toluenesulfonic acid (38.0 mg, 0.20 mmol, 0.20 equiv.) in EtOH (40 mL) was prepared in a 100-mL round-bottomed flask fitted with a Dean-Stark condenser. The solution was heated to reflux for 48 h, then cooled to room temperature, filtered, and washed with EtOH (30 mL) and then Et_2O (30 mL). After filtration, the product was dissolved in $CHCl_3$ and the solution passed through a 5 cm thick Celite pad on a glass-fritted Büchner funnel and a clear solution was seen. The solvent was evaporated from the clear solution using rotary evaporator to afford a pure solid of compound **25c** (yield: 588 mg, 0.61 mmol, 61%, m.p. > 450 ºC, with decomposition). ^{1}H NMR (500 MHz, $CDCl_3$) δ 7.91 (t, J=9.2 Hz, 8H), 7.53 (s, 16H) ppm. ^{13}C NMR (125 MHz, $CDCl_3$) δ 154.06 (Cq), 152.24 (Cq), 151.85 (Cq), 138.86 (Cq), 130.79 (+), 130.15 (+), 114.94 (+) ppm. ^{19}F-NMR (470 MHz, $CDCl_3$) δ –128.28 (t, J=9.0 Hz, 8F) ppm. IR (neat): $\tilde{\nu}$ = 1489, 1350, 1336, 1216, 1052, 1016, 976, 866, 780, 754, 613, 584, 546 cm^{-1}. ESI-HRMS: *m/z* $[M+H]^+$: Calcd for $[C_{56}H_{24}N_8F_8 \cdot H]^+$: 960.20; Found 961.21, with correct isotope distribution.

3.4.2.7 Synthesis and Characterization of Compound 25d

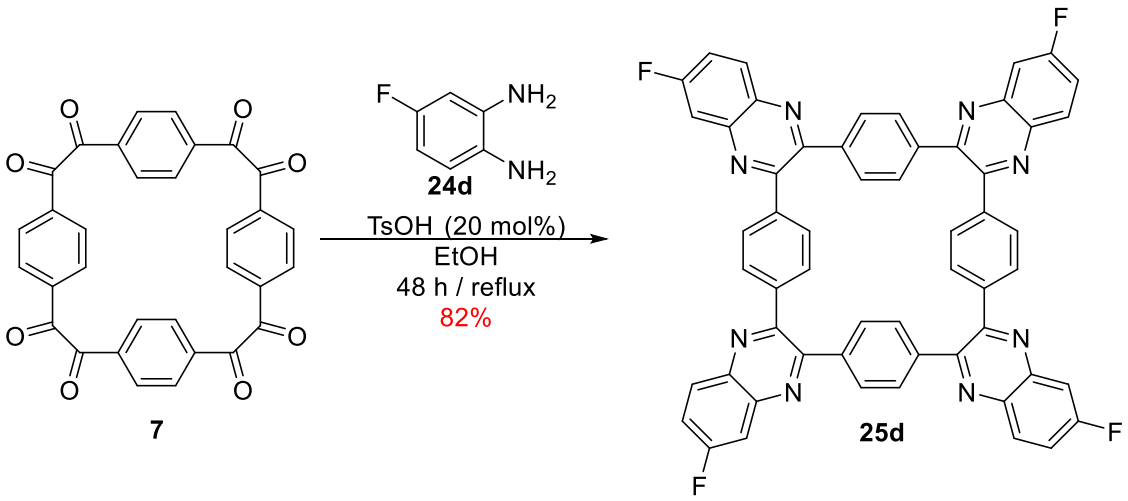

A solution of **7** (0.05 g, 0.10 mmol), 4-fluoro-1,2-phenylenediamine **24d** (0.05 g, 0.40 mmol, 4.00 equiv.), and *p*-toluenesulfonic acid (3.8 mg, 0.02 mmol, 0.20 equiv.) in EtOH (4 mL) was prepared in a 10-mL round-bottomed flask fitted with a Dean-Stark condenser. The solution was heated to reflux for 48 h, then cooled to room temperature, filtered, and washed with EtOH (30 mL) and then Et_2O (30 mL). After filtration, the product was dissolved in $CHCl_3$ and the solution passed through a 5 cm thick Celite pad on a glass-fritted Büchner funnel and a clear solution was seen. The solvent was evaporated from the clear solution using rotary evaporator to afford a pure solid of compound **25d** (yield: 73 mg, 0.082 mmol, 82%, m.p. > 450 ºC, with decomposition). ^{1}H NMR (500 MHz, $CDCl_3$) δ 8.17 (dd, *J*=9.3 Hz, 4H), 7.79 (dd, *J*=9.0 Hz, 4H), 7.58 (t, *J*=8.5 Hz, 4H), 7.55 (t, *J*=4.0, 16H) ppm. ^{13}C NMR (125 MHz, $CDCl_3$) δ 164.24 (Cq), 162.23 (Cq), 152.91 (Cq), 151.53 (Cq), 142.26 (Cq), 139.15 (Cq), 138.87 (Cq), 131.51 (+), 130.21 (+), 121.19 (+), 112.73 (+) ppm. ^{19}F-NMR (470 MHz, $CDCl_3$) δ –106.85 (m, 4F) ppm. IR (neat): $\tilde{\nu}$ = 1620, 1481, 1339, 1205, 1157, 1112, 1063, 1017, 980, 958, 852, 834, 615, 561 cm^{-1}. ESI-HRMS: *m/z* $[M+H]^+$: Calcd for $[C_{56}H_{28}N_8F_4 \cdot H]^+$: 888.24; Found 889.25, with correct isotope distribution. Elemental analysis

Calcd (%) for $C_{56}H_{28}N_8F_4$: C 75.67, H 3.18, N 12.61, F 8.55; Found: C 73.69, H 2.99, N 12.00, F 9.74.

3.4.2.8 Synthesis and Characterization of Compound 25ac

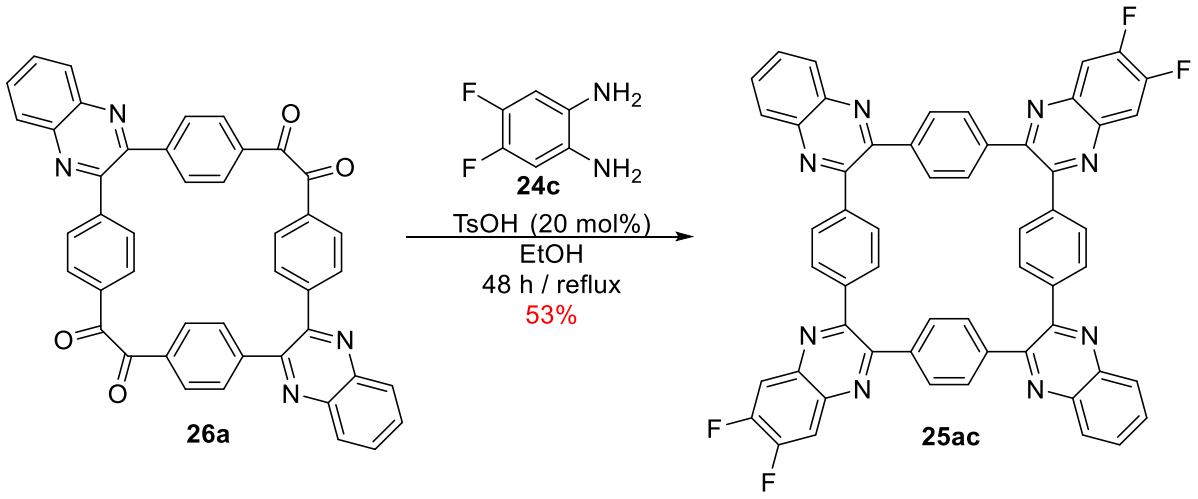

A solution of **26a** (20.1 mg, 0.03 mmol), 4,5-difluoro-1,2-phenylenediamine **24c** (8.6 mg, 0.06 mmol, 2.00 equiv.), and *p*-toluenesulfonic acid (1.2 mg, 0.006 mmol, 0.20 equiv.) in EtOH (2 mL) was prepared in a 5-mL round-bottomed flask fitted with a Dean-Stark condenser. The solution was heated to reflux for 48 h, then cooled to room temperature, filtered, and washed with EtOH (10 mL) and then Et_2O (10 mL). After filtration, the product was dissolved in $CHCl_3$ and the solution passed through a 2 cm thick Celite pad on a glass-fritted Büchner funnel and a clear solution was seen. The solvent was evaporated from the clear solution using rotary evaporator to afford a pure solid of compound **25ac** (yield: 14 mg, 0.015 mmol, 53%, m.p. > 450 ºC, with decomposition). ^{1}H NMR (500 MHz, $CDCl_3$) δ 8.17 (dd, *J*=3.2 Hz, 4H), 7.91 (t, *J*=9.2 Hz, 4H), 7.80 (dd, *J*=3.2 Hz, 4H), 7.56 (d, *J*=8.0 Hz, 8H), 7.54 (d, *J*=8.0 Hz, 8H) ppm. ^{13}C NMR (125 MHz, $CDCl_3$) δ 152.6 (Cq), 152.04 (Cq), 141.44 (Cq), 139.44 (Cq), 138.77 (Cq), 138.59 (Cq), 130.68 (+), 130.24 (+), 130.13 (+), 129.37 (+), 115.04 (Cq), 114.89 (Cq) ppm. ^{19}F-NMR (470 MHz, $CDCl_3$) δ –128.59 (t, *J*=9.0 Hz, 4F)

ppm. IR (neat): $\tilde{\nu}$ = 1631, 1496, 1399, 1360, 1337, 1220, 1063, 1015, 980, 978, 848, 661, 522, 492 cm^{-1}. ESI-HRMS: *m/z* $[M+H]^+$: Calcd for $[C_{56}H_{28}N_8F_4 \cdot H]^+$: 888.24; Found 889.25, with correct isotope distribution. Elemental analysis Calcd (%) for $C_{56}H_{28}N_8F_4$: C 75.67, H 3.18, N 12.61, F 8.55; Found: C 74.18, H 1.33, N 12.61, F 8.49.

3.4.2.9 Synthesis and Characterization of Compound 25ad

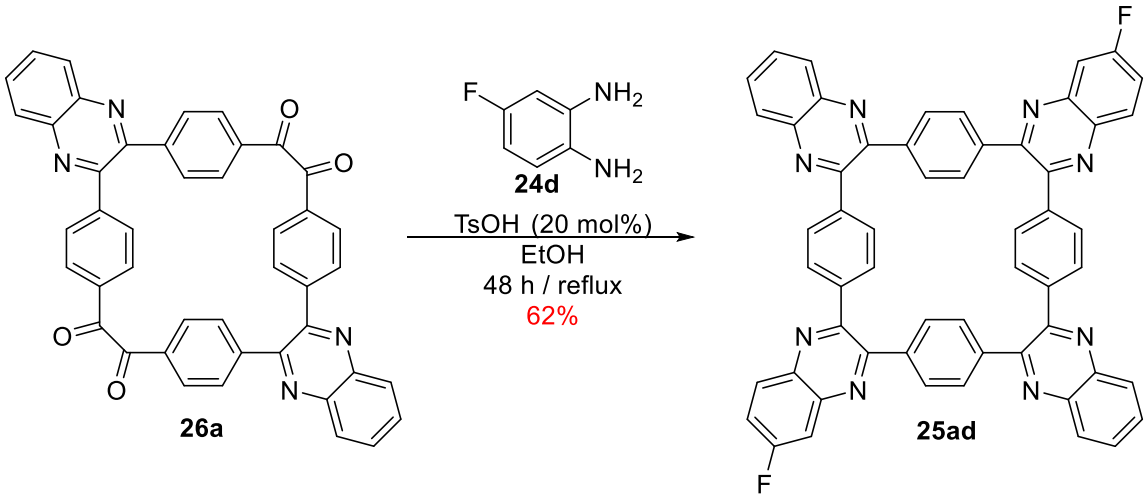

A solution of **26a** (0.10 g, 0.15 mmol), 4-fluoro-1,2-phenylenediamine **24d** (0.04 g, 0.30 mmol, 2.00 equiv.), and *p*-toluenesulfonic acid (5.7 mg, 0.03 mmol, 0.20 equiv.) in EtOH (6 mL) was prepared in a 10-mL round-bottomed flask fitted with a Dean-Stark condenser. The solution was heated to reflux for 48 h, then cooled to room temperature, filtered, and washed with EtOH (10 mL) and then Et_2O (10 mL). After filtration, the product was dissolved in $CHCl_3$ and the solution passed through a 2 cm thick Celite pad on a glass-fritted Büchner funnel and a clear solution was seen. The solvent was evaporated from the clear solution using rotary evaporator to afford a pure solid of compound **25ad** (yield: 78 mg, 0.091 mmol, 62%, m.p. > 450 ºC, with decomposition). ^{1}H NMR (500 MHz, $CDCl_3$) δ 8.16–8.18 (m, 6H), 7.80 (m, 6H), 7.53–7.59 (m, 18H) ppm. ^{13}C NMR (125 MHz, $CDCl_3$) δ 153.00 (Cq), 152.16 (Cq), 152.11 (Cq), 151.63 (Cq), 142.25 (Cq), 142.14 (Cq), 141.44 (Cq), 139.67

(Cq), 139.39 (Cq), 139.23 (Cq) 138.92 (Cq), 138.80 (Cq), 138.65 (Cq), 131.50 (+), 131.30 (+), 130.61 (+), 130.22 (+), 130.13 (+), 129.37 (+), 121.13 (+), 120.92 (+), 112.90 (+), 112.73 (+) ppm. ^{19}F-NMR (470 MHz, $CDCl_3$) δ –107.01 (m, 2F) ppm. IR (neat): $\tilde{\nu}$ = 1620, 1481, 1399, 1340, 1219, 1155, 1125, 1112, 1063, 1050, 1017, 978, 957, 893, 849,760, 718, 624, 546, 506 cm^{-1}. ESI-HRMS: *m/z* $[M+H]^+$: Calcd for $[C_{56}H_{30}N_8F_2 \cdot H]^+$: 852.26; Found 853.26, with correct isotope distribution. Elemental analysis Calcd (%) for $C_{56}H_{30}N_8F_2$: C 78.86, H 3.55, N 13.14, F 4.45; Found: C 76.97, H 1.24, N 12.64, F 5.15.

3.4.2.10 Synthesis and Characterization of Compound 25e

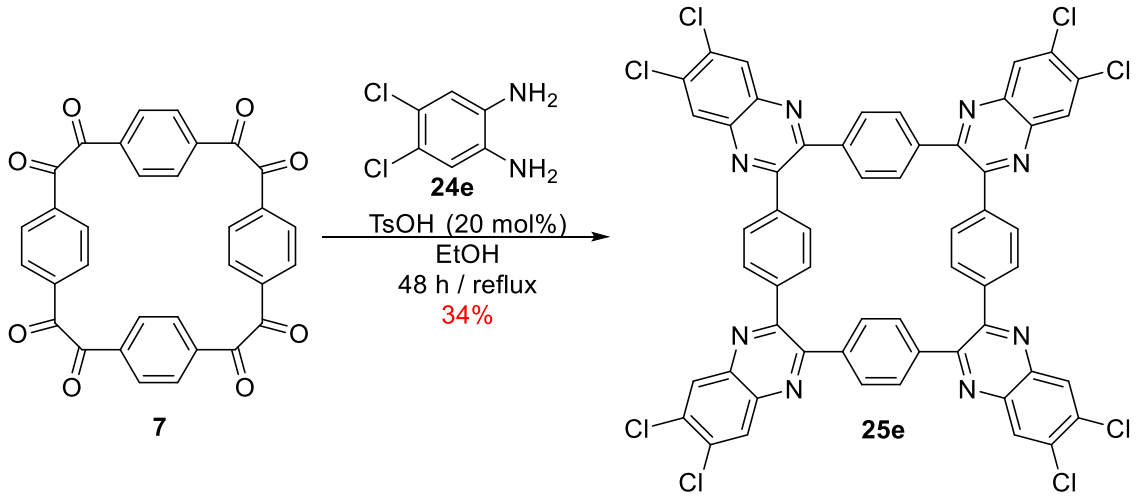

A solution of **7** (0.53 g, 1.00 mmol), 4,5-dichloro-1,2-phenylenediamine **24e** (1.42 g, 8.00 mmol, 8.00 equiv.), and *p*-toluenesulfonic acid (38.0 mg, 0.20 mmol, 0.20 equiv.) in EtOH (40 mL) was prepared in a 100-mL round-bottomed flask fitted with a Dean-Stark condenser. The solution was heated to reflux for 48 h, then cooled to room temperature, filtered, and washed with EtOH (30 mL) and then Et_2O (30 mL). After filtration, the product was dissolved in $CHCl_3$ and the solution passed through a 5 cm thick Celite pad on a glass-fritted Büchner funnel and a clear solution was seen. The solvent was evaporated from the clear solution using rotary evaporator to afford a pure solid of compound **25e** (yield: 370 mg,

0.34 mmol, 34%, m.p. > 450 ºC, with decomposition). ^{1}H NMR (500 MHz, $CDCl_3$) δ 8.29 (s, 8H), 7.54 (s, 16H) ppm. ^{13}C NMR (125 MHz, $CDCl_3$) δ 152.99 (Cq), 140.11 (Cq), 138.89 (Cq), 135.32 (Cq), 130.19 (+), 129.92 (+) ppm. IR (neat): $\tilde{\nu}$ = 1530, 1444, 1328, 1249, 1191, 1103, 1015, 962, 876, 751, 689, 560, 451 cm^{-1}. ESI-HRMS: *m/z* $[M+H]^+$: Calcd for $[C_{56}H_{24}N_8Cl_8 \cdot H]^+$: 1092.46; Found 1092.97, with correct isotope distribution. Elemental analysis Calcd (%) for $C_{56}H_{24}N_8Cl_8$: C 61.57, H 2.21, N 10.26, Cl 25.96; Found: C 60.24, H 0.71, N 9.79, Cl 23.99.

3.4.2.11 Synthesis and Characterization of Compound 25f

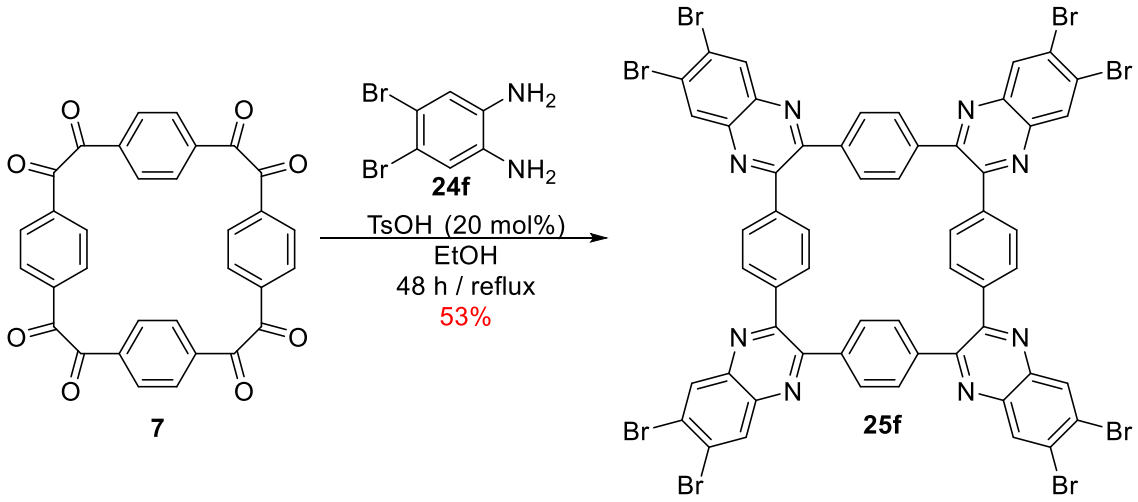

A solution of **7** (0.53 g, 1.00 mmol), 4,5-dibromo-1,2-phenylenediamine **24f** (2.13 g, 8.00 mmol, 8.00 equiv.), and *p*-toluenesulfonic acid (38.0 mg, 0.20 mmol, 0.20 equiv.) in EtOH (40 mL) was prepared in a 100-mL round-bottomed flask fitted with a Dean-Stark condenser. The solution was heated to reflux for 48 h, then cooled to room temperature, filtered, and washed with EtOH (30 mL) and then Et_2O (30 mL). After filtration, the product was dissolved in $CHCl_3$ and the solution passed through a 5 cm thick Celite pad on a glass-fritted Büchner funnel and a clear solution was seen. The solvent was evaporated from the clear solution using rotary evaporator to afford a pure solid of compound **25f** (yield: 764 mg,

0.53 mmol, 53%, m.p. > 450 ºC, with decomposition). ^{1}H NMR (500 MHz, $CDCl_3$) δ 8.48 (s, 8H), 7.53 (s, 16H) ppm. ^{13}C NMR (125 MHz, $CDCl_3$) δ 153.08 (Cq), 140.56 (Cq), 138.90 (Cq), 133.34 (+), 130.18 (+), 127.41 (Cq) ppm. IR (neat): $\tilde{\nu}$ = 1591, 1529, 1443, 1329, 1248, 1191, 1115, 1103, 1064, 1052, 962, 878, 856, 844, 688, 608, 593, 569 cm^{-1}. ESI-HRMS: *m/z* $[M+H]^+$: Calcd for $[C_{56}H_{24}N_8Br_8 \cdot H]^+$: 1448.10; Found 1448.56, with correct isotope distribution. Elemental analysis Calcd (%) for $C_{56}H_{24}N_8Br_8$: C 46.45, H 1.67, N 7.74, Br 44.14; Found: C 47.34, H < 0.1, N 7.38, Br 42.11.

3.4.2.12 Synthesis and Characterization of Compound 25g

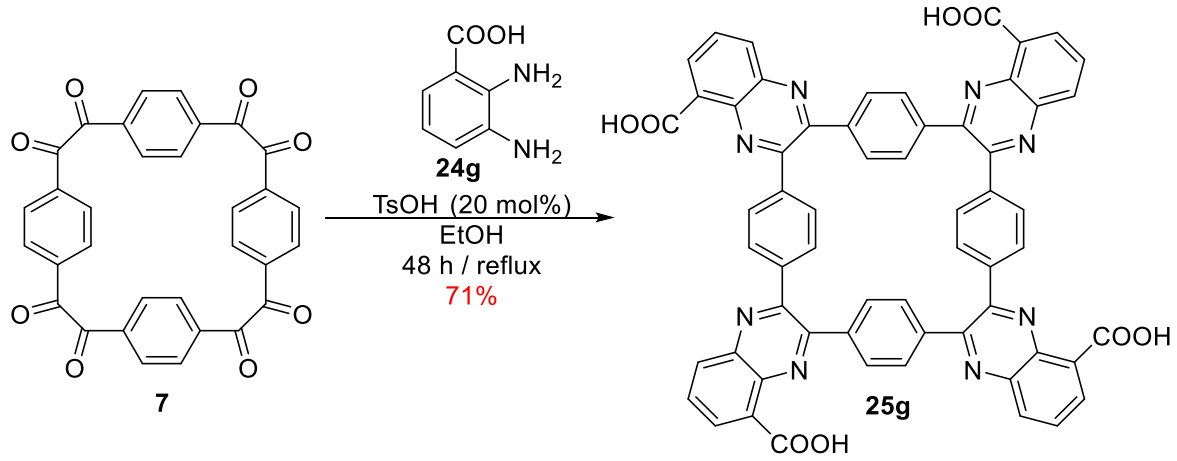

A solution of **7** (0.53 g, 1.00 mmol), 2,3-diamino benzoic acid **24g** (1.23 g, 8.00 mmol, 8.00 equiv.), and *p*-toluenesulfonic acid (38.0 mg, 0.20 mmol, 0.20 equiv.) in EtOH (40 mL) was prepared in a 100-mL round-bottomed flask fitted with a Dean-Stark condenser. The solution was heated to reflux for 48 h, then cooled to room temperature, filtered, and washed with EtOH (30 mL) and then Et_2O (30 mL). After filtration, the product was dissolved in $CHCl_3$ and the solution passed through a 5 cm thick Celite pad on a glass-fritted Büchner funnel and a clear solution was seen. The solvent was evaporated from the clear solution using rotary evaporator to afford a pure solid of compound **25g** (yield: 705 mg, 0.71 mmol, 71%, m.p. > 450 ºC, with decomposition). ^{1}H NMR (500 MHz, $CDCl_3$) δ 8.85–8.87

(m, 4H), 8.44–8.49 (m, 4H), 8.01–8.04 (m, 4H), 7.58–7.71 (m, 16H) ppm. ^{13}C NMR (125 MHz, $CDCl_3$) δ 165.52 (Cq), 165.38 (Cq), 152.81 (Cq), 150.32 (Cq), 141.79 (Cq), 139.10 (Cq), 138.31 (Cq), 138.20 (Cq), 136.65 (Cq), 136.54 (+), 134.82 (+), 131.40 (+), 130.72 (+), 130.66 (+), 130.60 (+), 130.42 (+), 130.25 (+), 125.00 (Cq), 124.93 (Cq) ppm. IR (neat): $\tilde{\nu}$ = 3470, 1716, 1699, 1598, 1575, 1475, 1447, 1393, 1344, 1279, 1176, 1073, 1011, 930, 839, 761, 620 cm^{-1}. ESI-HRMS: *m/z* $[M+H]^+$: Calcd for $[C_{60}H_{32}N_8O_8 \cdot H]^+$: 992.23; Found 993.24, with correct isotope distribution.

3.4.2.13 Synthesis and Characterization of Compound 25h

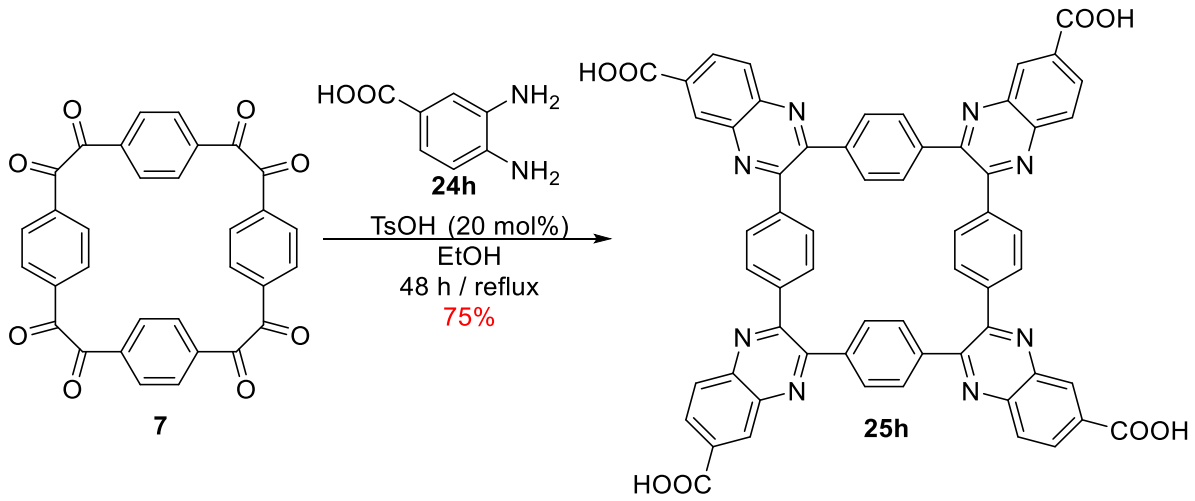

A solution of **7** (0.53 g, 1.00 mmol), 3,4-diamino benzoic acid **24h** (0.67 g, 4.40 mmol, 4.40 equiv.), and *p*-toluenesulfonic acid (38.0 mg, 0.20 mmol, 0.20 equiv.) in EtOH (40 mL) was prepared in a 100-mL round-bottomed flask fitted with a Dean-Stark condenser. The solution was heated to reflux for 48 h, then cooled to room temperature, filtered, and washed with EtOH (30 mL) and then Et_2O (30 mL). After filtration, the product was dissolved in tetrahydrofuran and the solution passed through a 5 cm thick Celite pad on a glass-fritted Büchner funnel and a clear solution was seen. The solvent was evaporated from the clear solution using rotary evaporator to afford a pure solid of compound **25h** (yield: 741

mg, 0.75 mmol, 75%, m.p. > 450 ºC, with decomposition). ^{1}H NMR (500 MHz, THF-d_8) δ 8.77 (s, 4H), 8.34 (d, J=8.6 Hz, 4H), 8.16 (d, J=8.6 Hz, 4H), 7.64 (s, 16H) ppm. ^{13}C NMR (125 MHz, THF-d_8) δ 166.00 (Cq), 153.72 (Cq), 153.12 (Cq), 143.09 (Cq), 140.54 (Cq), 139.31 (Cq), 139.42 (Cq), 132.47 (Cq), 131.50 (+), 130.03 (+), 129.89 (+), 129.19 (+) ppm. IR (neat): $\tilde{\nu}$ = 3390, 1688, 1620, 1531, 1486, 1435, 1338, 1253, 1196, 1054, 1014, 977, 848, 765, 651, 615, 550 cm^{-1}. ESI-HRMS: m/z $[M+H]^+$: Calcd for $[C_{60}H_{32}N_8O_8 \cdot H]^+$: 992.23; Found 993.24, with correct isotope distribution.

3.4.2.14 Synthesis and Characterization of Compound 25i

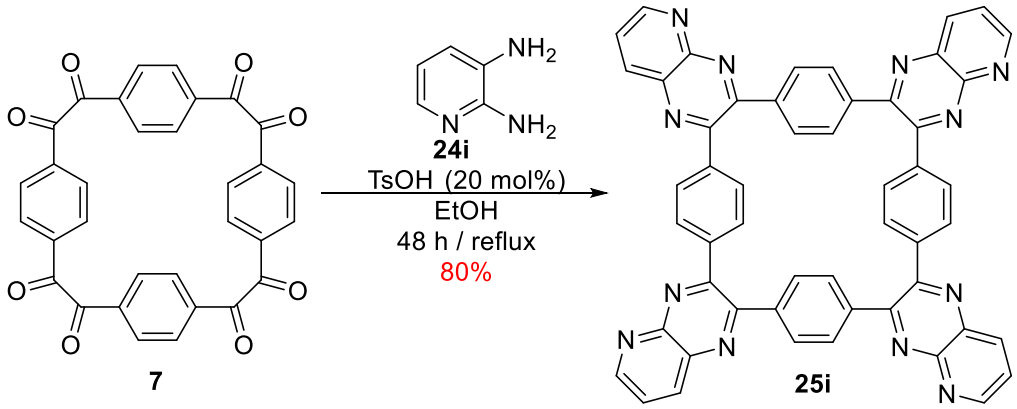

A solution of **7** (0.53 g, 1.00 mmol), 2,3-diamino pyridine **24i** (0.67 g, 10.00 mmol, 10.00 equiv.), and *p*-toluenesulfonic acid (38.0 mg, 0.20 mmol, 0.20 equiv.) in EtOH (40 mL) was prepared in a 100-mL round-bottomed flask fitted with a Dean-Stark condenser. The solution was heated to reflux for 48 h, then cooled to room temperature, filtered, and washed with EtOH (30 mL) and then Et_2O (30 mL). After filtration, the product was dissolved in $CHCl_3$ and the solution passed through a 5 cm thick Celite pad on a glass-fritted Büchner funnel and a clear solution was seen. The solvent was evaporated from the clear solution using rotary evaporator to afford a pure solid of compound **25i** (yield: 653 mg, 0.80 mmol, 80%, m.p. > 450 ºC, with decomposition). ^{1}H NMR (500 MHz, DMSO-d_6) δ 9.17 (m, 4H),

8.60 (m, 4H), 7.90 (m, 4H), 7.60 (d, *J*=8.0 Hz, 8H), 7.57 (d, *J*=8.0 Hz, 8H) ppm. ^{13}C NMR (125 MHz, DMSO-d_6) δ 155.53 (+), 154.90 (Cq), 154.83 (Cq), 153.32 (Cq), 149.72 (Cq), 138.98 (Cq), 138.53 (+), 136.53 (Cq), 130.50 (+), 130.45 (+), 126.87 (+) ppm. IR (neat): $\tilde{\nu}$ = 3390, 1688, 1620, 1531, 1486, 1435, 1338, 1253, 1196, 1054, 1014, 977, 848, 765, 651, 615, 550 cm^{-1}. ESI-HRMS: *m/z* [M+H]$^+$: Calcd for [$C_{52}H_{28}N_{12}$·H]$^+$: 820.26; Found 821.26, with correct isotope distribution.

3.4.2.15 Synthesis and Characterization of Compound 26i

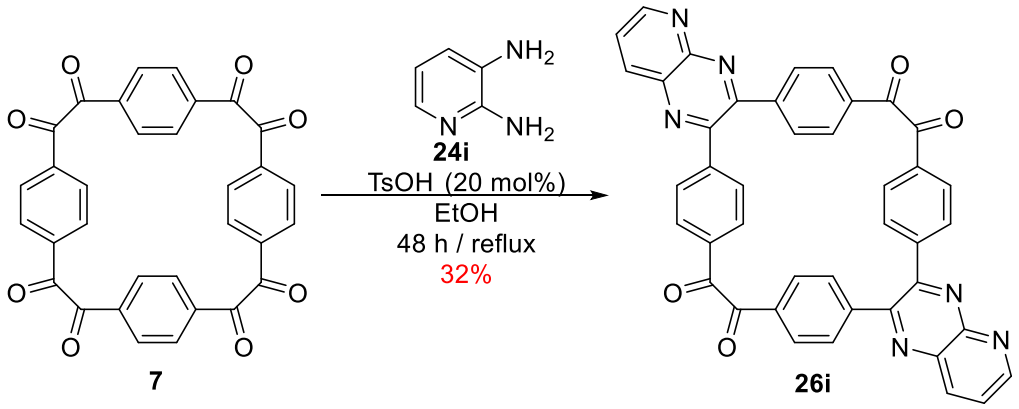

A solution of **7** (0.53 g, 1.00 mmol), 2,3-diamino pyridine **24i** (0.44 g, 4.00 mmol, 4.00 equiv.), and *p*-toluenesulfonic acid (38.0 mg, 0.20 mmol, 0.20 equiv.) in EtOH (40 mL) was prepared in a 100-mL round-bottomed flask fitted with a Dean-Stark condenser. The solution was heated to reflux for 48 h, then cooled to room temperature, filtered, and washed with EtOH (30 mL) and then Et_2O (30 mL). After filtration, the product was dissolved in mixture of $CHCl_3$ and ethyl acetate in a 3:1 ratio and the solution passed through a 10 cm thick silica gel pad on a glass-fritted Büchner funnel and a clear solution was seen. The solvent was evaporated from the clear solution using rotary evaporator to afford a pure solid of compound **26i** (yield: 219 mg, 0.32 mmol, 32%, m.p. > 450 ºC, with decomposition). ^{1}H NMR (500 MHz, $CDCl_3$) δ 9.28 (d, *J*=4.0 Hz, 2H), 8.59 (d, *J*=8.5 Hz, 2H), 7.90 (d, 8H), 7.84

(dd, *J*=8.5 Hz, 2H), 7.70 (d, 8H) ppm. ^{13}C NMR (125 MHz, $CDCl_3$) δ 194.37 (Cq), 155.61 (+), 154.47 (Cq), 152.82 (Cq), 149.79 (Cq), 144.33 (Cq), 144.06 (Cq), 138.46 (+), 136.90 (Cq), 133.13 (Cq), 133.04 (Cq), 132.94 (Cq), 131.19 (+), 130.91 (+), 129.86 (+), 129.71 (+), 126.47 (+) ppm. IR (neat): $\tilde{\nu}$ = 1668, 1605, 1548, 1506, 1443, 1406, 1318, 1246, 1177, 1059, 1013, 975, 891, 798, 691, 605, 544 cm^{-1}. ESI-HRMS: *m/z* $[M+H]^+$: Calcd for $[C_{42}H_{22}N_6O_4 \cdot H]^+$: 674.17; Found 675.18, with correct isotope distribution. Elemental analysis Calcd (%) for $C_{42}H_{22}N_6O_4$: C 74.77, H 3.29, N 12.46, O 9.49; Found: C 72.65, H 3.31, N 12.36, O 9.52.

3.4.2.16 Synthesis and Characterization of Compound 26j

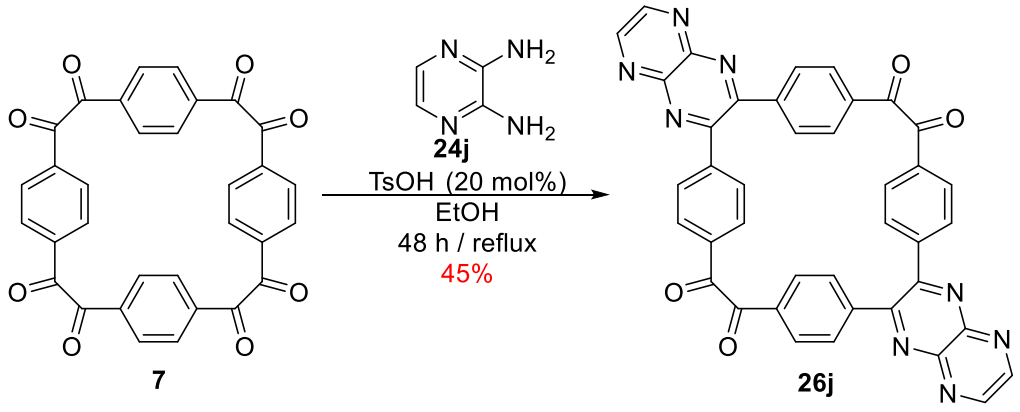

A solution of **7** (0.53 g, 1.00 mmol), 2,3-diamino pyrazine **24j** (0.48 g, 4.40 mmol, 4.40 equiv.), and *p*-toluenesulfonic acid (38.0 mg, 0.20 mmol, 0.20 equiv.) in EtOH (40 mL) was prepared in a 100-mL round-bottomed flask fitted with a Dean-Stark condenser. The solution was heated to reflux for 48 h, then cooled to room temperature, filtered, and washed with EtOH (30 mL) and then Et_2O (30 mL). After filtration, the product was dissolved in $CHCl_3$ and the solution passed through a 5 cm thick Celite pad on a glass-fritted Büchner funnel and a clear solution was seen. The solvent was evaporated from the clear solution using rotary evaporator to afford a pure solid of compound **26j** (yield: 305 mg, 0.45 mmol,

45%, m.p. > 450 ºC, with decomposition). ^{1}H NMR (500 MHz, $CDCl_3$) δ 9.25 (s, 4H), 7.91 (d, 8H), 7.91 (d, 8H) ppm. ^{13}C NMR (125 MHz, $CDCl_3$) δ 194.14 (Cq), 155.81 (Cq), 149.99 (+), 144.90 (Cq), 143.32 (Cq), 133.41 (Cq), 131.23 (+), 129.84 (+) ppm. IR (neat): $\tilde{\nu}$ = 1672, 1604, 1561, 1437, 1405, 1388, 1317, 1250, 1213, 1179, 1012, 930, 892, 768, 691, 609, 508 cm^{-1}. ESI-HRMS: *m/z* $[M+Na]^+$: Calcd for $[C_{40}H_{20}N_8O_4 \cdot Na]^+$: 676.16; Found 699.15, with correct isotope distribution. Elemental analysis Calcd (%) for $C_{40}H_{20}N_8O_4$: C 71.00, H 2.98, N 16.56; Found: C 68.42, H 2.95, N 16.26.

3.4.3 X-ray Crystallographic Analyses of Cyclic Oligoazaacenes

3.4.3.1 Crystal Growth and Crystal Data of Compound 25a

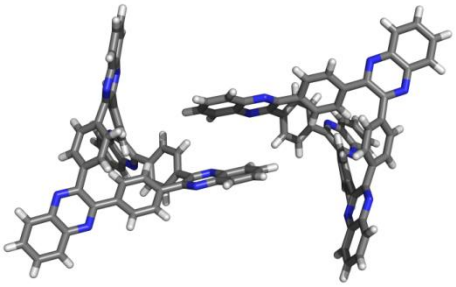

Single crystals of compound **25a** suitable for X-ray diffraction analysis were obtained by dissolving crude product **25a** (15 mg) in $CHCl_3$ (3 mL). The product solution was heated and filtered using PTFE syringe filters (0.22 μm, 30 mm). The resulting filtrate (0.15 mL) was added to a 0.75 mL round-bottomed culture tube, and this tube was placed inside a 2-dram scintillation vial containing ethyl acetate (1 mL) as the diffusing solvent. The vial was tightly closed and kept at ambient conditions without external disturbance. After two days, light-brown crystals were obtained by vapor diffusion technique.

Table 3.2 Crystallographic Data and Structure Refinement of Compound **25a**

Empirical formula	$C_{56}H_{32}N_8$
Formula weight	816.89
Temperature	123(2) K
Wavelength	CuKα (λ = 1.54178 Å)
Crystal system	Trigonal
Space group	$R\bar{3}$
Unit cell dimensions	a = 35.3660(4) Å α = 90°
	b = 35.3660(4) Å β = 90°
	c = 36.9318(4) Å γ = 120°
Volume	40003.9(10) Å^3
Z	36
Density (calculated)	1.221 Mg/m^3
Absorption coefficient	0.579 mm^{-1}
F(000)	15264
Crystal size	0.40 × 0.36 × 0.32 mm^3
2θ range for data collection	1.874 to 68.297°
Index ranges	$-38 \le h \le 39$, $-42 \le k \le 39$, $-44 \le l \le 44$
Reflections collected	66684
Independent reflections	16303 [$R_{(int)}$ = 0.0259]
Completeness to 2θ = 68.297°	99.8 %
Absorption correction	Empirical
Refinement method	Full-matrix least-squares on F^2
Data / restraints / parameters	16303 / 0 / 1153
Goodness-of-fit on F^2	1.031
Final R indices [I>2σ(I)]	R_1 = 0.0424, wR_2 = 0.1114
R indices (all data)	R_1 = 0.0465, wR_2 = 0.1155
Largest diff. peak and hole	0.68 and –0.24 e Å^{-3}

3.4.3.2 Crystal Growth and Crystal Data of Compound 26a

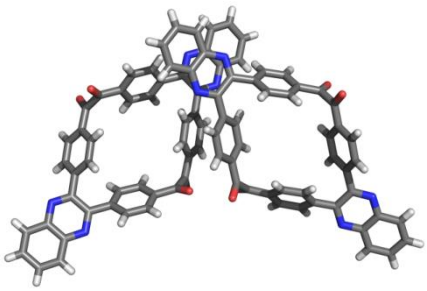

Single crystals of compound **26a** suitable for X-ray diffraction analysis were obtained by dissolving crude product **26a** (15 mg) in dichloroethane (3 mL). The product solution was heated and filtered using PTFE syringe filters (0.22 μm, 30 mm). The resulting filtrate (0.15 mL) was added to a 0.75 mL round-bottomed culture tube, and this tube was placed inside a 2-dram scintillation vial containing Et_2O (1 mL) as the diffusing solvent. The vial was tightly closed and kept at ambient conditions without external disturbance. After two days, pale-yellow crystals were obtained by vapor diffusion technique.

Table 3.3 Crystallographic Data and Structure Refinement of Compound **26a**

Empirical formula	$C_{92}H_{58}O_9N_8$	
Formula weight	1419.46	
Temperature	173(2) K	
Wavelength	CuKα (λ = 1.54178 Å)	
Crystal system	Triclinic	
Space group	$P\bar{1}$	
Unit cell dimensions	a = 10.1784(4) Å	α = 106.285(2)°
	b = 16.4318(7) Å	β = 92.906(3)°
	c = 26.9488(11) Å	γ = 105.787(3)°
Volume	4123.6(3) $Å^3$	
Z	2	
Density (calculated)	1.143 Mg/m^3	

Table 3.3 Continued

Absorption coefficient	0.603 mm^{-1}
$F(000)$	1476
Crystal size	0.18 × 0.06 × 0.02 mm^3
2θ range for data collection	1.724 to 67.057°
Index ranges	$-12 \leq h \leq 10$, $-19 \leq k \leq 19$, $-32 \leq l \leq 32$
Reflections collected	47771
Independent reflections	14161 [$R_{(int)} = 0.0731$]
Completeness to $2\theta = 67.057°$	96.2 %
Absorption correction	Empirical
Refinement method	Full-matrix least-squares on F^2
Data / restraints / parameters	14161 / 59 / 1073
Goodness-of-fit on F^2	1.047
Final R indices [$I>2\sigma(I)$]	$R_1 = 0.0834$, w$R_2 = 0.2458$
R indices (all data)	$R_1 = 0.1018$, w$R_2 = 0.2623$
Largest diff. peak and hole	0.55 and –0.40 e $Å^{-3}$

3.4.3.3 Crystal Growth and Crystal Data of Compound 25b

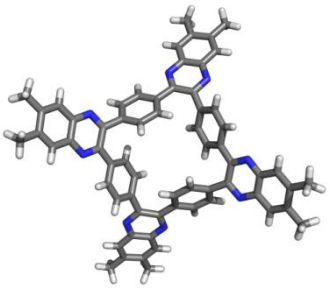

Single crystals of compound **25b** suitable for X-ray diffraction analysis were obtained by dissolving crude product **25b** (15 mg) in dichloroethane (3 mL). The product solution was heated and filtered using PTFE syringe filters (0.22 μm, 30 mm). The resulting filtrate (0.15 mL) was added to a 0.75 mL round-bottomed culture tube, and this tube was placed inside a 2-dram scintillation vial containing ethyl acetate (1 mL) as the diffusing solvent. The vial was

tightly closed and kept at ambient conditions without external disturbance. After two days, pale-yellow crystals were obtained by vapor diffusion technique.

Table 3.4 Crystallographic Data and Structure Refinement of Compound **25b**

Empirical formula	$C_{64}H_{48}N_8$
Formula weight	929.10
Temperature	173(2) K
Wavelength	CuKα (λ = 1.54178 Å)
Crystal system	Tetragonal
Space group	$I4_1/a$
Unit cell dimensions	a = 31.0988(16) Å α = 90°
	b = 31.0988(16) Å β = 90°
	c = 4.9366(4) Å γ = 90°
Volume	4774.4(6) Å^3
Z	4
Density (calculated)	1.293 Mg/m^3
Absorption coefficient	0.601 mm^{-1}
F(000)	1952
Crystal size	0.60 × 0.04 × 0.02 mm^3
2θ range for data collection	2.842 to 66.572°
Index ranges	$-35 \le h \le 36$, $-35 \le k \le 36$, $-5 \le l \le 5$
Reflections collected	9164
Independent reflections	2100 [$R_{(int)}$ = 0.0720]
Completeness to 2θ = 66.572°	99.7 %
Absorption correction	Empirical
Refinement method	Full-matrix least-squares on F^2
Data / restraints / parameters	2100 / 0 / 165
Goodness-of-fit on F^2	1.001
Final R indices [I>2σ(I)]	R_1 = 0.0494, wR_2 = 0.1215
R indices (all data)	R_1 = 0.0766, wR_2 = 0.1364
Largest diff. peak and hole	0.20 and –0.26 e Å^{-3}

3.4.3.4 Crystal Growth and Crystal Data of Compound 25c

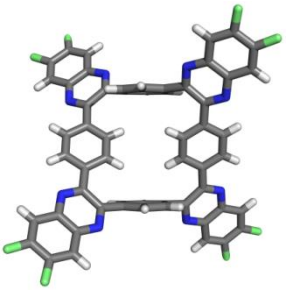

Single crystals of compound **25c** suitable for X-ray diffraction analysis were obtained by dissolving crude product **25c** (15 mg) in dichloroethane (3 mL). The product solution was heated and filtered using PTFE syringe filters (0.22 μm, 30 mm). The resulting filtrate (0.15 mL) was added to a 0.75 mL round-bottomed culture tube, and this tube was placed inside a 2-dram scintillation vial containing Et_2O (1 mL) as the diffusing solvent. The vial was tightly closed and kept at ambient conditions without external disturbance. After two days, brown crystals were obtained by vapor diffusion technique.

Table 3.5 Crystallographic Data and Structure Refinement of Compound **25c**

Empirical formula	$C_{56}H_{24}N_8F_8$	
Formula weight	960.83	
Temperature	123(2) K	
Wavelength	CuKα (λ = 1.54178 Å)	
Crystal system	Monoclinic	
Space group	*C*2/*c*	
Unit cell dimensions	a = 8.3101(5) Å	α = 90°
	b = 33.443(2) Å	β = 99.135(4)°
	c = 18.5442(10) Å	γ = 90°
Volume	5088.3(5) $Å^3$	
Z	4	
Density (calculated)	1.254 Mg/m^3	

Table 3.5 Continued

Absorption coefficient	0.819 mm^{-1}
$F(000)$	1952
Crystal size	0.11 × 0.08 × 0.05 mm^3
2θ range for data collection	2.642 to 66.712°
Index ranges	$-9 \leq h \leq 9$, $-39 \leq k \leq 37$, $-21 \leq l \leq 22$
Reflections collected	16271
Independent reflections	4495 [$R_{(int)} = 0.0422$]
Completeness to $2\theta = 66.712°$	99.7 %
Absorption correction	Empirical
Refinement method	Full-matrix least-squares on F^2
Data / restraints / parameters	4495 / 0 / 325
Goodness-of-fit on F^2	1.043
Final R indices [$I>2\sigma(I)$]	$R_1 = 0.0698$, w$R_2 = 0.1938$
R indices (all data)	$R_1 = 0.0934$, w$R_2 = 0.2065$
Largest diff. peak and hole	0.34 and –0.24 e $Å^{-3}$

3.4.3.5 Crystal Growth and Crystal Data of Compound 25d

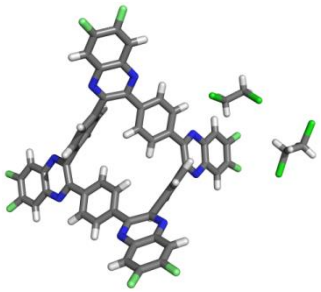

Single crystals of compound **25d** suitable for X-ray diffraction analysis were obtained by dissolving crude product **25d** (15 mg) in dichloroethane (3 mL). The product solution was heated and filtered using PTFE syringe filters (0.22 μm, 30 mm). The resulting filtrate (0.15 mL) was added to a 0.75 mL round-bottomed culture tube, and this tube was placed inside a 2-dram scintillation vial containing acetonitrile (1 mL) as the diffusing solvent. The vial was

tightly closed and kept at ambient conditions without external disturbance. After two days, brown crystals were obtained by vapor diffusion technique.

Table 3.6 Crystallographic Data and Structure Refinement of Compound **25d**

Empirical formula	$C_{60}H_{32}N_8F_4Cl_4$
Formula weight	1082.73
Temperature	173(2) K
Wavelength	CuKα (λ = 1.54178 Å)
Crystal system	Orthorhombic
Space group	$Pna2_1$
Unit cell dimensions	a = 20.0524(4) Å α = 90°
	b = 9.2012(2) Å β = 90°
	c = 26.6247(5) Å γ = 90°
Volume	4912.42(17) Å^3
Z	4
Density (calculated)	1.464 Mg/m^3
Absorption coefficient	2.748 mm^{-1}
F(000)	2208
Crystal size	0.40 × 0.22 × 0.02 mm^3
2θ range for data collection	3.320 to 66.672°
Index ranges	$-23 \le h \le 22$, $-10 \le k \le 10$, $-31 \le l \le 31$
Reflections collected	38330
Independent reflections	8637 [$R_{(int)}$ = 0.0410]
Completeness to 2θ = 66.672°	99.0 %
Absorption correction	Empirical
Refinement method	Full-matrix least-squares on F^2
Data / restraints / parameters	8637 / 674 / 726
Goodness-of-fit on F^2	1.040
Final R indices [I>2σ(I)]	R_1 = 0.0446, wR_2 = 0.1252
R indices (all data)	R_1 = 0.0451, wR_2 = 0.1261
Largest diff. peak and hole	0.70 and –0.65 e Å^{-3}

3.4.3.6 Crystal Growth and Crystal Data of Compound 25ac

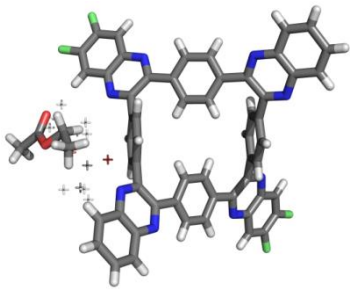

Single crystals of compound **25ac** suitable for X-ray diffraction analysis were obtained by dissolving crude product **25ac** (15 mg) in dichloroethane (3 mL). The product solution was heated and filtered using PTFE syringe filters (0.22 μm, 30 mm). The resulting filtrate (0.15 mL) was added to a 0.75 mL round-bottomed culture tube, and this tube was placed inside a 2-dram scintillation vial containing ethyl acetate (1 mL) as the diffusing solvent. The vial was tightly closed and kept at ambient conditions without external disturbance. After two days, brown crystals were obtained by vapor diffusion technique.

Table 3.7 Crystallographic Data and Structure Refinement of Compound **25ac**

Empirical formula	$C_{56}H_{28}N_8F_4$	
Formula weight	888.86	
Temperature	173(2) K	
Wavelength	CuKα (λ = 1.54178 Å)	
Crystal system	Monoclinic	
Space group	*Cc*	
Unit cell dimensions	a = 8.63450(10) Å	α = 90°
	b = 33.1038(4) Å	β = 98.6090(10)°
	c = 18.0901(2) Å	γ = 90°
Volume	5112.52(10) Å^3	
Z	4	
Density (calculated)	1.155 Mg/m^3	

Table 3.7 Continued

Absorption coefficient	0.659 mm^{-1}
$F(000)$	1824
Crystal size	0.18 × 0.15 × 0.03 mm^3
2θ range for data collection	2.669 to 66.594°
Index ranges	$-10 \leq h \leq 10$, $-29 \leq k \leq 39$, $-21 \leq l \leq 20$
Reflections collected	16851
Independent reflections	7271 [$R_{(int)} = 0.0186$]
Completeness to $2\theta = 66.594°$	96.0 %
Absorption correction	Empirical
Refinement method	Full-matrix least-squares on F^2
Data / restraints / parameters	7271 / 2 / 614
Goodness-of-fit on F^2	1.067
Final R indices [$I>2\sigma(I)$]	$R_1 = 0.0537$, w$R_2 = 0.1551$
R indices (all data)	$R_1 = 0.0568$, w$R_2 = 0.1606$
Largest diff. peak and hole	0.51 and –0.17 e $Å^{-3}$

3.4.3.7 Crystal Growth and Crystal Data of Compound 25ad

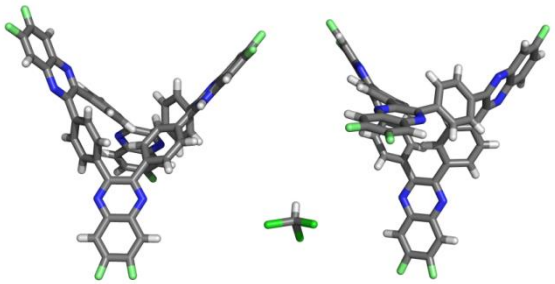

Single crystals of compound **25ad** suitable for X-ray diffraction analysis were obtained by dissolving crude product **25ad** (15 mg) in $CHCl_3$ (3 mL). The product solution was heated and filtered using PTFE syringe filters (0.22 μm, 30 mm). The resulting filtrate (0.15 mL) was added to a 0.75 mL round-bottomed culture tube, and this tube was placed inside a 2-dram scintillation vial containing *n*-hexane (1 mL) as the diffusing solvent. The

vial was tightly closed and kept at ambient conditions without external disturbance. After two days, brown crystals were obtained by vapor diffusion technique.

Table 3.8 Crystallographic Data and Structure Refinement of Compound **25ad**

Empirical formula	$C_{13}H_{52}N_{16}F_4Cl_3$
Formula weight	1816.05
Temperature	123(2) K
Wavelength	CuKα (λ = 1.54178 Å)
Crystal system	Trigonal
Space group	$R\bar{3}$
Unit cell dimensions	a = 35.5987(11) Å α = 90°
	b = 35.5987(11) Å β = 90°
	c = 37.1750(19) Å γ = 120°
Volume	40799.0(3) Å^3
Z	18
Density (calculated)	1.330 Mg/m^3
Absorption coefficient	1.486 mm^{-1}
F(000)	16722.0
Crystal size	0.21 × 0.18 × 0.03 mm^3
2θ range for data collection	3.724 to 135.598°
Index ranges	$-42 \le h \le 42$, $-42 \le k \le 41$, $-44 \le l \le 44$
Reflections collected	210663
Independent reflections	16351 [$R_{(int)}$ = 0.0628]
Completeness to 2θ = 67.799°	99.4 %
Absorption correction	Empirical
Refinement method	Full-matrix least-squares on F^2
Data / restraints / parameters	16351 / 1269 / 1315
Goodness-of-fit on F^2	1.026
Final R indices [I>2σ(I)]	R_1 = 0.0701, wR_2 = 0.2078
R indices (all data)	R_1 = 0.0834, wR_2 = 0.2230
Largest diff. peak and hole	1.60 and –0.91 e Å^{-3}

3.4.3.8 Crystal Growth and Crystal Data of Compounds 25e and 25f

Single crystals of compound **25e** suitable for X-ray diffraction analysis were obtained by dissolving crude product **25e** (15 mg) in dichloroethane (3 mL). The product solution was heated and filtered using PTFE syringe filters (0.22 μm, 30 mm). The resulting filtrate (0.15 mL) was added to a 0.75 mL round-bottomed culture tube, and this tube was placed inside a 2-dram scintillation vial containing Et_2O (1 mL) as the diffusing solvent. The vial was tightly closed and kept at ambient conditions without external disturbance. After four days, yellow crystals were obtained by vapor diffusion technique. Unfortunately, the structure of **25e** was solved but not refined. The single crystal of **25f** was obtained under similar conditions by dissolving the crude product **25f** (15 mg) in dichloroethane (3 mL) and acetonitrile was used as a diffuser solvent. The structure of **25f** was neither solved nor refined due to the very fast deterioration and severe structural disorder which makes the diffractions at high angles very weak.

3.4.3.9 Crystal Growth and Crystal Data of Compound 25i

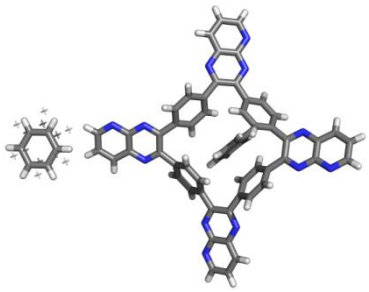

Single crystals of compound **25i** suitable for X-ray diffraction analysis were obtained by dissolving crude product **25i** (15 mg) in AcOH (3 mL). The product solution was heated and filtered using PTFE syringe filters (0.22 μm, 30 mm). The resulting filtrate (0.15 mL) was added to a 0.75 mL round-bottomed culture tube, and this tube was placed inside a 2-dram scintillation vial containing benzene (1 mL) as the diffusing solvent. The vial was

tightly closed and kept at ambient conditions without external disturbance. After two weeks, brown crystals were obtained by vapor diffusion technique.

Table 3.9 Crystallographic Data and Structure Refinement of Compound **25i**

Empirical formula	$C_{69.43}H_{45.43}N_{12}$
Formula weight	1047.73
Temperature	123(2) K
Wavelength	CuKα (λ = 1.54178 Å)
Crystal system	Tetragonal
Space group	*I*4/*m*
Unit cell dimensions	a = 21.1048(10)Å α = 90°
	b = 21.1048(10) Å β = 90°
	c = 15.8439(9) Å γ = 90°
Volume	7057.1(8) Å^3
Z	4
Density (calculated)	0.986 Mg/m^3
Absorption coefficient	0.473 mm^{-1}
F(000)	2184
Crystal size	0.33 × 0.30 × 0.02 mm^3
2θ range for data collection	5.922 to 134.578°
Index ranges	$-25 \le h \le 22$, $-25 \le k \le 25$, $-18 \le l \le 17$
Reflections collected	34218
Independent reflections	3278 [$R_{(int)}$ = 0.0731]
Completeness to 2θ = 67.289°	99.4 %
Absorption correction	Empirical
Refinement method	Full-matrix least-squares on F^2
Data / restraints / parameters	3278 / 324 / 234
Goodness-of-fit on F^2	1.077
Final *R* indices [$I>2\sigma(I)$]	R_1 = 0.0698, wR_2 = 0.1818
R indices (all data)	R_1 = 0.0785, wR_2 = 0.1884
Largest diff. peak and hole	0.40 and –0.19 e Å^{-3}

3.4.3.10 Crystal Growth and Crystal Data of Compound 26i

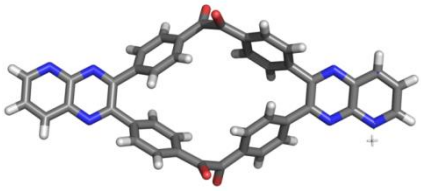

Single crystals of compound **26i** suitable for X-ray diffraction analysis were obtained by dissolving crude product **26i** (15 mg) in $CHCl_3$ (3 mL). The product solution was heated and filtered using PTFE syringe filters (0.22 μm, 30 mm). The resulting filtrate (0.15 mL) was added to a 0.75 mL round-bottomed culture tube, and this tube was placed inside a 2-dram scintillation vial containing MeOH (1 mL) as the diffusing solvent. The vial was tightly closed and kept at ambient conditions without external disturbance. After two days, yellow crystals were obtained by vapor diffusion technique.

Table 3.10 Crystallographic Data and Structure Refinement of Compound **26i**

Empirical formula	$C_{42}H_{22}N_6O_4$	
Formula weight	674.65	
Temperature	173(2) K	
Wavelength	CuKα (λ = 1.54178 Å)	
Crystal system	Monoclinic	
Space group	*C*2/*c*	
Unit cell dimensions	a = 21.0393(3) Å	α = 90°
	b = 17.7591(3) Å	β = 129.5220(10)°
	c = 14.1551(2) Å	γ = 90°
Volume	4079.75(12) $Å^3$	
Z	4	
Density (calculated)	1.098 Mg/m^3	
Absorption coefficient	0.593 mm^{-1}	
F(000)	1392	

Table 3.10 Continued

Crystal size	0.12 × 0.07 × 0.05 mm^3
2θ range for data collection	10.902 to 133.138°
Index ranges	$-25 \leq h \leq 17$, $-21 \leq k \leq 20$, $-16 \leq l \leq 16$
Reflections collected	11693
Independent reflections	3594 [$R_{(int)}$ = 0.0210]
Completeness to 2θ = 66.569°	99.7 %
Absorption correction	Empirical
Refinement method	Full-matrix least-squares on F^2
Data / restraints / parameters	3594 / 0 / 235
Goodness-of-fit on F^2	1.028
Final R indices [$I>2\sigma(I)$]	R_1 = 0.0429, wR_2 = 0.1323
R indices (all data)	R_1 = 0.0467, wR_2 = 0.1363
Largest diff. peak and hole	0.21 and –0.21 e $Å^{-3}$

3.4.3.11 Crystal Growth and Crystal Data of Compound 26i-Cu

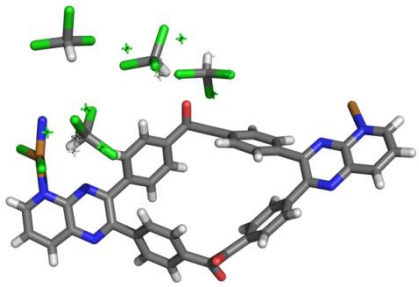

Single crystals of compound **26i-Cu** suitable for X-ray diffraction analysis were obtained by dissolving 0.1 mmol of **26i** (67.5 mg) in $CHCl_3$ (15 mL). The product solution was heated and filtered using PTFE syringe filters (0.22 μm, 30 mm). The resulting filtrate (1.00 mL) was added to 2-dram scintillation vial and layered with 1.00 mL of 0.007 M solution of $CuCl_2.2H_2O$ in MeOH. The vial was tightly closed and kept at ambient conditions without external disturbance. After one day, blue crystals were obtained.

Table 3.11 Crystallographic Data and Structure Refinement of Compound **26i-Cu**

Empirical formula	$C_{46}H_{26}Cl_{14}CuN_6O_4$
Formula weight	1286.57
Temperature	123(2) K
Wavelength	CuKα (λ = 1.54178 Å)
Crystal system	Monoclinic
Space group	*C*2/*c*
Unit cell dimensions	a = 41.1770(3) Å α = 90°
	b = 10.9002(7) Å β = 122.480(4)°
	c = 27.9217(18) Å γ = 90°
Volume	10572.0(13) Å^3
Z	8
Density (calculated)	1.617 Mg/m^3
Absorption coefficient	7.509 mm^{-1}
F(000)	5144
Crystal size	0.09 × 0.07 × 0.04 mm^3
2θ range for data collection	6.418 to 136.652°
Index ranges	$-49 \le h \le 49$, $-13 \le k \le 8$, $-33 \le l \le 33$
Reflections collected	34400
Independent reflections	9599 [$R_{(int)}$ = 0.0437]
Completeness to 2θ = 66.569°	99.7 %
Absorption correction	Empirical
Refinement method	Full-matrix least-squares on F^2
Data / restraints / parameters	9599 / 516 / 738
Goodness-of-fit on F^2	1.029
Final *R* indices [I>2σ(I)]	R_1 = 0.0561, wR_2 = 0.1532
R indices (all data)	R_1 = 0.0753, wR_2 = 0.1668
Largest diff. peak and hole	0.57 and –0.59 e Å^{-3}

3.4.3.12 Crystal Growth and Crystal Data of Compound 26j

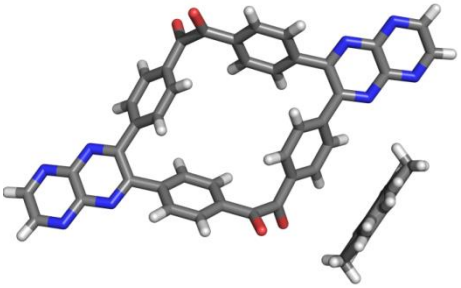

Single crystals of compound **26j** suitable for X-ray diffraction analysis were obtained by dissolving crude product **26j** (15 mg) in $CHCl_3$ (3 mL). The product solution was heated and filtered using PTFE syringe filters (0.22 μm, 30 mm). The resulting filtrate (0.15 mL) was added to a 0.75 mL round-bottomed culture tube, and this tube was placed inside a 2-dram scintillation vial containing PhMe (1 mL) as the diffusing solvent. The vial was tightly closed and kept at ambient conditions without external disturbance. After three days, yellow crystals were obtained by vapor diffusion technique. The X-ray diffraction data for compound **26j** were collected at ChemMatCARS beamline at Advanced Photon Source in Argonne National Laboratory and refined by Dr. Xiqu Wang (UH).

Table 3.12 Crystallographic Data and Structure Refinement of Compound **26j**

Empirical formula	$C_{47}H_{28}N_8O_4$	
Formula weight	768.77	
Temperature	100(2) K	
Wavelength	synchrotron (λ = 0.61992 Å)	
Crystal system	Orthorhombic	
Space group	*Pbcn*	
Unit cell dimensions	a = 14.041(4) Å	α = 90°
	b = 17.030(6) Å	β = 90°
	c = 15.553(4) Å	γ = 90°
Volume	3719.0(19) $Å^3$	

Table 3.12 Continued

Z	4
Density (calculated)	1.373 Mg/m^3
Absorption coefficient	0.068 mm^{-1}
F(000)	1592
Crystal size	0.08 × 0.02 × 0.01 mm^3
2θ range for data collection	3.280 to 48.186°
Index ranges	$-15 \leq h \leq 14$, $-19 \leq k \leq 21$, $-17 \leq l \leq 18$
Reflections collected	59962
Independent reflections	3752 [$R_{(int)}$ = 0.0520]
Completeness to 2θ = 24.093°	84.1 %
Absorption correction	Empirical
Refinement method	Full-matrix least-squares on F^2
Data / restraints / parameters	3752 / 122 / 300
Goodness-of-fit on F^2	1.134
Final R indices [I>2σ(I)]	R_1 = 0.0460, wR_2 = 0.1227
R indices (all data)	R_1 = 0.0647, wR_2 = 0.1492
Largest diff. peak and hole	0.46 and –0.26 e Å^{-3}

3.4.4 UV-Vis and Fluorescence Spectra of Selected Cyclic Oligoazaacenes

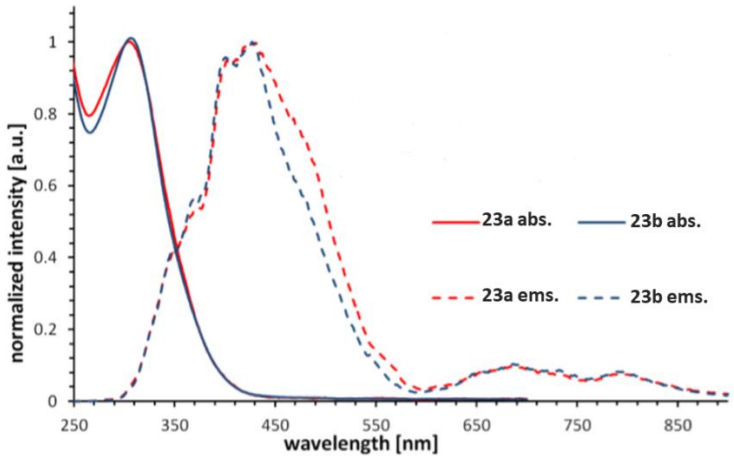

Figure 3.19 Normalized absorption and emission spectra of **23a**–**b** (1×10^{-6} M) recorded in CH_2Cl_2.

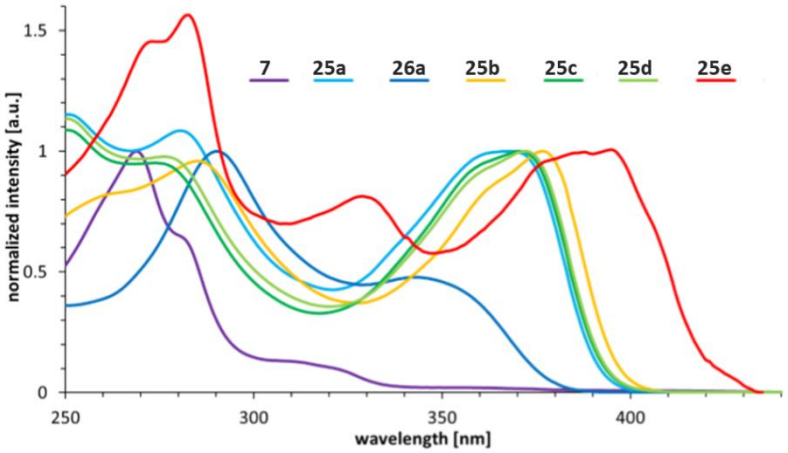

Figure 3.20 Normalized absorption spectra of **7**, **25a**–**e**, and **26a** (1×10^{-6} M) recorded in CH_2Cl_2.

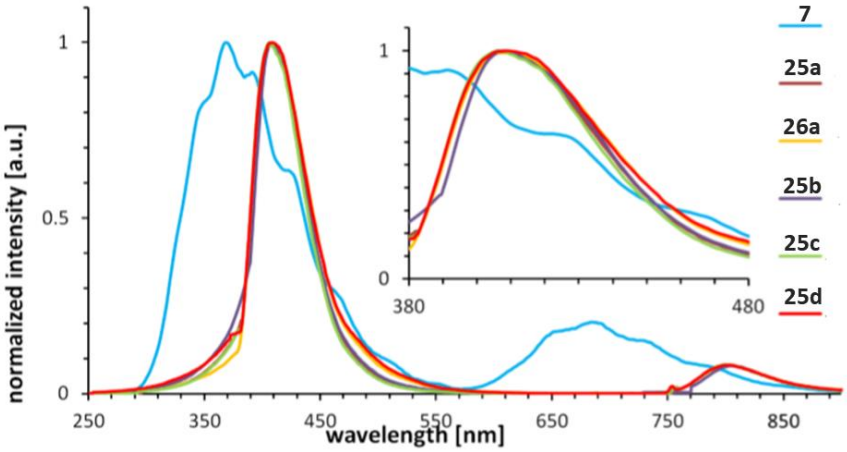

Figure 3.21 Normalized emission spectra of **7**, **25a**–**d**, and **26a** (1×10^{-6} M) recorded in CH_2Cl_2.

3.4.5 Cyclic Voltammograms of Selected Cyclic Oligoazaacenes

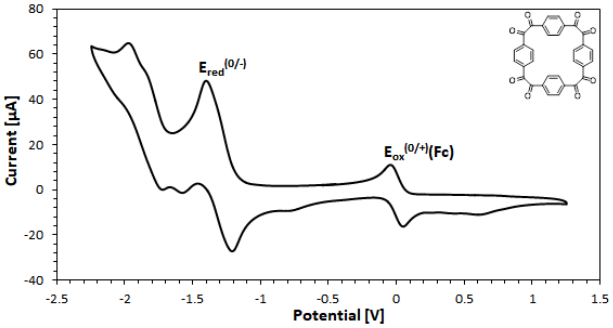

Figure 3.22 Cyclic voltammogram of compound **7**.

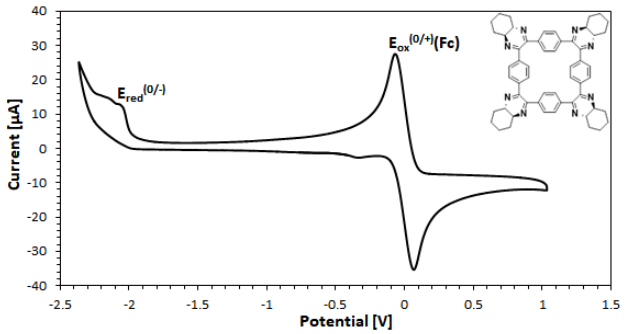

Figure 3.23 Cyclic voltammogram of compound **23a**.

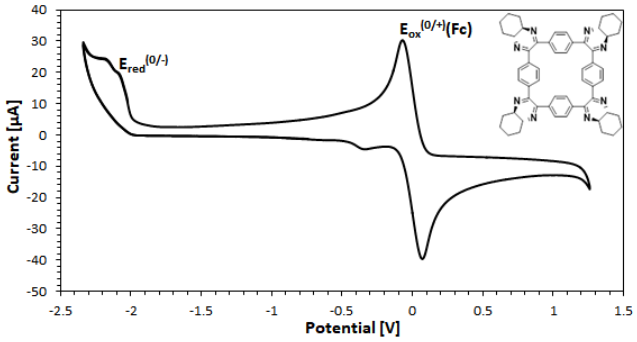

Figure 3.24 Cyclic voltammogram of compound **23b**.

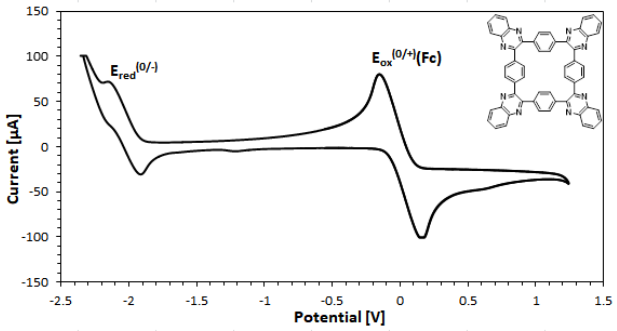

Figure 3.25 Cyclic voltammogram of compound **25a**.

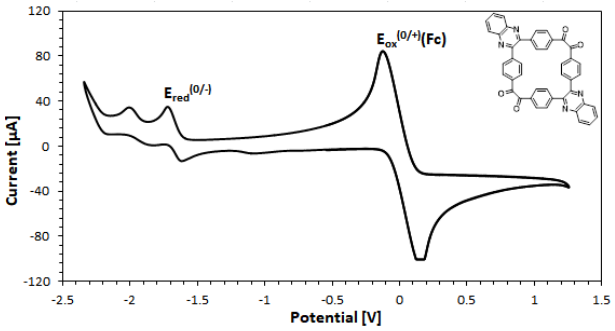

Figure 3.26 Cyclic voltammogram of compound **26a**.

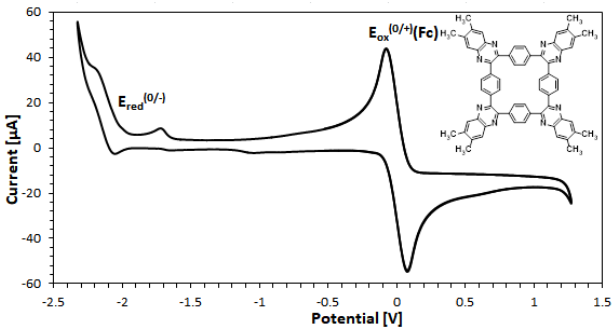

Figure 3.27 Cyclic voltammogram of compound **25b**.

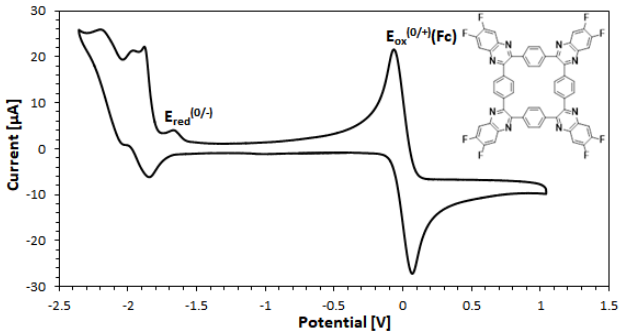

Figure 3.28 Cyclic voltammogram of compound **25c**.

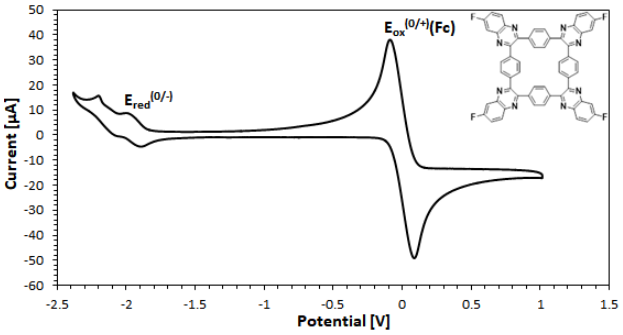

Figure 3.29 Cyclic voltammogram of compound **25d**.

Chapter Four

Synthesis and Characterization of Cyclotetra(bisarylhydrazone)benzils

4.1 Introduction

4.1.1 Chemistry of Hydrazones

Azomethines are secondary aldimines or ketimine compounds which have a chemical formula R–CR'=NR", where R" ≠ H. Hydrazones are considered as azomethine compounds with two connected nitrogen atoms (R–CR'=N–NH–R"), which distinguishes them from other members of this class such as imines and oximes.[380] The burgeoning research on the compounds containing the hydrazone functional group has received increasing interest recently in many fields, ranging from organic synthesis[381–384] and medicinal chemistry[385–390] to supramolecular chemistry,[391–393] and has been used in metal and covalent organic frameworks,[394–396] dynamic combinatorial chemistry,[397–400] dye[401] and hole-transporting materials,[402] as well as in molecular switches,[403–410] among other applications.[411] This popularity was attained due to the hydrazone functional group's modularity, straightforward synthesis, and stability towards hydrolysis, as well as the functional diversity which provides the physical and chemical properties for hydrazones.[412,413] The chemistry of the hydrazone functional group (Figure 4.1) is dominated by the nucleophilic imine and amino-type (more reactive) nitrogen atoms, an imine carbon that has both electrophilic and nucleophilic character, configurational isomerism stemming from the intrinsic nature of the C=N double bond, and in most cases an acidic N–H proton.

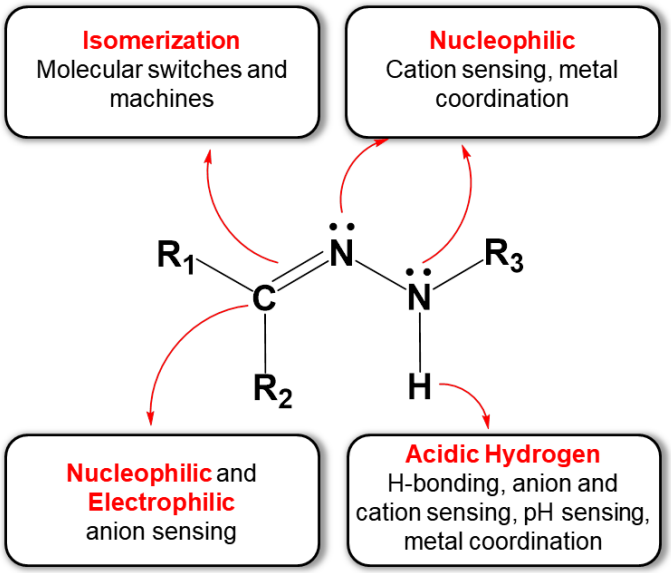

Figure 4.1 The structural and functional diversity of the hydrazone functional group.

4.1.2 Conformational Changes in Hydrazones' Structures

Using hydrazines with electron withdrawing substituents to prepare hydrazones can enhance the acidity of the hydrazone N–H proton that can be used as acid/base sensors or molecular switches, in which conformational changes can occur.[413–419] In general, the aryl substituents on either side of the hydrazones may lead to a π-conjugated system upon deprotonation or tautomerization (Scheme 4.1). This π-conjugated system may be extended across the entire molecule, leading to a resonance system which enhances the stability of the anionic hydrazones.

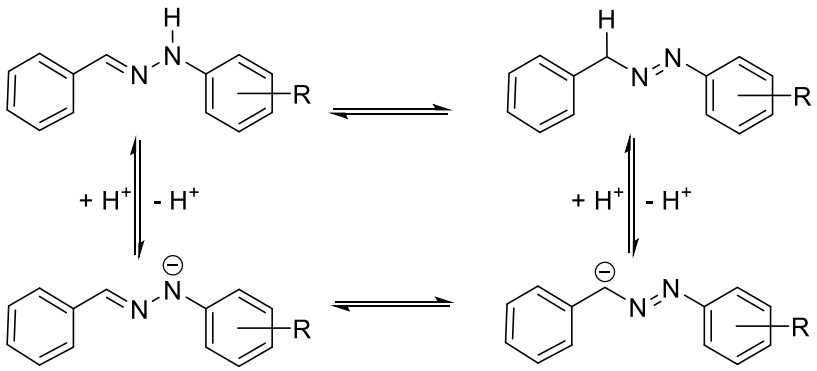

Scheme 4.1 Solvent or pH induced tautomerization in hydrazones, where R is an electron-withdrawing group.

4.1.3 Configurational Changes in Hydrazones' Structures

Owing to the presence of an additional nitrogen atom in hydrazones that facilitates the reversible configurational changes (*E*/*Z* isomerization), hydrazones have been used in molecular switches.[403–410,413] These changes in the configuration of the produced systems can be reversibly modulated using various external stimuli: light,[420-425] heat,[403,426] addition of metal ions,[427,428] pH changes,[411,429,430] or electrochemical potentials.[431] The uncatalyzed *E*/*Z* isomerization in hydrazones can proceed via either of two different mechanisms: rotation and inversion; the latter is considered to be the common mechanistic pathway in hydrazones.[432–435] The rotation mechanism occurs through a polar transition state, and results in the rotation of the substituents around the C=N double bond, while the inversion mechanism occurs through an inversion around the imine nitrogen, and goes through a nonpolar transition state (Scheme 4.2).[415,427] Accordingly, the polarity of the solvent can affect the isomerization rates in the rotation mechanism, and no such effects are observed in the inversion mechanism.

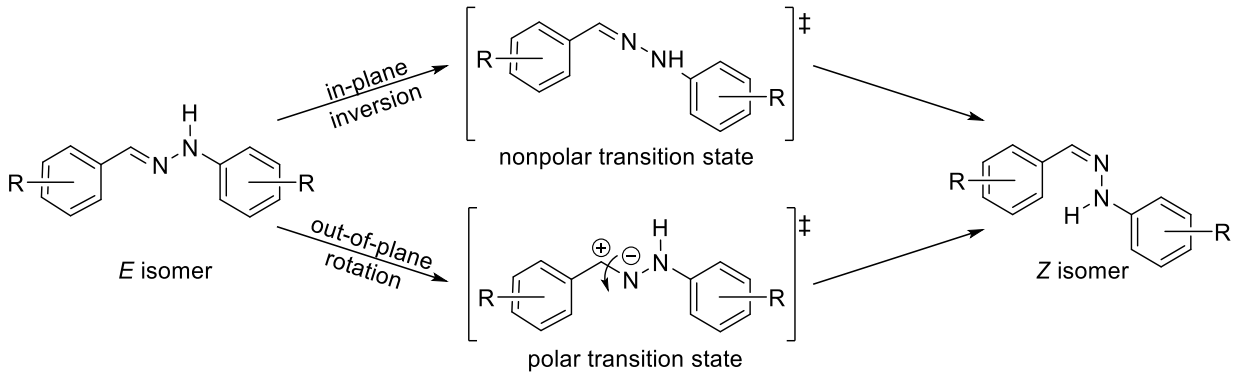

Scheme 4.2 *E*/*Z* isomerization mechanisms in hydrazones.

In this study, the rotation mechanism may be restricted by using the rigid octaketone macrocyclic scaffold. Four new hydrazones were synthesized through a condensation reaction of arylhydrazines with cyclotetrabenzil (**7**) [120,363] that could orient eight arylhydrazones arms around the central macrocyclic core. Structural properties of the resulting compounds were investigated.

4.2 Results and Discussion

4.2.1 Syntheses of Cyclotetra(bisarylhydrazone)benzils

Four cyclotetra(bisarylhydrazone)benzils **29a**–**d** were obtained using acid-catalyzed hydrazone condensation reaction of arylhydrazines **28a**–**d** (12–32 equivalents) with the previously prepared cycloterabenzil (**7**) in EtOH, PhMe, or *p*-xylene (Scheme 4.3). These mixtures were stirred under nitrogen at reflux for 48 h. After purification by crystallization, the desired macrocycles appended with eight arylhydrazone groups **29a**–**d** were obtained in moderate yields.

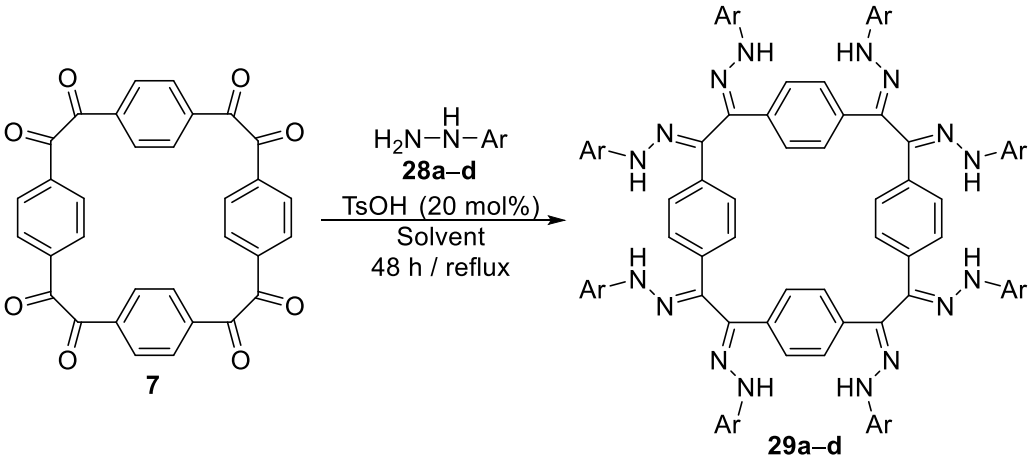

	28a / 29a	28b / 29b	28c / 29c	28d / 29d
Ar	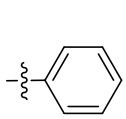	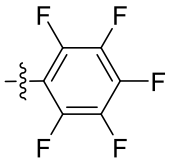	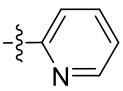	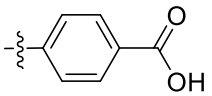
Solvent	PhMe	*p*-xylene	PhMe	EtOH
Yield%	53	39	66	49

Scheme 4.3 Hydrazone condensation reaction of cyclotetrabenzil (**7**) with arylhydrazines **28a**–**d**.

In these reactions, the precursor, cycloterabenzil (**7**), has a cyclic framework which prevented the collapse of the cyclic structure when further functionalities were introduced within the macrocycle backbone; therefore the final yields were enhanced.[360]

4.2.2 X-ray Crystallographic Analyses of Cyclotetra(bisarylhydrazone)benzils

Single crystals of four cyclotetra(bisarylhydrazone)benzils **29a**–**d** have been analyzed by X-ray crystallography. The results exhibited that the square structure of the scaffold, cyclotetrabenzil, is maintained in all four hydrazone derivatives **29a**–**d** with slight variations in the dimensions and angles; these variations are summarized in Table 4.1.

According to these results, the macrocyclic scaffold for **29a**–**d** possibly has a boat-like conformation because the rotation directions of the opposite dihedral angles are same, unlike the chair-like conformation structure, in which the rotation directions of the opposite dihedral angles are different. The X-ray results of single crystals for all four cyclotetra(bisarylhydrazone)benzils **29a**–**d** also demonstrated that each molecule has a bistetrapodal structure: four arylhydrazone units oriented above, and the other four oriented below the plane of central cavity of the macrocyclic scaffold, forming a double-decker structure. The appended arylhydrazone units are arranged in "*aabbaabb*" fashion, where "*a*" refers to the units oriented above the plane of the central cavity and "*b*" refers to the units oriented below the plane of the central cavity. In crystal structures of compounds **29a**–**d**, the mobile proton resides on the closest nitrogen atom to the aryl unit of the arylhydrazone moieties with N–H distance is 0.88 Å. This refers to the presence of only one stable structure at ambient conditions which is hydrazone (R–CR'=N–NH–R"); the other possible constitutional isomer, diazene (R–CHR'–N=N–R"), was not observed.[436,437]

Table 4.1 The distances and angles measured from the core macrocycles of **29a–d** and their corresponding measurements from the two conformers of cyclotetrabenzil (**7**).

	7		**29a**	**29b**	**29c**	**29d**
	chair	**boat**				
The distances between the centroids of each opposite phenyl rings in the core macrocycles, Å	7.62 7.33	7.39 7.22	7.38 7.37	7.19 7.09	7.34 7.34	7.31 7.28
The tilt angles between the planes of each opposite phenyl rings in the core macrocycles, º	0.0 0.0	23.0 40.8	54.6 56.4	41.2 46.1	50.8 50.8	52.2 35.2
The distances between the centroids of C–C bonds of each opposite corners in core macrocycle, Å	9.45 8.79	9.31 8.77	9.35 9.02	9.38 8.87	9.18 8.97	9.02 9.02
The [Ph–C–C–Ph] torsion angles in core macrocycle, º	–91.5 77.7 91.5 –77.7	–89.3 77.8 –89.3 77.8	–80.3 71.1 –85.6 76.2	–72.0 62.4 –72.8 57.0	–91.0 82.6 –91.6 82.6	–86.2 86.2 –85.2 85.2

4.2.2.1 Crystal Structure and Packing of Compound 29a

Diffraction-quality single crystals of compound **29a** were grown by slow vapor diffusion of EtOH into the chloroform solution of the compound, analyzed by single crystal X-ray diffraction, and the resulting solved structure is shown in Figure 4.2. This structure contains eight phenylhydrazone moieties oriented above and below the plane of the central macrocycle cavity. Compound **29a** crystallizes in the $P2_1/n$ centrosymmetric space group which belongs to the monoclinic system, with four molecules per unit cell.

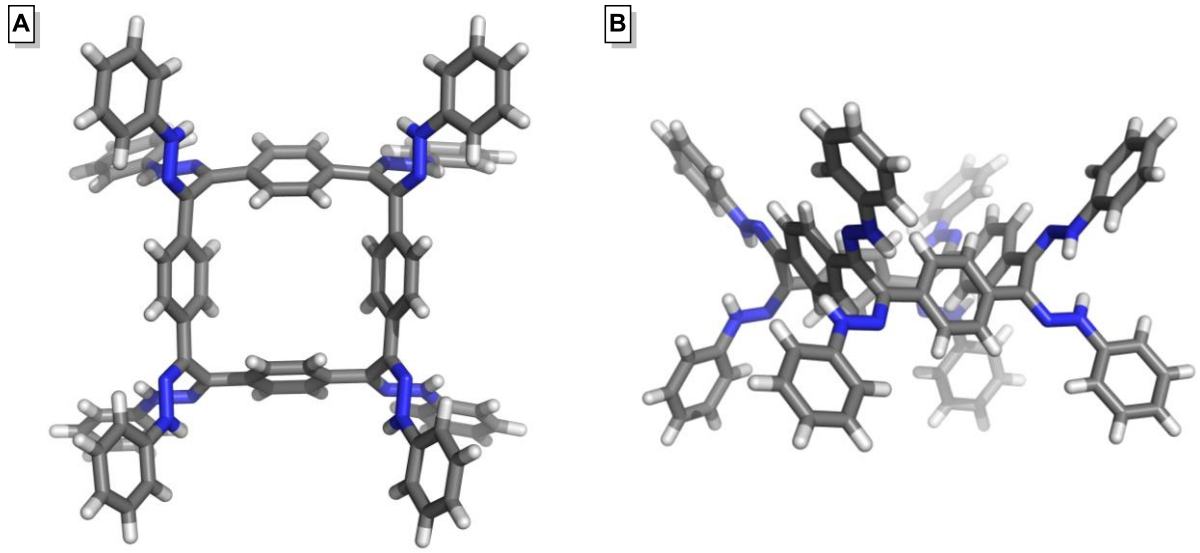

Figure 4.2 *(A)* Top-down view and *(B)* side view of the X-ray crystal structure of compound **29a**. Element colors: C—gray, N—blue, H—white.

The stereochemical arrangements for each adjacent phenylhydrazone moieties in compound **29a** are synclinal: two opposite pairs of them rotated in a clockwise direction with [N=C–C=N] dihedral angles of 72.1 and 77.1°, and the other two opposite pairs rotated in a counterclockwise direction with [N=C–C=N] dihedral angles of –78.6 and –89.8°. The nearest two phenylhydrazone moieties to each phenyl ring in the core macrocycle are pointing in the same direction (above or below the plane of the central cavity) with tilt angles measured between the planes of phenyl ring in the core macrocycle and phenyl rings in its neighboring phenylhydrazone moieties ranging from 6.4 to 22.3º. These angles indicate that phenyl rings in the core macrocycle and phenyl rings in their neighboring phenylhydrazone moieties are almost coplanar. All phenylhydrazone moieties in compound **29a** have *E*-configuration of hydrazone bridges. The [C=N–N–C(Ar)] torsion angles are ranging between 168.5 and 180.0º, and the distances between the atoms range between 1.28 and 1.31 Å for C=N, 1.35 and 1.36 Å for N–N, and 1.38 and 1.40 Å for N–C(Ar). These bond lengths fall in the same range as the average values reported for organic molecules with the same functional groups,[438–441] therefore there is no π-delocalization in the bonds from either the macrocycle

core or the aryl arms. This result proved the presence of only one structural isomer which is hydrazone and denied the possibility to find the other constitutional isomer which is diazene.

The molecules of compound **29a** packed with voids occupying 33.3% of unit cell volume, and their crystal packing diagram viewed along the crystallographic *a* axis is shown in Figure 4.3. Each molecule of **29a** makes weak short contacts to ten neighboring molecules involving the phenyl rings of the core macrocycle, the phenyl rings in the phenylhydrazone moieties, and the hydrazone functional groups. They established short [C–H···C] contacts ranging from 2.69 to 2.90 Å, short [C–H···N] contacts of 2.51 Å, and short [C···C–H] contacts of 3.21 and 3.39 Å in length; some of these short contacts established due to the appearance of large artifacts in the electron density near some atoms during solving the structure, which is common in needle- or plate-shaped crystals.[442]

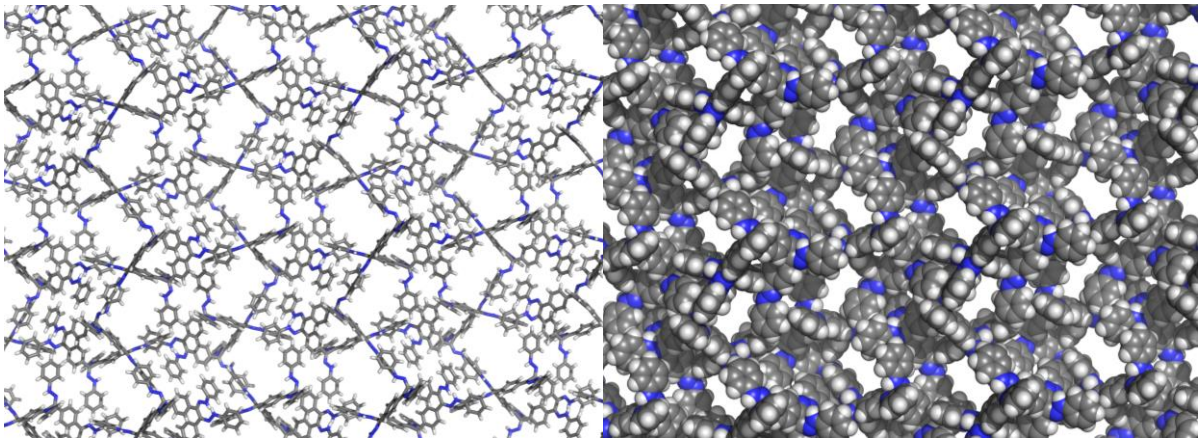

Figure 4.3 Segment of the crystal packing diagram of compound **29a** viewed along the crystallographic *a* axis. Element colors: C—gray, N—blue, H—white.

4.2.2.2 Crystal Structure and Packing of Compound 29b

Single crystals of compound **29b** suitable for X-ray diffraction analyses were grown by slow vapor diffusion of *n*-hexane into the chloroform solution of the compound, and the resulting analyzed structure is shown in Figure 4.4. Same as compound **29a**, the crystal structure of compound **29b** comprises eight pentafluorophenyl-hydrazone moieties extending

above and below the plane of the central macrocycle cavity. Compound **29b** crystallizes in the $P\bar{1}$ centrosymmetric space group which belongs to the triclinic system, with two molecules per unit cell.

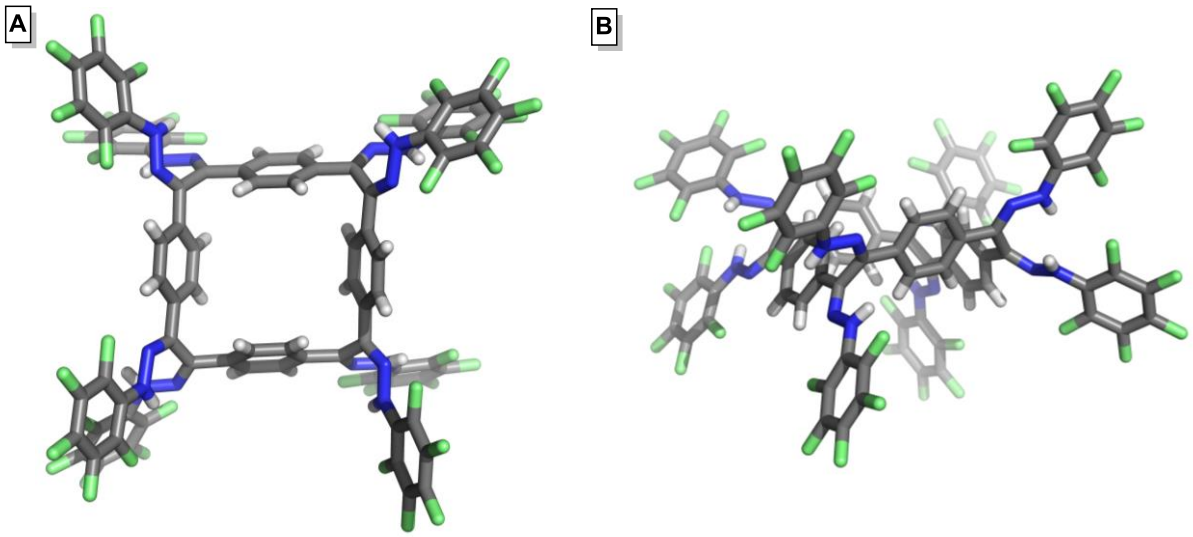

Figure 4.4 *(A)* Top-down view and *(B)* side view of the X-ray crystal structure of compound **29b**. Element colors: C—gray, N—blue, H—white, F—lime.

Neighboring pentafluorophenyl-hydrazone moieties in compound **29b** are stereochemically organized in synclinal arrangement: two opposite pairs of them are rotated in a clockwise direction with [N=C–C=N] dihedral angles of 58.3 and 60.0°, and the other two opposite pairs are rotated in a counterclockwise direction with [N=C–C=N] dihedral angles of –71.3 and –76.7°. The closest two pentafluorophenyl-hydrazone moieties to each phenyl ring in the core macrocycle point in the same direction (above or below the plane of the central cavity) with tilt angles measured between the planes of phenyl ring in the core macrocycle and phenyl rings in its neighboring pentafluorophenyl-hydrazone moieties ranging from 2.9 to 13.2º for six arms, and the remaining two arms have 33.8 and 45.7º tilt angles, which means these two arms are deviated from the coplanarity of phenyl rings in the core macrocycle with phenyl rings in their neighboring pentafluorophenyl-hydrazone

moieties. In structure of compound **29b**, all pentafluorophenyl-hydrazone moieties found in *E*-configuration with regard to hydrazone bridges. The [C=N–N–C(Ar)] torsion angles are ranging between 165.6 and 178.4º, and the distances between the atoms range between 1.28 and 1.31 Å for C=N, 1.34 and 1.37 Å for N–N, and 1.38 and 1.43 Å for N–C(Ar). These bond lengths agree with the average values for the reported organic molecules with the same functional groups.[63–66] Consequently, the π-delocalization between the bonds from either the macrocycle core or the aryl arms was not observed. Similar to compound **29a**, this result proved the presence of only one structural isomer for compound **29b**, which is hydrazone, and the other constitutional isomer (diazene) was not observed.

The extended crystal structure (seen along the crystallographic *a* axis in Figure 4.5A) for compound **29b** displays voids occupying 25.3% of the unit cell volume. In this extended structure, the molecules of **29b** stacked together by slipped-parallel [π···π] interaction between the four phenyl rings (electron rich units) in the core macrocycle with pentafluorophenyl rings (electron poor units) from four neighboring molecules and vice versa as it is shown in Figure 4.5B. The centroid-centroid distances between the phenyl and pentafluorophenyl rings in these [π···π] stacks ranging from 3.55 to 3.57 Å, which is in agreement with the average distances between benzene and hexafluorobenzene molecules reported in the literature.[443] The crystal lattice of compound **29b** is further stabilized by an assortment of weak short contacts whose lengths are ranging from 2.29 to 3.38 Å.

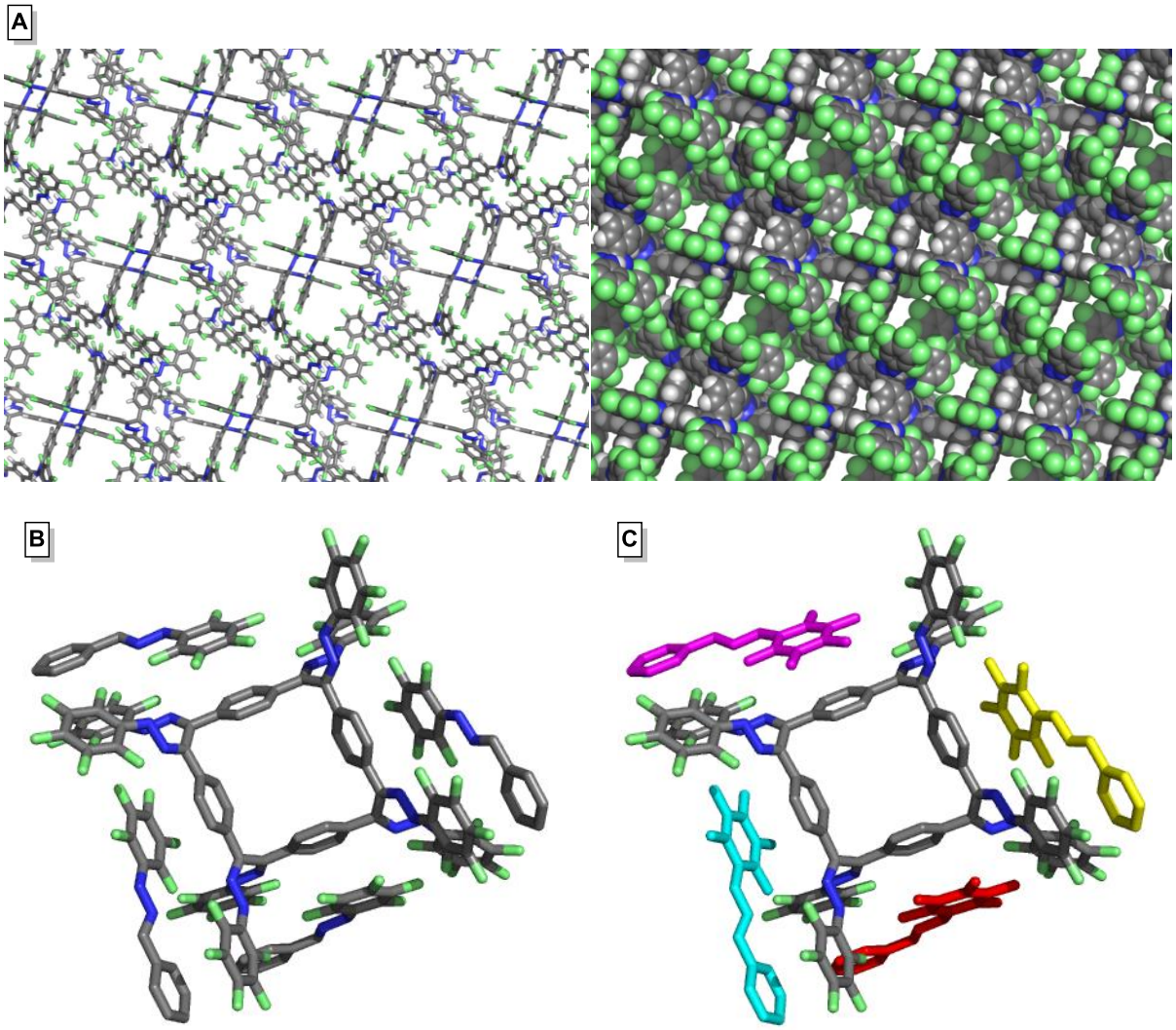

Figure 4.5 *(A)* Segment of the crystal packing diagram of compound **29b** viewed along the crystallographic *a* axis. *(B)* Crystal structure of compound **29b** and the fragments of four neighboring molecules that interact with it by [π···π] stacking; and *(C)* same as *(B)*, but with fragments of neighboring molecules highlighted in different colors. Hydrogen atoms have been omitted from *(B)* and *(C)* for clarity. Element colors: C—gray, N—blue, H—white, F—lime.

4.2.2.3 Crystal Structure and Packing of Compound 29c

Slow vapor diffusion of Et_2O into the AcOH solution of the compound **29c** afforded single crystal qualified to analyze by X-ray diffraction, and the resulting solved structure is shown in Figure 4.6. The crystal structure of compound **29c** exhibits eight 2-pyridylhydrazone moieties distributed above and below the plane of the central macrocycle

cavity. Compound **29c** crystallizes in the *P*2/*c* centrosymmetric space group which belongs to the monoclinic system, with two molecules of compound **29c** and eight molecules of AcOH per unit cell.

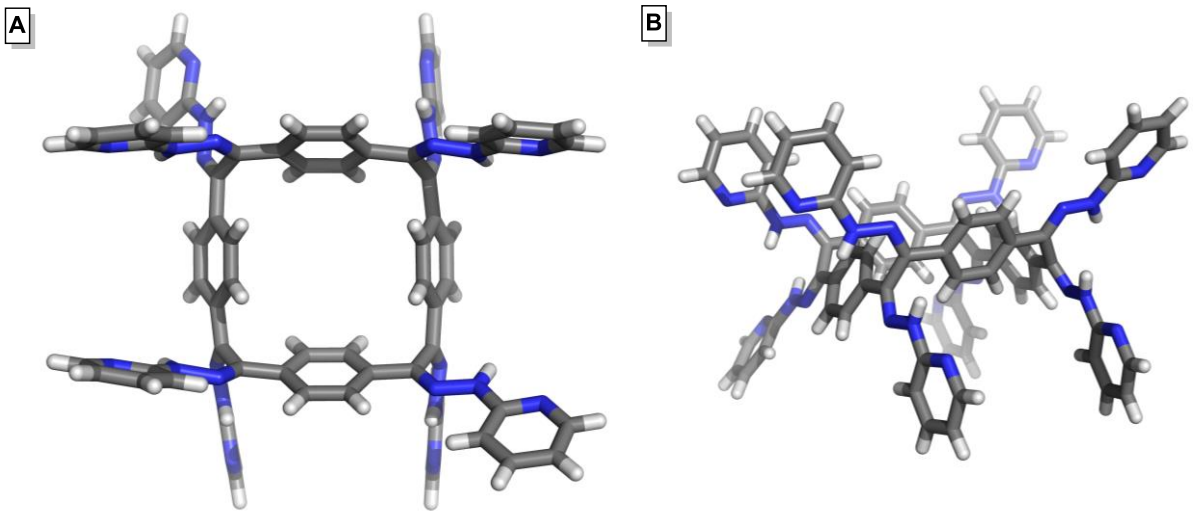

Figure 4.6 *(A)* Top-down view and *(B)* side view of the X-ray crystal structure of compound **29c**. Element colors: C—gray, N—blue, H—white. All solvent molecules are omitted for clarity.

The stereochemical arrangements for each neighboring 2-pyridylhydrazone moieties in compound **29c** are anticlinal: two opposite pairs of them rotated in a clockwise direction with [N=C–C=N] identical dihedral angles of 90.9°, and the other two opposite pairs rotated in a counterclockwise direction with [N=C–C=N] dihedral angles of –107.2 and –110.2°. The nearest two 2-pyridylhydrazone moieties to each phenyl ring in the core macrocycle are oriented in the same direction (above or below the plane of the central cavity) and they are almost coplanar with slight deviation measured by the tilt angles, the angle between the planes of phenyl ring in the core macrocycle and pyridyl rings in its adjacent 2-pyridylhydrazone moieties, which range from 12.9 to 27.1º. The substituents around hydrazone functional groups in all 2-pyridylhydrazone moieties in compound **29c** are found in *E*-configuration. The measured torsion angles [C=N–N–C(Ar)] are ranging between 167.5 and 173.5º, and the measured distances between the atoms range from 1.28 to 1.29 Å for

C=N, from 1.36 to 1.37 Å for N–N, and from 1.37 to 1.38 Å for N–C(Ar). The measured bond lengths match the average values reported for the organic molecules with the same functional groups.[63–66] As a result; there is no π-delocalization in the bonds from either the macrocycle core or the aryl arms. This result proved the presence of only one structural isomer which is hydrazone, and excluded the probability to find the other constitutional isomer (diazene).

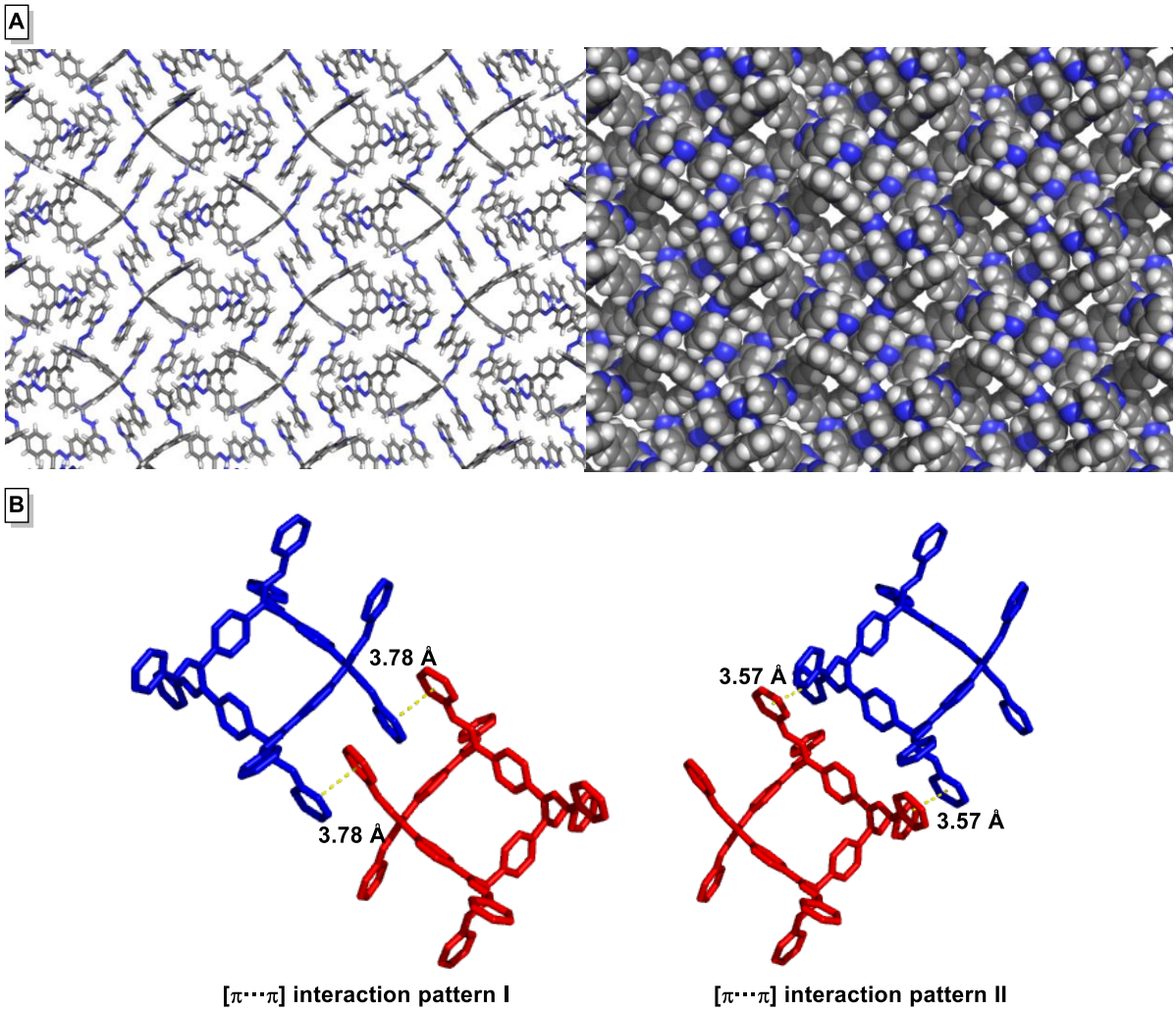

Figure 4.7 *(A)* Segment of the crystal packing diagram of compound **29c** viewed along the crystallographic *a* axis, *(B)* The two patterns of [π···π] interaction which are shown in the crystal lattice of compound **29c** highlighted in different colors. Element colors: C—gray, N—blue, H—white. All solvent molecules are omitted for clarity.

Closer inspection of the packing diagram of compound **29c**, seen along the crystallographic *a* axis in Figure 4.7A, shows voids occupying 38.1% of the unit cell volume. In this packing diagram, the molecules of **29c** stacked together by antiparallel-displaced [π···π] interaction between the pyridyl rings in the 2-pyridylhydrazone moieties from neighboring molecules. The centroid-centroid distances in such [π···π] stacks are 3.78 Å (Figure 4.7B), which is in the same range of the calculated distances between two antiparallel-displaced pyridine molecules in the literature.[444,445] The other displaced [π···π] interaction was found between the pyridyl rings in the 2-pyridylhydrazone moieties from neighboring molecules, where the angles between the two nitrogen atoms from each ring were 120º. The centroid-centroid distances in these [π···π] stacks are 3.57 Å. The crystal lattice of compound **29c** is further stabilized by a variety of weak short contacts ranging from 2.30 to 3.39 Å.

4.2.2.4 Crystal Structure and Packing of Compound 29d

X-ray diffraction was used to analyze the single crystals of compound **29d** which were grown by slow vapor diffusion of *n*-pentane into the 1,4-dioxane solution of the compound, and the resulting solved preliminary structure is shown in Figure 4.8. Compound **29d** crystallizes in a structure similar to the structures of the previous compounds with eight 4-carboxyphenylhydrazone moieties oriented above and below the plane of the central macrocyclic cavity. This compound crystallizes in the *I*4/*m* centrosymmetric space group which belongs to the tetragonal system, with sixteen molecules of compound **29d** per unit cell. Each adjacent pair of 4-carboxyphenylhydrazone moieties in compound **29d** stereochemically organizes in anticlinal arrangement: two opposite pairs of them rotated in a clockwise direction with [N=C–C=N] dihedral angles of 96.1 and 105.2°, and the other two opposite pairs rotated in a counterclockwise direction with [N=C–C=N] dihedral angles of –

96.1 and –105.2°. The closest two 4-carboxyphenylhydrazone moieties to each phenyl ring in the core macrocycle are oriented in the same direction (above or below the plane of the central cavity) with tilt angles measured between the planes of phenyl ring of the core macrocycle and 4-carboxyphenyl rings in its neighboring 4-carboxyphenylhydrazone moieties ranging from 9.7 to 17.2º. These angles indicated that phenyl rings in the core macrocycle and 4-carboxyphenyl rings in their neighboring 4-carboxyphenylhydrazone moieties are almost coplanar.

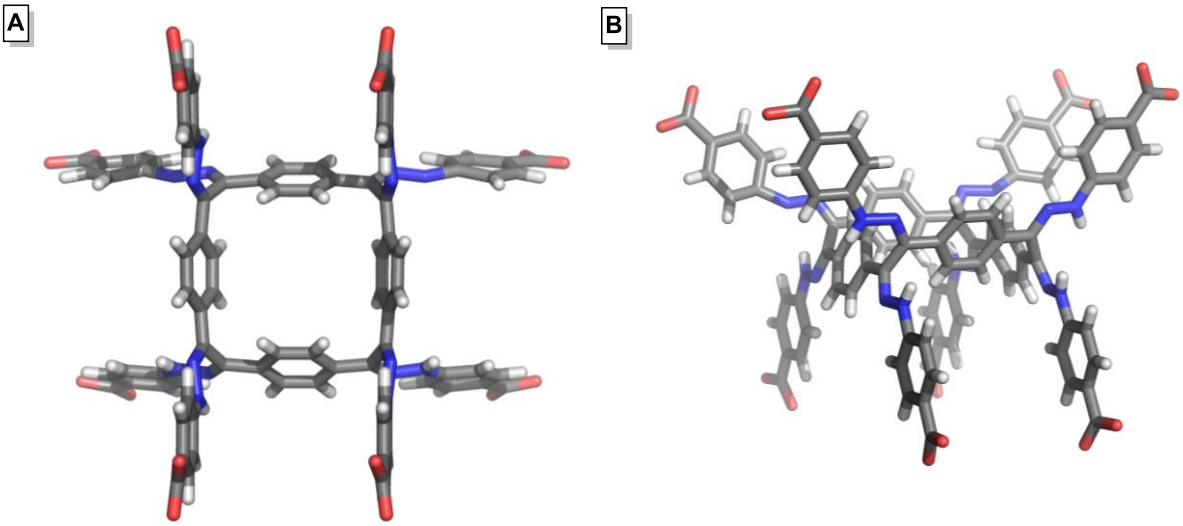

Figure 4.8 *(A)* Top-down view and *(B)* side view of the X-ray crystal structure of compound **29d**. Element colors: C—gray, N—blue, H—white, O—red.

The 4-carboxyphenylhydrazone moieties in compound **29d** possess *E*-configuration around their hydrazone bridges. The [C=N–N–C(Ar)] torsion angles are ranging between 166.8 and 174.8º, and the distances between the atoms in most 4-carboxyphenylhydrazone arms range between 1.29 and 1.32 Å for C=N, 1.33 and 1.35 Å for N–N, and 1.35 and 1.41 Å for N–C(Ar). These bond lengths fall in the same range as the average values reported for the same functionalized organic molecules,[63–66] thus the π-delocalization between the bonds from either the macrocycle core or the aryl arms was not seen. This result confirmed the existence of only one structural isomer which is hydrazone, and omitted the possibility to see the other

expected structural isomer which is diazene. The exception was seen in two identical 4-carboxyphenylhydrazone arms which have slightly longer N–N and N–C(Ar) bonds, measuring 1.40 and 1.45 Å, and these two longer arms overlapped with the neighboring molecule causing a twinned crystal. These two longer bonds could be a result of poor refinement of crystal structure of compound **29d**.[442,446]

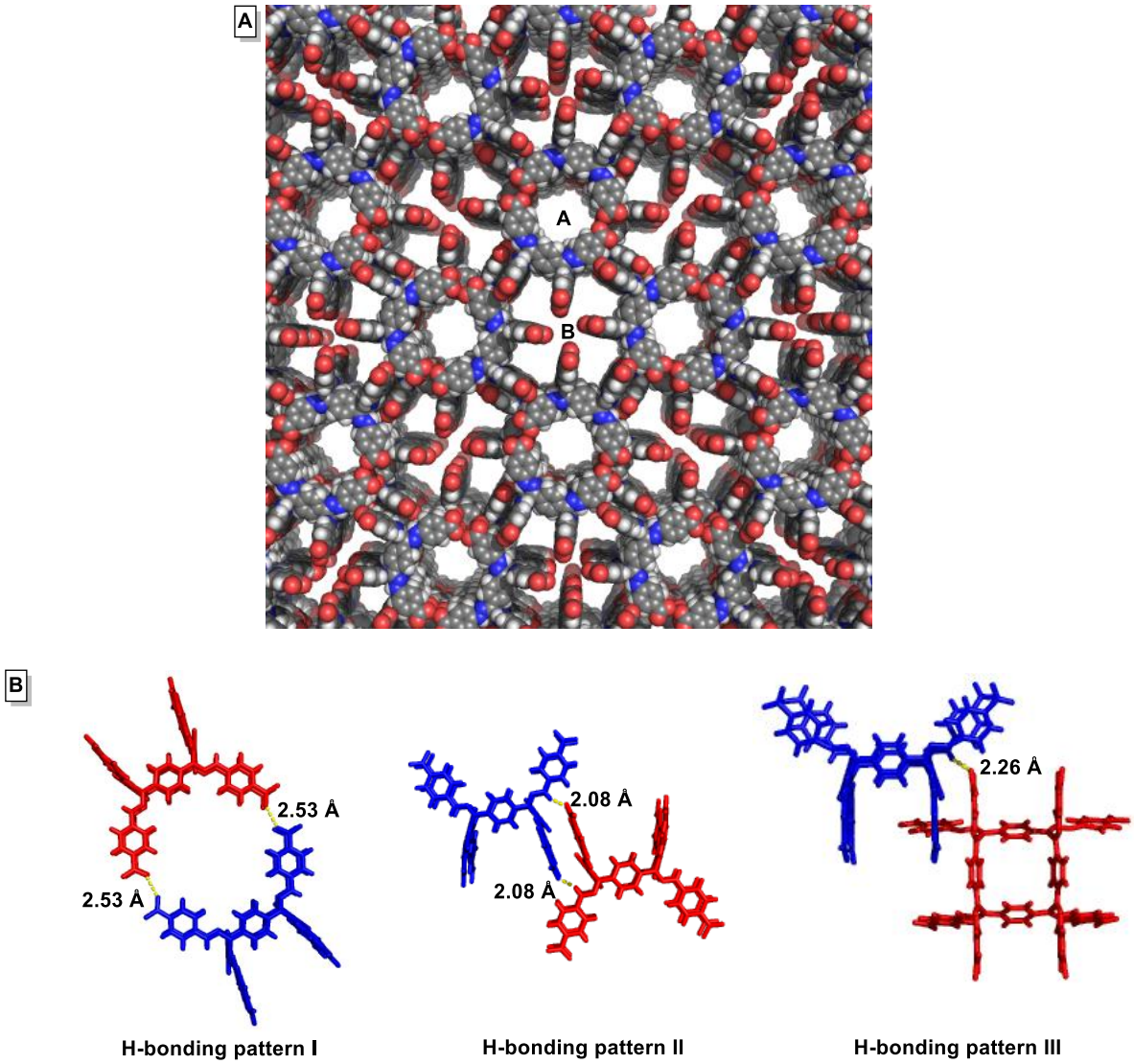

Figure 4.9 *(A)* Segment of the crystal packing diagram of compound **29d** viewed along the crystallographic *c* axis, *(B)* The three patterns of H-bonding which are shown in the crystal lattice of compound **29d**. Element colors: C—gray, N—blue, H—white, O—red.

The extended structure of compound **29d** showed three-dimensional porous network, viewed along the crystallographic *c* axis. In this packing, four molecules of compound **29d**

come together to enclose one-dimensional cylindrical channels (pore A in Figure 4.9A) with an average diameter of approximately 16.24 Å, measured between the centroids of each opposite pair of phenyl rings which enclosing the pores. Four 4-carboxyphenylhydrazone arms from each molecules of compound **29d** arranged themselves in order to let their carboxylate units approach each other to form hydrogen bonds and enclose the pores (H-bonding pattern I in Figure 4.9B; [O···O] distance of 2.53 Å).

Other two arms participated in stabilizing the porous self-assembled structure through another pattern of hydrogen bonds between the oxygen atoms of the carboxylate units and the hydrogen atoms of the hydrazone units from a neighboring molecule (H-bonding pattern II in Figure 4.8B; [N–H···O] bond distance 2.08 Å). The last two arms were involved in generating another set of pores between the cylindrical channels with a clover leaf-like shape (pore B in Figure 4.9A). The shortest distance is 7.32 Å for two opposite oxygen atoms from carboxylate units, and the widest distance is 24.72 Å between the centroids of two opposite phenyl rings enclosing the pores. Another hydrogen bond contributed in enclosing the extrinsic pores generated between the oxygen atoms of the carboxylate units and the hydrogen atoms of the hydrazone units from a neighboring molecule (H-bonding pattern III in Figure 4.9B; [N–H···O] bond distance 2.26 Å). Materials Studio software package was used to estimate the accessible surface area for this hydrogen-bonding organic framework by following the procedures reported in the literature by Kim and co-workers.[447] The probe molecule with diameter equal to the kinetic diameter of N_2 (3.68 Å) was used, and the calculated accessible surface area was 3531.7 $m^{2}{\cdot}g^{-1}$.

The presence of two types of pores within the crystal lattice of compound **29d** produced voids occupying 63.3% of the unit cell volume which is filled with highly disordered solvent molecules; this disordered solvent was likely the culprit behind the poor refinement of the structure. Therefore, the data were corrected for the influence of these

solvents using the SQUEEZE routine in PLATON,[448,449] resulting in high *R* values. The calculated density of the solvent free network was affected and measured as 0.624 Mg m^{-3}, which is much lower than the upper limit (0.9 Mg m^{-3}) suggested by McKeown and co-workers for potentially porous compounds.[450]

4.2.3 Dynamic ^{1}H NMR Study of the Barrier to Inversion in Compounds 29b–d

At ambient conditions, the ^{1}H NMR spectra of cyclotetra(bisarylhydrazone)benzils **29a**–**d** exhibit two equal intensity broad signals for the symmetrical hydrogens of the phenyl rings in the core macrocycle. This opservation is a consequence of the slow E/Z isomerization around the imine nitrogen in the bulk hydrazone arms which causes slow exchange and hinders the rotation freedom of these protons and increase the spin-spin relaxation time.

Results of the dynamic ^{1}H NMR study of the cyclotetra(bisarylhydrazone)benzils **29b**–**d** are shown in Table 4.2; the dynamic ^{1}H NMR study did not include compound **29a** due to its poor solubility in high boiling point solvents. Gradual heating of the samples broadens the two equal intensity signals of the hydrogens in phenyl rings in the core macrocycle until they are vanished, and then they coalesce at higher temperatures forming one signal. Additionally, the signal of the proton in (N–H) group is shielded to lower chemical shifts by increasing the temperature in DMSO-d_6 (polar aprotic solvent) due to the decrease of the hindrance around hydrogens of phenyl rings during *E*/*Z* inversion (Scheme 4.4). The same signal (N-H) is disappeared or being very weak in AcOH-d_4 (polar protic solvent), probably due to the intermolecular exchange between (N–H) proton and deuterated AcOH solvent.

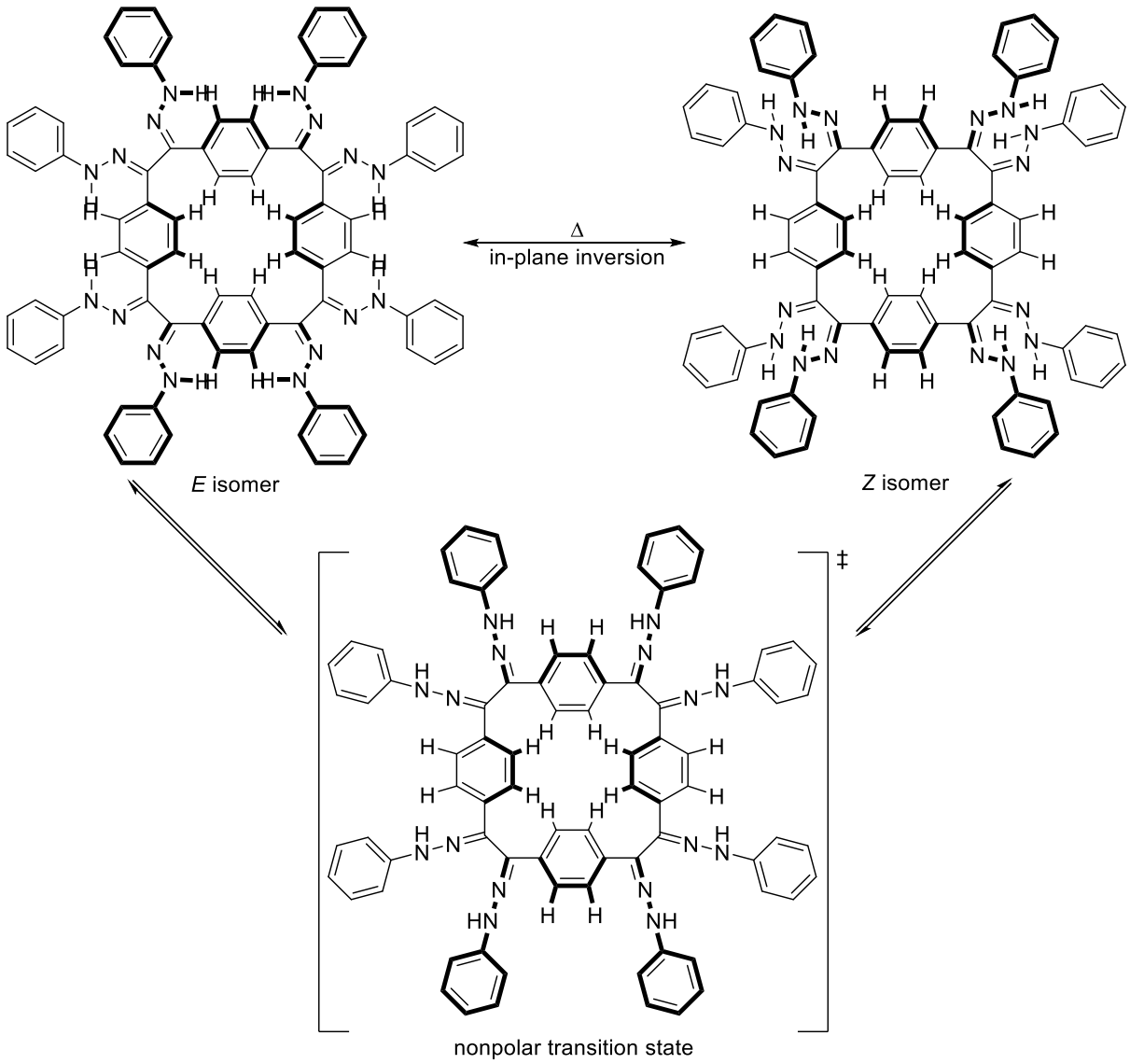

Scheme 4.4 The suggested mechanism of *E/Z* isomerization occurring through an in-plane inversion of the rotors (NH–Ar) around the imine nitrogen atoms, Ar = phenyl in this scheme.

The rate constants (k_c) for the present dynamic process in the cyclotetra(bisarylhydrazone)benzils **29b**–**d** were calculated at the coalescence temperature (T_c) employing the Gutowsky–Holm equation ($k_c = 2.22\ \Delta\nu$), where $\Delta\nu$ is the difference between the chemical shifts of the hydrogens of phenyl rings in the core macrocycle in Hz, and assuming the transmission coefficient (κ) to be unity, the Gibbs free energies of activation ($\Delta G^{\ddagger}$) were calculated according to the Eyring equation ($\Delta G^{\ddagger} = RT_c[\ln T_c - \ln k_c + 23.76]$).[451–456]

Table 4.2 Rate constants and Gibbs activation energy parameters for the *E*/*Z* isomerization calculated from the dynamic ^{1}H NMR data of compounds **29b–d** in DMSO-d_6 and AcOH-d_4.

	solvent	δ [Hz][a]	T_c [K]	k_c [s^{-1}]	$\Delta G^{\ddagger}$ [kcal mol^{-1}]	$t_{1/2} \times 10^{-4}$ [s]	$\tau \times 10^{-4}$ [s]
29b	DMSO-d_6	4110, 4730	323	1376	14.35	5.0	7.2
	AcOH-d_4	4156, 4946	323	1754	14.19	4.0	5.7
29c	DMSO-d_6	4003, 4945	363	2091	15.90	3.3	4.8
	AcOH-d_4	4163, 5128	363	2143	15.89	3.2	4.7
29d	DMSO-d_6	3967, 4973	383	2234	16.77	3.1	4.5
	AcOH-d_4	4077, 5050	383	2161	16.79	3.2	4.6

[a] Chemical shifts of the protons of phenyl rings of the core macrocycle in ppm × NMR-instrument frequency, which was 600 MHz in this study.

Barriers to inversion, thus obtained for the cyclotetra(bisarylhydrazone)benzils **29b**−**d**, are given in Table 4.2 and proved to be slightly unsensitive to the different functional groups in (NH–Ar) rotor: the isomerization rate and the Gibbs activation energy showed a little difference by changing the functionality of aryl groups, and subsequently the lifetime slightly changed. Additionally, the differences in rate constants and the free energies of activation when changing the solvent are not substantial; i.e. they are almost the same in both the aprotic (DMSO-d_6) and the protic (AcOH-d_4) solvents. One might conclude that the isomerization process goes through the inversion mechanism which is known to be a solvent-independent mechanism.[413] The inversion mechanism proceeds via changing the hybridization of the imine nitrogen atoms from sp^2 to sp at the linear transition state, and the sp^2 lone pair changes to a transitory filled p orbital to facilitate the inversion process.

4.3 Conclusions and Outlook

In summary, based on cyclotetrabenzil (**7**), four new cyclotetra(bisarylhydrazone)benzils **29a**–**d**, bearing eight arylhydrazone pendant arms at the bridges between the phenyl rings in the core macrocycle, were synthesized and characterized. The effect of attaching different arylhydrazone substituents on the cyclic backbone structure was examined. The crystal packing of these macrocycles showed different interaction patterns between molecules to stabilize the crystal lattice: only short contacts in **29a**, [$\pi\cdots\pi$] stacking in **29b** and **29c**, and hydrogen bonding in **29d**. The crystal lattice of **29d** exhibited two types of pores which could provide a high surface area hydrogen-bonding organic framework to use for gas storage or separation. The *E*/*Z* isomerization rate and the Gibbs activation energies for compounds **29b**–**d** were studied using dynamic ^{1}H NMR analysis. This analysis opened up the future opportunities to use other external stimuli such as light or addition of metal ions to study the reversible change in configuration. Additionally, these compounds provided inspiration for the direction for future work by expansion of these compounds to other larger and more stable metal-organic frameworks or coordination polymers. Also, these compounds could participate in inclusion complexes due to the existence of many chelating zones in their structures.

4.4 Experimental Section

4.4.1 General Materials and Physical Methods

Materials. All reactions were performed in a fume hood in oven-dried glassware. All starting materials and solvents, which were used for syntheses or crystal growth, were obtained from the commercial sources and used without further purification. Cyclotetrabenzil (**7**) was synthesized according to the procedures described in Chapter Two.

Physical Methods. All NMR spectra were recorded on a JEOL ECA-600 spectrometer, with working frequencies for ^{1}H nuclei of 600, for ^{13}C nuclei of 150, and for ^{19}F nuclei of 565 MHz. ^{1}H, ^{13}C , and ^{19}F NMR chemical shifts (δ) were reported in parts per million (ppm) units relative to the residual signals of deuterated solvent (^{1}H: DMSO-d_6 = 2.50 ppm; $CDCl_3$ = 7.24 ppm; AcOH-d_4 = 11.65 and 2.04 ppm; ^{13}C: DMSO-d_6 = 39.50 ppm; $CDCl_3$ = 77.23 ppm; AcOH-d_4 = 178.99 and 20.00 ppm). All NMR spectra were recorded at ambient temperature. The multiplicities of ^{1}H NMR signals were described as follows: s = singlet, d = doublet, t = triplet, q = quartet, m = multiplet, dd = doublet of doublet. The ^{13}C NMR signal structure was analyzed by DEPT (Distortionless Enhancement by Polarization Transfer), which is a tool used to assign ^{13}C NMR peaks, and described as follows: (+) = primary or tertiary C atom "positive signal", (−) = secondary C atom "negative signal", and (Cq) = quaternary C atom "no signal". Melting points were measured in a Barnstead International 1101D MeL-Temp capillary MP apparatus equipped with a Fluke 51-2 Thermometer, and are uncorrected. Mass spectra were recorded using electrospray ionization high resolution mass spectrometry (ESI-HRMS) and were collected at University of Texas at Austin by Dr. Ian M Riddington and his assistants. Infrared spectra (IR) were recorded on a Nicolet iS10 FT-IR spectrometer equipped with a Thermo Scientific iTR for multi-purpose ATR sampling and reported in wavenumbers (cm^{-1}) as a solid phase measurement. Elemental analyses were conducted by Intertek USA Inc. Single crystal XRD measurements were performed by Dr. Xiqu Wang (UH) using a Bruker DUO platform diffractometer equipped with a 4K CCD APEX II detector and an Incoatec 30 Watt Cu microsource with compact multilayer optics.

4.4.2 Syntheses and Characterization of Cyclotetra(bisarylhydrazone)benzils

4.4.2.1 Synthesis and Characterization of Compound 29a

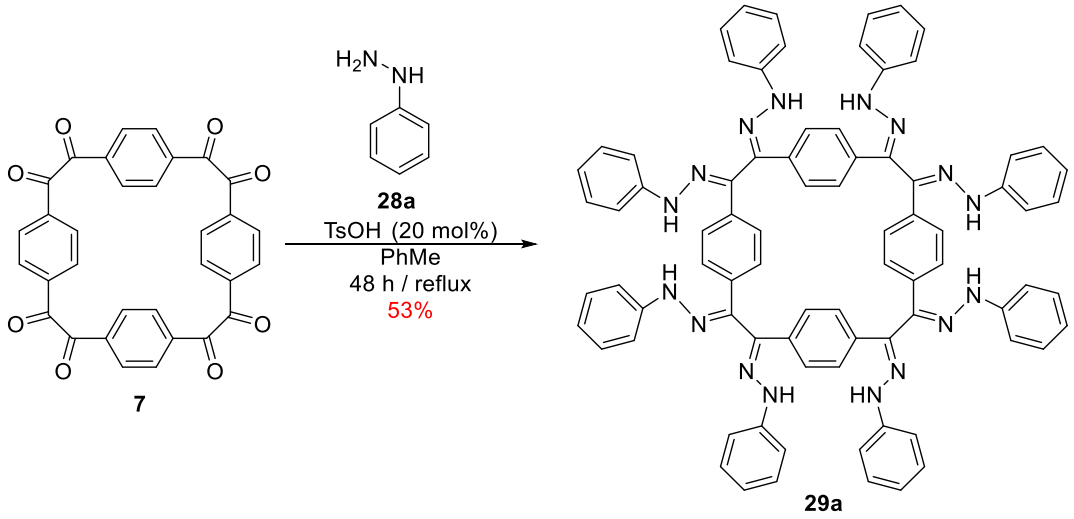

A solution of **7** (0.53 g, 1.00 mmol), phenylhydrazine **28a** (1.30 g, 12.00 mmol, 12.00 equiv.), and *p*-toluenesulfonic acid (38.0 mg, 0.20 mmol, 0.20 equiv.) in PhMe (50 mL) was prepared in a 100-mL round-bottomed flask equipped with a magnetic stirrer and a Dean-Stark condenser. The solution was heated to reflux for 48 h, and then the solvent was evaporated from the reaction mixture using rotary evaporator. The resulting orange solid was suspended in EtOH (50 mL), filtered, and washed with EtOH (50 mL) and then Et_2O (50 mL). After filtration, the product was dissolved in chloroform (100 mL) and the solution was passed through a 2 cm thick Celite pad on a glass-fritted Büchner funnel fitted onto 500-mL round-bottomed flask; a clear orange solution was seen. Then, hot EtOH (100 mL) was carefully layered on the top of the orange solution and the round-bottomed flask was sealed with a septum. After 3 d, the obtained precipitate was filtered and washed with EtOH (50 mL) and Et_2O (50 mL), to afford pure **29a** as an orangish-yellow solid (yield: 0.66 g, 0.53 mmol, 53%, m.p. 210–212 ºC). ^{1}H NMR (600 MHz, $CDCl_3$) δ 8.40 (s, broad, 16H), 7.73 (s, 8H), 7.25 (t, *J*=7.6 Hz, 16 H), 7.13 (d, *J*=8.2 Hz, 16H), 6.90 (t, *J*=7.2 Hz, 8H), 6.72 (s, broad, 16H) ppm. ^{13}C NMR (150 MHz, $CDCl_3$) δ 143.69 (Cq), 134.87 (Cq), 134.70 (Cq), 129.40

(+), 127.43 (+), 121.50 (+), 113.68 (+) ppm. IR (neat): $\tilde{\nu}$ = 3312, 1599, 1566, 1497, 1245, 1141, 1005, 966, 845, 747, 688, 503 cm^{-1}. ESI-HRMS: *m/z* $[M+H]^+$: Calcd for $[C_{80}H_{64}N_{16}\cdot H]^+$: 1249.50; Found 1249.55, with correct isotope distribution. Elemental analysis Calcd (%) for $C_{80}H_{64}N_{16}$: C 76.90, H 5.16, N 17.94; Found: C 75.52, H 5.09, N 17.23.

4.4.2.2 Synthesis and Characterization of Compound 29b

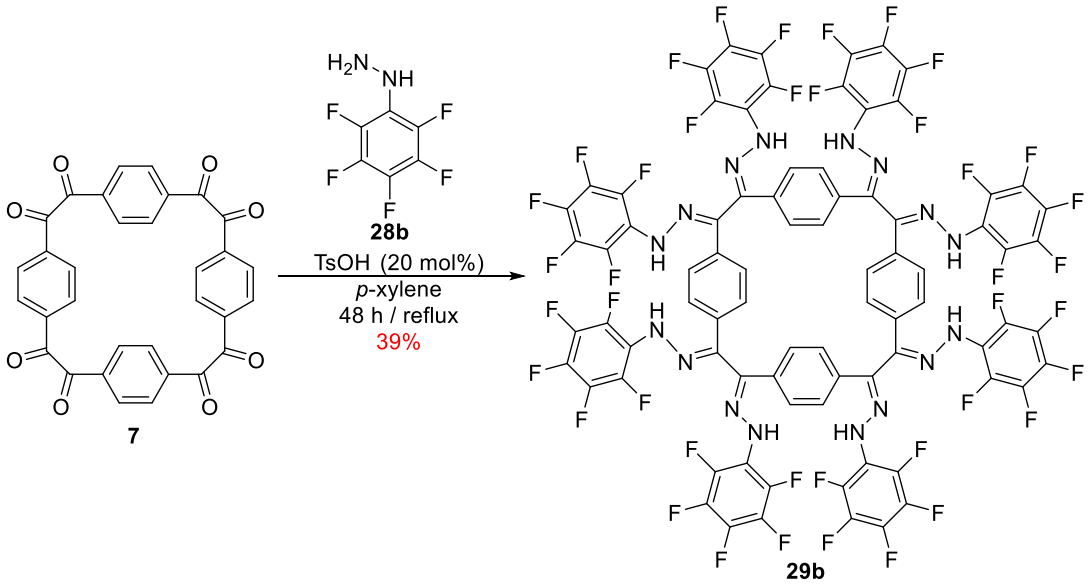

A solution of **7** (0.53 g, 1.00 mmol), phenylhydrazine **28b** (2.38 g, 12.00 mmol, 12.00 equiv.), and *p*-toluenesulfonic acid (38.0 mg, 0.20 mmol, 0.20 equiv.) in *p*-xylene (50 mL) was prepared in a 100-mL round-bottomed flask equipped with a magnetic stirrer and a Dean-Stark condenser. The solution was heated to reflux for 48 h, then quenched with *n*-hexane (50 mL), cooled to room temperature, filtered, and washed with EtOH (50 mL) and then Et_2O (50 mL). After filtration, the product was dissolved in chloroform (100 mL) and the solution was passed through a 2 cm thick Celite pad on a glass-fritted Büchner funnel fitted onto 500-mL round-bottomed flask; a clear yellowish solution was seen. Then, hot *n*-hexane (100 mL) was carefully layered on the top of the yellowish solution and the round-

bottomed flask was sealed with a septum. After 3 d, the obtained precipitate was filtered and washed with EtOH (50 mL) and Et_2O (50 mL), to afford pure **29b** as a yellowish solid (yield: 0.76 g, 0.39 mmol, 39%, m.p. 154–156 ºC). ^{1}H NMR (600 MHz, $CDCl_3$) δ 8.28 (s, broad, 16H), 7.43 (s, 8H), 6.80 (s, broad, 16H) ppm. ^{13}C NMR (150 MHz, $CDCl_3$) δ 140.09 (Cq), 139.08 (Cq), 138.44 (Cq), 137.42 (Cq), 134.17 (Cq), 125.88 (+), 119.42 (Cq) ppm. ^{19}F-NMR (565 MHz, $CDCl_3$) δ –154.78 (d, *J*=21.7, 16F), –162.11 (t, *J*=19.5, 16F), –162.87 (t, *J*=21.7, 8F) ppm. IR (neat): $\tilde{\nu}$ = 3323, 1658, 1520, 1486, 1451, 1409, 1278, 1181, 1139, 1030, 1011, 973, 849, 726, 632, 574 cm^{-1}. ESI-HRMS: *m/z* $[M+K]^+$: Calcd for $[C_{80}H_{24}F_{40}N_{16}\cdot K]^+$: 2007.08; Found 2007.14, with correct isotope distribution. Elemental analysis Calcd (%) for $C_{80}H_{24}F_{40}N_{16}$: C 48.80, H 1.23, N 11.38; Found: C 49.17, H 1.20, N 11.67.

4.4.2.3 Synthesis and Characterization of Compound 29c

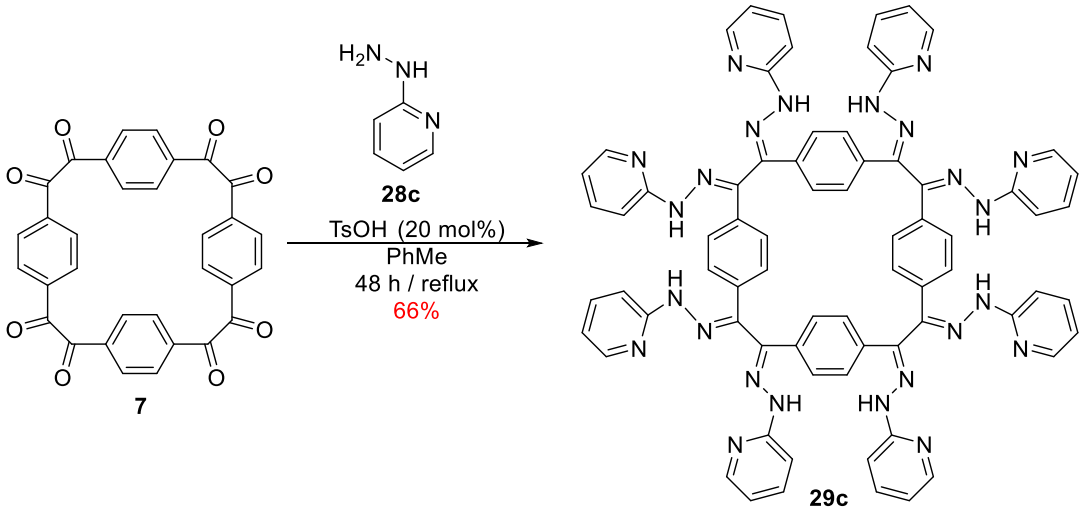

A solution of **7** (0.53 g, 1.00 mmol), 2-hydrazinopyridine **28c** (3.49 g, 32.00 mmol, 32.00 equiv.), and *p*-toluenesulfonic sulfonic acid (38.0 mg, 0.20 mmol, 0.20 equiv.) in PhMe (50 mL) was prepared in a 100-mL round-bottomed flask equipped with a magnetic stirrer and a Dean-Stark condenser. The solution was heated to reflux for 48 h, then cooled to room temperature, filtered, and washed with EtOH (50 mL) and then Et_2O (50 mL). After filtration,

the product was dissolved in chloroform (150 mL) and the solution was passed through a 2 cm thick Celite pad on a glass-fritted Büchner funnel fitted onto 500-mL round-bottomed flask; a clear yellowish solution was seen. Then, hot MeOH (150 mL) was carefully layered on the top of the yellowish solution and the round-bottomed flask was sealed with a septum. After 3 d, the obtained precipitate was filtered and washed with EtOH (50 mL) and Et_2O (50 mL), to afford pure **29c** as a yellowish solid (yield: 0.83 g, 0.66 mmol, 66%, m.p. 320–322 °C). ^{1}H NMR (600 MHz, $CDCl_3$) δ 8.98 (s, broad, N-H), 8.23 (s, broad, 16H), 7.82 (d, *J*=1.2 Hz, 8H), 7.61 (t, *J*=7.2 Hz, 8H), 7.35 (d, *J*=7.6 Hz, 8H), 6.76 (t, *J*=5.8 Hz, 8H), 6.69 (s, broad, 16H) ppm. ^{13}C NMR (150 MHz, $CDCl_3$) δ 156.37 (Cq), 147.83 (+), 137.97 (+), 136.46 (Cq), 134.80 (Cq), 127.67 (+), 124.99 (+), 116.77 (+), 108.47 (+) ppm. IR (neat): $\tilde{\nu}$ = 3316, 1593, 1568, 1489, 1435, 1305, 1250, 1138, 1005, 988, 837, 768, 735, 614, 509 cm^{-1}. ESI-HRMS: *m/z* $[M+2H]^{+2}$: Calcd for $[C_{72}H_{56}N_{24}\cdot 2H]^{+2}$: 629.71; Found 629.27, with correct isotope distribution. Elemental analysis Calcd (%) for $C_{72}H_{56}N_{24}$: C 68.78, H 4.49 N 26.73; Found: C 66.56, H 4.09, N 25.39.

4.4.2.4 Synthesis and Characterization of Compound 29d

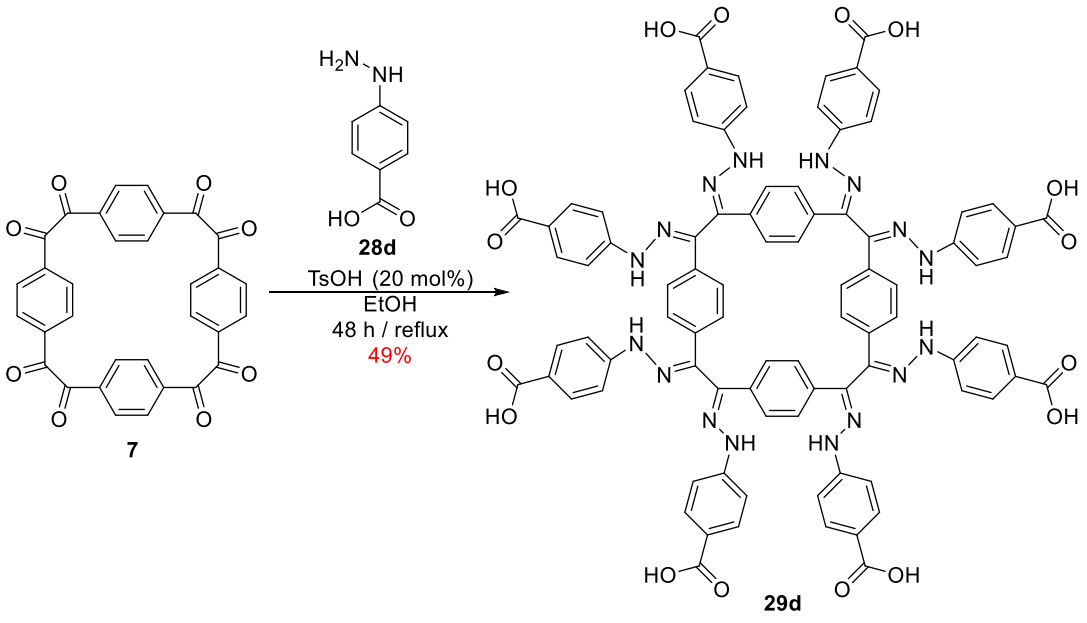

A solution of **7** (0.53 g, 1.00 mmol), 4-hydrazinobenzoic acid **28d** (1.83 g, 12.00 mmol, 12.00 equiv.), and *p*-toluenesulfonic acid (38.0 mg, 0.20 mmol, 0.20 equiv.) in EtOH (50 mL) was prepared in a 100-mL round-bottomed flask equipped with a magnetic stirrer and a Dean-Stark condenser. The solution was heated to reflux for 48 h, then cooled to room temperature, filtered, and washed with EtOH (50 mL) and then Et_2O (50 mL). After filtration, the product was dissolved in dioxane or THF (150 mL) and the solution was passed through a 2 cm thick Celite pad on a glass-fritted Büchner funnel fitted in 500-mL round-bottomed flask; a clear reddish solution was seen. Then, hot PhMe (150 mL) was carefully layered on the top of the reddish solution and the round-bottomed flask was sealed with a septum. After 3 d, the obtained precipitate was filtered and washed with EtOH (50 mL) and Et_2O (50 mL), to afford pure **29d** as a reddish solid (yield: 0.78 g, 0.49 mmol, 49%, m.p. 275–277 °C). ^{1}H NMR (600 MHz, DMSO-d_6) δ 12.35 (s, broad, O–H), 10.15 (s, N–H), 8.28 (s, broad, 16H), 7.74 (d, J=7.8 Hz, 16H), 7.33 (d, J=7.8 Hz, 16H), 6.62 (s, broad, 16H) ppm. IR (neat): $\tilde{\nu}$ = 2996, 1677, 1599, 1515, 1404, 1310, 1237, 1157, 1093, 1026, 1004, 961, 843, 766, 695 cm^{-1}. ESI-HRMS: *m/z* $[M–2H]^{-2}$: Calcd for $[C_{88}H_{64}N_{16}O_{16}\cdot 2H]^{-2}$: 799.78; Found 799.23, with correct isotope distribution. Elemental analysis Calcd (%) for $C_{88}H_{64}N_{16}O_{16}$: C 66.00, H 4.03 N 13.99; Found: C 63.66, H 4.08, N 12.79.

4.4.3 X-ray Crystallographic Analyses of Cyclotetra(bisarylhydrazone)benzils

4.4.3.1 Crystal Growth and Crystal Data of Compound 29a

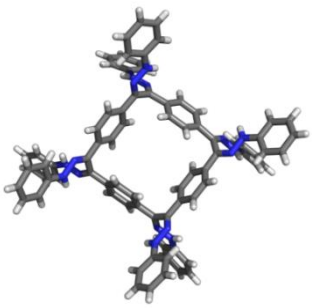

To obtain single crystals of compound **29a** suitable for X-ray diffraction analysis, we begun by dissolving crude product **29a** (15 mg) in chloroform (3 mL). The product solution was heated and filtered using a PTFE syringe filter (0.22 μm, 30 mm). The resulting filtrate (0.15 mL) was added to a small round-bottomed 0.75 mL culture tube, and this tube was placed inside a 2-dram scintillation vial containing EtOH (1 mL) as the diffusing solvent. The vial was tightly closed and kept at ambient conditions without external disturbance. Thin needle-like yellow crystals were harvested after 3 d by vapor diffusion technique.

Table 4.3 Crystallographic Data and Structure Refinement of Compound **29a**

Empirical formula	$C_{80}H_{64}N_{16}$
Formula weight	1249.47
Temperature	173(2) K
Wavelength	CuKα (λ = 1.54178 Å)
Crystal system	Monoclinic
Space group	$P2_1/n$
Unit cell dimensions	a = 11.2200(7) Å α = 90°
	b = 34.7220(2) Å β = 93.868(4)°
	c = 23.4803(17) Å γ = 90°
Volume	9126.8(10) Å^3
Z	4
Density (calculated)	0.909 Mg/m^3
Absorption coefficient	0.438 mm^{-1}
F(000)	2624
Crystal size	0.56 × 0.06 × 0.02 mm^3
2θ range for data collection	2.275 to 66.876°
Index ranges	$-13 \le h \le 13$, $-38 \le k \le 40$, $-23 \le l \le 27$
Reflections collected	81271
Independent reflections	16051 [$R_{(int)}$ = 0.0943]
Completeness to 2θ = 66.876°	98.9 %

Table 4.3 Continued

Absorption correction	Empirical
Refinement method	Full-matrix least-squares on F^2
Data / restraints / parameters	16051 / 756 / 865
Goodness-of-fit on F^2	1.047
Final R indices [$I>2\sigma(I)$]	R_1 = 0.0819, wR_2 = 0.2384
R indices (all data)	R_1 = 0.1095, wR_2 = 0.2571
Largest diff. peak and hole	0.25 and –0.28 e Å^{-3}

4.4.3.2 Crystal Growth and Crystal Data of Compound 29b

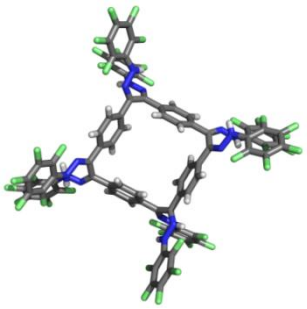

To obtain single crystals of compound **29b** suitable for X-ray diffraction analysis, we begun by dissolving crude product **29b** (15 mg) in chloroform (3 mL). The product solution was heated and filtered using a PTFE syringe filter (0.22 μm, 30 mm). The resulting filtrate (0.15 mL) was added to a small round-bottomed 0.75 mL culture tube, and this tube was placed inside a 2-dram scintillation vial containing *n*-hexane (1 mL) as the diffusing solvent. The vial was tightly closed and kept at ambient conditions without external disturbance. Prismatic yellow crystals were harvested after 48 h by vapor diffusion technique.

Table 4.4 Crystallographic Data and Structure Refinement of Compound **29b**

Empirical formula	$C_{80}H_{24}O_{40}N_{16}$
Formula weight	1969.15
Temperature	123(2) K
Wavelength	CuKα (λ = 1.54178 Å)
Crystal system	Triclinic
Space group	$P\bar{1}$
Unit cell dimensions	a = 11.9175(4) Å α = 110.459(2)°
	b = 20.6330(7) Å β = 91.480(2)°
	c = 21.1795(6) Å γ = 98.540(2)°
Volume	4808.3(3) Å^3
Z	2
Density (calculated)	1.360 Mg/m^3
Absorption coefficient	1.244 mm^{-1}
F(000)	1952
Crystal size	0.28 × 0.16 × 0.01 mm^3
2θ range for data collection	4.468 to 137.040°
Index ranges	$-14 \le h \le 14$, $-24 \le k \le 24$, $-25 \le l \le 24$
Reflections collected	53369
Independent reflections	17113 [$R_{(int)}$ = 0.0518]
Completeness to 2θ = 68.520°	96.5 %
Absorption correction	Empirical
Refinement method	Full-matrix least-squares on F^2
Data / restraints / parameters	17113 / 2842 / 1423
Goodness-of-fit on F^2	1.124
Final R indices [I>2σ(I)]	R_1 = 0.0722, wR_2 = 0.2031
R indices (all data)	R_1 = 0.1048, wR_2 = 0.2322
Largest diff. peak and hole	0.46 and –0.44 e Å^{-3}

4.4.3.3 Crystal Growth and Crystal Data of Compound 29c

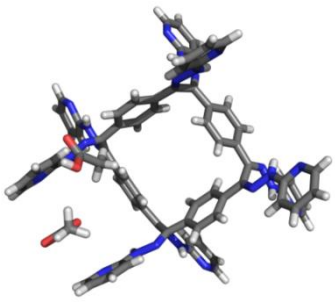

To obtain single crystals of compound **29c** suitable for X-ray diffraction analysis, we begun by dissolving crude product **29c** (15 mg) in AcOH (3 mL). The product solution was heated and filtered using a PTFE syringe filter (0.22 μm, 30 mm). The resulting filtrate (0.15 mL) was added to a small round-bottomed 0.75 mL culture tube, and this tube was placed inside a 2-dram scintillation vial containing Et_2O (1 mL) as the diffusing solvent. The vial was tightly closed and kept at ambient conditions without external disturbance. Cubic bright yellow crystals were harvested after 5 d by vapor diffusion technique.

Table 4.5 Crystallographic Data and Structure Refinement of Compound **29c**·2AcOH

Empirical formula	$C_{80}H_{72}N_{24}O_8$	
Formula weight	1497.61	
Temperature	123(2) K	
Wavelength	CuKα (λ = 1.54178 Å)	
Crystal system	Monoclinic	
Space group	*P*2/*c*	
Unit cell dimensions	a = 11.8280(8) Å	α = 90°
	b = 19.7880(14) Å	β = 98.362(3)°
	c = 20.2282(15) Å	γ = 90°
Volume	4684.1(6) $Å^3$	
Z	2	
Density (calculated)	1.062 Mg/m^3	

Table 4.5 Continued

Absorption coefficient	0.590 mm^{-1}
$F(000)$	1568
Crystal size	0.14 × 0.11 × 0.01 mm^3
2θ range for data collection	3.777 to 67.567°
Index ranges	$-14 \leq h \leq 14$, $-23 \leq k \leq 23$, $-22 \leq l \leq 23$
Reflections collected	51218
Independent reflections	8344 [$R_{(int)} = 0.0627$]
Completeness to $2\theta = 67.567°$	98.7 %
Absorption correction	Empirical
Refinement method	Full-matrix least-squares on F^2
Data / restraints / parameters	8344 / 0 / 511
Goodness-of-fit on F^2	1.036
Final R indices [$I>2\sigma(I)$]	$R_1 = 0.0651$, w$R_2 = 0.1769$
R indices (all data)	$R_1 = 0.0744$, w$R_2 = 0.1845$
Largest diff. peak and hole	0.52 and –0.20 e $Å^{-3}$

4.4.3.4 Crystal Growth and Crystal Data of Compound 29d

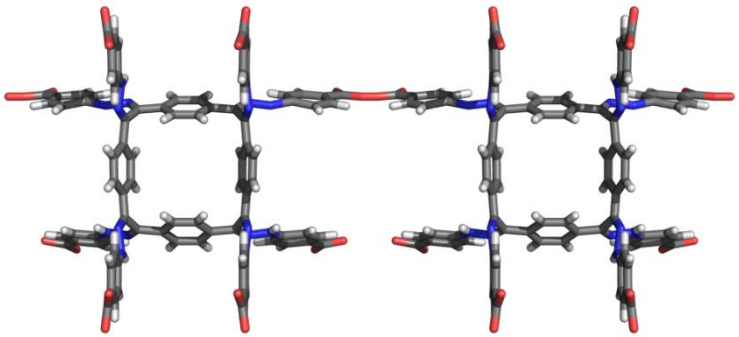

To obtain single crystals of compound **29d** suitable for X-ray diffraction analysis, we begun by dissolving crude product **29d** (15 mg) in 1,4-dioxane (3 mL). The product solution was heated and filtered using a PTFE syringe filter (0.22 μm, 30 mm). The resulting filtrate (0.15 mL) was added to a small round-bottomed 0.75 mL culture tube, and this tube was placed inside a 2-dram scintillation vial containing *n*-pentane (1 mL) as the diffusing solvent.

The vial was tightly closed and kept at ambient conditions without external disturbance. Cubic bright reddish-brown crystals were harvested after 7 d by vapor diffusion. The same crystals can be obtained by dissolving the crude product of **29d** in THF instead of 1,4-dioxane at the beginning and using a 1:1 mixture of *n*-pentane and 1-pentanol or PhMe as the diffusing solvent instead of *n*-pentane, and then following the same previously mentioned procedures. The structure of **29d** was solved but unfortunately refined poorly due to the very fast deterioration and severe disorder in solvent molecules which screened the diffractions at high angles.

Table 4.6 Crystallographic Data and Structure Refinement of Compound **29d**

Empirical formula	$C_{44}H_{27}N_8O_8$
Formula weight	795.73
Temperature	123(2) K
Wavelength	CuKα (λ = 1.54178 Å)
Crystal system	Tetragonal
Space group	*I*4/*m*
Unit cell dimensions	a = 39.6241(11) Å α = 90°
	b = 39.6241(11) Å β = 90°
	c = 21.5883(7) Å γ = 90°
Volume	33895(2) Å^3
Z	16
Density (calculated)	0.624 Mg/m^3
Absorption coefficient	0.368 mm^{-1}
F(000)	6576
Crystal size	0.18 × 0.14 × 0.04 mm^3
2θ range for data collection	2.230 to 50.740°
Index ranges	$-32 \le h \le 39$, $-37 \le k \le 39$, $-21 \le l \le 20$
Reflections collected	45005
Independent reflections	9273 [$R_{(int)}$ = 0.0576]

Table 4.6 Continued

Completeness to 2θ = 50.740°	99.7 %
Absorption correction	Empirical
Refinement method	Full-matrix least-squares on F^2
Data / restraints / parameters	9273 / 407 / 622
Goodness-of-fit on F^2	1.418
Final R indices [$I>2\sigma(I)$]	R_1 = 0.1114, wR_2 = 0.3445
R indices (all data)	R_1 = 0.1536, wR_2 = 0.3859
Largest diff. peak and hole	0.38 and –0.30 e Å^{-3}

4.4.4 ^{1}H NMR Spectra of Cyclotetra(bisarylhydrazone)benzils

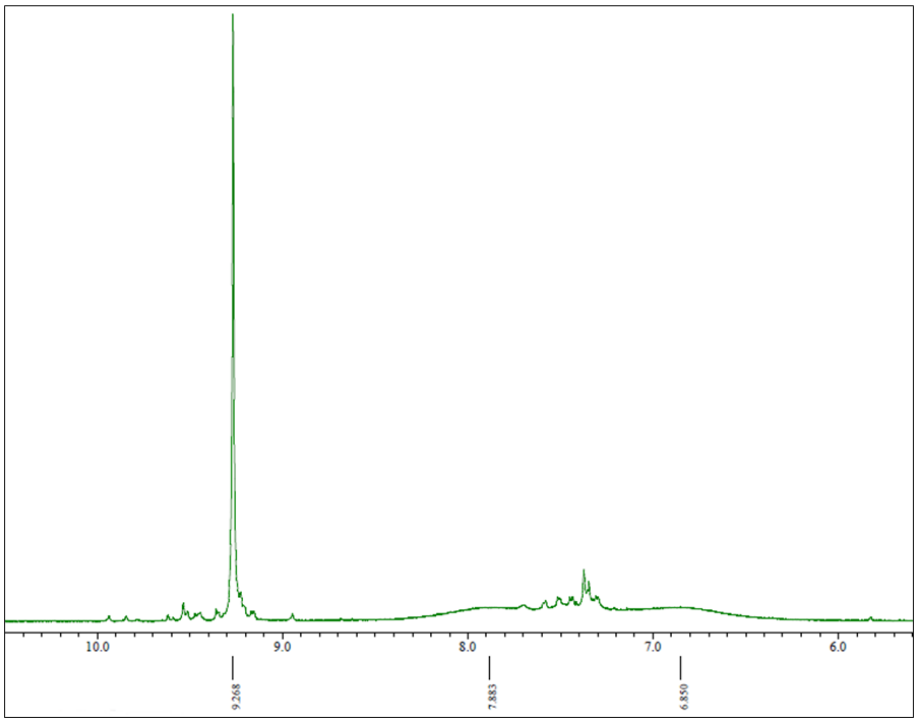

Figure 4.10 ^{1}H NMR spectrum of compound **29b** in DMSO-d_6.

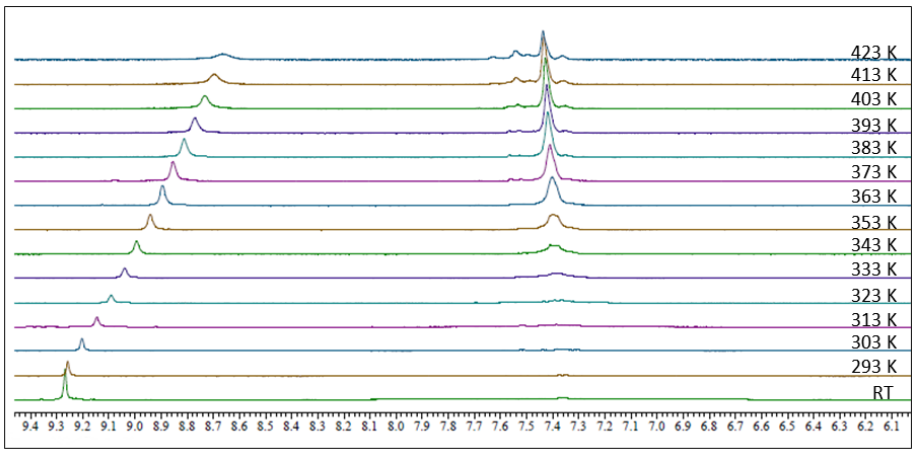

Figure 4.11 Variable-temperature ^{1}H NMR spectra of compound **29b** in DMSO-d_6.

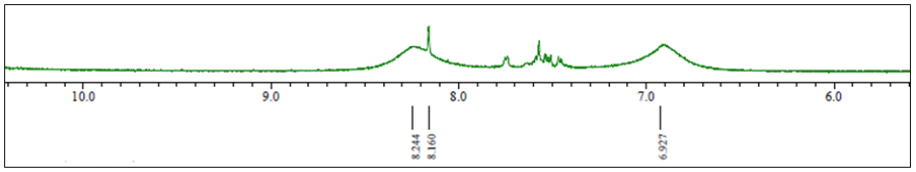

Figure 4.12 ^{1}H NMR spectrum of compound **29b** in AcOH-d_4.

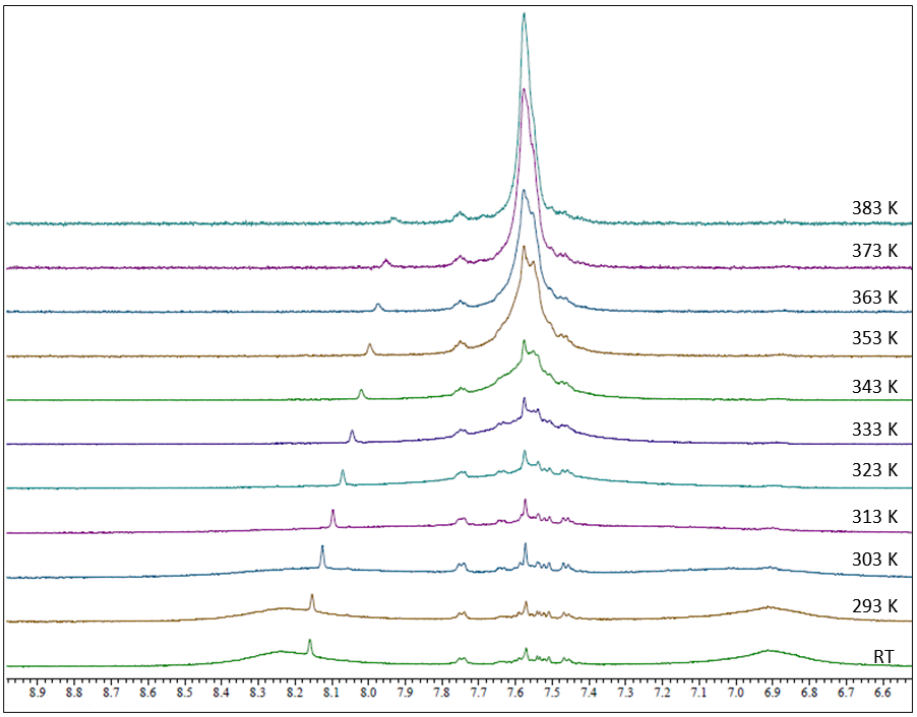

Figure 4.13 Variable-temperature ^{1}H NMR spectra of compound **29b** in AcOH-d_4.

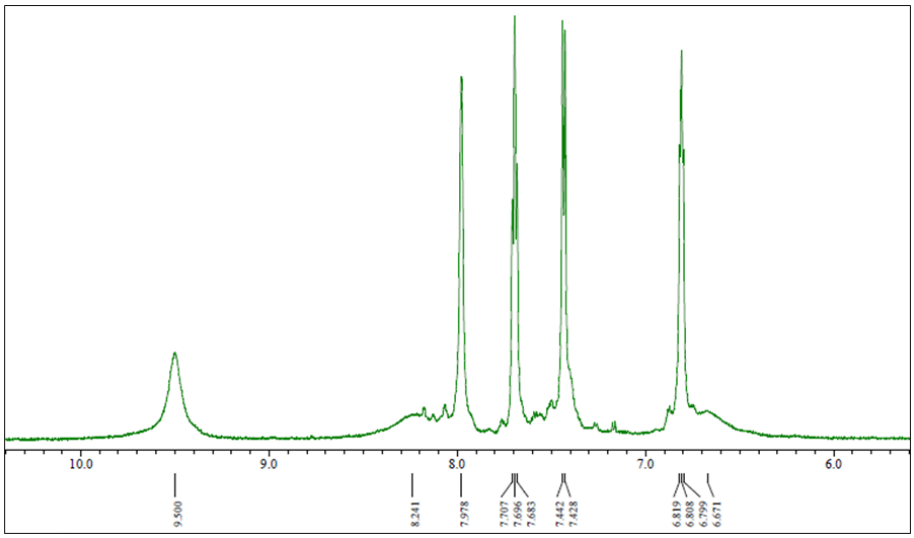

Figure 4.14 ^{1}H NMR spectrum of compound **29c** in DMSO-d_6.

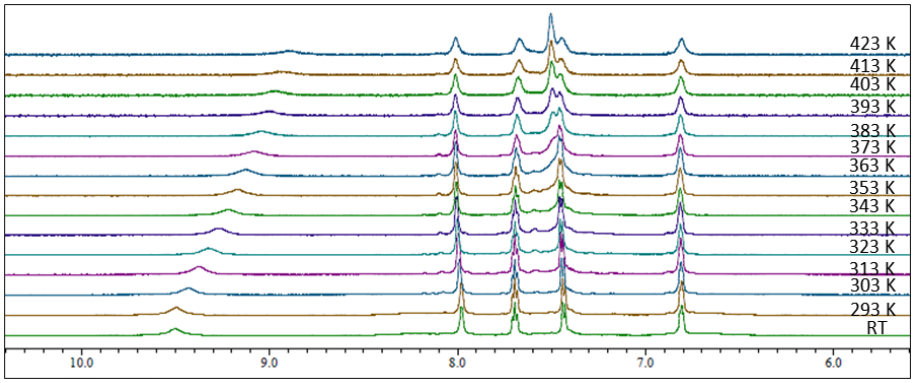

Figure 4.15 Variable-temperature ^{1}H NMR spectra of compound **29c** in DMSO-d_6.

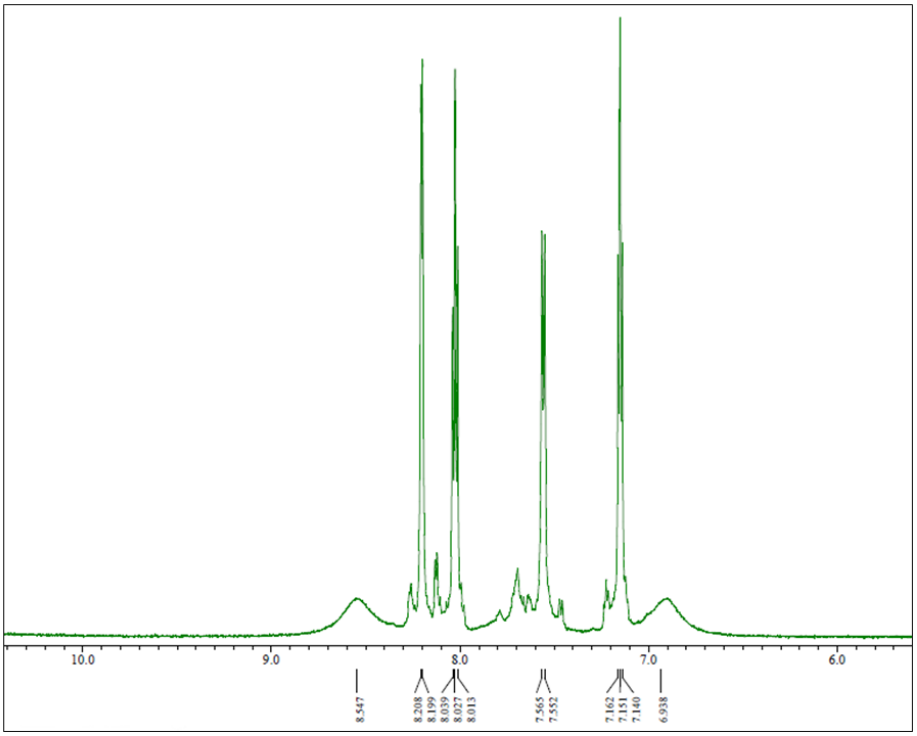

Figure 4.16 ^{1}H NMR spectrum of compound **29c** in AcOH-d_4.

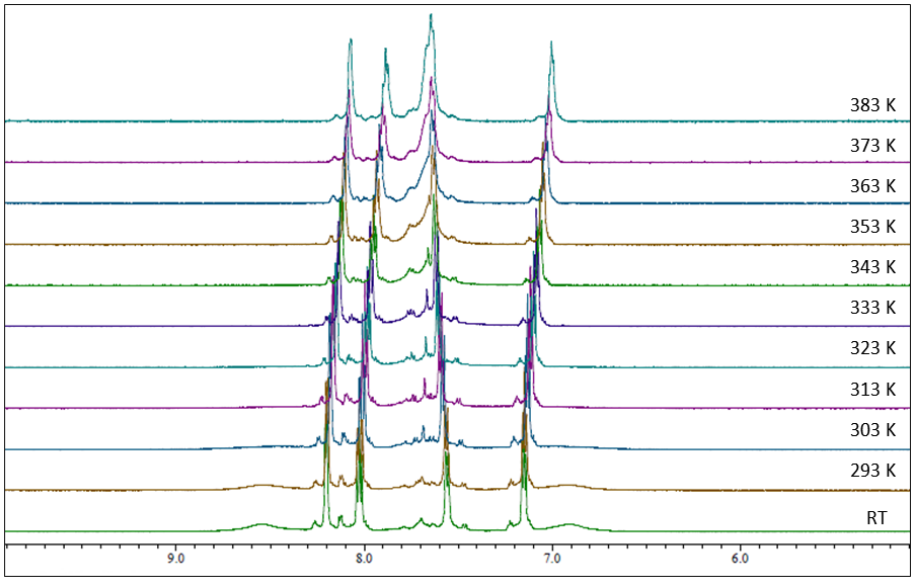

Figure 4.17 Variable-temperature ^{1}H NMR spectra of compound **29c** in AcOH-d_4.

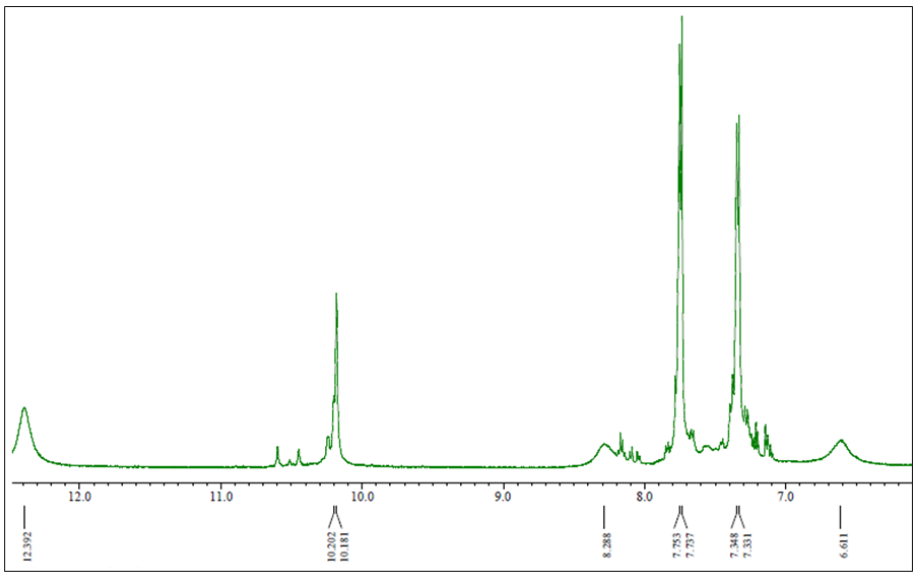

Figure 4.18 ^{1}H NMR spectrum of compound **29d** in DMSO-d_6.

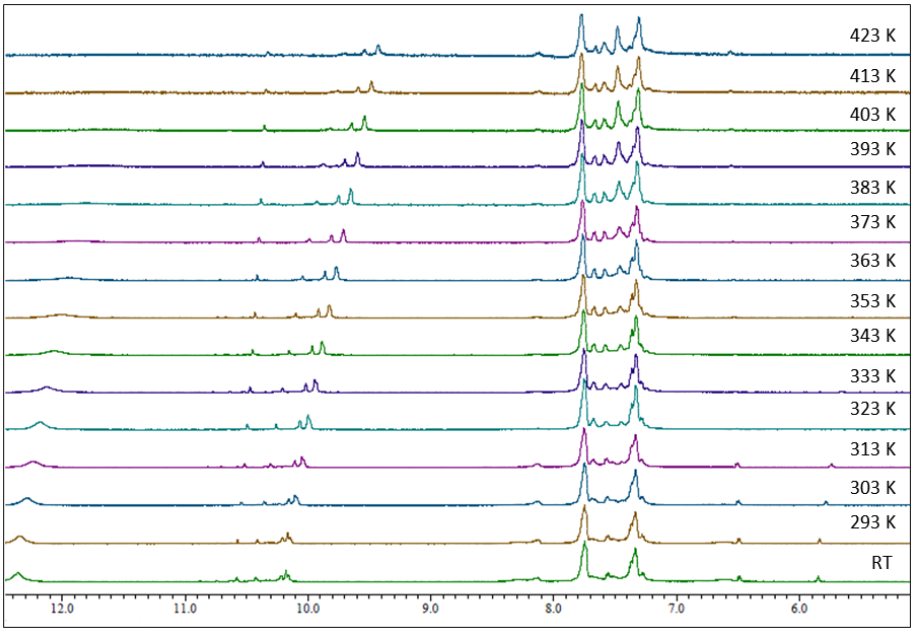

Figure 4.19 Variable-temperature ^{1}H NMR spectra of compound **29d** in DMSO-d_6.

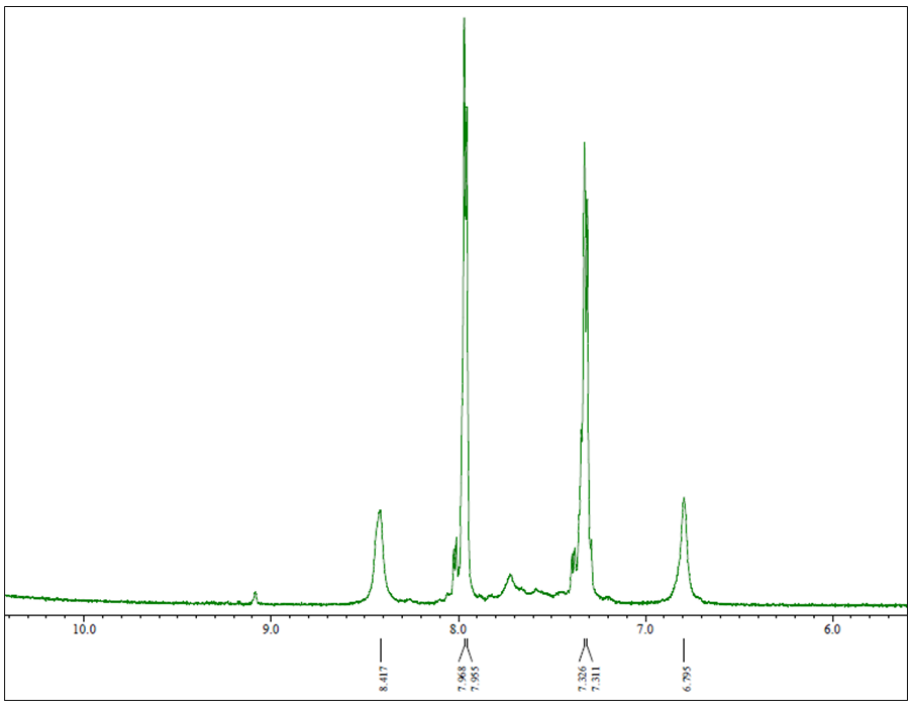

Figure 4.20 ^{1}H NMR spectrum of compound **29d** in AcOH-d_4.

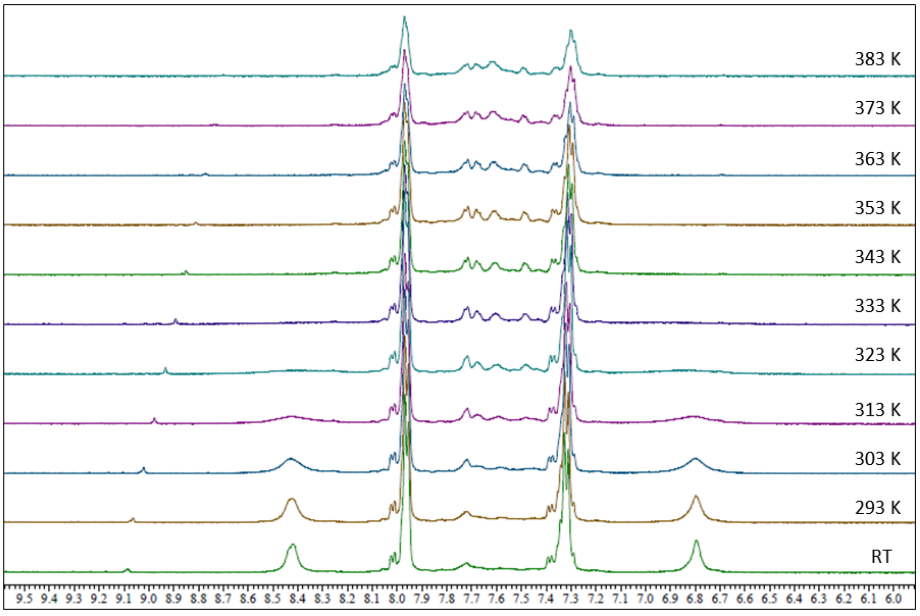

Figure 4.21 Variable-temperature ^{1}H NMR spectra of compound **29d** in AcOH-d_4.

The reason behind the presence of noisy peaks in ^{1}H NMR spectra was that the intensities of the broad signals were very weak; the increasing of their intensity leads to showing up of the noisy peaks which were on the baseline.

Bibliography

1. Mortensen, K. T.; Osberger, T. J.; King, T. A.; Sore, H. F.; Spring, D. R. *Chem. Rev.* **2019**, *119*, 10288−10317.
2. Pedersen, C. J. *J. Am. Chem. Soc.* **1967**, *89*, 2495−2496.
3. Pedersen, C. J. *J. Am. Chem. Soc.* **1967**, *89*, 7017−7036.
4. Lehn, J.-M. *Acc. Chem. Res.* **1978**, *11*, 49−57.
5. Cram, D. J. *Science* **1983**, *219*, 1177−1183.
6. Pedersen, C. J. *Angew. Chem., Int. Ed. Engl.* **1988**, *27*, 1021−1027.
7. Lehn, J.-M. *Angew. Chem., Int. Ed. Engl.* **1988**, *27*, 89−112.
8. Cram, D. J. *Angew. Chem., Int. Ed. Engl.* **1988**, *27*, 1009−1020.
9. Bell, T. W.; Firestone, A. *J. Am. Chem. Soc.* **1986**, *108*, 8109−8111.
10. Bell, T. W.; Firestone, A.; Guzzo, F.; Hu L.-Y. *J. Incl. Phenom.* **1987**, *5*, 149-152.
11. Bell, T. W.; Cragg, P. J.; Drew, M. G. B.; Firestone, A.; Kwok, A. D.-I.; Liu, J.; Ludwig, R. T.; Papoulis, A. T. *Pure Appl. Chem.* **1993**, *65*, 361−366.
12. Gutsche, C. D. *Calixarenes: An Introduction*. 2nd Ed, Royal Society of Chemistry: Cambridge, **2008**.
13. Freeman, W. A.; Mock, W. L.; Shih, N. Y. *J. Am. Chem. Soc.* **1981**, *103*, 7367−7368.
14. Kim, J.; Jung, I.-S.; Kim, S.-Y.; Lee, E.; Kang, J.-K.; Sakamoto, S.; Yamaguchi, K.; Kim, K. *J. Am. Chem. Soc.* **2000**, *122*, 540−541.
15. Lagona, J.; Mukhopadhyay, P.; Chakrabarti, S.; Isaacs, L. *Angew. Chem., Int. Ed.* **2005**, *44*, 4844−4870.
16. Svec, J.; Necas, M.; Sindelar, V. *Angew. Chem., Int. Ed.* **2010**, *49*, 2378−2381.
17. Ogoshi, T.; Kanai, S.; Fujinami, S.; Yamagishi, T.-A.; Nakamoto, Y. *J. Am. Chem. Soc.* **2008**, *130*, 5022−5023.

18. Xue, M.; Yang, Y.; Chi, X.; Zhang, Z.; Huang, F. *Acc. Chem. Res.* **2012**, *45*, 1294−1308.

19. Ogoshi, T.; Yamagishi, T.-A. *Eur. J. Org. Chem.* **2013**, *2013*, 2961−2975.

20. Cao, D.-R.; Meier, H. *Asian J. Org. Chem.* **2014**, *3*, 244−262.

21. Saenger, W. *Angew. Chem., Int. Ed. Engl.* **1980**, *19*, 344−362.

22. Uekama, K.; Hirayama, F.; Irie, T. *Chem. Rev.* **1998**, *5*, 2045−2076.

23. Zhao, D.; Moore, J. S. *Chem. Commun.* **2003**, 807−818.

24. Zhang, W.; Moore, J. S. *Angew. Chem., Int. Ed.* **2006**, *45*, 4416−4439.

25. Zang, L.; Che, Y.; Moore, J. S. *Acc. Chem. Res.* **2008**, *41*, 1596−1608.

26. Gross, D. E.; Zang, L.; Moore, J. S. *Pure Appl. Chem.* **2012**, *84*, 869−878.

27. Popov, I.; Chen, T.-H.; Belyakov, S.; Daugulis, O.; Wheeler, S. E.; Miljanić, O. Š. *Chem. Eur. J.* **2015**, *21*, 2750-2754.

28. Odell, B.; Reddington, M. V.; Slawin, A. M. Z.; Spencer, N.; Stoddart, J. F.; Williams, D. J. *Angew. Chem., Int. Ed. Engl.* **1988**, *27*, 1547−1550.

29. Barnes, J. C.; Juríček, M. ; Strutt, N. L.; Frasconi, M.; Sampath, S.; Giesener, M. A.; McGrier, P. L.; Bruns, C. J.; Stern, C. L.; Sarjeant, A. A.; Stoddart, J. F. *J. Am. Chem. Soc.* **2013**, *135*, 183−192.

30. Juríček, M.; Barnes, J. C.; Dale, E. J.; Liu, W.-G.; Strutt, N. L.; Bruns, C. J.; Vermeulen, N. A.; Ghooray, K. C.; Sarjeant, A. A.; Stern, C. L.; Botros, Y. Y.; Goddard III, W. A.; Stoddart, J. F. *J. Am. Chem. Soc.* **2013**, *135*, 12736−12746.

31. Young, R. M.; Dyar, S. M.; Barnes, J. C.; Juríček, M.; Stoddart, J. F.; Co, D. T.; Wasielewski, M. R. *J. Phys. Chem. A* **2013**, *117*, 12438−12448.

32. Barnes, J. C.; Juríček, M.; Vermeulen, N. A.; Dale, E. J.; Stoddart, J. F. *J. Org. Chem.* **2013**, *78*, 11962−11969.

33. Dyar, S. M.; Barnes, J. C.; Juríček, M.; Stoddart, J. F.; Co, D. T.; Young, R. M.; Wasielewski, M. R. *Angew. Chem., Int. Ed.* **2014**, *53*, 5371−5375.

34. Sun, J.; Frasconi, M.; Liu, Z.; Barnes, J. C.; Wang, Y.; Chen, D.; Stern, C. L.; Stoddart, J. F. *Chem. Commun.* **2015**, *51*, 1432−1435.

35. Roy, I.; Bobbala, S.; Zhou, J.; Nguyen, M. T.; Nalluri, S. K. M.; Wu, Y.; Ferris, D. P.; Scott, E. A.; Wasielewski, M. R.; Stoddart, J. F. *J. Am. Chem. Soc.* **2018**, *140*, 7206−7212.

36. Gong, H.-Y.; Rambo, B. M.; Karnas, E.; Lynch, V. M.; Sessler, J. L. *Nat. Chem.* **2010**, *2*, 406−409.

37. Rambo, B. M.; Gong, H.-Y.; Oh, M.; Sessler, J. L. *Acc. Chem. Res.* **2012**, *45*, 1390−1401.

38. Chi, X.; Cen, W.; Queenan, J. A.; Long, L.; Lynch, V. M.; Khashab, N. M.; Sessler, J. L. *J. Am. Chem. Soc.* **2019**, *141*, 6468−6472.

39. Lee, S.; Chen, C.-H.; Flood, A. H. *Nat. Chem.* **2013**, *5*, 704−710.

40. Singharoy, A.; Venkatakrishnan, B.; Liu, Y.; Mayne, C. G.; Lee, S.; Chen, C.-H.; Zlotnick, A.; Schulten, K.; Flood, A. H. *J. Am. Chem. Soc.* **2015**, *137*, 8810−8818.

41. Benson, C. R.; Fatila, E. M.; Lee, S.; Marzo, M. G.; Pink, M.; Mills, M. B.; Preuss, K. E.; Flood, A. H. *J. Am. Chem. Soc.* **2016**, *138*, 15057−15065.

42. Fatila, E. M.; Twum, E. B.; Sengupta, A.; Pink, M.; Karty, J. A.; Raghavachari, K.; Flood, A. H. *Angew. Chem., Int. Ed.* **2016**, *55*, 14057−14062.

43. Zhao, W.; Qiao, B.; Chen, C.-H., Flood, A. H. *Angew. Chem., Int. Ed.* **2017**, *56*, 13083−13087.

44. Fatila, E. M.; Pink, M.; Twum, E. B.; Karty, J. A.; Flood, A. H. *Chem. Sci.* **2018**, *9*, 2863−2872.

45. Zhao, W.; Qiao, B.; Tropp, J.; Pink, M.; Azoulay, J.; Flood, A. H. *J. Am. Chem. Soc.* **2019**, *141*, 4980−4989.

46. Chen, H.; Fan, J.; Hu, X.; Ma, J.; Wang, S.; Li, J.; Yu, Y.; Jia, X.; Li, C. *Chem. Sci.* **2015**, *6*, 197−202.

47. Ma, S.; Chen, H.; Li, J.; Jia, X.; Li, C. *Chem. Asian J.* **2016**, *11*, 3449−3453.

48. Dai, L.; Ding, Z.-J.; Cui, L.; Li, J.; Jia, X.; Li, C. *Chem. Commun.* **2017**, *53*, 12096−12099.

49. Guo, Q.-H.; Fu; Z.-D.; Zhao, L.; Wang, M.-X. *Angew. Chem., Int. Ed.* **2014**, *53*, 13548−13552.

50. Guo, Q.-H.; Zhao, L.; Wang, M.-X. *Angew. Chem., Int. Ed.* **2015**, *54*, 8386−8389.

51. Guo, Q.-H.; Zhao, L.; Wang, M.-X. *Chem. Eur. J.* **2016**, *22*, 6947−6955.

52. Jin, Y.; Zhang, A.; Huang, Y.; Zhang, W. *Chem. Commun.* **2010**, *46*, 8258−8260.

53. Fu, H.; Liu, Y.; Zeng, H. *Chem. Commun.* **2013**, *49*, 4127−4144.

54. Schneebeli, S. T.; Frasconi, M.; Liu, Z.; Wu, Y.; Gardner, D. M.; Strutt, N. L.; Cheng, C.; Carmieli, R.; Wasielewski, M. R.; Stoddart, J. F. *Angew. Chem., Int. Ed.* **2013**, *52*, 13100−13104.

55. Liu, Z.; Liu, G.; Wu, Y.; Cao, D.; Sun, J.; Schneebeli, S. T.; Nassar, M. S.; Mirkin, C. A.; Stoddart, J. F. *J. Am. Chem. Soc.* **2014**, *136*, 47, 16651−16660.

56. Chen, C.-F. *Chem. Commun.* **2011**, *47*, 1674−1688.

57. Xin, P.; Zhang, L.; Su, p.; Hou, J.-L.; Li, Z.-T. *Chem. Commun.* **2015**, *51*, 4819−4822.

58. Jia, F.; He, Z.; Yang, l.-P.; Pan, Z.-S.; Yi, M.; Jiang, R.-W.; Jiang, W. *Chem. Sci.* **2015**, *6*, 6731−6738.

59. Davis, F; Higson, S. *Macrocycles: Construction, Chemistry and Nanotechnology Applications*. 1st Ed, John Wiley & Sons: Hoboken, **2011**.

60. Stoddart, J. F. *Angew. Chem., Int. Ed.* **2017**, *56*, 11094−11125.

61. Sauvage, J.-P. *Angew. Chem., Int. Ed.* **2017**, *56*, 11080−11093.

62. Feringa, B. L. *Angew. Chem., Int. Ed.* **2017**, *56*, 11060−11078.

63. Yudin, A. *Chem. Sci.* **2015**, 6, 30−49.

64. Martí-Centelles, V.; Pandey, M. D.; Burguete, M. I.; Luis, S. V. *Chem. Rev.* **2015**, *115*, 8736−8834.

65. Ruggli, P. *Justus Liebigs Ann. Chem.* **1912**, *392*, 92−100.

66. Kotha, S.; Shirbhate, M.; Waghule, G. *Beilstein J. Org. Chem.* **2015**, *11*, 1274−1331.

67. Ghasemabadi, P.; Yao, T.; Bodwell, G. *Chem. Soc. Rev.* **2015**, *44*, 6494−6518.

68. Pellegrin, M. M. *Recl. Trav. Chim. Pays-Bas* **1899**, *18*, 457−465.

69. Brown, C. J.; Farthing, A. C. *Nature* **1949**, *164*, 915−916.

70. Cram, D. J.; Steinberg, H. *J. Am. Chem. Soc.* **1951**, *73*, 5691−5704.

71. Mitchell, R. H. *Heterocycles* **1978**, *11*, 563−586.

72. Bodwell, G. J.; Ernst, L.; Hopf, H. *Chem. Ber.* **1989**, *122*, 1013−1016.

73. Semmelhack, M. F.; Harrison, J. J.; Young, D. C.; Gutiérrez, A.; Rafii, S.; Clardy, J. *J. Am. Chem. Soc.* **1985**, *107*, 7508−7514.

74. Jenneskens, L. W.; de Kanter, F. J. J.; Kraakman, P. A.; Turkenburg, L. A. M.; Koolhaas, W. E.; de Wolf, W. H.; Bickelhaupt, F.; Tobe, Y.; Kakiuchi, K.; Odaira, Y. *J. Am. Chem. Soc.* **1985**, *107*, 3716−3717.

75. Cai, K.; Lipke, M. C.; Liu, Z.; Nelson, J.; Cheng, T.; Shi, Y.; Cheng, C.; Shen, D.; Han, J.-M.; Vemuri, S.; Feng, Y.; Stern, C. L.; Goddard III, W. A.; Wasielewski, M. R.; Stoddart, J. F. *Nat. Commun.* **2018**, *9*, 5275−5282.

76. Berville, M.; Karmazin, L.; Wytko, J. A.; Weiss, *J. Chem. Commun.* **2015**, *51*, 15772−15775.

77. Miyake, M.; Kirisawa, M.; Koga, K. *Tetrahedron Lett.* **1991**, *32*, 7295−7298.

78. Virués, C.; Velázquez, E. F.; Inoue, M. B.; Inoue, M. *J. Incl. Phenom. Macro.* **2004**, *48*, 141−146.

79. Virués, C.; Velázquez, E. F.; Navarro, R. E.; Inoue, M. *Supramolecular Chemistry* **2009**, *21*, 344−350.

80. Iwanaga, T.; Nakamoto, R.; Yasutake, M.; Takemura, H.; Sako, K.; Shinmyozu, T. *Angew. Chem., Int. Ed.* **2006**, *45*, 3643−3647.

81. Rajakumar, P.; Srisailas, M. *Tetrahedron* **2003**, *59*, 5373−5376.

82. Cram, D. J.; Wilkinson, D. I. *J. Am. Chem. Soc.* **1960**, *82*, 5721−5723.

83. Ohno, H.; Horita, H.; Otsubo, T.; Sakata, Y.; Misumi, S. ***Tetrahedron*** *Lett.* **1977**, *18*, 265−268.

84. Elschenbroich, C.; Möckel, R.; Zenneck, U. *Angew. Chem., Int. Ed. Engl.* **1978**, *17*, 531−532.

85. Laganis, E. D.; Finke, R. G.; Boekelheide, V. *Tetrahedron Lett.* **1980**, *21*, 4405−4408.

86. Laganis, E. D.; Finke, R. G.; Boekelheide, V. *Proc. Natl. Acad. Sci. USA* **1981**, *78*, 2657−2658.

87. Plitzko, K. D.; Boekelheide, V. *Organometallics* **1988**, *7*, 1573−1582.

88. Ashton, P. R.; Balzani, V.; Credi, A.; Kocian, O.; Pasini, D.; Prodi, L.; Spencer, N.; Stoddart, J. F.; Tolley, M. S.; Venturi, M.; White, A. J. P.; Williams, D. J. *Chem. Eur. J.* **1998**, *4*, 590−607.

89. Inoue, M. B.; Medrano, F.; Inoue, M.; Raitsimring, A.; Fernando, Q. *Inorg. Chem.* **1997**, *36*, 2335−2340.

90. Inoue, M. B.; Velázquez, E. F.; Medrano, F.; Ochoa, K. L.; Galvez, J. C.; Inoue, M.; Fernando, Q. *Inorg. Chem.* **1998**, *37*, 4070−4075.

91. Nikolaeva, Y. A.; Balueva, A. S.; Ignatéva, S. N.; Musina, E. I.; Karasik, A. A. *Russ. Chem. Bull., Int. Ed.* **2016**, *65*, 1319−1324.

92. Hopf, H. *Angew. Chem., Int. Ed.* **2008**, *47*, 9808−9812.

93. Morisaki, Y.; Chujo, Y. *Angew. Chem., Int. Ed.* **2006**, *45*, 6430− 6437.

94. Morisaki, Y.; Chujo, Y. *Prog. Polym. Sci.* **2008**, *33*, 346−364.

95. Morisaki, Y.; Chujo, Y. *Polym. Chem.* **2011**, *2*, 1249−1257.

96. Gorham, W. F. *J. Polym. Sci. Part A-1* **1966**, *4*, 3027−3039.

97. Nandivada, H.; Chen, H.Y.; Bondarenko, L.; Lahann, J. *Angew. Chem., Int. Ed.* **2006**, *45*, 3360−3363.

98. Mizogami, S.; Yoshimura, S. *J. Chem. Soc., Chem. Commun.* **1985**, 427−428.

99. Mizogami, S.; Yoshimura, S. *J. Chem. Soc., Chem. Commun.* **1985**, 1736−1738.

100. Morisaki, Y.; Chujo, Y. *Macromolecules* **2002**, *35*, 587−589.

101. Morisaki, Y.; Ishida, T.; Chujo, Y. *Macromolecules* **2002**, *35*, 7872−7877.

102. Jagtap, S. P.; Collard, D. M. *J. Am. Chem. Soc.* **2010**, *132*, 12208−12209.

103. Morisaki, Y.; Gon, M.; Tsuji, Y.; Kajiwara, Y.; Chujo, Y. *Macromol. Chem. Phys.* **2012**, *213*, 572−579.

104. Morisaki, Y.; Gon, M.; Chujo, Y. *J. Polym. Sci., Pol. Chem.* **2013**, *51*, 2311−2316.

105. Iwatsuki, S.; Itoh, T.; Kubo, M.; Okuno, H. *Polym. Bull.* **1994**, *32*, 27−34.

106. Nandajan, P. C.; Neelakandan, P. P.; Ramaiah, D. *RSC Adv.* **2013**, *3*, 5624−5630.

107. Venkatesan, N.; Singh, V.; Rajakumar, P.; Mishra, A. K. *RSC Adv.* **2014**, *4*, 53484−53489.

108. Yu, C.-T.; Hsu, C.-C. *Polymer* **2018**, *137*, 30−37.

109. Elacqua, E.; Bučar, D.-K.; Skvortsova, Y.; Baltrusaitis, J.; Geng, M. L.; MacGillivray, L. R. *Org. Lett.* **2009**, *11*, 5106−5109. **109**

110. Morisaki, Y.; Gon, M.; Sasamori, T.; Tokitoh, N.; Chujo, Y. *J. Am. Chem. Soc.* **2014**, *136*, 3350−3353.

111. Gon, M.; Morisaki, Y.; Chujo, Y. *Eur. J. Org. Chem.* **2015**, *2015*, 7756−7762.

112. Lin, R.-B.; He, Y.; Li, P.; Wang, H.; Zhou, W.; Chen, B. *Chem. Soc. Rev.* **2019**, *48*, 1362−1389.

113. Zhou, H.-C.; Long, J. R.; Yaghi, O. M. *Chem. Rev.* **2012**, *112*, 673−674.

114. Shimizu, L.S.; Hughes, A. D.; Smith, M. D.; Davis, M. J.; Zhang, B. P.; zur Loye, H.-C.; Shimizu, K. D. *J. Am. Chem. Soc.* **2003**, *125*, 14972−14973.

115. Dewal, M. B.; Lufaso, M. W.; Hughes, A. D.; Samuel, S. A.; Pellechia, P.; Shimizu, L. S. *Chem. Mater.* **2006**, *18*, 4855−4864.

116. Hisaki, I.; Nakagawa, S.; Ikenaka, N.; Imamura, Y.; Katouda, M.; Tashiro, M.; Tsuchida, H.; Ogoshi, T.; Sato, H.; Tohnai, N.; Miyata, M. *J. Am. Chem. Soc.* **2016**, *138*, 6617−6628.

117. Hisaki, I.; Nakagawa, S.; Tohnai, N.; Miyata, M. *Angew. Chem., Int. Ed.* **2015**, *54*, 3008−3012.

118. Chen, T.-H.; Popov, I.; Chuang, Y.-C.; Chen, Y.-S.; Miljanić, O. Š. *Chem. Commun.* **2015**, *51*, 6340−6342.

119. Chen, T.-H.; Popov, I.; Miljanić, O. Š. *Chem. Eur. J.* **2017**, *23*, 286−290.

120. Alrayyani, M.; Miljanić, O. Š. *Chem. Commun.* **2018**, *54*, 11989–11997.

121. Nagendrappa, G. *Resonance* **2008**, *13*, 355–368.

122. Wöhler, F.; Liebig, J. *Ann. Pharm.* **1832**, *3*, 249–282.

123. Esteban, S. *J. Chem. Educ.* **2008**, *85*, 1201–1203.

124. Zinin, N. *Ann. Pharm.* **1839**, *31*, 329–332.

125. Zinin, N. *Ann. Pharm.* **1840**, *34*, 186–192.

126. Lapworth, A. *J. Chem. Soc., Trans.* **1903**, *83*, 995.

127. Morton, A; Stevens, J. *J. Am. Chem. Soc.* **1930**, *52*, 2031–2037.

128. Schowen, R. L.; Kuebrich, J. P.; Wang, M.-S.; Lupes, M. E. *J. Am. Chem. Soc.* **1971**, *93*, 1214–1220.

129. Ide, W. S.; Buck, J. S. *Org. React.* **1948**, *4*, 269–304.

130. Safari, J.; Arani, N. M.; Isfahani, A. R. *Asian J. Chem.* **2011**, *23*, 495–498.

131. Linghu, X.; Johnson, J. S. *Angew. Chem., Int. Ed.* **2004**, *42*, 2534–2536.

132. Linghu, X.; Potnick, J. S.; Johnson, J. S. *J. Am. Chem. Soc.* **2004**, *126*, 3070–3071.

133. Arnold, R.; Fuson, R. *J. Am. Chem. Soc.* **1936**, *58*, 1295–1296.

134. Menon, R. S.; Biju, A. T.; Nair, V. *Beilstein J. Org. Chem.* **2016**, *12*, 444–461.

135. Ugai, T.; Tanaka, R.; Dokawa, T. *J. Pharm. Soc. Jpn.* **1943**, *63*, 296–300.

136. Breslow, R. *J. Am. Chem. Soc.* **1958**, *80*, 3719–3726.

137. Arduengo, III, A. J.; Harlow, R. L.; Kline, M. *J. Am. Chem. Soc.* **1991**, *113*, 361–363.

138. Bourissou, D.; Guerret, O.; Gabbaï, F. P.; Bertrand, G. *Chem. Rev.* **2000**, *100*, 39–92.

139. Sheehan, J. C.; Hunneman, D. H. *J. Am. Chem. Soc.* **1966**, *88*, 3666–3667.

140. Sheehan, J. C.; Hara, T. *J. Org. Chem.* **1974**, *39*, 1196–1199.

141. Knight, R. L.; Leeper, F. J. *Tetrahedron Lett.* **1997**, *38*, 3611–3614.

142. Gerhards, A. U.; Leeper, F. J. *Tetrahedron Lett.* **1997**, *38*, 3615–3618.

143. Waichiro, T.; Yoshiharu, T.; Yumihiko, Y. *Bull. Chem. Soc. Jpn.* **1980**, *53*, 478–480.

144. Enders, D.; Breuer, K.; Teles, J. H. *Helv. Chim. Acta* **1996**, *79*, 1217–1221.

145. Knight, R. L.; Leeper, F. J. *J. Chem. Soc., Perkin Trans. 1* **1998**, 1891–1894.

146. Enders, D; Kallfass, U. *Angew. Chem., Int. Ed.* **2002**, *41*, 1743–1745.

147. Enders, D.; Balensiefer, T. *Acc. Chem. Res.* **2004**, *37*, 534–541.

148. Baragwanath, L.; Rose, C. A.; Zeitlerand, K.; Connon, S. J. *J. Org. Chem.* **2009**, *74*, 9214–9217.

149. Tachibana, Y.; Kihara, N.; Takata, T. *J. Am. Chem. Soc.* **2004**, *126*, 3438–3439.

150. Ma, Y.; Wei, S.; Wu, J.; Yang, F.; Liu, B.; Lan, J.; Yang, S.; You, J. *Adv. Synth. Catal.* **2008**, *350*, 2645–2651.

151. O'Toole, S. E.; Connon, S. J. *Org. Biomol. Chem.* **2009**, *7*, 3584–3593.

152. Rafiński, Z.; Kozakiewicz, A.; Rafińska, K. *Tetrahedron* **2014**, *70*, 5739–5745.

153. Yan, J.; Sun, R.; Shi, K.; Li, K.; Yang, L.; Zhong, G. *J. Org. Chem.* **2018**, *83*, 7547–7552.

154. Inoue, K.; Nakagawa, N.; Tanigaki, T. *Polym. J.* **1976**, *8*, 254–259.

155. Lewis, F. D.; Lauterbach, R. T.; Heine, H. G.; Hartmann, W.; Rudolph, H. *J. Am. Chem. Soc.* **1975**, *97*, 1519–1525.

156. Masahiro, M.; Seigo, Y.; Noboru, H.; Motohiko, K.; Hiroshi, F. *Bull. Chem. Soc. Jpn.* **1992**, *65*, 1679–1684.

157. Shrestha, N. K.; Yagi, E. J.; Takatori, Y.; Kawai, A.; Kajii, Y.; Shibuya, K.; Obi, K. *J. Photochem. Photobiol. A Chem.* **1998**, *116*, 179–185.

158. Esen, D.; Arsu, N.; Da Silva, J.; Jockusch, S.; Turro, N. *J. Polym. Sci., Part A: Polym. Chem.* **2013**, *51*, 1865–1871.

159. Deka, S. R.; Kakati, D. K. *J. Appl. Polym. Sci.* **2009**, *111*, 3089–3093.

160. Kizilcan, N.; Akar, A. *J. Appl. Polym. Si.* **2002**, *85*, 500–508.

161. Kaynak, N.; Önen, A.; Karahasanoğlu, M. *J. Mater. Sci.* **2018**, *53*, 9598–9610.

162. Uyar, Z.; Durgun, M.; Yavuz, M.; Abaci, M.; Arslan, U.; Degirmenci, M. *Polymer* **2017**, *123*, 153–168.

163. Timpe, H.; Rajendran, A. *Eur. Polym. J.* **1991**, *27*, 77–83.

164. Jones, J. I.; Tinker, P. B. *J. Chem. Soc.* **1955**, 1286–1287.

165. Oppenheimer, H. *Ber. Dtsch. Chem. Ges.* **1886**, *19*, 1814.

166. Kuriakose, S.; Pillai, V. *Eur. Polym. J.* **1994**, *30*, 881–884.

167. Angiolini, L.; Carlini, C.; Tramontini, M; Altomare, A. *Polymer* **1990**, *31*, 212–219.

168. Zhao, Y.; Wang, T.; Zhang, L.; Cui, Y.; Han, B. *ACS Appl. Mater. Interfaces* **2012**, *4*, 6975–6981.

169. Itakura, T.; Torigoe, K.; Esumi, K. *Langmuir* **1995**, *11*, 4129–4134.

170. Cui, F.; Dou, L.; Yang, Q.; Yu, Y.; Niu, Z.; Sun, Y.; Liu, H.; Dehestani, A.; Schierle-Arndt, K.; Yang, P. *J. Am. Chem. Soc.* **2017**, *139*, 3027–3032.

171. Niu, Z.; Cui, F.; Kuttner, E.; Xie, C.; Chen, H.; Sun, Y.; Dehestani, A.; Schierle-Arndt, K.; Yang, P. *Nano Lett.* **2018**, *18*, 5329–5334.

172. Ghaedi, M.; Asadpour, E.; Vafaie, A. *Spectrochim. Acta, Part A* **2006**, *63*, 182–188.

173. Attia, A. S.; El-Mashtouly, S. F.; El-Shahat, M. F. *Synth. React. Inorg. Met.-Org. Chem.* **2002**, *32*, 509–527.

174. Koumousi, E. S.; Manos, M. J.; Lampropoulos, C.; Tasiopoulos, A. J., Wernsdorfer, W.; Christou, G.; Stamatatos, T. C. *Inorg. Chem.* **2010**, *49*, 3077–3079.

175. Joshi, S. R.; Habib, S. I. *J. Chem. Pharm. Res.* **2014**, *6*, 1085–1088.

176. Narang, K. K.; Lal, R. A.; Thapa, R. K.; Gautam, V. K. *Transition Met. Chem.* **1988**, *13*, 212–216.

177. Zakir, H. M., Jesmin, M.; Ali, S. M. M. *Asian J. Med. Pharm. Res.* **2016**, *6*, 32–40.

178. El-Shahawi, M. S.; Al-Jahdali, M. S.; Bashammakh, A. S.; Al-Sibaai, A. A.; Nassef, H. M. *Spectrochim. Acta, Part A* **2013**, *113*, 459–465.

179. Aliyu, H. N.; Abdullahi, H. J. *Bayero J. Pure Appl. Sci.* **2009**, *2*, 110–112.

180. Dahikar, P.; Kedar, R. *IJSER* **2013**, *4*, 508–511.

181. Aliyu, H. N.; Mohammed, A. S. *Bayero J. Pure Appl. Sci.* **2009**, *2*, 132–134.

182. Al-Saadawy, N. H.; Alyassin, F. F.; Faraj, H. R. *Global J. Pure Appl. Chem. Res.* **2016**, *4*, 13–20.

183. Hu, H.; Gao, H.; Song, K.; Liu, F.; Long, J.; Zhang, L.; Zhu, F.; Wu, Q. *Polymer* **2008**, *49*, 4552–4558.

184. Rahaman, R.; Paria, S.; Paine, T. K. *Inorg. Chem.* **2015**, *54*, 10576–10586.

185. El-ajaily, M. M.; Maihub, A. A. *Int. J. ChemTechRes.* **2010**, *2*, 1579–1580.

186. Itoh, S.; Kondo, T.; Komatsu, M.; Ohshiro, Y.; Li, C.; Kanehisa, N.; Kai, Y.; Fukuzumi, S. *J. Am. Chem. Soc.* **1995**, *117*, 4714–4715.

187. Ji, Q.; Do, L. H.; Miljanić, O. Š. *Synlett* **2015**, *26*, 1625–1627.

188. Ji, Q.; Le, H. T. M.; Wang, X.; Chen, Y.-S.; Makarenko, T.; Jacobson, A. J.; Miljanić, O. Š. *Chem. Eur. J.* **2015**, *21*, 17205–17209.

189. McHale, C. M.; Stegemoller, C. R.; Hashim, M. I.; Wang, X.; Miljanić, O. Š. *Cryst. Growth Des.* **2019**, *19*, 562–567.

190. McNaught, A. D.; Wilkinson, A. *Compendium of Chemical Terminology (IUPAC Chemical Data)*. 2nd Ed, Blackwell Scientific Publications: Oxford, **1997**.

191. Schlesinger, H. I.; Sanderson, R. T.; Burg, A. B. *J. Am. Chem. Soc.* **1940**, *62*, 3421–3425.

192. Schlesinger, H. I.; Brown, H. C.; Schaeffer, G. W. *J. Am. Chem. Soc.* **1943**, *65*, 1786–1787.

193. Downs, A. J.; Thomas, P. D. P. *J. Chem. Soc., Chem. Commun.* **1976**, 825–827.

194. Burg, A. B.; Schlesinger, H. I. *J. Am. Chem. Soc.* **1940**, *62*, 3425–3429.

195. Schlesinger, H. I.; Brown, H. C. *J. Am. Chem. Soc.* **1940**, *62*, 3429–3435.

196. Nystrom, R. F.; Chaikin, S. W.; Brown, W. G. *J. Am. Chem. Soc.* **1949**, *71*, 3245–3246.

197. Meschino, J. A.; Bond, C. H. *J. Org. Chem.* **1963**, *28*, 3129–3134.

198. Brown, M. S.; Rapoport, H. *J. Org. Chem.* **1963**, *28*, 3261–3263.

199. Finholt, A. E.; Bond Jr., A. C.; Schlesinger, H. I. *J. Am. Chem. Soc.* **1947**, *69*, 1199–1203.

200. Chaikin, S. W.; Brown, W. G. *J. Am. Chem. Soc.* **1949**, *71*, 122–125.

201. Wigfield, D. C. *Tetrahedron* **1979**, *35*, 449–462.

202. Mengel, A.; Reiser, O. *Chem. Rev.* **1999**, *99*, 1191–1224.

203. Okano, K. *Tetrahedron* **2011**, *67*, 2483–2512.

204. Junzo, Y.; Masaaki, M.; Akihiro, S.; Shoichi, O.; Misao, K.; Kunitoshi, S.; Harukichi, H. *Chem. Lett.* **1982**, 1409–1412.

205. Crosby, J.; Fakley, M. E.; Gemmell, C.; Martin, K.; Quick, A.; Slawin, A. M. Z.; Shahriari-Zavareh, H., Stoddart, J. F.; Williams, D. J. *Tetrahedron Lett.* **1989**, *30*, 3849–3852.

206. Pennington, W. T.; Chakraborty, S.; Paul, I. C.; Curtin, D. Y. *J. Am. Chem. Soc.* **1988**, *110*, 6498–6504.

207. Superchi, S.; Donnoli, M. I.; Proni, G.; Spada, G. P.; Rosini, C. *J. Org. Chem.* **1999**, *64*, 4762–4767.

208. Percino, M. J., Chapela, V. M.; Ortega-Martinez, R. *Des. Monomers Polym.* **2004**, *7*, 435–444.

209. Nakata, T.; Tanaka, T.; Oishi, T. *Tetrahedron Lett.* **1983**, *24*, 2653–2656.

210. Yamada, M.; Horie, T.; Kawai, M.; Yamamura, H.; Araki, S. *Tetrahedron* **1997**, *53*, 15685–15690.

211. Eriks, K.; Hayden, T. D.; Yang, S. H.; Chan, I. Y. *J. Am. Chem. Soc.* **1983**, *105*, 3940–3942.

212. Laurent, A. *Ann. Chim.***1835**, *59*, 397–423.

213. Wisniak, J. *Educ. Quím.* **2009**, *20*, 166–175.

214. Corson, B. B.; McAllister, R. W. *J. Am. Chem. Soc.* **1929**, *51*, 2822–2825.

215. Weiss, M.; Appel, M. *J. Am. Chem. Soc.* **1948**, *70*, 3666–3667.

216. McKillop, A.; Swann, B. P.; Ford, M. E.; Taylor, E. C. *J. Am. Chem. Soc.* **1973**, *95*, 3641–3645.

217. Ranganathan, S.; Ranganathan, D.; Ramachandran, P. V. *Tetrahedron* **1984**, *40*, 3145–3151.

218. Masao, H.; Masaki, O.; Takashi, M. *Bull. Chem. Soc. Jpn.* **1991**, *64*, 1046–1047.

219. Tymonko, S. A.; Nattier, B. A.; Mohan, R. S. *Tetrahedron Lett.* **1999**, *40*, 7657–7659.

220. Namboodiri, V. V.; Polshettiwar, V.; Varma, R. S. *Tetrahedron Lett.* **2007**, *48*, 8839–8842.

221. Shei, C.-T.; Chien, H.-L.; Sung, K. *Synlett* **2008**, 1021–1026.

222. Joo, C.; Kang, S.; Kim, S. M.; Han, H.; Yang, J. W. *Tetrahedron Lett.* **2010**, *51*, 6006–6007.

223. Kirihara, M.; Ochiai, Y.; Takizawa, S.; Takahata, H.; Nemoto, H. *Chem. Commun.* **1999**, 1387–1388.

224. Choudary, B. M.; Kantam, M. L.; Rahman, A.; Reddy, Ch. V.; Rao, K. K. *Angew. Chem., Int. Ed.* **2001**, *40*, 763–766.

225. Alamsetti, S. K.; Muthupandi, P.; Sekar, G. *Chem. Eur. J.* **2009**, *15*, 5424–5427.

226. Qin, C.; Chen, J.; Wu, H.; Cheng, J.; Zhang, Q.; Zuo, B.; Su, W.; Ding, J. *Tetrahedron Lett.* **2008**, *49*, 1884–1888.

227. Zhang, W.; Liu, M.; Wu, H.; Ding, J.; Cheng, J. *Tetrahedron Lett.* **2008**, *49*, 5336–5338.

228. Zhang, Q.; Xu, C.-M.; Chen, J.-X.; Xu, X.-L.; Ding, J.-C.; Wu, H.-Y. *Appl. Organometal. Chem.* **2009**, *23*, 524–526.

229. Balalaie, S.; Golizeh, M.; Hashtroudi, M. S. *Green Chem.* **2000**, *2*, 277–278.

230. Wadkins, R. M.; Hyatt, J. L.; Wei, X.; Yoon, K. J. P.; Wierdl, M.; Edwards, C. C.; Morton, C. L.; Obenauer, J. C.; Damodaran, K.; Beroza, P.; Danks, M. K.; Potter, P. M. *J. Med. Chem.* **2005**, 48, 2906–2915.

231. Li, J. J.; Norton, M. B.;Reinhard, E. J.; Anderson, G. D.; Gregory, S. A.; Isakson, P. C.; Koboldt, C. M.; Masferrer, J. L.; Perkins, W. E.; Seibert, K.; Zhang, Y.; Zweifel, B. S.; Reitz, D. B. *J. Med. Chem.* **1996**, *39*, 1846–1856.

232. Campillo, N.; García, C.; Goya, P.; Páez, J. A.; Carrasco, E.; Grau, M. *J. Med. Chem.* **1999**, *42*, 1698–1704.

233. Muccioli, G. G.; Martin, D.; Scriba, G. K. E.; Poppitz, W.; Poupaert, J. H.; Wouters, J.; Lambert, D. M. *J. Med. Chem.* **2005**, *48*, 2509–2517.

234. Singh, D. P.; Kumar, R.; Singh, J. *Eur. J. Med. Chem.* **2009**, *44*, 1731–1736.

235. Friedman, M. *J. Org. Chem.* **1965**, *30*, 859–863.

236. Kadish, K. M.; Van Caemelbecke, E.; D'Souza, F.; Lin, M.; Nurco, D. J.; Medforth, C. J.; Forsyth, T. P.; Krattinger, B.; Smith, K. M.; Fukuzumi, S.; Nakanishi, I.; Shelnutt, J. A. *Inorg. Chem.* **1999**, *38*, 2188–2198.

237. Du, G.; Mirafzal, G. A.; Woo, L. K. *Organometallics* **2004**, *23*, 4230–4235.

238. Yu, D. H. S.; Torkelson, J. M. *Macromolecules* **1988**, *21*, 852–853.

239. Catalina, F.; Peinado, C.; Blanco, M.; Alonso, A.; Allen, N. S. *J. Photochem. Photobiol. A: Chem.* **2000**, *131*, 141–146.

240. Roy, P. K.; Surekha, P.; Rajagopal, C.; Chatterjee, S. N.; Choudhary, V. *Polym. Degrad. Stab.* **2005**, *90*, 577–585.

241. Szablan, Z.; Lovestead, T. M.; Davis, T. P.; Stenzel, M. H.; Barner-Kowollik, C. *Macromolecules* **2007**, *40*, 26–39.

242. Alrayyani, M.; Wang, X.; Miljanić, O. Š. *Chem. Eur. J.* **2017**, *23*, 16476–16478.

243. Ludwig, R. *Angew. Chem., Int. Ed.* **2001**, *40*, 1808–1827.

244. Do, H.; Besley, N. A. *J. Phys. Chem. A* **2013**, *117*, 5385–5391.

245. Infantes, L.; Motherwell, S. *CrystEngComm* **2002**, *4*, 454–461.

246. Yoshizawa, M.; Kusukawa, T.; Kawano, M.; Ohhara, T.; Tanaka, I.; Kurihara, K.; Niimura, N.; Fujita, M. *J. Am. Chem. Soc.* **2005**, *127*, 2798–2799.

247. Walrafen, G. E. *J. Chem. Phys.* **1964**, *40*, 3249–3256.

248. Walrafen, G. E. *J. Chem. Phys.* **1967**, *47*, 114–126.

249. Monosmith, W. B.; Walrafen, G. E. *J. Chem. Phys.* **1984**, *81*, 669–674.

250. Walrafen, G. E.; Hokmabadi, M. S.; Yang, W.-H. *J. Chem. Phys.* **1986**, *85*, 6964–6969.

251. Walrafen, G. E.; Fisher, M. R.; Hokmabadi, M. S.; Yang, W.-H. *J. Chem. Phys.* **1986**, *85*, 6970–6982.

252. Walrafen, G. E.; Yang, W.-H.; Chu, Y. C.; Hokmabadi, M. S. *J. Phys. Chem.* **1996**, *100*, 1381–1391.

253. Wang, Q.-Q.; Day, V. W.; Bowman-James, K. *Angew. Chem., Int. Ed.* **2012**, *51*, 2119–2123.

254. Wang, Q.-Q.; Day, V. W.; Bowman-James, K. *J. Am. Chem. Soc.* **2013**, *135*, 392–399.

255. Yamasaki, K. *J. Phys. Soc. Jpn.* **1962**, *17*, 1262–1267.

256. Nyburg, S. C. *J. Chem. Phys.* **1964**, *40*, 2493–2501.

257. Hillier, I. H.; Rice, S. A. *J. Chem. Phys.* **1967**, *46*, 3881–3889.

258. Ramasubbu, N.; Parthasarathy, R.; Murray-Rust, P. *J. Am. Chem. Soc.* **1986**, *108*, 4308–4314.

259. Desiraju, G. R.; Parthasarathy, R. *J. Am. Chem. Soc.* **1989**, *111*, 8725–8726.

260. Awwadi, F. F.; Willett, R. D.; Peterson, K. A.; Twamley, B. *Chem. Eur. J.* **2006**, *12*, 8952–8960.

261. Bui, T. T. T.; Dahaoui, S.; Lecomte, C.; Desiraju, G. R.; Espinosa, E. *Angew. Chem., Int. Ed.* **2009**, *48*, 3838–3841.

262. Sarma, J. A. R. P.; Desiraju, G. R. *Acc. Chem. Res.* **1986**, *19*, 222–228.

263. Capdevila-Cortada, M.; Castellóa, J.; Novoa, J. J. *CrystEngComm* **2014**, *16*, 8232–8242.

264. Capdevila-Cortada, M.; Novoa, J. J. *CrystEngComm* **2015**, *17*, 3354–3365.

265. Sovers, O. J.; Kern, C. W.; Pitzer, R. M.; Karplus, M. *J. Chem. Phys.* **1968**, *49*, 2592–2599.

266. Christiansen, P. A.; Palke, W. E. *Chem. Phys. Lett.* **1975**, *31*, 462–466.

267. Brunck, T. K.; Weinhold, F. *J. Am. Chem. Soc.* **1979**, *101*, 1700–1709.

268. Barbour, L. J. *Nat. Chem.* **2015**, **7**, 97–99.

269. Kitaigorodskii, A. I. *Acta Cryst.* **1965**, *18*, 585–590.

270. Batsanov, S. S. *Inorg. Mater.* **2001**, *37*, 871–885.

271. Shannon, R. D. *Acta Cryst.* **1976**, *A32*, 751–761.

272. Karpusas, M.; Baase, W. A.; Matsumura, M.; Matthews, B.,W. *Proc. Natl. Acad. Sci. USA* **1989**, *86*, 8237–8241.

273. Morii, H.; Uedaira, H.; Ogata, K.; Ishii, S.; Sarai, A. *J. Mol. Biol.* **1999**, *292*, 909–920.

274. Hahn, S.; Koser, S.; Hodecker, M.; Seete, P.; Rominger, F.; Miljanić, O. Š.; Dreuw, A.; Bunz, U. H. F. *Chem. Eur. J.* **2018**, *24*, 6968–6974.

275. Eddaoudi, M.; Kim, J.; Wachter, J. B.; Chae, H. K.; O'Keeffe, M.; Yaghi, O. M. *J. Am. Chem. Soc.* **2001**, *123*, 4368–4369.

276. Li, H.; Eddaoudi, M.; O'Keeffe, M.; Yaghi, O. M. *Nature* **1999**, *402*, 276–279.

277. Karl, N. *Crystals, Growth, Properties and Applications*. Freyhardt, H. C. Ed., Springer: Berlin, **1980**, Vol. 4.

278. Gribble, G. W.; Perni, R. B.; Onan, K. D. *J. Org. Chem.* **1985**, *50*, 16, 2934–2939.

279. Clar, E.; John. F. *Ber. Dtsch. Chem. Ges. B* **1930**, *63*, 2967–2977.

280. Santato, C.; Capelli, R.; Loi, M. A.; Murgia, M.; Cicoira, F.; Roy, V. A. L.; Stallinga, P.; Zamboni, R.; Rost, C.; Karg, S. F.; Muccini, M. *Synth. Met.* **2004**, *146*, 329–334.

281. Takahashi, T.; Takenobu, T.; Takeya, J.; Iwasa, Y. *Adv. Funct. Mater.* **2007**, *17*, 1623–1628.

282. Dimitrakopoulos, C.D.; Malenfant, P. R. L. *Adv. Mater.* **2002**, *14*, 99–117.

283. Murphy, A. R.; Fréchet, J. M. J. *Chem. Rev.* **2007**, *107*, 1066–1096.

284. Anthony, J. E. *Angew. Chem., Int. Ed.* **2008**, *47*, 452–483.

285. Sirringhaus, H. *Adv. Mater.* **2014**, *26*, 1319–1335.

286. Roncali, J.; Leriche, P.; Blanchard, P. *Adv. Mater.* **2014**, *26*, 3821–3838.

287. Xiang, D.; Wang, X.; Jia, C.; Lee, T.; Guo, X. *Chem. Rev.* **2016**, 116, 4318–4440.

288. Jancarik, A.; Levet, G.; Gourdon, A. *Chem. Eur. J.* **2019**, *25*, 2366–2374.

289. Marschalk, C. *Bull. Soc. Chim.* **1939**, *6*, 1112–1121.

290. Clar, E. *Ber. Dtsch. Chem. Ges. B* **1939**, *72*, 1817–1821.

291. Clar, E. *Chem. Ber.* **1942**, *75*, 1330–1338.

292. Marschalk, C. *Bull. Soc. Chim.* **1943**, *10*, 511.

293. Bailey, W. J.; Liao, C.-W. *J. Am. Chem. Soc.* **1955**, *77*, 992–993.

294. Boggiano, B.; Clar, E. *J. Chem. Soc.* **1957**, 2681–2689.

295. Mondal, R.; Shah, B. K.; Neckers, D. C. *J. Am. Chem. Soc.* **2006**, *128*, 9612–9613.

296. Einholz, R.; Fang, T.; Berger, R.; Grüninger, P.; Früh, A.; Chassé, T.; Fink, R. F.; Bettinger, H. F. *J. Am. Chem. Soc.* **2017**, *139*, 4435–4442.

297. Anthony, J. E.; Brooks, J. S.; Eaton, D. L.; Parkin, S. R. *J. Am. Chem. Soc.* **2001**, *123*, 9482–9483.

298. Payne, M. M.; Parkin, S. R.; Anthony, J. E. *J. Am. Chem. Soc.* **2005**, *127*, 8028–8029.

299. Tönshoff, C.; Bettinger, H. F. *Angew. Chem., Int. Ed.* **2010**, *49*, 4125–4128.

300. Clar, E. *Polycyclic Hydrocarbons*. Academic Press: London, **1964**, Vol. 1.

301. Krüger, J.; García, F.; Eisenhut, F.; Skidin, D.; Alonso, J. M.; Guitián, E.; Pérez, D.; Cuniberti, G.; Moresco, F.; Peña, D. *Angew. Chem., Int. Ed.* **2017**, *56*, 11945–11948.

302. Zuzak, R.; Dorel, R.; Kolmer, M.; Szymonski, M.; Godlewski, S.; Echavarren, A. M. *Angew. Chem., Int. Ed.* **2018**, *57*, 10500–10505.

303. Eisenhut, F.; Kühne, T.; García, F.; Fernández, S.; Guitián, E.; Pérez, D.; Trinquier, G.; Cuniberti, G.; Joachim, C.; Peña, D.; Moresco, F. *ACS Nano* **2020**, *14*, 1011–1017.

304. Wudl , F.; Koutentis, P. A.; Weitz, A.; Ma, B.; Strassner, T.; Houk, K. N.; Khan, S. I. *Pure Appl. Chem.* **1999**, *71*, 295–302.

305. Nishida, J.-I.; Naraso; Murai, S.; Fujiwara, E.; Tada, H.; Tomura, M.; Yamashita, Y. *Org. Lett.* **2004**, *6*, 2007–2010.

306. Winkler, M.; Houk, K. N. *J. Am. Chem. Soc.* **2007**, *129*, 1805–1815.

307. Bunz, U. H. F. *Acc. Chem. Res.* **2015**, *48*, 1676–1686.

308. Bunz, U. H. F.; Engelhart, J. U. *Chem. Eur. J.* **2016**, *22*, 4680–4689.

309. Ji, L.; Friedrich, A.; Krummenacher, I.; Eichhorn, A.; Braunschweig, H.; Moos, M.; Hahn, S.; Geyer, F. L.; Tverskoy, O.; Han, J.; Lambert, C.; Dreuw, A.; Marder, T. B.; Bunz, U. H. F. *J. Am. Chem. Soc.* **2017**, *139*, 15968–15976.

310. Lindner, B. D.; Engelhart, J. U.; Tverskoy, O.; Appleton, A. L.; Rominger, F.; Peters, A.; Himmel, H. J.; Bunz, U. H. F. *Angew. Chem., Int. Ed.* **2011**, *50*, 8588–8591.

311. Engelhart, J. U.; Tverskoy, O.; Bunz, U. H. F. *J. Am. Chem. Soc.* **2014**, *136*, 15166–15169.

312. Miao, S.; Brombosz, S. M.; Schleyer, P. v. R.; Wu, J. I.; Barlow, U. S.; Marder, S. R.; Hardcastle, K. I.; Bunz, U. H. F. *J. Am. Chem. Soc.* **2008**, *130*, 7339–7344.

313. Hofstetter, Y. J.; Hopkinson, P. E.; Bakulin, A. A.; Vaynzof, Y. *J. Mater. Chem. C* **2016**, *4*, 1111–1116.

314. Lindner, B. D.; Zhang, Y.; Höfle, S.; Berger, N.; Teusch, C.; Jesper, M.; Hardcastle, K. I.; Qian, X.; Lemmer, U.; Colsmann, A.; Bunz, U. H. F.; Hamburger, M. *J. Mater. Chem. C* **2013**, *1*, 5718–5724.

315. Herz, J.; Buckup, T.; Paulus, F.; Engelhart, J. U.; Bunz, U. H. F.; Motzkus, M. *J. Phys. Chem. A* **2015**, *119*, 6602–6610.

316. Appleton, A. L.; Brombosz, S. M.; Barlow, S.; Sears, J. S.; Bredas, J.-L.; Marder, S. R.; Bunz, U. H. F. *Nat. Commun.* **2010**, *91*, 1–6.

317. Engelhart, J. U.; Paulus, F.; Schaffroth, M.; Vasilenko, V.; Tverskoy, O.; Rominger, F.; Bunz, U. H. F. *J. Org. Chem.* **2016**, *81*, 1198–1205.

318. Iyoda, M.; Yamakawa, J.; Rahman, M. J. *Angew. Chem., Int. Ed.* **2011**, *50*, 10522–10553.

319. Zang, L.; Che, Y.; Moore, J. S. *Angew. Chem., Int. Ed.* **2006**, *45*, 4416–4439. **319**

320. Vogel, E.; Roth, H. D. *Angew. Chem., Int. Ed. Engl.* **1964**, *3*, 228–229.

321. Vogel, E.; Böll, W. A. *Angew. Chem., Int. Ed. Engl.* **1964**, *3*, 642–642.

322. Hoeben, F. J. M.; Jonkheijm, P.; Meijer, E. W.; Schenning, A. P. H. J. *Chem. Rev.* **2005**, *105*, 1491–1546.

323. Zang, L.; Che, Y.; Moore, J. S. *Acc. Chem. Res.* **2008**, *41*, 1596–1608.

324. De Greef, T. F. A.; Smulders, M. M. J.; Wolffs, M.; Schenning, A. P. H. J.; Sijbesma, R. P.; Meijer, E. W. *Chem. Rev.* **2009**, *109*, 5687–5754.

325. Kudernac, T.; Lei, S.; Elemans, J. A. A. W.; De Feyter, S. *Chem. Soc. Rev.* **2009**, *38*, 402–421.

326. Höger, S. *Pure Appl. Chem.* **2010**, *82*, 821–830.

327. Mohnani, S.; Bonifazi, D. *Coord. Chem. Rev.* **2010**, *254*, 2342–2362.

328. Kawase, T.; Kurata, H. *Chem. Rev.* **2006**, *106*, 5250–5273.

329. Kawase, T.; Oda, M. *Pure Appl. Chem.* **2006**, *78*, 831–839.

330. Tahara, K.; Tobe, Y. *Chem. Rev.* **2006**, *106*, 5274–5290.

331. Rapson, W. S.; Shuttleworth, R. G.; van Niekerk, J. N. *J. Chem. Soc.* **1943**, 326–327.

332. Rajca, A.; Rajca, S.; Pink, M.; Miyasaka, M. *Synlett* **2007**, *12*, 1799–1822.

333. Huang, H.; Hau, C.-K.; Law, C. C. M.; Wong, H. N. C. *Org. Biomol. Chem.* **2009**, *7*, 1249– 1257.

334. Rajca, A.; Rajca, S *Angew. Chem., Int. Ed.* **2010**, *49*, 672– 674.

335. Staab, H, A.; Binnig, F. *Tetrahedron Lett.* **1964**, *5*, 319–321.

336. Irngartinger, H.; Leiserowitz, L.; Schmidt, G. M. J. *Chem. Ber.* **1970**, *103*, 1132–1156.

337. Pisula, W.; Kastler, M.; Yang, C.; Enkelmann, V.; Müllen, K. *Chem. Asian J.* **2007**, *2*, 51–56.

338. Xue, J. Y.; Ikemoto, K.; Takahashi, N.; Izumi, T.; Taka, H.; Kita, H.; Sato, S.; Isobe, H. *J. Org. Chem.* **2014**, *79*, 9735–9739.

339. Jasti, R.; Bhattacharjee, J.; Neaton, J. B.; Bertozzi, C. R. *J. Am. Chem. Soc.* **2008**, *130*, 17646–17647.

340. Steinberg, B. D.; Scott, L. T. *Angew. Chem., Int. Ed.* **2009**, *42*, 5400–5402.

341. Takaba, H.; Omachi, H.; Yamamoto, Y.; Bouffard, J.; Itami, K. *Angew. Chem., Int. Ed.* **2009**, *48*, 6112–6116.

342. Jasti, R.; Bertozzi, C. R. *Chem. Phys. Lett.* **2010**, *494*, 1–7.

343. Yamago, S; Watanabe, Y.; Iwamoto, T. *Angew. Chem., Int. Ed.* **2010**, *49*, 757–759.

344. Omachi, H.; Matsuura, S.; Segawa, Y.; Itami, K. *Angew. Chem., Int. Ed.* **2010**, *49*, 10202–10205.

345. Iwamoto, T.; Watanabe, Y.; Sakamoto, Y.; Suzuki, T.; Yamago, S. *J. Am. Chem. Soc.* **2011**, *133*, 8354–8361.

346. Kayahara, E.; Patel, V. K.; Yamago, S. *J. Am. Chem. Soc.* **2014**, *136*, 2284–2287.

347. Meyer, H.; Staab, H. A. *Justus Liebigs Ann. Chem.* **1969**, *724*, 30–33.

348. Yasuhiro, F. *Bull. Chem. Soc. Jpn.* **1984**, *57*, 3494–3506.

349. Shibata, T.; Fujimoto, M.; Hirashima, H.; Chiba, T.; Endo, K. *Synthesis* **2012**, *44*, 3269–3284.

350. Sakamoto, Y.; Suzuki, T. *J. Am. Chem. Soc.* **2013**, *135*, 14074–14077.

351. Kaikawa, T.; Takimiya, K.; Aso, Y.; Otsubo, T. *Org. Lett.* **2000**, *2*, 4197– 4199.

352. Krömer, J.; Rios-Carreras, I.; Fuhrmann, G.; Musch, C.; Wunderlin, M.; Debaerdemaeker, T.; Mena-Osteritz, E.; Bäuerle, P. *Angew. Chem., Int. Ed.* **2000**, *39*, 3481–3486.

353. Chmielewski, P. J. *Angew. Chem., Int. Ed.* **2010**, *49*, 1359–1361.

354. Maier, S. K.; Jester, S.-S.; Müller, U.; Müller, W. M.; Höger, S. *Chem. Commun.* **2011**, *47*, 11023–11025.

355. Matsui, K.; Segawa, Y.; Itami, K. *Org. Lett.* **2012**, *14*, 1888–1891.

356. Yang, F.; Wang, Z.; Song, F.; Liu, X.; Lan, J.; You, J. *Chem. Commun.* **2013**, *49*, 5975–5977.

357. Roznyatovskiy, V. V.; Leeb, C.-H.; Sessler, J. L. *Chem. Soc. Rev.* **2013**, *42*, 1921–1933.

358. Iyoda, M.; Shimizu, H. *Chem. Soc. Rev.* **2015**, *44*, 6411–6424.

359. Tanaka, T.; Osuka, A. *Chem. Soc. Rev.* **2015**, *44*, 943–969.

360. Marin, L.; Kudrjasova, J.; Verstappen, P.; Penxten, H.; Robeyns, K.; Lutsen, L.; Vanderzande, D. J. M.; Maes, W. *J. Org. Chem.* **2015**, *80*, 2425–2430.

361. Jiang, H.; Zhang, Y.; Chen, D.; Zhou, B.; Zhang, Y. *Org. Lett.* **2016**, *18*, 2032–2035.

362. Li, P.; Wong, B. M.; Zakharov, L. N.; Jasti, R. *Org. Lett.* **2016**, *18*, 1574–1577.

363. Hahn, S.; Alrayyani, M.; Sontheim, A.; Wang, X.; Rominger, F.; Miljanić, O. Š.; Bunz, U. H. F. *Chem. Eur. J.* **2017**, *23*, 10543–10550.

364. Dopper, J. H.; Wynberg, H. *Tetrahedron Lett.* **1972**, *13*, 763–766.

365. Song, X.; Kong, L.; Du, H.; Li, X.; Feng, H.; Zhao, J.; Xie, Y. *Materials* **2018**, *11*, 2063–2082.

366. Stoklosa, H. J.; Wasson, J. R.; Brown, E. V.; Richardson, H. W.; Hatfield, W. E. *Inorg. Chem.* **1975**, *14*, 2378–2382.

367. Staniewicz, R. J.; Sympson, R. F.; Hendricker, D. G. *Inorg. Chem.* **1977**, *16*, 2166–2171.

368. Wheeler, M. T.; Walmsley, F. *Thermochim. Acta* **1986**, *108*, 325–336.

369. Bessenbacher, C.; Kaim, W. *J. Organomet. Chem.* **1989**, *369*, 83−103.

370. Choi; Y.-Y.; Wong, W.-T. *J. Organomet. Chem.* **1999**, *573*, 189–201.

371. Manson, J. L. *Inorg. Chem.* **2003**, *42*, 2602−2605.

372. Barrios, L. A.; Aromí, G.; Frontera, A.; Quiñonero, D.; Deyà, P. M.; Gamez, P.; Roubeau, O.; Shotton; E. J.; Teat S. J. *Inorg. Chem.* **2008**, *47*, 5873–588.

373. van Albada, G. A.; van der Horst, M. G.; Fu, W. T.; Roubeau, O.; Mutikainen, I.; Turpeinen, U.; Reedijk, J. *Inorg. Chim. Acta* **2009**, *362*, 4422–4429.

374. van Albada, G. A.; Ghazzali, M.; Al-Farhan, K.; Mutikainen, I.; Reedijk, J. *Inorg. Chem. Commun.* **2011**, *14*, 162–165.

375. van Albada, G. A.; Mutikainen, I.; Ghazzali, M.; Al-Farhan, K.; Reedijk, J. *Dalton Trans.* **2012**, *41*, 4566–4574.

376. Cheeseman, G. W. H.; Cookson, R. F. *Chemistry of Heterocyclic Compounds: Condensed Pyrazines*. John Wiley & Sons: New York, **1979**, Vol. 35.

377. Lu, P.; Wu, Y.; Kang, H.; Wei, H.; Liu, H.; Fang, M. *J. Mater. Chem. A* **2014**, 2, 16250–16267.

378. Okuniewski, A.; Rosiak, D.; Chojnacki, J.; Becker, B. *Polyhedron* **2015**, *90*, 47–57.

379. Würth, C.; Grabolle, M.; Pauli, J.; Spieles, M.; Resch-Genger, U. *Nat. Protoc.* **2013**, *8*, 1535–1550.

380. Singh, R. B.; Jain, P.; Singh, R. P. *Talanta* **1982**, *29*, 77–84.

381. Hidai, M.; Mizobe, Y. *Chem. Rev.* **1995**, *95*, 1115–1133.

382. Enders, D.; Wortmann, L.; Peters, R. *Acc. Chem. Res.* **2000**, *33*, 157–169.

383. Lazny, R.; Nodzewska, A. *Chem. Rev.* **2010**, *110*, 1386–1434.

384. Kobayashi, S.; Mori, Y.; Fossey, J. S.; Salter, M. M. *Chem. Rev.* **2011**, *111*, 2626–2704.

385. Vicini, P.; Zani, F.; Cozzini, P.; Doytchinova, I. *Eur. J. Med. Chem.* **2002**, *37*, 553–564.

386. Loncle, C.; Brunel, J.; Vidal, N.; Dherbomez, M.; Letourneux, Y. *Eur. J. Med. Chem.* **2004**, *39*, 1067–1071.

387. Savini, L.; Chiasserini, L.; Travagli, V.; Pellerano, C.; Novellino, E.; Cosentino, S.; Pisano, M. *Eur. J. Med. Chem.* **2004**, *39*, 113–122.

388. Cocco, M.; Congiu, C.; Lilliu, V.; Onnis, V. *Bioorg. Med. Chem.* **2006**, *14*, 366–372.

389. Masunari, A.; Tavares, L. C. *Bioorg. Med. Chem.* **2007**, *15*, 4229–4236.

390. Vicini, P.; Incerti, M.; La Colla, P.; Loddo, R. *Eur. J. Med. Chem.* **2009**, *44*, 1801–1807.

391. Lehn, J.-M. *Chem. Soc. Rev.* **2007**, *36*, 151–160.

392. Lehn, J.-M. *Angew. Chem., Int. Ed.* **2013**, *52*, 2836–2850.

393. Lehn, J.-M. *Topics in Current Chemistry*. Springer: Berlin, **2012**.

394. Uribe-Romo, F. J.; Doonan, C. J.; Furukawa, H.; Oisaki, K.; Yaghi, O. M. *J. Am. Chem. Soc.* **2011**, *133*, 11478–11481.

395. Bunck, D. N.; Dichtel, W. R. *J. Am. Chem. Soc.* **2013**, *135*, 14952–14955.

396. Zhou, X.-P.; Wu, Y.; Li, D. *J. Am. Chem. Soc.* **2013**, *135*, 16062–16065.

397. Rowan, S.; Cantrill, S.; Cousins, G.; Sanders, J.; Stoddart, J. F. *Angew. Chem., Int. Ed.* **2002**, *41*, 898–952.

398. Corbett, P. T.; Leclaire, J.; Vial, L.; West, K. R.; Wietor, J.-L.; Sanders, J. K. M.; Otto, S. *Chem. Rev.* **2006**, *106*, 3652–3711.

399. Jin, Y.; Yu, C.; Denman, R. J.; Zhang, W. *Chem. Soc. Rev.* **2013**, *42*, 6634–6654.

400. Miller, B. L. *Dynamic Combinatorial Chemistry, Drug Discovery, Bioorganic Chemistry, and Materials Science*. John Wiley and Sons: New Jersey (Hoboken), **2010**.

401. Raue, R.; Brack, A.; Lange, K. *Angew. Chem., Int. Ed. Engl.* **1991**, *30*, 1643–1644.

402. Lygaitis, R.; Getautis, V.; Grazulevicius, J. V. *Chem. Soc. Rev.* **2008**, *37*, 770–788.

403. Landge, S.M.; Tkatchouk, E.; Benítez, D.; Lanfranchi, D. A.; Elhabiri, M.; Goddard, III, W. A.; Aprahamian, I. *J. Am. Chem. Soc.* **2011**, *133*, 25, 9812–9823.

404. Romero, E. L.; D'Vries, R. F.; Zuluaga, F.; Chaur, M. N. *J. Braz. Chem. Soc.* **2015**, *26*, S1–S6.

405. Lehn, J.-M. *Chem. Eur. J.* **2006**, *12*, 5910–5915.

406. Tatum, L.; Su, X.; Aprahamian, I. *Acc. Chem. Res.* **2014**, *47*, 2141–2149.

407. Lehn, J. M.; Ulrich, S. *J. Am. Chem. Soc.* **2009**, *131*, 5546–5559.

408. Ruben, M.; Lehn, J-M.; Müller, P. *Chem. Soc. Rev.* **2006**, *35*, 1056–1067.

409. Hardy, J. G. *Chem. Soc. Rev.* **2013**, *42*, 7881–7899.

410. Dugave, C.; Demange, L. *Chem. Rev.* **2003**, *103*, 2475–2532.

411. Serbutoviez, C.; Bosshard, C.; Knopfle, G.; Wyss, P.; Pretre, P.; Gunter, P.; Schenk, K.; Solari, E.; Chapuis, G. *Chem. Mater.* **1995**, *7*, 1198–1206.

412. Lawrence, M. A.W.; Lorraine, S. C.; Wilson, K.-A.; Wilson, K. *Polyhedron* **2019**, *173*, 1–18.

413. Su, X.; Aprahamian, I. *Chem. Soc. Rev.* **2014**, *43*, 1963-1981.

414. Adegoke, O.A.; Adesuji, T.E.; Thomas, O.E. *Spectrochim. Acta, Part A* **2014**, *128*, 147–152.

415. Bakir, M.; Brown, O. *J. Mol. Struct.* **2011**, *1006*, 402–408.

416. Bakir, M.; Green, O.; Gyles, C. *Spectrochim. Acta, Part A* **2009**, *72*, 50–55.

417. Bakir, M.; Green, O.; Gyles, C.; Mangaro, B.; Porter, R. *Talanta* **2004**, *62*, 781–789.

418. Bakir, M.; Gyles, C. *J. Mol. Struct.* **2007**, *833*, 161–168.

419. Burdette, S. C. *Nat. Chem.* **2012**, *4*, 695–696.

420. Cnossen, A.; Browne, W. R.; Feringa, B. L. *Molecular Machines and Motors: Unidirectional Light-Driven Molecular Motors Based on Overcrowded Alkenes*. Berlin: Springer-Verlag, **2014**.

421. Yamamura, S.; Tamaki, T.; Seki, T.; Sakuragi, M.; Kawanishi, Y.; Ichimura, K. *Chem. Lett.* **1992**, 21, 543–546.

422. Chaur, M. N.; Collado, D.; Lehn, J.-M. *Chem. Eur. J.* **2011**, *17*, 248–258.

423. Hirose, K. *J. Inclusion Phenom. Macrocyclic Chem.* **2010**, *68*, 1–24.

424. Kay, E. R.; Leigh, D. A.; Zerbetto, F. *Angew. Chem., Int. Ed. Engl.* **2006**, *46*, 72–191.

425. Sun, W.-T.; Huang, S.-L.; Yao, H.-H.; Chen, I.-C.; Lin, Y.-C.; Yang, J. S. *Org. Lett.* **2012**, *14*, 4154–4157.

426. Coskun, A.; Friedman, D. C.; Li, H.; Patel, K.; Khatib, H.; Stoddart, J. F. *J. Am. Chem. Soc.* **2009**, *131*, 2493–2495.

427. Kelly, T. R.; Bowyer, M. C.; Bhaskar, K. V.; Bebbington, D.; García, A.; Lang, F.; Kim, M. H.; Jette, M. P. *J. Am. Chem. Soc.* **1994**, *116*, 3657–3658.

428. Ray, D.; Foy, J. T.; Hughes, R. P.; Aprahamian, I. *Nat. Chem.* **2012**, *4*, 757–762.

429. Landge, S. M.; Aprahamian, I. *J. Am. Chem. Soc.* **2009**, *131*, 18269–18271.

430. Su, X.; Voskian, S.; Hughes, R. P.; Aprahamian, I. *Angew. Chem., Int. Ed.* **2013**, *52*, 10734–10739.

431. Yang, C.-H.; Prabhakar, C.; Huang, S.-L.; Lin, Y.-C.; Tan, W. S.; Misra, N. C.; Sun, W.-T.; Yang, J.-S. *Org. Lett.* **2011**, *13*, 5632–5635.

432. Patai, S. *Chemistry of the Carbon-Nitrogen Double Bond*. John Wiley and Sons: New York, **1970**.

433. Kessler, H. *Tetrahedron* **1974**, *30*, 1861–1870.

434. Padwa, A.; Albrecht, F. *J. Am. Chem. Soc.* **1974**, *96*, 4849–4857.

435. Padwa, A. *Chem. Rev.* **1977**, *77*, 37–68.

436. Lemal, D. M.; Menger, F.; Coats, E. *J. Am. Chem. Soc.* **1964**, *86*, 2395–2401.

437. Ioffe, B.V.; Kartsova, L.A. *Tetrahedron Lett.* **1973**, *14*, 623–626.

438. Allen, F. H.; Kennard, O.; Watson, D. G.; Brammer, L.; Orpen, A. G.; Taylor, R. *J. Chem. Soc., Perkin Trans. 2* **1987**, S1–S19.

439. Benson, S. W. *J. Chem. Educ.* **1965**, *42*, 502–518.

440. Cottrell, T. L. *The Strengths of Chemical Bonds*. 2nd Ed, Butterworths: London, **1958**.

441. Kitaev, Y. P.; Arbuzov, A. E. *Russ. Chem. Bull.* **1960**, *9*, 1306–1311.

442. Jones, P. G. *Chem. Soc. Rev.* **1984**, *13*, 157–172.

443. Tsuzuki, S.; Uchimaru, T., Mikami, M. *J. Phys. Chem. A* **2006**, *110*, 2027–2033.

444. Mishra, B. K.; Sathyamurthy, N. *J. Phys. Chem. A* **2005**, *109*, 6–8.

445. Sierański, T. *J. Mol. Model.* **2017**, *23*, 338–353.

446. Müller, P. *Crystallogr. Rev.* **2009**, *15*, 57–83.

447. Sim, J.; Yim, H.; Ko, N.; Choi, S. B.; Oh, Y.; Park, H. J.; Park, S. Y.; Kim, J. *Dalton Trans.* **2014**, *43*, 18017–18024.

448. Van der Sluis, P, Spek, A. L. *Acta Crystallogr. Sect. A* **1990**, *46*, 194–201.

449. Spek, A. L. *Acta Crystallogr. Sect. D* **2009**, *65*, 148–155.

450. Msayib, K. J.; Book, D.; Budd, P. M.; Chaukura, N.; Harris, K. D. M.; Helliwell, M.; Tedds, S.; Walton, A.; Warren, J. E.; Xu, M.; McKeown, N. B. *Angew. Chem., Int. Ed.* **2009**, *48*, 3273–3277.

451. Garratt, P. J.; Thom, S. N.; Wrigglesworth, R. *Tetrahedron* **1994**, *50*, 12211−12218.

452. Yamagami, C.; Takao, N.; Takeuchi, Y. *Aust. J. Chem.* **1986**, *39*, 457−463.

453. Dabbagh, H. A.; Modarresi-Alam, A. R. *J. Chem. Res., Synop.* **2000**, 190−192.

454. Modarresi-Alam, A. R.; Keykha, H.; Khamooshi, F.; Dabbagh, H. A. *Tetrahedron* **2004**, *60*, 1525−1530.

455. Günther, H. *NMR Spectroscopy*. 2nd Ed, John Wiley and Sons: New York, **1995**.

456. Ōki, M. *Application of Dynamic NMR Spectroscopy to Organic Chemistry*. In: VCH Publishers: New York, **1985**, Vol. 4.